

Sheffield Hallam University

Creep settlement of opencast mine backfill.

O'NEILL, Mark A.

Available from the Sheffield Hallam University Research Archive (SHURA) at:

<http://shura.shu.ac.uk/20148/>

A Sheffield Hallam University thesis

This thesis is protected by copyright which belongs to the author.

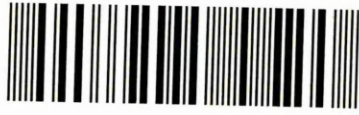
The content must not be changed in any way or sold commercially in any format or medium without the formal permission of the author.

When referring to this work, full bibliographic details including the author, title, awarding institution and date of the thesis must be given.

Please visit <http://shura.shu.ac.uk/20148/> and <http://shura.shu.ac.uk/information.html> for further details about copyright and re-use permissions.

Sheffield S1 1WB

101 907 908 8



Sheffield Hallam University
Learning and IT Services
Adsetts Centre City Campus
Sheffield S1 1WB

REFERENCE

ProQuest Number: 10697455

All rights reserved

INFORMATION TO ALL USERS

The quality of this reproduction is dependent upon the quality of the copy submitted.

In the unlikely event that the author did not send a complete manuscript and there are missing pages, these will be noted. Also, if material had to be removed, a note will indicate the deletion.



ProQuest 10697455

Published by ProQuest LLC (2017). Copyright of the Dissertation is held by the Author.

All rights reserved.

This work is protected against unauthorized copying under Title 17, United States Code
Microform Edition © ProQuest LLC.

ProQuest LLC.
789 East Eisenhower Parkway
P.O. Box 1346
Ann Arbor, MI 48106 – 1346

Creep Settlement of Opencast Mine Backfill

Mark A O'Neill

A thesis submitted in partial fulfilment of the requirements of
Sheffield Hallam University
for the degree of Doctor of Philosophy

May 2007

Collaborating Organisation: University of Sheffield



Abstract

The extraction of a significant amount coal in the United Kingdom has over the last four or so decades been made using opencast mining methods. This method involves large-scale excavation to reach the coal seams (with depths often exceeding 100m). Following extraction various forms of restoration have been employed, including backfilling the mine void with material excavated in order to extract the coal. This backfilling was frequently undertaken in an uncontrolled fashion. In recent years it has been more usual to engineer the restoration such that further development of the site can take place. However, settlement remains the major obstacle to development.

One mode of settlement commonly encountered on restored sites is creep settlement. Further, on older sites whose restoration was, most probably, undertaken in an uncontrolled way, the potential for creep settlement is the major obstacle.

Creep settlement is understood to be that component of total settlement which, in a coarse granular soil, takes place under conditions of constant stress. It is generally accepted to occur linearly with the decadic logarithm of time. This study investigates the phenomenon from the visualisation of the granular particle mechanics.

The technique used for the visualisations is computed tomography (CT), a technique which is common in medical diagnostics but has rarely been exploited in soil mechanics and never at the scale employed in the study. The use of CT supplements a programme of high quality, large scale laboratory testing, which models typical opencast coal mine backfill.

The testing programme has revealed that compaction and the diagenesis of the source materials have a significant effect on the creep rate. Further, that the creep rate is defined in the most part by the aggregation of small or minor movements rather being dominated by large or major movements.

Affirmation

The work submitted in this thesis is my own work and has not been previously submitted for any other degree.

Signed: Mark A O'Neill

Date:15 October 2008.....

Contents

| | Page |
|---|------------|
| Abstract | i |
| Affirmation | ii |
| Contents | iii |
| List of Figures | vii |
| List of Tables | xi |
| Acknowledgements | xii |
| 1 Introduction | 1 |
| 1.1 Opencast mining and restoration in the U.K. | 3 |
| 1.1.1 Background | 3 |
| 1.1.2 History of Opencast Coal Mining in the U.K. | 4 |
| 1.1.3 Scale and Operation of Opencast Mine Sites | 5 |
| 1.2 Post-Restoration Development | 9 |
| 1.3 Research Context | 11 |
| 1.4 Research Aims and Objectives | 12 |
| 2 Literature Review | 14 |
| 2.1 Geology and Coal Measures Rock | 14 |
| 2.1.1 Introduction | 14 |
| 2.1.2 Coal Geology | 14 |
| 2.1.3 Mudstone Classification | 16 |
| 2.1.4 Mineralogy | 21 |
| 2.1.5 Engineering Properties | 22 |
| 2.1.6 Weathering | 24 |
| 2.2 Opencast Coal Mine Backfill Behaviour and Properties | 27 |
| 2.2.1 Introduction | 27 |
| 2.2.2 Types of Movement | 27 |
| 2.2.3 Typical Opencast Backfill Material | 28 |
| 2.2.4 Backfill Placement | 30 |
| 2.2.5 Compaction Theory | 31 |
| 2.2.6 Compaction Specification | 33 |
| 2.2.7 Compaction Plant and Methods | 34 |
| 2.2.8 Compaction Monitoring and Testing | 34 |
| 2.2.9 Particle and Soil Characteristics | 36 |
| 2.2.10 Stress Distribution, Soil Structure and Fills | 44 |
| 2.3 Mechanisms of Creep | 52 |
| 2.3.1 Effect of Water on Behaviour | 52 |
| 2.3.2 Brittle Fracture | 55 |
| 2.3.3 Particle Crushing. | 55 |
| 2.3.4 Asperity Indentation and Ploughing in Rock Friction | 57 |
| 2.3.5 Potential for Particle Breakage | 62 |
| 2.4 Creep Theories, Analysis and Prediction | 63 |

| | Page | |
|----------|---|------------|
| 2.4.1 | Introduction | 63 |
| 2.4.2 | Creep Settlement Definitions | 63 |
| 2.4.3 | Alpha (α) Coefficient | 63 |
| 2.4.4 | Typical Values of the α Parameter | 65 |
| 2.4.5 | Theory of Rate Processes | 66 |
| 2.4.6 | Secondary Compression in Clay | 70 |
| 2.5 | Discussion and Summary | 73 |
| 2.5.1 | Creep Definition | 73 |
| 2.5.2 | Stress Path Development | 74 |
| 2.5.3 | Primary, Secondary and Component Mechanisms | 74 |
| 2.5.4 | Fill Composition | 75 |
| 2.5.5 | Changes in Material after Compaction | 76 |
| 2.5.6 | Suction | 77 |
| 3 | Methodology | 78 |
| 3.1 | Laboratory based testing | 78 |
| 3.1.1 | Schedule of testing | 79 |
| 3.1.2 | Test Preparation (Cell and Specimen) | 80 |
| 3.1.3 | Testing Procedure | 83 |
| 3.2 | Non-destructive Testing | 85 |
| 3.2.1 | Methodology Development | 85 |
| 3.2.2 | Computered Tomography Procedures | 89 |
| 4 | Equipment | 92 |
| 4.1 | Laboratory Equipment | 93 |
| 4.1.1 | The Laboratory | 93 |
| 4.1.2 | Compression Cells | 93 |
| 4.1.3 | Cell Commissioning | 101 |
| 4.1.4 | Loading and Load Control System | 104 |
| 4.1.5 | Data Acquisition Equipment and Systems | 105 |
| 4.1.6 | Specimen Compaction Equipment | 106 |
| 4.1.7 | Laboratory Equipment Failures | 107 |
| 4.2 | Computed Tomography | 108 |
| 4.2.1 | Introduction | 108 |
| 4.2.2 | CT, An Overview | 108 |
| 4.2.3 | CT, Applications in Soil Mechanics | 112 |
| 4.2.4 | CT Equipment Used | 113 |
| 5 | Test Materials | 115 |
| 5.1 | Origin and Description of Samples | 115 |
| 5.1.1 | Houghton Main Samples | 117 |
| 5.1.2 | Orgreave Sample | 119 |
| 5.2 | Particle Density | 121 |
| 5.3 | Particle Size Distribution (PSD) | 121 |
| 5.4 | Particle Shape Analysis | 123 |
| 5.4.1 | Houghton Main Sample | 125 |
| 5.4.2 | Orgreave Sample | 126 |

| | Page | |
|----------|---|------------|
| 5.5 | Moisture Content | 127 |
| 5.6 | Atterberg Limits | 128 |
| 5.7 | Standard Compaction Test | 128 |
| 6 | Results and Analysis | 130 |
| 6.1 | Introduction | 130 |
| 6.2 | Laboratory Test Data | 130 |
| 6.2.1 | Detailed results for Test 1 | 131 |
| 6.2.2 | Detailed results for Test 2 | 134 |
| 6.2.3 | Detailed results for Test 3 | 137 |
| 6.2.4 | Detailed results for Test 4 | 140 |
| 6.2.5 | Detailed results for Test 5 | 143 |
| 6.2.6 | Detailed results for Test 6 | 146 |
| 6.2.7 | Detailed results for Test 7 | 149 |
| 6.2.8 | Detailed results for Test 8 | 152 |
| 6.2.9 | Detailed results for Test 9 | 155 |
| 6.2.10 | Detailed results for Test 10 | 158 |
| 6.2.11 | Detailed results for Test 11 | 161 |
| 6.2.12 | Detailed results for Test 12 | 164 |
| 6.2.13 | Detailed results for Test 13 | 167 |
| 6.2.14 | Detailed results for Test 14 | 170 |
| 6.2.15 | Detailed results for Test 15 | 173 |
| 6.3 | Laboratory Test Data – Summary | 176 |
| 6.4 | Computed Tomography Data | 177 |
| 6.4.1 | Introduction | 177 |
| 6.4.2 | Analysis of CT Scans | 177 |
| 6.4.3 | Computed Tomography Data - Summary | 220 |
| 6.5 | Other Observations | 221 |
| 7 | Interpretation and Discussion | 223 |
| 7.1 | Methodology | 223 |
| 7.2 | Equipment | 223 |
| 7.2.1 | Laboratory Based | 223 |
| 7.2.2 | Computed Tomography Equipment & Procedures | 227 |
| 7.3 | Materials | 228 |
| 7.3.1 | Material sources | 228 |
| 7.3.2 | Engineering Properties | 229 |
| 7.3.3 | Houghton Main – Orgreave Sample Differences | 231 |
| 7.4 | Results | 233 |
| 7.4.1 | Specimen Preparation | 233 |
| 7.4.2 | Laboratory Results | 238 |
| 7.4.3 | Computed Tomography Results | 248 |
| 7.4.4 | Laboratory and Computed Tomography Results Comparison | 251 |
| 8 | Conclusions & Recommendations | 254 |
| 8.1 | Summary of work | 254 |

| | Page | |
|-------------------|-------------------------------------|------------|
| 8.2 | Conclusions | 255 |
| 8.2.1 | General Creep Settlement Behaviour | 255 |
| 8.2.2 | Field Creep Values | 255 |
| 8.2.3 | Repeatability | 256 |
| 8.2.4 | Source Materials | 256 |
| 8.2.5 | Compaction Regime | 257 |
| 8.2.6 | Test Scale | 257 |
| 8.2.7 | Non-linear and Inundation Behaviour | 258 |
| 8.3 | Recommendations | 258 |
| References | | 260 |

Appendix A Metal Cell Component Design Calculations

List of Figures

| | Page |
|--|------|
| Figure 1-1: Typical operation of an opencast coal site. | 5 |
| Figure 1-2: The “Ace of Spades” walking dragline at work. | 6 |
| Figure 1-3: Dumper truck being loaded by a face shovel. | 7 |
| Figure 1-4: Division of sales, of coal won by opencasting, by consumer (data from British Coal Opencast, 1993). | 8 |
| Figure 1-5: UK: The coal supply chain, 2005 (source DTI cited by BGS, 2006) | 8 |
| Figure 1-6: Distribution of coal resources in the UK as of September 2006 (after BGS 2006). | 10 |
| Figure 2-1: Sandstone, a detrital sedimentary rock. | 17 |
| Figure 2-2: Mudstone, a detrital sedimentary rock. | 18 |
| Figure 2-3: A “geological” classification of clays and mudrocks based upon clay content and combined alumina to silica ratio, further indicative of clastics, after Taylor (1988). | 18 |
| Figure 2-4: Engineering classification of argillaceous Materials, after Morgenstern and Eigenbrod (1974). | 19 |
| Figure 2-5: The composition of mudrocks and the origins of the different fractions, after Taylor and Spears (1981). | 22 |
| Figure 2-6: Typical compaction curve. | 32 |
| Figure 2-7: Effect of compaction Energy, after Lambe and Whitman (1969). | 33 |
| Figure 2-8: Three dimensional shape categories bounded by arbitrary limits of elongation ratio and flatness ratio, after Lees (1964). | 38 |
| Figure 2-9: Chart for the determining, visually, the degree of angularity of particles, after Lees (1963). | 39 |
| Figure 2-10: Chart for the determining, visually, the degree of roundness of particles, after Krumbein (1941). | 39 |
| Figure 2-11: Compression of broken rock fill and river gravel, after Penman (1971). | 41 |
| Figure 2-12: Effect of particle size of shearing resistance of Ballotini, after Kolbuszewski and Frederick (1963). | 42 |
| Figure 2-13: False colour image showing ‘stress chains’ in a collection of photo-elastic particles (after Howell, 2000). | 45 |
| Figure 2-14: Soil skeleton (simplified). | 46 |
| Figure 2-15: Contact forces, after Marsal 1963. | 46 |
| Figure 2-16: Clay and silt particles within a mass of soil. | 47 |
| Figure 2-17: Categorisation of partially saturated soils based on various | |

| | Page |
|---|------|
| degrees of saturation (Fredlund, 1995). | 49 |
| Figure 2-18: Air/water interface forming a meniscus. | 50 |
| Figure 2-19: Properties of a purely thixotropic material, after Mitchell (1960). | 54 |
| Figure 2-20: Previous measures of particle breakage, after Hardin (1985). | 56 |
| Figure 2-21: Crushing test apparatus, after Marsal (1973). | 57 |
| Figure 2-22: Bi-axial loading frame as used in Scholz and Engelder (1976a). | 58 |
| Figure 2-23: Experimental equipment used in Scholz and Engelder (1976a). | 58 |
| Figure 2-24: Area of indent as a function of loading duration for quartz and olivine, after Scholz and Engelder (1976a). | 59 |
| Figure 2-25: Friction between a metal sheet of varying hardness, after Scholz and Engelder (1976b). | 62 |
| Figure 2-26: Observed settlements of rockfill dams after completion of construction, as cited in Sowers <i>et al.</i> (1965). | 65 |
| Figure 2-27: Settlement- \log_{10} time curves for laboratory confined compression tests of broken rock for constant vertical pressures applied in increments, after Sowers <i>et al.</i> (1965). | 66 |
| Figure 2-28: Energy barriers in rate process theory, after Feda (1989). | 67 |
| Figure 3-1 Radiograph of sample, taken as part of the investigations into suitable non-destructive imaging techniques. | 87 |
| Figure 4-1: Photograph showing much of the laboratory equipment. | 93 |
| Figure 4-2: Sample laboratory temperature monitoring data. | 94 |
| Figure 4-3: Schematic of the compression cells used in this project. | 95 |
| Figure 4-4: Creep data from testing carried out on behalf of North West Water (natural scale). | 97 |
| Figure 4-5: Creep data from testing carried out on behalf of North West Water (\log_{10} scale). | 98 |
| Figure 4-6: Top plate, piston bush, housing, o-ring and piston rod section. | 99 |
| Figure 4-7: Side wall friction investigation, cell set ups. | 103 |
| Figure 4-8: Side wall friction investigation, detailed results of the Stage 2 testing for the large cells. | 104 |
| Figure 4-9: Schematic of loading and load control system. | 105 |
| Figure 4-10: Schematic sketch of a CT scanner and its components. | 109 |
| Figure 4-11: a) Energy absorption, b) Scattering of rays. | 110 |
| Figure 4-12: GE Medical Systems HiSpeed CT/i Pro CT Scanner, gantry and table. | 114 |
| Figure 4-13: GE Medical Systems Advantage Windows Workstation. | 114 |
| Figure 5-1: Locations of Houghton Main and Orgreave Opencast Coal Mine sites. | 116 |

| | Page |
|--|------|
| Figure 5-2: Houghton Main Opencast Site Geology. | 118 |
| Figure 5-3: Orgreave Opencast Site Geology. | 120 |
| Figure 5-4: Graph of particle size distributions for the specimens used in the testing. | 122 |
| Figure 5-5: Photographs of particles (20mm, 28mm, 37.5mm & 50mm) taken from the Houghton Main specimens. | 123 |
| Figure 5-6: Photographs of particles (75mm) taken from the Houghton Main specimens. | 124 |
| Figure 5-7: Photograph of particles (75mm & 50mm) taken from the Orgreave specimens | 124 |
| Figure 5-8: Photograph of particles taken from the Orgreave specimens. | 125 |
| Figure 5-9: Distribution of particles from the Houghton specimen by shape factor. | 126 |
| Figure 5-10: Distribution of particles from the Orgreave specimen by shape factor. | 127 |
| Figure 5-11: Graph of mean results from standard compaction testing of the Houghton Main Sample. | 129 |
| Figure 5-12: Graph of mean results from standard compaction testing of the Orgreave Sample. | 129 |
| Figure 6-1: Graph of Pressure and Displacement against Time for Test 1. | 133 |
| Figure 6-2: Graph of Pressure and Strain against \log_{10} Time for Test 1. | 133 |
| Figure 6-3: Graph of Pressure and Displacement against Time for Test 2. | 136 |
| Figure 6-4: Graph of Pressure and Strain against \log_{10} Time for Test 2. | 136 |
| Figure 6-5: Graph of Pressure and Displacement against Time for Test 3. | 139 |
| Figure 6-6: Graph of Pressure and Strain against \log_{10} Time for Test 3. | 139 |
| Figure 6-7: Graph of Pressure and Displacement against Time for Test 4. | 142 |
| Figure 6-8: Graph of Pressure and Strain against \log_{10} Time for Test 4. | 142 |
| Figure 6-9: Graph of Pressure and Displacement against Time for Test 5. | 145 |
| Figure 6-10: Graph of Pressure and Strain against \log_{10} Time for Test 5. | 145 |
| Figure 6-11: Graph of Pressure and Displacement against Time for Test 6. | 148 |
| Figure 6-12: Graph of Pressure and Strain against \log_{10} Time for Test 6. | 148 |
| Figure 6-13: Graph of Pressure and Displacement against Time for Test 7. | 151 |
| Figure 6-14: Graph of Pressure and Strain against \log_{10} Time for Test 7. | 151 |
| Figure 6-15: Graph of Pressure and Displacement against Time for Test 8. | 154 |
| Figure 6-16: Graph of Pressure and Strain against \log_{10} Time for Test 8. | 154 |
| Figure 6-17: Graph of Pressure and Displacement against Time for Test 9. | 157 |
| Figure 6-18: Graph of Pressure and Strain against \log_{10} Time for Test 9. | 157 |

| | Page |
|---|------|
| Figure 6-19: Graph of Pressure and Displacement against Time for Test 10. | 160 |
| Figure 6-20: Graph of Pressure and Strain against \log_{10} Time for Test 10. | 160 |
| Figure 6-21: Graph of Pressure and Displacement against Time for Test 11. | 163 |
| Figure 6-22: Graph of Pressure and Strain against \log_{10} Time for Test 11. | 163 |
| Figure 6-23: Graph of Pressure and Displacement against Time for Test 12. | 166 |
| Figure 6-24: Graph of Pressure and Strain against \log_{10} Time for Test 12. | 166 |
| Figure 6-25: Graph of Pressure and Displacement against Time for Test 13. | 169 |
| Figure 6-26: Graph of Pressure and Strain against \log_{10} Time for Test 13. | 169 |
| Figure 6-27: Graph of Pressure and Displacement against Time for Test 14. | 172 |
| Figure 6-28: Graph of Pressure and Strain against \log_{10} Time for Test 14. | 172 |
| Figure 6-29: Graph of Pressure and Displacement against Time for Test 15. | 175 |
| Figure 6-30: Graph of Pressure and Strain against \log_{10} Time for Test 15. | 175 |
| Figure 6-31: CT section locations. | 177 |
| Figure 7-1: Graph showing compaction achieved for each test specimen compared to MDD and 90% of MDD. | 236 |
| Figure 7-2: Graph showing relative effectiveness of compaction energies used in specimen preparation for creep testing. | 236 |
| Figure 7-3: Graph showing relative effects of compaction energies on each material type. | 238 |
| Figure 7-4: Comparison of test α values with typical values observed in the field. | 241 |
| Figure 7-5: Graph of α values against cell size. | 242 |
| Figure 7-6: Comparison of test α value with sample dry density. | 243 |
| Figure 7-7: Graph of α values against compaction treatment. | 243 |
| Figure 7-8: Graph of α values against material source. | 244 |
| Figure 7-9: Comparison of sample dry density of Repeatability Pairs. | 245 |
| Figure 7-10: Comparison of sample strain of Repeatability Pairs. | 246 |
| Figure 7-11: Comparison of sample α values of Repeatability Pairs. | 246 |
| Figure 7-12: Comparison of test difference score with sample dry density. | 250 |
| Figure 7-13: Graph of difference score against material source. | 250 |
| Figure 7-14: Graph of difference score against compaction treatment. | 251 |
| Figure 7-15: Comparison of total differences scores against α values for each test. | 252 |
| Figure 7-16: Comparison of differences scores against α values for each test. | 253 |

List of Tables

| | Page |
|---|------|
| Table 2-1: Terms relevant to the Carboniferous time period, after Challinor (1967). | 15 |
| Table 2-2: General cyclothem sequence, after Hassani <i>et al.</i> (1979). | 16 |
| Table 2-3: Classification in terms of slaking characteristics, after Morgenstern and Eigenbrod (1974). | 20 |
| Table 2-4: Classification of weathered mudrocks, after Cripps and Taylor (1981). | 20 |
| Table 2-5: Average mineralogy of mudrocks, after Taylor (1988). | 22 |
| Table 2-6: List of Coal Measures rocks in order of geotechnical importance, after Hassani <i>et al.</i> (1979). | 23 |
| Table 2-7: Engineering properties of UK minestone (Rainbow, 1987) | 23 |
| Table 2-8: Physical Properties, after Rainbow (1987) and Blanchfield (1998). | 30 |
| Table 2-9: Types of compaction plant. | 35 |
| Table 2-10: Shape classification of particles as proposed by Lees (1963). | 40 |
| Table 3-1: Summary list of the testing producing a complete set of results. | 81 |
| Table 3-2: Typical cell and test specimen preparation times. | 82 |
| Table 3-3: Specimen loading regime | 83 |
| Table 4-1: Results of side wall friction investigation. | 103 |
| Table 5-1: Summary of particle density results. | 121 |
| Table 5-2: Results of Atterberg limit determinations. | 128 |
| Table 6-1: Summary of Laboratory Testing Results. | 176 |
| Table 6-2: Scale of differences used in the analysis of the CT results. | 178 |
| Table 6-3: Example of calculation of 'differences score'. | 179 |
| Table 6-4: Summary of Laboratory and CT Data. | 222 |
| Table 7-1: Comparison of the compaction achieved in specimen preparation with standard compaction. | 235 |
| Table 7-2: Repeatability pairs. | 245 |
| Table 7-3: Summary of totals of differences scores. | 249 |

Acknowledgements

It has become apparent to me that, generally, the nature of research is one of isolation; this is true for the researcher and for the research undertaken. So it is with grateful thanks that the following acknowledgements are given.

- To my supervisors (Dr A. K. Goodwin and Prof. W. F. Anderson) and other reviewers for their patient support and frequent, if sometimes painful, questioning.
- To Mr S Linskill, Senior Technician at Sheffield Hallam University, who has provided much welcome technical support throughout the research programme.
- To RJB Mining Ltd. for access to materials and their sites at Houghton Main and Orgreave.
- To the staff (especially A. Heseltine) and the organisation of the Royal Hallamshire Hospital, Sheffield, who have enabled much of my innovative work.
- To my girlfriend (Miss E. Cubitt) and brother (Mr J. O'Neill) who have given up much of their time in order to support me and my efforts.
- To the rest of my family and friends.

1 Introduction

The mechanics of particulate materials is of importance in a number of fields including chemistry, physics, pharmaceuticals, food production, as well as in soil mechanics and geotechnical engineering. In many of these fields the interest in particulates is focused on storage and transport of the particulate material or the mixing of two or more materials to produce a consistent final product. Given that geotechnical engineering is most often concerned with soils and their interaction with structures the interest in particulate material in this field is obvious and broad.

In geotechnical engineering one significant behaviour of particulate materials (i.e. soil) is settlement. This behaviour can be separated out into a number of modes. Broadly speaking these modes fall into two types: elastic settlements, i.e. those movements that recover following the removal of the load causing them, and plastic movements, i.e. those movements that do not recover.

Restored opencast coal mines embody a number of problems relating to the mechanics of coarse grained soils. When such a site is identified as having sufficient potential for a development to take place, it is these problems that often provide the greatest technical challenges and obstacles. As is discussed Section 1.2, due to the proximity of these potential development sites to urban centres it is common for them to be built upon. These built developments are often sensitive to settlements. This research is focused on a behaviour exhibited by coarse grained soils, identified as creep compression or creep settlement.

Plastic modes of settlement usually dominate the geotechnical concerns in these situations. Other considerations such as bearing pressure and elastic stiffness are not normally an issue for most developments. Plastic settlements occurring in fill can be sub-divided into different modes and these are listed, defined and described in Chapter 2. As can be seen from the review made in Chapter 2 work to advance the understanding of the various modes of settlement has been undertaken. However, it is considered that creep

settlement, i.e. settlement occurring under conditions of constant stress, is the one that is least well understood and is therefore the subject of this work.

The following chapter (Chapter 2) expands on the concept of creep settlement and describes the various methods proposed for its prediction and the mechanisms postulated to cause it. Chapter 2 also describes the generally accepted model for the understanding of soil structure and typical properties and characteristics of the particular materials used in the restoration of opencast sites.

X-ray computed tomography is utilised in this research to obtain three-dimensional images through the samples. Chapter 4 includes a review of the technique and its use in geotechnical engineering thus far. Chapter 4 also includes details the equipment used in the research. The materials used are detailed in Chapter 5.

The results of the laboratory testing and the computed tomography are contained in Chapter 6. The interpretation of the results and discussion on them is given in Chapter 7.

Chapters 8 and Section 8.3 present the conclusions and recommendations, respectively, drawn from the work outlined in the preceding chapters.

By way of further introduction the subsequent sections of this chapter provide a concise history and description of the operation of opencast coal mining in the United Kingdom. Also, details of the geographic spread of opencast operations are provided. Reference to this is made in a brief explanation of some of the constraints and motivations for the development of opencast coal mines and how this provides a context for the research.

1.1 Opencast mining and restoration in the U.K.

1.1.1 Background

The mining of coal has been a massive industry in the United Kingdom for well over a century, providing coal for use as a fuel for powering industry and heating homes. This need for coal has in recent decades been relieved in part by other fuels - such as nuclear and gas. However, this need is still present, but in a form of reduced intensity. Historically, the coal supplying industrial Britain has been coal won using deep mining techniques. However, the extraction of coal by excavation was usually restricted to coal outcrops, where only shallow excavation would be needed.

Deep mining probably would have developed from ancient techniques of mining such as bell pit mining (Grimshaw, 1992). Bell pit mining involved the excavation of a shaft down to a shallow seam of coal, generally at a depth of less than 12 m below ground level. The coal would then be removed from the shaft and for a distance away considered safe when unsupported. The bell pit would then be abandoned or backfilled and adjacent pit formed. This progressed to extraction by radial drives and galleries from a central shaft into pillar and stall type workings. The further development from this to forming tunnels into the coal seam would have been small and would have proved more economically viable than excavating all of the coals' overburden and then extracting the coal. Deep mining was – but with automation became less so - very labour intensive requiring large numbers of men and small tools to be employed at depth within the mines. Winning coal from within seams at depth by deep mining methods continues today. However, deep mining is still seen, by some, to be labour intensive; even with the technical advance in mining and tunnelling machinery made to date. With the advancements made in the utilisation of the petrol engine to provide mechanical assistance the economics of extracting coal by first removing all of its overburden became more attractive. Thus in the later part of the twentieth century, opencast coal mining became a significant contribution to the coal industry's output.

1.1.2 History of Opencast Coal Mining in the U.K.

A comprehensive review of opencast coal mining history in the United Kingdom is given by Grimshaw (1992) and is summarised here with the focus on the relevant historical facts to this study.

On the 27th December 1941 the first coal was excavated by open casting methods as part of a national strategy initiated to provide coal to aid the war effort. From this beginning the opencast coal industry grew, such that in 1950 the annual production of coal by this method was 12.1 million tons, with 78 million tons of coal having been produced between 1942 and 1992.

Opencast coal mining was always expected to be a temporary industry set in place to make up the shortfall in coal production from deep mining, which was a great source of employment. However, even with the large numbers of returning soldiers as labour, the deep mines were unable to produce enough coal to meet the post-war demand and so opencast mining continued.

Opencast mining for coal took a downturn in fortunes during the late 1950s and early 1960s, with a drop in the coal market. Rather than reduce deep mining operations it was thought that reducing opencast mining operations offered a better choice for reducing coal production while minimising unemployment. Some long-term contracts of special interest, such as those producing special coals (such as anthracite), did continue. During the mid- and late- 1960s the opencast coal industry stabilised and in the 1970s a reverse to the downward trend began. The coal produced and stockpiled by opencast mining was to take up some of the shortfall produced by the 1972 miner's strike. Its strong position was further reinforced by the higher oil prices of the time, an effect of the oil crisis of the early 1970s.

More recent attempts to use the opencast mining industry as an economic regulator to save deep mining were unsuccessful.

In the first years of the twenty-first century, the UK opencast mining industry supplied around 20 million tonnes of coal per annum at a profit per tonne of

about £15.00, with all but a very few sites producing more than 1 million tonnes, but some producing as much as 15 million tonnes (Hughes and Clarke, 2003).

1.1.3 Scale and Operation of Opencast Mine Sites

1.1.3.1 Operation of Opencast sites

The operation of opencast sites is, in general, the systematic removal of overburden, followed by the extraction of the coal in one area of the site. This is followed by the same operation, of excavation and extraction, in an adjacent area of the site with the overburden being placed in the void of the previous area of excavation. Such a system of operation is illustrated in Figure 1-1. The overburden excavated from the first section may be stored somewhere on the site, possibly used as an aesthetic screen. This overburden mound may be added to when appropriate.

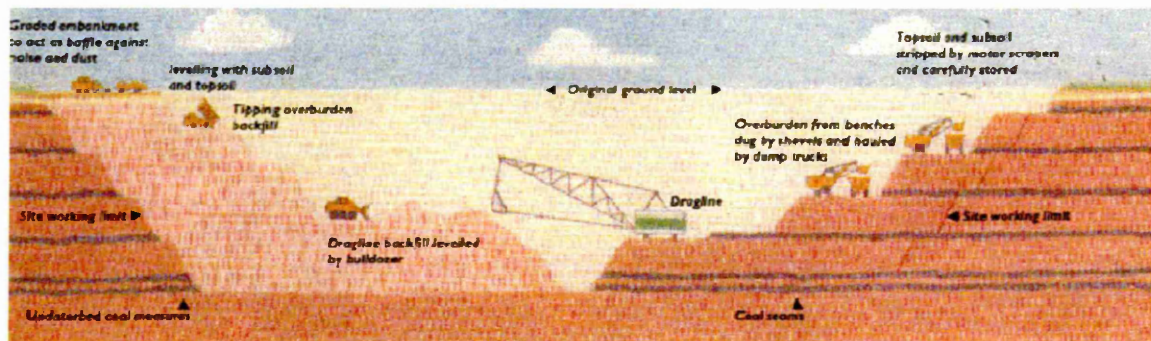


Figure 1-1: Typical operation of an opencast coal site.

As can be seen from Figure 1-1 a number of coal seams within one site can be worked. Seams that can be worked economically can be as thin as 100mm.

The overburden placed behind the working face of the mine can be, where prescribed by an agreed specification, compacted ready for development.

The economic viability of opencast mining continued after the Second World War for the reasons presented in Section 1.1.2. This was further strengthened by the improved and improving technology available in excavation and quarrying. Thus, the opencast mining industry moved rapidly from a labour intensive operation comprising lots of men with picks and shovels, small steam and diesel driven excavators and trucks to massive dragline excavators and dump trucks. The new machinery was better able to cope with both the large volumes of material involved in opencast mining and the continually changing environment in which it must operate.

Plant on a very large modern opencast mine site may include walking draglines; for example the dragline shown in Figure 1-2 is capable of excavating 50m³ of material in one scoop of its bucket to a depth of 190m below its working position. Smaller and more typical plant include tracked hydraulic backhoe excavators with 10m³ capacity buckets (Figure 1-3), weighing ~100 tonnes. These ‘smaller’ excavators often work alongside dumper trucks weighing more than 70 tonnes and capable of carrying their own equivalent weight in load (Figure 1-3).



Figure 1-2: The “Ace of Spades” walking dragline at work.



Figure 1-3: Dumper truck being loaded by a face shovel.

Once the overburden has been removed by the large capacity plant, both man power and smaller plant (typically 13 tonne tracked excavators) are used to clean, then excavate and load the coal on to 20 tonne capacity road-going trucks.

1.1.3.3 Economic and Physical Scale (British Coal Opencast. 1993)

Opencast mining is a massive operation and each site in the UK can typically cover an area in excess of 30 hectares, though much larger sites exist in the U.S.A and other countries. The average depth of an opencast site is around 60m but can be as deep as 150m where coal seams are plentiful and coal production remains economically profitable. The true measure of economic viability is the stripping ratio. The stripping ratio is the ratio of volume of coal extracted to the volume of overburden material that must be removed in order to access and extract the coal beneath. Average stripping ratios have increased from 7:1 in the early days to over 20:1 with the utilisation of modern equipment. Again, in the U.S.A. opencast mine sites can be found where the stripping ratio is around 30:1.

As of 2005 the economic scale of opencast mining is based on the 10.5 million tonnes of coal extracted per annum, which is approximately half of the total coal extracted in the UK at a value of £722 million (British Geological Survey, 2006). This is a fall in extraction since 1993 when 17.5 million tonnes of coal was extracted by opencasting at a profit of £246 million (British Coal Opencast,

1993). The coal extracted by opencast methods is supplied to the consumers shown in Figure 1-4 and Figure 1-5.

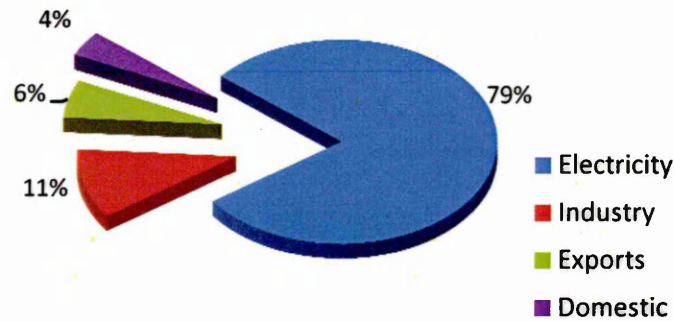


Figure 1-4: Division of sales, of coal won by opencasting, by consumer (data from British Coal Opencast, 1993).

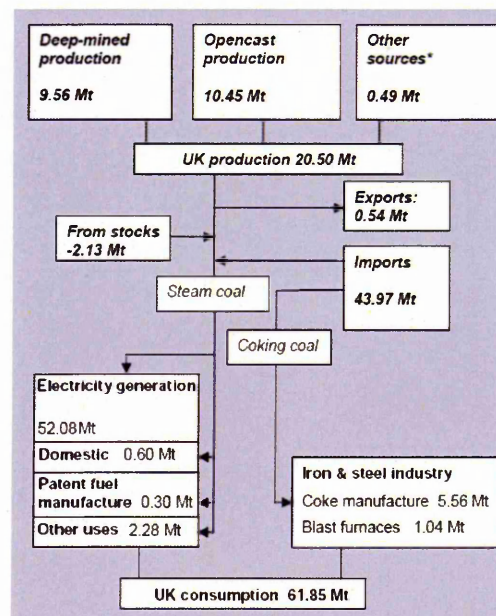


Figure 1-5: UK: The coal supply chain, 2005 (source Department for Trade and Industry cited by British Geological Survey, 2006)

As can be seen whilst the volume of coal supplied from opencast mining has fallen the proportions of coal used in the UK by individual sectors has not changed greatly. That is, for example, approximately:

- 5% of coal extracted in the UK in 2005 is used domestically which compares to the 4% of opencast coal used in 1993, and
- 80% of all coal (including imports) used in 2005 is for electricity generation which compares to the 79% of opencast coal used in 1993.

1.2 Post-Restoration Development

As can be seen from Figure 1-6 the areas that could potentially be exploited for coal production by opencasting methods are situated close to some of the large cities of the U.K. It is not difficult to understand how this situation has come about, with these large industrially based cities being located near to the reserves of deep coal that lie below the shallower deposits. Further, it is generally accepted that the cities concerned, and outlying communities, must continue to develop and grow if they are to remain prosperous.

This close proximity leads to several problems for those wishing to exploit these coal reserves and the authorities that are tasked with the regulation of land use. Any of the land that may be seen as suitable for development by the local authority would, in the extreme, sterilise the land for the extraction of a shallow coal deposit. Thus, the problem facing those concerned is to identify a means that can satisfy the continued suitability of the site for development while allowing the extraction of the coal beneath it.

A number of sources including Beynon et al. (2000), Hughes and Clarke (2003) and Grimshaw (1992) give accounts of the history of opencast coal mine restoration and the regulatory and legislative frameworks which govern it. A summary of these accounts follows. When the first sites were opened and ultimately restored the imposed conditions were to restore the sites to their original condition. The Ministry of Works more rigorously defined this in 1943 as restoration of the ground to a condition suitable for agricultural purposes. This was to include the filling of the void with the removed overburden and the replacement of the topsoil. However, the resulting land would still be of a poor quality and subject to problems, such as large settlements and difficult drainage; these were dealt with by compensation. This was reviewed in 1947, due to problems with the low agricultural productivity of early sites. The Ministry of Agriculture, Food and Fisheries (MAFF) produced a code of practice, in 1951, based on a review of these early regulations. The 1951 code of practice included more emphasis on rehabilitation and less on compensation.

The concept of rehabilitation was to form the basis of the argument to convince the authorities of the suitability of land for development after opencasting. Research and development driven in the U.K. by a profitable industry has led to a great deal of knowledge in the area of quarry and opencast coal site restoration. This is illustrated by the U.S. Surface Mining Control and Reclamation Act 1977, which is based on Britain's restoration policies and practices. In the U.K. opencast mining is allowed in accordance with the Town and Country Planning Act 1990 under which the local Mineral Planning Authorities gain their powers and The Urban White Paper: "Our Towns and Cities: the Future" (Office of the Deputy Prime Minister, 2000).

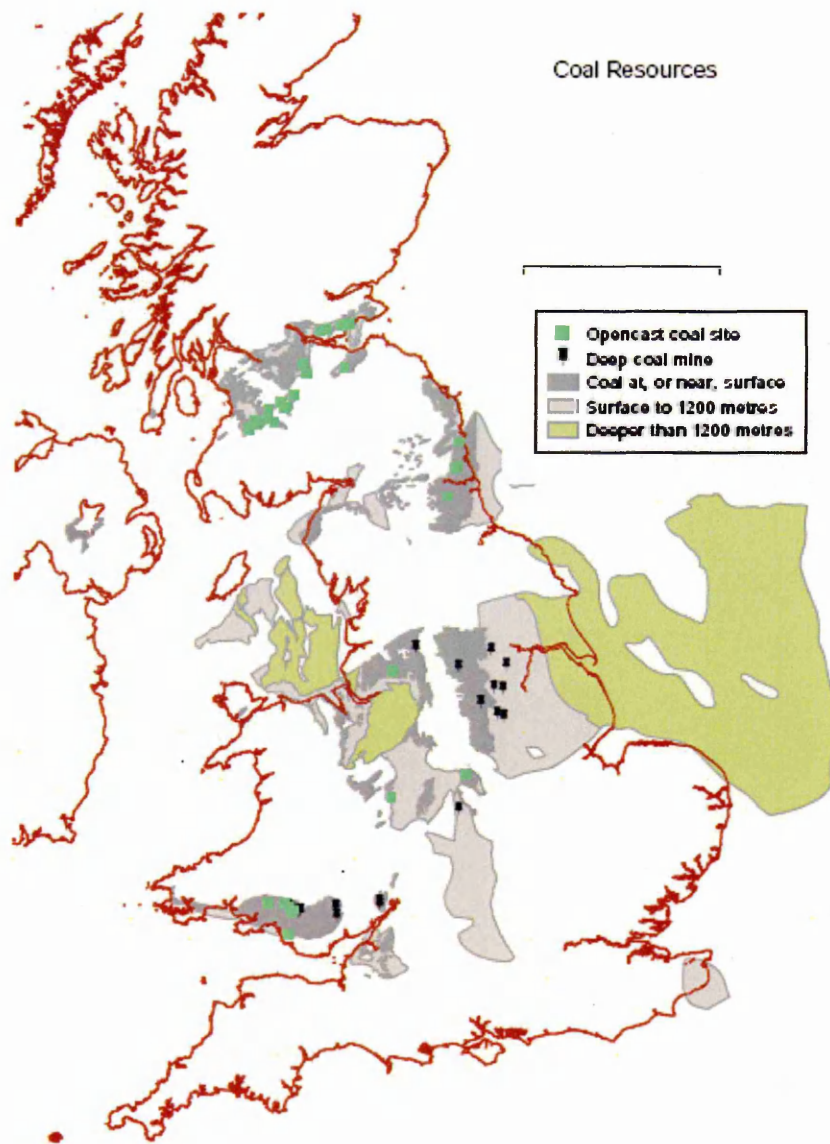


Figure 1-6: Distribution of coal resources in the UK as of September 2006 (after British Geological Survey 2006).

Other documents also play part in the opencast mining regulations such as the Mineral Planning Guidance Notes, in particular Note 3 (MPG3,1999), which stated that "... there is always a presumption in favour of allowing applications for development..." as opencast mine sites. Despite MPG3, obtaining permission for the operation of a new mine has always been the opencast mining industry's largest problem.

The pressure on the planning process to prevent the development of mine sites has meant that this presumption in favour of development has been eroded. In the early 21st century, the prevailing general presumption is now against development (Beynon *et al.*, 2000). Therefore, convincing the mineral planning authorities that development following opencasting would still be possible would be of significant advantage to any proposal, particularly if the future development could be undertaken at little or no extra cost. If planned development is other than agricultural or recreational, the understanding, control and prediction of long-term settlement of the opencast backfill is essential.

1.3 Research Context

The context of this research is given by its potential applications. As is outlined above, in order for new opencast mine sites to be developed an intended restoration strategy must be in place. Therefore, it follows that this strategy must address the technical issues, including long-term settlement. This is particularly true when the intended restoration and subsequent redevelopment includes having to deal with a large body of fill.

Two scenarios present themselves when considering the case of developments needing to address problems associated with the backfill used in a mine's restoration:

- The first of these occurs when a development's economic feasibility requires mineral extraction. This situation may occur when funds are required to deal with problems, such as the treatment of contamination.

- The other scenario occurs when an attempt is made to realise a development opportunity on a site over a restored opencast coal site.

1.4 Research Aims and Objectives

As can be seen from the literature review in Chapter 2 in order to fully understand the long-term settlement behaviour of a large body of coarse grained fill it is necessary to consider the micromechanics of the fill. Without such consideration any resulting prediction method will be largely if not purely empirical. The theory, proposed by Sowers *et. al.* 1965, currently used to predict the long-term settlements in opencast coal mine backfill is empirical. It is postulated that settlements predicted by this theory are due to the gradual redistribution of forces within the soil. Further, that this redistribution occurs by rearrangement of the particles of the soil through rotation and/or breakage of individual particles. This research tests this hypothesis.

In order to further the understanding of the behaviour of granular materials the following aims and objective for this research have been derived. It should be noted that this increase in understanding should extend beyond the specifics of opencast mine restoration, soil mechanics and geotechnical engineering.

1.4.1 Aims and Objectives

To better define the mechanisms involved in the phenomenon of creep settlement of opencast coal mine backfill. That is, to identify and establish the extent to which the component mechanisms of creep settlement occur in opencast coal mine backfill. This will be achieved through:

- the use of non-standard methods (to geotechnical engineering) of data acquisition to aid in better defining the mechanisms.
- investigating the effects of compaction on creep behaviour. By simulating field compaction regimes and observing creep settlement behaviour in the controlled environment of the laboratory
- investigating the effects of backfill material composition on creep behaviour.
- investigating the effects of inundation events on creep behaviour.

2 Literature Review

2.1 Geology and Coal Measures Rock

2.1.1 Introduction

In order to appreciate the nature of the situation resulting from coal extraction by opencasting and then the subsequent restoration operations a brief study of the nature of coal and associated strata must be made.

2.1.2 Coal Geology

2.1.2.1 Coal

Coal is a readily combustible rock containing more than 50% by weight and more than 70% by volume of carbonaceous material, including inherent moisture, formed from the compaction and induration of variously altered plant remains similar to those of peat (Bates and Jackson, 1980). In bog like conditions when decomposing vegetable matter sinks to the bottom it is covered by other sedimentary detritus, thus, an anaerobic environment is formed. In an anaerobic environment the decomposition processes would effectively cease, as the bacteria that decompose the vegetable matter are not able to survive. Bacterial non-survival depends not on the absence of oxygen but on the build up of the bacteria's own waste products (Monroe & Wicander, 1992). These environments still exist today, where this is true the partially decomposed vegetable matter is called Peat, which can and is excavated for use as a fuel.

Coal is graded in terms of its carbon content, with very high grades - such as anthracite coal - having more than 90% carbon. Bituminous coal is the more commonly occurring coal in the United Kingdom.

Seatearth is found usually beneath a seam of coal and is often termed fire-clay due to its use, when fired, as a high heat resistant brick. The seatearth itself can take the form of a bed of heavily over-consolidated clay or rock.

If the coal is seen as the vegetation of ancient plants the seatearth represents the soil in which these plants grew. This is supported by observations made of “roots” of coal protruding into the seatearth strata (Ramsbottom et al., 1981).

2.1.2.3 Coal Measure Rock

The coal and rocks that commonly accompany a coal seam are collectively termed “Coal Measures”. Coal Measures usually comprise a series of sandstones and shales*. In England and Wales “Coal Measures” strata were deposited during the Upper Carboniferous period, which is further sub-divided into the Upper, Middle and Lower Coal Measures. Table 2-1 depicts the relevance of the terms within the context of geological time, the corresponding terminology of the carboniferous system as taken from common American, English and mainland European terms.

| Long-established names still very generally used | | Names particularly on the Continent | American |
|--|--|-------------------------------------|----------------------|
| Upper | Upper Coal Measures Middle Coal Measures Lower Coal Measures | Stephanian Westphalian | Pennsylvanian system |
| | Millstone Grit | Namurian | |
| Lower Carboniferous | Dinantian | Viséan | Mississippian system |
| Limestone (Avonian) | | Tournaisian | |

Table 2-1: Terms relevant to the Carboniferous time period, after Challinor (1967).

* The term “shales” is used to describe argillaceous rocks that are classified further into claystones, mudstones and siltstones see section 2.1.3.

These argillaceous rocks have been formed from the sediments of older rocks. The particles of the parent rock would be deposited over the coal seam in a similar environment to that which the coal-vegetation was deposited *i.e.* a low energy environment. This low energy environment would have allowed the very fine particles that make up such rocks to settle. If the environment had been one of high energies then the fine particles would have remained in suspension. The small particles were probably present in large numbers and may have formed a mud with the liquid of this low energy environment.

The occurrence of sandstones in series with shales would suggest that the environment of deposition was one that fluctuated between low and higher energies with sand sized particles being deposited in periods of higher energies and silt and clay size particles being deposited in periods of lower energies.

The Rock of the Coal Measures typically follows a cycle of occurrence; this is termed a cyclothem. The terms siltstone and mudstone are introduced in Table 2-2 and are explained in Section 2.1.3.

| Rock Type | | Average Thickness (m) |
|------------|------------------|-----------------------|
| Seat earth | Next sequence | 1.0 |
| Sandstone | General sequence | 4.0 |
| Siltstone | | 2.5 |
| Mudstone | | 6.0 |
| Coal | | 1.5 |
| Seat earth | | 1.0 |
| Sandstone | Next sequence | 4.0 |

Table 2-2: General cyclothem sequence, after Hassani *et al.* (1979).

2.1.3 Mudstone Classification

It should be stated that there are clearly differing definitions of mudstones and siltstones in the literature, which has a major effect on the classification systems derived.

Coal Measures' rock, as has already been stated, is predominantly sandstones and mudstones (also sometimes termed shales). Sandstone is consolidated, cemented sand forming a rock that is most recognisable by its grainy texture

and can be defined as sandstone when sand sized particles are clearly visible, see Figure 2-1.



Figure 2-1: Sandstone, a detrital sedimentary rock.

The term 'shale', that has been used thus far, has been to describe argillaceous rocks that are made up of particles smaller than sand. It has become common place for geologists to group siltstone and claystone under the term mudstone as claystone and siltstone both, usually, contain silt and clay sized particles (Taylor, 1988). This is not true in the geotechnics field, where the terms mudrock, mudstone and claystone are widely considered as inter-changeable, although BS5390:1999 only uses the term mudstone. Siltstone is considered only to include rocks made predominately of silt sized particles.

The most predominant classification system for claystone and siltstone depends upon the ratio of clay to silt sized particles, *i.e.* if the ratio is greater than one the rock is classed as a claystone, less than one the rock would classed as a siltstone.

The classification situation is further confused when the term mudstone is used to encompass many of the soils (as well as rocks) encountered within the Coal Measures. These soils are usually over-consolidated to heavily over-consolidated CLAY and silty to very silty CLAY (Taylor and Spears, 1981). This is further complicated by the inclusion of the term shale. Shale is used to describe a mudstone that is fissile; the fissility can also be used to further describe the soils that fall under the term mudstone.

For a period of time the term mudstone was not seen to include rocks that contained laminations (Figure 2-2).



Figure 2-2: Mudstone, a detrital sedimentary rock.

A classification of mudrocks based upon clastic content (Taylor, 1988) can be made, as shown in Figure 2-3.

As described in Section 2.1.2.3, the sedimentary environment for the mudstone would have been an environment of low energies and the liquid in it would have been heavy with suspended solids forming a mud. Thus, the term mudstone can be seen as appropriate “mud that has become a stone”. However, its original use was probably to describe the weathering process that takes place when a mudstone is wetted and degrades into a mud, *i.e.* “rock that becomes mud” on weathering and wetting (Challinor, 1967).

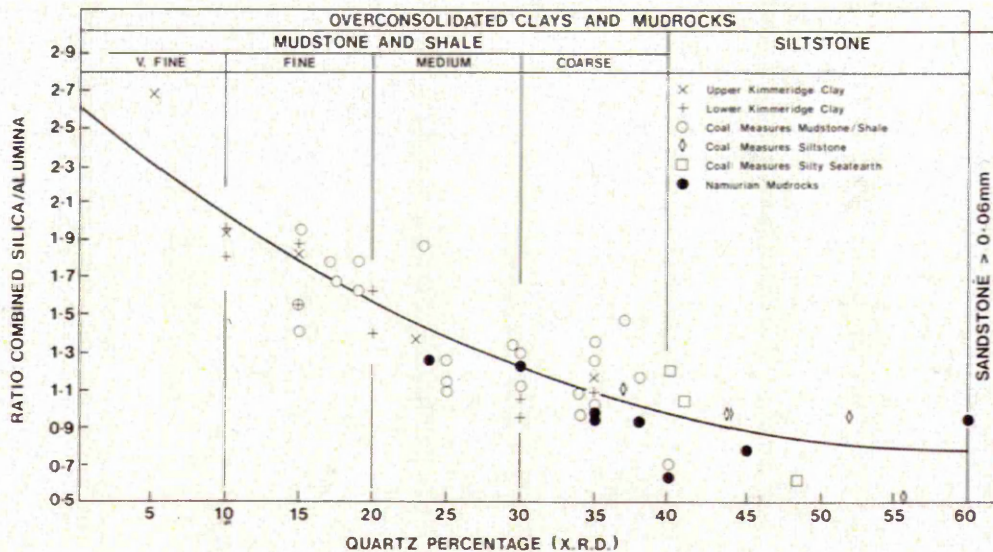


Figure 2-3: A “geological” classification of clays and mudrocks based upon clay content and combined alumina to silica ratio, further indicative of clastics, after Taylor (1988).

When submerged in water less indurated mudrock softens and/or slakes forming platelets along laminations within its structure. Slaking could also be

described as flaking. It is the softening and slaking properties of mudstones that forms the basis of a classification system proposed by Morgenstern and Eigenbrod (1974). The system comprises of two parts the first testing the softening of the mudrock. The test requires a number of samples of the mudrock to be submerged in water from where samples are removed at certain time intervals between one hour and one day, when they are tested to determine their unconfined shear strength. A comparison between the initial, final and tested unconfined shear strength gives the distinction between mudstone and clay, see Figure 2-4. The slaking part of the classification tests is two-fold: both the quantitative slaking test and rate of slaking test are used to define the mudstone's classification (see Table 2-3). The slaking test involved the cyclic wetting and drying of the samples followed by the measuring of the moisture content of the sample. The rate of slaking test involved measuring the change in liquidity index.

The insitu process of slaking and softening degrades a mudrock, ultimately resulting in a residual clay soil. A classification system given by Cripps and Taylor (1981) allows the severity of any mudstone weathering to be described, see Table 2-4.

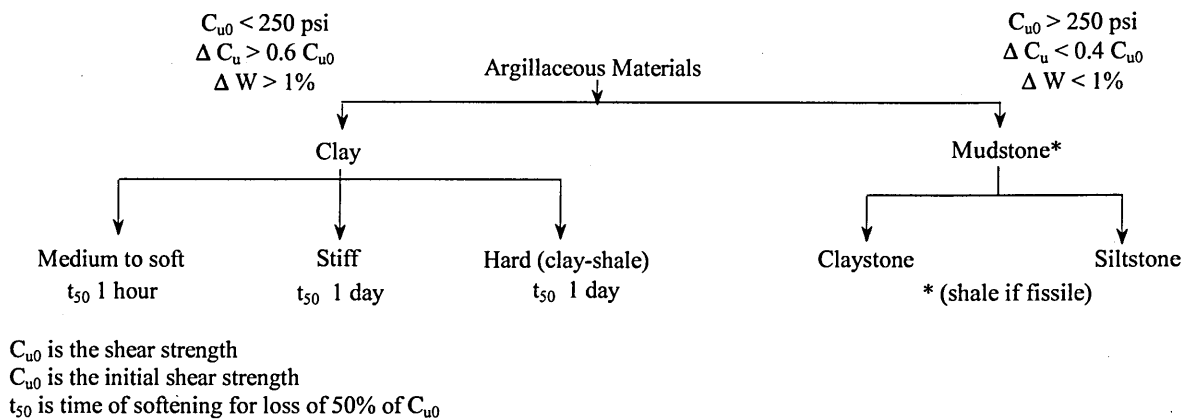


Figure 2-4: Engineering classification of argillaceous Materials, after Morgenstern and Eigenbrod (1974).

| | | Amount of slaking $w_s = w_l$ | | | | |
|---|--------------------------------------|-------------------------------|-----------------------------|--------------------------------|-------------------------------|--------------------------------|
| | | very low VL $w_L < 20$ | low L $20 < w_L < 50$ | medium M $50 < w_L < 90$ | high H $90 < w_L < 140$ | very high VH $w_L > 140$ |
| Rate of slaking: $\Delta I_{L,1} = \frac{I_{L,1} - I_{L,0}}{\text{Water immersion}}$ | Slow S $\Delta I_L < 0.75$ | VS | L | M | H | VH |
| | | S | S | S | S | S |
| | fast F $0.75 < \Delta I_L < 1.25$ | VS | L | M | H | VH |
| | | F | F | F | F | F |
| | very fast VF $\Delta I_L > 1.25$ | VS | L | M | H | VH |
| | | VF | VF | VF | VF | VF |

Notes: I_L is the liquidity index
 ΔI_L is the change in liquidity index
 w_L is the liquid limit

Table 2-3: Classification in terms of slaking characteristics, after Morgenstern and Eigenbrod (1974).

| Term | Grade | Description |
|----------------------|-------|--|
| Fresh | IA | No visible sign of weathering |
| Faintly Weathered | IB | Discoloration on a major discontinuity surfaces |
| Slightly Weathered | II | Discoloration |
| Moderately Weathered | III | Less than half of rock material decomposed |
| Highly Weathered | IV | More than half of rock material decomposed |
| Completely Weathered | V | All rock material decomposed; original mass structure still largely intact. |
| Residual soil | VI | All rock material converted to soil; Mass structure and material fabric are destroyed. |

Table 2-4: Classification of weathered mudrocks, after Cripps and Taylor (1981).

Other systems of classification do exist, such as that given in BS 5930; these are not specific to mudstones however.

As can be seen from the above discussion, different classification systems for mudrocks are plentiful with no true consensus existing between all of them. The most common and understood classification system seems to be classification by clastic grain size content and, thus, this system shall be adopted, in this research. The specific system adopted here is described here.

2.1.3.1 Clastic grain size content based classification system

Mudrocks are classed as those rocks with more than 50% of their clastic grains sized at less than 60 μ m (Stow, 1981). With those mudrocks with less than two-thirds silt content being prefixed with a suitable term. Many North American authors suggest 3 sub-divisions:

- $>2/3$ silt \equiv siltstone,
- $2/3 - 1/3$ silt \equiv mudstone/mudshale,
- $<1/3$ silt size \equiv claystone/clayshale.

The major drawback to this classification system is the lack of distinction between an over consolidated clay and an indurated rock.

2.1.4 Mineralogy

The mineralogy of a mudrock will, to some extent, define how it behaves under a number of different conditions. For example the weathering characteristics of a mudrock when exposed to an oxygen rich environment will be greatly defined by the pyrite content. Pyrite is quantitatively the most important sulphide and in an oxidising weathering environment its breakdown, to ferrous sulphate and sulphuric acid, involves a free energy change comparable with hydrocarbon combustion (Curtis, 1976).

Argillaceous rocks consist of the clastic debris eroded off the landmass. This debris grades down in size from larger particles through sands (sandstone) to silts (siltstone) and clays (claystone). With this gradation the mineralogy changes from mainly quartz to clay minerals (fine particles). The debris making up mudrock consists of two fractions: resistate and hydroltate. Quartz dominates the former of these while clay minerals dominate the latter. These fractions are illustrated in Figure 2-5 and Table 2-5.

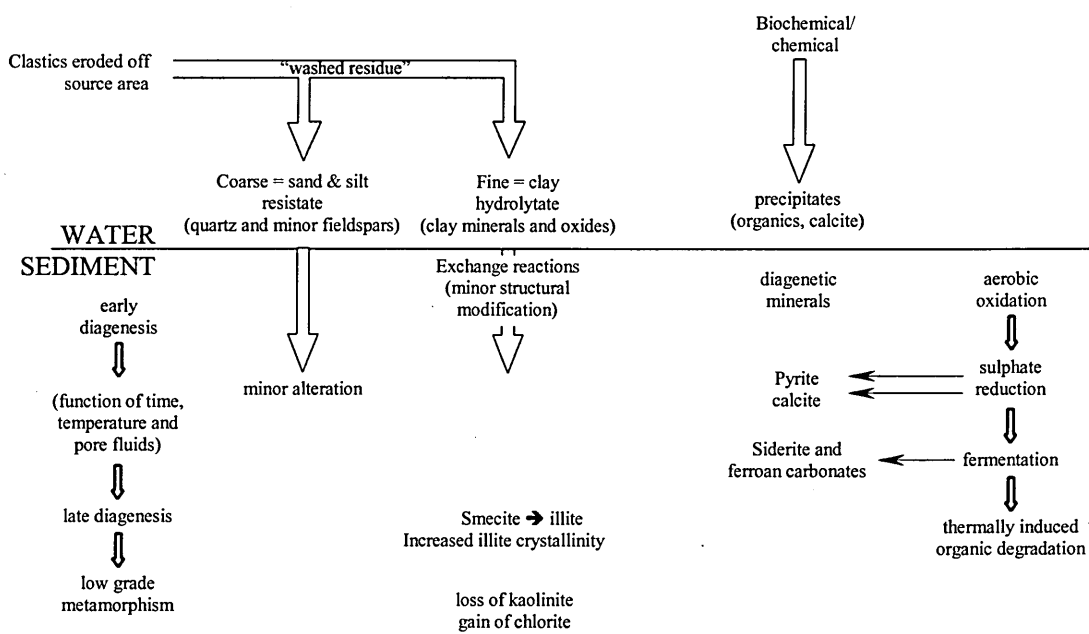


Figure 2-5: The composition of mudrocks and the origins of the different fractions, after Taylor and Spears (1981).

| Mineral | United Kingdom Lower Eocene-Westphalian Coal Measures | United Kingdom Coal Measures colliery tips |
|------------------|---|--|
| Smectite | 9.0 | 0.0 |
| Mixed-layer clay | 17.0 | 29.0 |
| Illite | 27.5 | 35.5 |
| Kaolinite | 20.0 | 12.0 |
| Chlorite | 0.5 | 0.5 |
| Quartz | 16.5 | 19.5 |
| Feldspar | 0.5 | 0.5 |
| Carbonates | 4.5 | 1.0 |
| Pyrite | 2.5 | 0.5 |
| Gypsum | 1.0 | Trace |
| Organic carbon | 1.0 | 2.3 |

Table 2-5: Average mineralogy of mudrocks, after Taylor (1988).

2.1.5 Engineering Properties

Identified in Table 2-6 are the rocks of the Coal Measures in order of geotechnical importance, due to the frequency of occurrence and engineering

properties as identified by Hassani *et al.* (1979). As can be seen the most importance is given to that of mudrock, including siltstone and mudstone, therefore, it is these types that are concentrated upon here.


| | | | |
|--|-----------|-----------------------|---|
| Most important  Least important | Mudrock | Siltstone Mudstone | Both massive and laminated types |
| | Sandstone | | Coarse, medium and fine grained types |
| | Seatearth | | Weakly structured types with organic matter |

Table 2-6: List of Coal Measures rocks in order of geotechnical importance, after Hassani *et al.* (1979).

Cripps and Taylor (1981) identified the lithology, type and method of testing, and the degree of weathering of a mudrock as influencing the values of its engineering properties.

Rainbow (1987) reported ‘typical’ values of engineering properties for UK minestone, these are reproduced in Table 2-7.

| Engineering Property (Units) | UK minestone | |
|--|--------------|------|
| | Range | Mean |
| Natural moisture content, w (%) | 6.7 – 11.6 | 9.9 |
| Liquid limit, LL (%) | 27 – 50 | 40 |
| Plastic limit, PL (%) | 18 – 29 | 24 |
| Plasticity index, PI (%) | 9 – 21 | 16 |
| Maximum dry density, ρ_d (Mg/m ³) | 1.6 – 2.2 | 1.8 |
| Optimum moisture content, w_{opt} (%) | 8.1 – 16.5 | 12 |
| Specific gravity, G_s | 2.2 – 2.7 | 2.5 |

Table 2-7: Engineering properties of UK minestone (Rainbow, 1987)

2.1.5.1 Lithology

This is taken to encompass the diagenesis of the mudrock. This is discussed within the geology and deposition sections (section numbers 2.1.2 and 2.1.3).

Another characteristic of mudrocks directly linked with lithology is anisotropy. Mudrocks are anisotropic mainly due to their nature of deposition and compounded by the compactive nature of the strata.

2.1.5.2 Geological history - Exhumation

The geological history of a mudrock is of major importance to its engineering properties when it is exhumed. In removing the mudrock's overburden the degradation process is begun. This process leads to the associated fissuring associated with stress release, an increase in water content and softening (Cripps and Taylor, 1981). The exhumation can be seen as the beginning of the physical weathering processes, discussed in Section 2.1.6.3.

2.1.5.3 Type and method of testing

The results of tests investigating most geotechnical properties are open to interpretation; this is also very true of mudrocks. Cripps and Taylor (1981) identified four factors that should be paid particular attention when reviewing published data; these are also important when reviewing collected data. These factors are:

- interpretation of “effective strength” and “apparent effective strength”
- effects of sample disturbance and anisotropy
- type of test - laboratory and insitu tests
- interpretation of residual shear strength.

Cripps and Taylor (1981) discuss these four factors and Coop (1997) reports on the a meeting of the British Geotechnical Society in which Professor Atkinson of City University, London, gave a summary lecture on the interpretation of geotechnical parameters in general.

2.1.6 Weathering

Mudrocks in their undisturbed stratified state are affected little by the effects of weathering, being largely protected by the relatively impervious nature of the adjacent rocks. Chemical and physical weathering of near surface strata takes place in the zones where both air and water are present. Over time this weathering reduces the rock to a residual soil.

Within a body of compacted backfill made up of mudrocks weathering will occur when it has access to both air and water (Blanchfield, 1998).

2.1.6.1 Degree of weathering

A description of weathering degradation has been given with the completed process resulting in a residual soil. It is understandable, therefore, that the degree of weathering will result in the greatest variation in engineering properties.

The major properties and engineering characteristics of mudrocks can be defined as:

- water content
- porosity
- plasticity
- clay fraction
- undrained shear strength
- effective and apparent effective shear strength parameters
- residual shear strength
- deformation parameters
- Slake durability

Values of these engineering properties for a range of rocks and clays are given in Cripps and Taylor (1981).

2.1.6.2 Chemical Weathering

The oxidation of the mineral pyrite has been identified (Taylor and Spears, 1970, Hawkins and Pinches, 1987 and Taylor, 1988) as the principal mechanism of the chemical breakdown of mudrocks. As the oxidation reaction (shown in Equation 2-1) requires both that air and water be present, a zone in which the reaction is likely to occur is identified as: to a depth of 3.8m (Spears *et al.*, 1971).

The sulphuric acid leachate is produced when undiluted acid reacts with other minerals present; the most significant of these is the buffering reaction with calcium carbonate (calcite) to form calcium sulphate (gypsum). Anderson and Cripps (1990) investigated the effects of acid leaching.

Swelling within the mudrock was identified by Taylor (1988) as a manifestation of the expansion of the mixed layer clay minerals (illite-smectite).

Taylor noted also that the effect of chemical weathering on the shear strength of mudrocks is small. Bell *et al.* (1997) supported this claim, stating that the breakdown of mudrocks is primarily due to physical rather than chemical factors. Curtis (1976) stated that the most important chemical weathering process was that of pyrite oxidation.

2.1.6.3 Physical weathering

Cripps and Taylor (1981), Spears (1969) and Bell *et al.* (1997) discussed the fact that mudrock will swell even when no clay minerals are present. Gillott (1968) termed this inter-particle swelling and results from the uptake of water into the pore space between the grains of the mudrock in accordance with the principles of effective stress.

The take up of water by capillary action was noted by Taylor and Spears (1970), as causing “air breakage” of the mudrock, where “air breakage” is caused by the pressurisation of the air held in the pore-spaces of the mudrock by the water under capillary action.

2.2 Opencast Coal Mine Backfill Behaviour and Properties

2.2.1 Introduction

Opencast coal mine backfill is made up of the arisings from the coal extraction process. The materials encountered in this process are described through Sections 2.1.2, but the made ground formed by its re-compaction is subject to massive variability laterally and vertically. This section is set out to provide the context for describing these variables, their description in engineering terms and goes on to discuss the transmission of stress through a soil body.

2.2.2 Types of Movement

Five types of movement can be identified in opencast coal mine backfills, these are:

Loading Compression - the strain due to the progressive placement and compaction of the overburden during reinstatement; includes settlement induced by compaction, which can reduce the magnitude of other modes.

Collapse/Inundation Settlement - the rapid settlement and reduction in voids due to the collapse of the soil structure, occurs mainly in non-engineered backfills, where the fill has large voids within it. The particle around these voids will, when stressed, collapse to fill the voids. Another form of collapse settlement is inundation settlement where rapid settlement is triggered by the inundation by water of the fill.

Creep Settlement - the long-term settlement and reduction of voids under conditions of constant moisture content and overburden pressure (see Section 2.3).

Heave or Swelling - increase in the volume of the particles and soil within the fill on wetting due to the reduction in effective

stress and physical or chemical swelling of the clay minerals (Blanchfield 1998).

Lateral Movement - secondary movement due to vertical settlement of the fill. When vertical settlement occurs over a sloping surface lateral movement may be induced.

2.2.3 Typical Opencast Backfill Material

In the case of coal mining the backfill material is that derived from the extracted coal's overburden. As such, it is predominantly made up of mudstone. This material has undergone mechanical weathering, initially, from its excavation, the stress relief caused by its exhumation and that caused by its transportation and placement as backfill. In addition this material may also have been stockpiled for a period of time and been subject to other mechanisms of weathering such as chemical weathering, e.g. due to pyrite oxidation.

The resulting material consists of a soil with particles ranging in size from clay sized particles to large boulders. The individual particles are derived from the various strata that were overburden to the extracted coal, including mudstones, siltstones, sandstones and shales.

2.2.3.1 Particle Structure

An opencast coal mine backfill – after excavation, transportation, dumping, placement and compaction – is a soil predominately made up of particles of mudrock and to a lesser extent sandstones of various sizes. Fragments can be up to the size of 0.5m in nominal diameter, and all the fragments are themselves agglomerates of smaller clay, silt and sand sized particles.

The discrete particle arrangement within the fill leads to the existence of two different levels of pore-spacing (Blanchfield, 1998). A system of larger voids exists around the particles and within those particles there exists a system of smaller voids due to the fissuring within the parent rock and physical weathering experienced in excavation etc. These fissures and micro-cracks

between the grains of the particles are commonly referred to as micro-pores with the larger system of voids being referred to as macro-pores (Blanchfield, 1998).

2.2.3.2 Material Description

The only suitable generic descriptions found for an opencast coal mine backfill were:

- for the intact material within a specific fill from Pithouse, Sheffield. These are summarised in the description:

"... a moderately strong, dark grey, fresh, slightly fissile, clayey mudstone. It had rare bedding fractures with conchoidal surfaces, much disseminated carbonaceous plant debris and occasional pyrite nodules ..." (Czerewko, 1997).

- This does not describe the assemblage of particles that form the fill. This was given by Knipe (1979) as:

"... backfill ... which ... consisted predominately of mudstone and silty mudstone fragments in a clay matrix with a smaller proportion of sandstone, siltstone, carbonaceous shales, sideritic clay-ironstone and coal fragments."

2.2.3.3 Physical Characteristics

The physical characteristics are Moisture Content (w) Plasticity, Specific Gravity (G_s), Dry Density (ρ_d) and Optimum Moisture Content (w_{opt}).

Values from the Pithouse opencast coal mine backfill (Blanchfield, 1998) are quoted along side the data gathered by Rainbow (1987) and shown in Table 2-8.

| Location | As-dug | Atterberg limits | | | ρ_d at w_{opt} | w_{opt} | G_s |
|-----------------------|------------------|------------------|------|------|-----------------------|-----------|---------------------|
| | w % | LL | PL | PI | Mg/m^3 | % | |
| Mellet (Belgium) | 6.7 | 42.0 | 24.0 | 18.0 | 2.16 | 8.1 | 2.70 |
| Bedwas | 11.6 | 27.0 | 18.0 | 9.0 | 2.02 | 9.0 | 2.61 |
| Oxcroft | 11.5 | 50.0 | 28.9 | 21.1 | 1.71 | 16.5 | 2.45 |
| Newmarket / Silkstone | 8.6 | 38.0 | 22.0 | 16.0 | 1.87 | 12.0 | 2.45 |
| Prince of Wales | 9.0 | 38.0 | 23.0 | 15.0 | 1.98 | 10.5 | 2.66 |
| Donisthorpe | 10.7 | 45.0 | 27.0 | 18.0 | 1.63 | 13.8 | 2.16 |
| Bleanant | 11.2 | 45.0 | 25.0 | 20.0 | 1.84 | 10.0 | 2.37 |
| Pithouse* | 2.9 (2.5-3.4) | 34.0 | 20.0 | 14.0 | - | - | 2.52 (2.16-2.66) |

Where: PL = Plastic Limit, LL = Liquid Limit and PI = Plastic Limit

* - Determined by Blanchfield (1998).

Table 2-8: Physical Properties, after Rainbow (1987) and Blanchfield (1998).

In addition to these values Cripps and Taylor (1981) provide the following ranges for Coal Measures mudstone: w – 6% to 8% PI – 9% to 19% and LL – 39% to 49% and for shale: w – 9% to 14% PI – 12% to 19% and LL – 42% to 51%.

2.2.3.4 Mineralogy and Geo-chemistry

Both mineralogy and geo-chemistry are covered in Section 2.1. Czerewko (1997) reports values specific to the Pithouse site referred to in Table 2-8.

2.2.4 Backfill Placement

The reinstatement of backfill can be completed in two ways either in a controlled (or compacted / engineered) fashion, or in an uncontrolled fashion (uncompacted).

2.2.4.1 Uncompacted Fills

In the case where the settlement and future behaviour of the fill are of little or no importance the reinstatement can take place utilising the most economically available plant. This uncompacted backfill is usually placed by the plant that was used to excavate it *i.e.* dragline, backhoe excavator and dump-truck or scraper. The resulting backfill would most likely contain large voids. A high void ratio would mean a high potential for settlement of all types.

2.2.4.2 Compacted Fills

In compacted fills the backfill material is placed in layers and subsequently compacted to a designed specification. The compliance of the backfill to a specification is confirmed by a regime of monitoring and testing.

2.2.5 Compaction Theory

Compaction is the elimination of voids by the addition of mechanical energy to layers of the soil as they are placed as fill. Compaction energy is used to reduce the volume of air voids by remoulding the lumps of clay and reorienting the grains of a coarse grained soil. Therefore, the greater in strength the clay lumps are, or the greater the amount of friction between the particles of the coarse grained soil, the more energy is required to compact the soil. The strength or friction of the soil governs the extent to which a soil can be economically compacted.

The main factors affecting compaction as identified by Barnes (2000) are:

- **Moisture Content** – an optimum value for moisture content (optimum moisture content, w_{opt}) can be identified above which the soil particles cannot move closer together due to an increased pore water pressure. Below this w_{opt} the soil friction or strength is large therefore the soil is more difficult to compact. For a definition of components see Figure 2-6. Further the moisture content of the material to be compacted is critical to where the suction exists between individual particles such that

they effectively increase the strength of the compaction material such that the compactive effort to be applied to achieve effective compact will need to be greater than if these forces were not present.

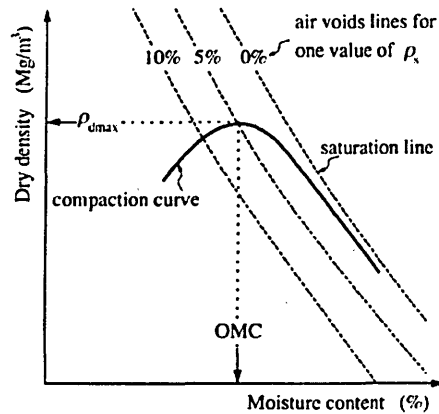


Figure 2-6: Typical compaction curve.

- Compactive effort (Figure 2-7) – the amount of energy applied to the soil in order to achieve compaction, based upon mass and number of passes made by compaction plant. The more compactive effort that is expended on a soil with a moisture content dry of w_{opt} the greater the state of compaction. However, it becomes wasteful to expend a large amount of compactive effort to a soil that is moist, due to the build up of high pore water pressures that will cause consolidation at a later stage. A point can be reached when increasing compactive effort offers very little or no benefit.
- Soil Type – The strength-moisture content relationship differs for different soils. So the compactability or ease of compaction will be, to some extent, determined by the soil type.

The strength or friction of the soil can be affected by the soil's moisture content, which is, therefore, of great importance in compaction. The degree of compaction achieved is usually measured relative to the maximum dry density, $\rho_{d(max)}$, of the soil.

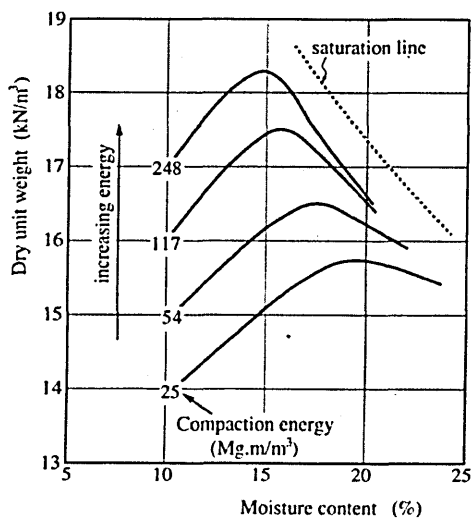


Figure 2-7: Effect of compaction Energy, after Lambe and Whitman (1969).

2.2.6 Compaction Specification

Specifications for opencast coal mine backfill compaction have usually been based on either the Department of Transport (DoT) Specification for Road and Bridge Works 1969, DoT Specification for Road and Bridge Works 1976 (“Blue Book”) or the DoT Specification for Highway Works 1986 (“Brown Book”), which are now superseded by the Highways Agency’s Manual for Highway Works, May 1998 and as subsequently amended. Other documents have in recent years been published in an attempt to provide generic specification tailored for opencast sites. These include: SARCOB (1993); Thompson *et al.*, 1990; Trenter and Charles, 1996. Trenter (2001) give a thorough review of the earthwork’s theory and practical application.

Compaction is aimed at achieving the closest possible density to that of the maximum dry density, usually set at 90% of $\rho d_{(max)}$ for opencast backfills or at 95% $\rho d_{(max)}$ as prescribed by Trenter and Charles (1996).

An alternative to this “maximum dry density” approach is discussed by Charles *et al.* (1998). It is suggested that control of compaction be made by the minimising the total air voids in the compacted material. Charles *et al.* (1998) advocate the restriction of the air voids content to less than 5% of the total volume of the compacted fill. The primary aim of including such a criterion is

to minimise the likelihood of the occurrence of settlement on inundation of the fill.

2.2.7 Compaction Plant and Methods

Many types of plant are available for the compaction of fill material. Table 2-9 summarises the types of plant listed in Barnes (2000) and in SARCOB (1993).

Not all of the compaction plant list is suitable for all soil types and environments so selection of the most suitable plant has to be made. Opencast coal mine backfills contain many types of soil and so a number of the compaction plant types are unsuitable for its compaction. Vibrating plate, grid rollers, pneumatic-tyred rollers are considered unsuitable for the compaction of opencast mine backfills by SARCOB (1993).

2.2.8 Compaction Monitoring and Testing

Monitoring and testing of completed areas of compacted material is essential to ensure that the fill material after compaction conforms to the requirements set down in the specification. Monitoring and testing should also be supported with a suitable record keeping system so as to enable future problems or monitoring data to be compared with the conditions at the time of placement.

| | |
|--|---|
| Smooth wheeled rollers | Comprising of a smooth steel drum roller which is either towed (singularly or in tandem) by a crawler tractor or can be self propelled (two or three-rollers tandem). |
| Vibratory rollers | Commonly a smooth drum which have either a vibratory attachment or have a vibratory mechanism integral to the roller. "Sheep's foot" roller may also utilise a vibratory mechanism. |
| Tamping rollers (also term a "sheep's foot" compactor) | Smooth drums with steel projections attached which add a kneading action to the compaction process. They provide lateral compaction as well as vertical compaction and can provide a good key between successive layers of fill. |
| Grid rollers | These consist of an open steel mesh drum with concrete blocks attached to the frame (as ballast). These are usually towed by a crawler tractor. |
| Pneumatic-tyred rollers | A number of rubber-tyred wheels mounted on one or two axle are towed over the ground to provide a kneading action. The two axles types often have the wheels offset thus providing a more complete coverage of the area. A "wobbly wheeled" type exists, which has the wheels mounted loosely so that they wobble from side to side, which further adds to the kneading action. |
| Vibrating plate compactors | Comprise of a vibrating unit mounted on a steel plate, which is manually operated. Weights vary up to approximately 2 tonnes with plate areas of 1.6 m ² . |
| Vibro-tampers | These weigh between 50 and 100 kg and apply compaction by vibration. |
| Power rammers | utilising the explosive reactions within a combustion engine these compactors impact the ground thus compacting it. |
| Dropping weight compactors | These consist of a weight (200-500kg) lifted by a hoist mechanism and dropped through a height of 1 to 3m. |

Table 2-9: Types of compaction plant.

Testing of the compacted material involves the determination of the state of compaction achieved in terms of the dry density and percentage air voids (SARCOB, 1993). Insitu testing methods that are commonly used include:

- Nuclear Density Gauge (NDG) – The use of a nuclear density gauge is the most common form of testing due to its simplicity. Testing with the nuclear density gauge is usually carried out in accordance with the ASTM D2922 (1991) and ASTM D3017 (1993). NDG tests should be correlated against one or more of the other types of test so as to calibrate the NRG to operation on that specific fill (SARCOB, 1993).
- Sand Replacement Test (SRT) – The sand replacement test consists of the excavation of a hole in the compacted material and the measurement of the amount of pre-weighed sand required to completely fill the hole. SRTs are conducted in accordance to BS 1377.
- Water Replacement Test (WRT) – Using the same principle as that of the SRT the WRT uses water to fill a polythene lined hole with the volume of water being measured.
- Gel Replacement Test – Again using the same principle as the SRT the gel-replacement test involves using a gel flowable enough to flow into the void while being viscose so that it will not permeate into the soil itself. The advantage of the gel replacement method is the elimination of the errors generated by the use of the polythene lining, which may bridge small voids caused by the unevenness of the excavation.

2.2.9 Particle and Soil Characteristics

The effects of particle shape, size and size distribution on the behaviour of a soil under load, particularly settlement behaviour, may intuitively be recognised as potentially significant. These sections review this potential significance in greater detail.

2.2.9.1 Particle shape

Particle shape has been identified as affecting the behaviour of a soil by many authors, including Kolbuszewski and Frederick (1963), and Lees (1963 &

1964). Porosity, shear strength and permeability of unbound aggregates are all known to be affected by particle shape (Lees, 1964).

Before going on to discuss these effects, a review of the common shapes and descriptors of those shapes is presented.

2.2.9.2 Particle Shape Description

Researchers and workers in the field of sedimentary petrology have developed methods of shape description and these were reviewed by Lees (1963 & 1964) and Kolbuszewski and Alyanak (1964). BS812:1989 also provides details for particle shape description.

Particle shape can be described by four broad classification names: discs, blades, rods and equi-dimensional. Each classification name describes the general particle shape, with discs resembling discs etc., equi-dimensional particles are those that have very approximately the same dimensions in all three planes. This descriptive system is given an analytical context with the specification of particles into each class using the ratios of elongation and flatness, defined as:

$$\text{elongation ratio, } q = \frac{\text{intermediate length (b)}}{\text{greatest length (a)}} \quad \text{Equation 2-2}$$

$$\text{flatness ratio, } p = \frac{\text{shortest length (c)}}{\text{intermediate length (b)}} \quad \text{Equation 2-3}$$

The shape factor (F) is the degree of prolateness or oblateness. This can alternatively be defined as the ratio of flatness to elongation, shown in Equation 2-4 and graphically in Figure 2-8.

$$\text{shapefactor, } F = \frac{p}{q} \quad \text{Equation 2-4}$$

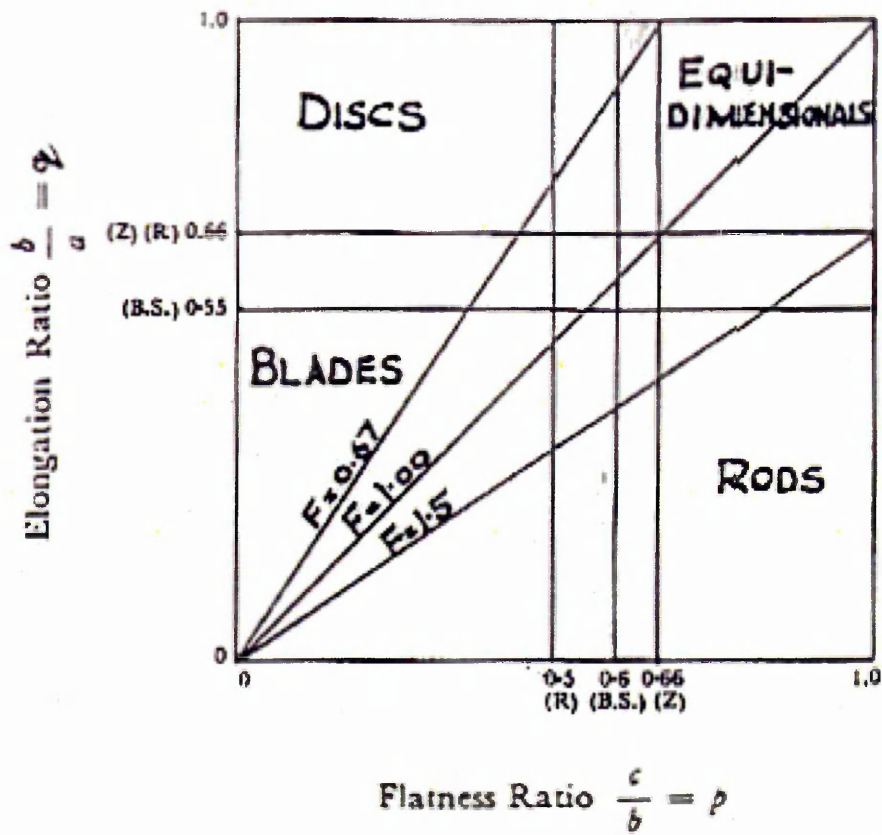


Figure 2-8: Three dimensional shape categories bounded by arbitrary limits of elongation ratio and flatness ratio, after Lees (1964).

Within the classification of equi-dimensional particles there exists another useful classification, that of roundness or angularity. The angularity of particles is dealt with, for the purposes of classification, by charts such as are shown in Figure 2-9 and Figure 2-10.

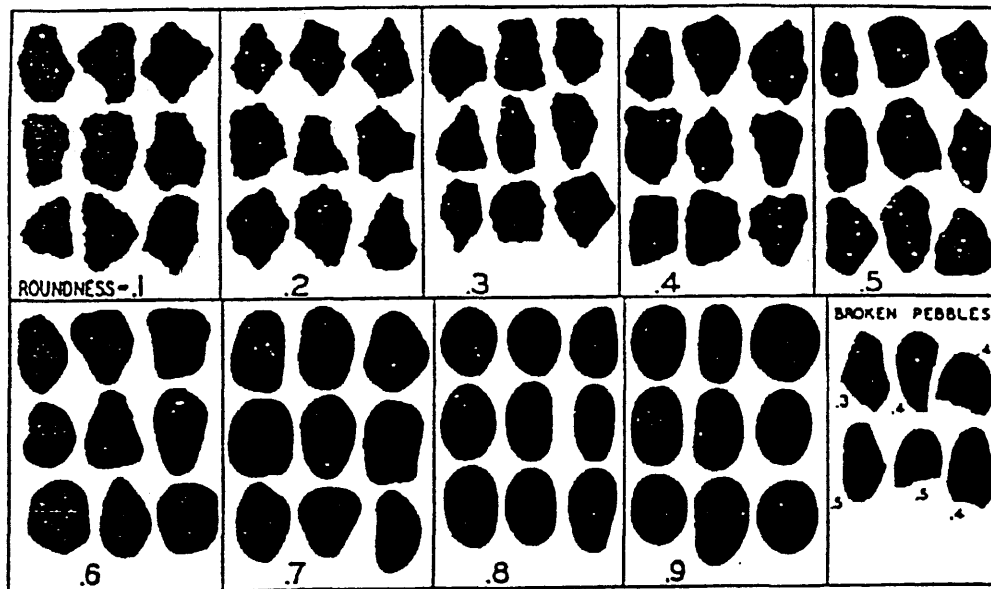


Figure 2-9: Chart for the determining, visually, the degree of angularity of particles, after Lees (1963).

| 0-99 | 100-199 | 200-299 | 300-399 | 400-499 | 500-599 | 600-699 | 700-799 |
|---------|---------|-----------|-----------|-----------|-----------|-----------|-----------|
| | | | | | | | |
| 800-899 | 900-999 | 1000-1099 | 1100-1199 | 1200-1299 | 1300-1399 | 1400-1499 | 1500-1599 |
| | | | | | | | |

Figure 2-10: Chart for the determining, visually, the degree of roundness of particles, after Krumbein (1941).

It is important to note that the angularity can be applied to the disc, rod and blade classes as well as the equi-dimensional particles.

Lees (1963) proposed a system that is shown in Table 2-10. The table has four columns representing the three-dimensional shape, angularity/roundness and

surface texture. The last of these is given separate attention so as not to confuse it with the angularity of the particle.

| 3-Dimensional Shape | Macrotopography (Angularity/Roundness) | | Microtopography (Surface Texture) |
|---|--|--|------------------------------------|
| | Type A: Fractured Particles | Type B: Worn Particles | |
| Equi-dimensional $p > 2/3$ $q > 2/3$ | Of High Angularity $A > 2000$ | Of High Roundness $R > 0.6$ | Rough Texture $RF > 10$ |
| Disc $p < 2/3$ $q > 2/3$ | | | |
| Rod $p > 2/3$ $q < 2/3$ | Of Medium Angularity $A = 1000$ to 2000 | Of Medium Roundness $R = 0.4 - 0.6$ | Medium Texture $RF = 7$ to 10 |
| Blade $p < 2/3$ $q < 2/3$ | Of Low Angularity $A < 1000$ | Of Low Roundness $R < 0.4$ | Smooth Texture $RF < 7$ |

Table 2-10: Shape classification of particles as proposed by Lees (1963).

In recent years work has been undertaken to describe and characterise particle shape mathematically using Fourier Analysis (e.g. Bowman *et al.*, 2000).

2.2.9.3 Effect of Particle Shape

Particle shape has been shown to affect the shear strength of a soil by Terzaghi and Peck (1948). However, the precise role of the shape of the particles was not clearly differentiated. Penman (1953) focussed attention on the importance of dilatancy in the variation in shear strength and porosity. The pilot study completed by Kolbuszewski and Frederick (1963) showed that the primary effect of particle shape was on the internal angle of shearing resistance. The pilot study did not include the investigation of compression with time.

Penman (1971) stated that the soils made up of angular particles were more likely to suffer greater degrees of compression. This can be seen in the results of confined compression tests on quarried rock fill and river gravel derived from the same rock origin, shown in Figure 2-11. Although this study does not consider the pre-treatment undergone by the river gravels in the dynamic river environment. Further Human (1992) and Leung *et al.* (1996) suggested that soils made up of angular particles are, under conditions of constant stress, more likely to exhibit creep behaviour.

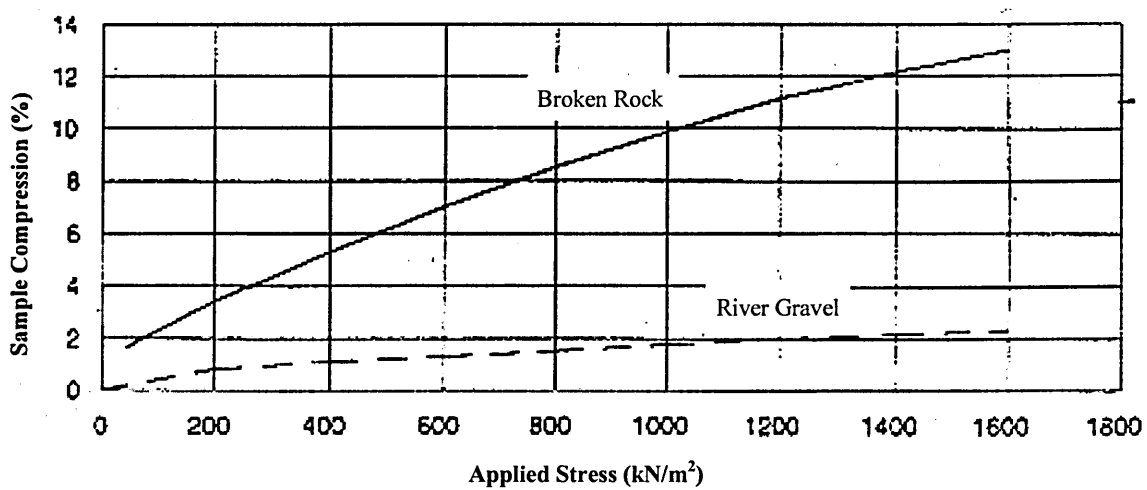


Figure 2-11: Compression of broken rock fill and river gravel, after Penman (1971).

2.2.9.4 Particle size

It was shown in a pilot study by Kolbuszewski and Frederick (1963) that particle size, for all practical purposes, does not affect the internal angle of friction of a soil. Rather they showed that the primary effect of increasing soil particle size is to increase the dilatancy component as size increases. Figure 2-12, an extract from Kolbuszewski and Frederick (1963), shows only the effects of particle size; particle size distribution (grading is discussed in Section 2.2.9.6.

The effect of particle size on the potential for particle breakage was not investigated in the pilot study. As the particle size increases so does the potential for particle breakage, due to increased normal stress transferred between particles and the likelihood of a defect existing within a given particle (Hardin, 1985). The effect of size of particles has been researched by Kettle (1990) with regard to cement bound minestone. Though not cemented together, particles within an opencast mine backfill may be held by a strong clay matrix which may induce particle failure.

Blanchfield and Anderson (2001) have shown that the maximum particle size tested influence the observed settlement behaviour of compacted mudstone.

The compression over time of a soil has been attributed in part to the crushing of asperities and contact points of the particles of the soil. Although recent work, such as that reported by McDowell and Bolton (1998), has examined the strength of single particles and related yield during normal one-dimensional compression to this particle strength for dry materials, it is considered that the situation with softer rock particles that can break and deform during compaction is more complex.

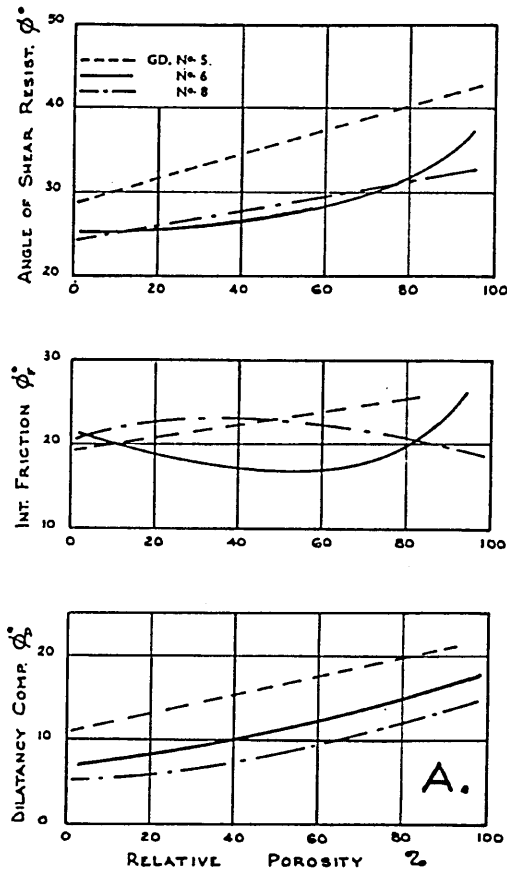


Figure 2-12: Effect of particle size of shearing resistance of Ballotini, after Kolbuszewski and Frederick (1963).

The compressive strength of a particle of rock derived from the Coal Measures has been shown by Hassani *et al.* (1979) to be dependent upon: weathering condition, degree of saturation, bedding planes and other anisotropic behaviour dependent upon orientation. Mitchell (1993) provide further discussion on this aspect.

2.2.9.6 Particle size distribution

The compressibility of a well graded fill is less than that of a fill containing only a small percentage of fine material (Kjaernsli and Sande, 1963). According to Penman (1971), settlements can be minimised by properly compacting a rockfill which has sufficient fine material to infill the void spaces between larger rock particles. It is thought that encasing the larger rock particles with finer material will reduce the potential for settlement by increasing the number of particle contacts, thus reducing the normal stress between each particle. With a reduction in normal stress on particles the potential for particle rotation and particle asperity breakage and particle breakage will also be reduced.

Particle size distribution has an effect on the potential for particle breakage similar to that of the particle size. This is given more attention in Section 2.3 below.

2.2.9.7 Particle packing state

Packing state is simply a measure of the density of a soil and, hence, is inversely proportional to the voids ratio of that soil. This can be extended to state that the potential for compression of a soil is proportional to its void ratio and thus inversely proportional to its packing state.

Marsal (1973) determined that in the case of the El Infiernillo Dam, Mexico, the principal cause of continuing settlement was the degradation of the particles, *i.e.* the crushing of contact points and the subsequent re-arrangement of particles into a denser state.

To assess the particle degradation Marsal carried out a series of experiments from which the following relationship was derived:

$$B = f. \left(\frac{\sigma}{N_s} \cdot \frac{1}{q_u} \right)$$

Equation 2-5

Where: B is a measure of degradation and hence that component of settlement due to degradation, f is a constant, σ is the normal stress, N_s is the number of contacts per unit area and q_u is the particle compressive strength. N_s is dependent upon the grading of the material (N_s increases as the grading goes from narrow to broad) and inversely proportional to void ratio (Kilkenny, 1968). The relationship between particle size distribution, packing state and particle strength and settlement can be clearly seen.

Early work studying packing states was undertaken by Kolbuszewski and Frederick (1963) and has since been built upon by other authors such as Feda (1982); only a brief summary is given here. For an initial state of packing to exist the soil must be under some stress e.g. self weight due to gravity. On the application of load this packing state will change to a packing state capable of carrying the original load plus the additional stress. This change in packing state will mean, providing that the stresses induced within the soil do not exceed the compressive strength of the particles, a change in the position and orientation of the soil particles. If this concept is considered at the limits of the particle strength then a limiting domain packing state will be achieved.

If the limiting state of packing is exceeded one of two things could happen. Firstly the particles could begin to crush, *i.e.* the nature of the soil will change, within whose limits the possible packing states can accommodate the loading. Secondly, the geometry of the packing state could continue to change continually *i.e.* plastic failure could be induced within the soil mass.

2.2.10 Stress Distribution, Soil Structure and Fills

In order to appreciate how the soil will react to any loading an understanding of the soil's structure must be gained. This is most easily achieved by forming a suitable model representing the structure. The theoretical soil has long been appreciated to be different from real soil (Terzaghi, 1943). The soil of theory can be seen as a continuous media in which stresses are distributed along linear paths, this model has been shown to be of great use when dealing with clay soils. However, in granular soil where the soil is made up of discrete particles

the stresses imposed must be transmitted particle to particle (Kuhn and Mitchell, 1993). The nature of this particle to particle contact has been investigated further in recent years and the work by Behringer et al. (1998) and Howell (2000) illustrates how the particle to particle contact stress may be distributed throughout a soil mass made up of discrete particles (see Figure 2-13).

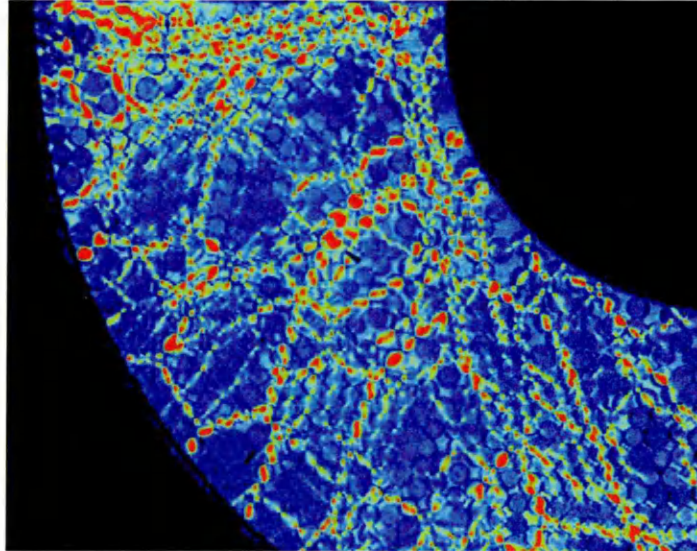


Figure 2-13: False colour image showing 'stress chains' in a collection of photo-elastic particles (after Howell, 2000).

2.2.10.1 Particle Contact Stress in Dry Soils

Stresses in a particular medium, such as opencast coal mine backfill, are transmitted in the soil skeleton, and the stresses on each discrete soil particle ultimately sum vectorially to equilibrium. This skeleton is shown in Figure 2-14, and the forces acting between the particles of the soil can be idealised as shown in Figure 2-15, assuming the soil is dry.

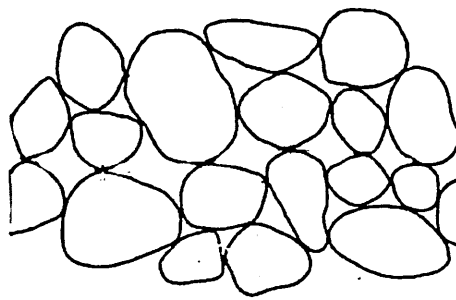


Figure 2-14: Soil skeleton (simplified).

As shown in Figure 2-15a, the force imposed from adjacent particles through the particle contacts, P_{ji} , are of differing magnitude and direction. $S_{x, y \text{ and } z}$ are the compressive forces in the directions x , y and z ; while $T_{xy, xz \text{ etc.}}$ are the frictional forces acting between the particles. A Cartesian system used to calculate the forces acting on an elementary cube was adopted by Marsal (1963). He went on to utilise the simplified forces, within the theory of probabilities, to provide a statistical distribution of the forces. Estimations of the inter-granular forces can then be obtained using three equilibrium equations derived about once face of the elementary cube.

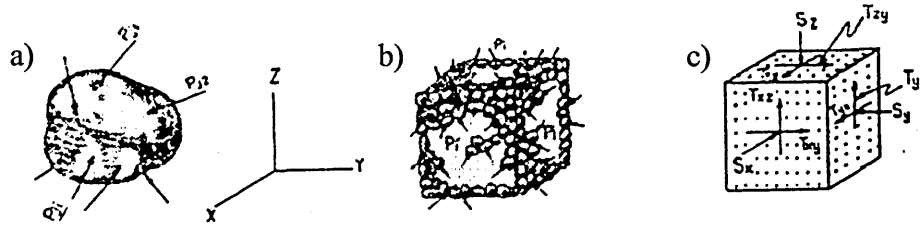


Figure 2-15: Contact forces, after Marsal 1963.

Assuming that the stress state of a discrete body in equilibrium could be determined by means of average values it was shown (Marsal 1963) that the estimated value of P_i becomes:

$$\frac{1}{n} \sum_{j=1}^n P_{ji} \cos \theta_{ij}, \text{ for face } (x,y)$$

Equation 2-6

Howell (2000) used a two-dimensional collection of photo-elastic polymer particles to exam stress transmission. The photo-elasticity of the polymer allowed the visualisation the stresses in the material. The collection of particles was then viewed through circular polarizers, revealing the location of higher stresses as brighter (red) regions (see Figure 2-13).

The modelling of a discrete particle material by simply modelling each individual particle is possible. However, this discrete element modelling (DEM) is generally not considered a suitable form of modelling in general. This is due to the logistics of the modelling process; it would require a massive amount of computing power to model just a 0.01m^2 sample of material (Kestenbaum, 1995). The increase in computing power in the intervening years has seen further work; for example, during recent years some academic work has been focused on developing DEM. Lu and McDowell (2007) provide a strong example of this work.

2.2.10.2 Other Forces

Cohesion between particles has not thus far been introduced, though it is clear that it will exist within an opencast mine backfill. The inclusion of this force into the soil skeleton model can be seen in Figure 2-16.

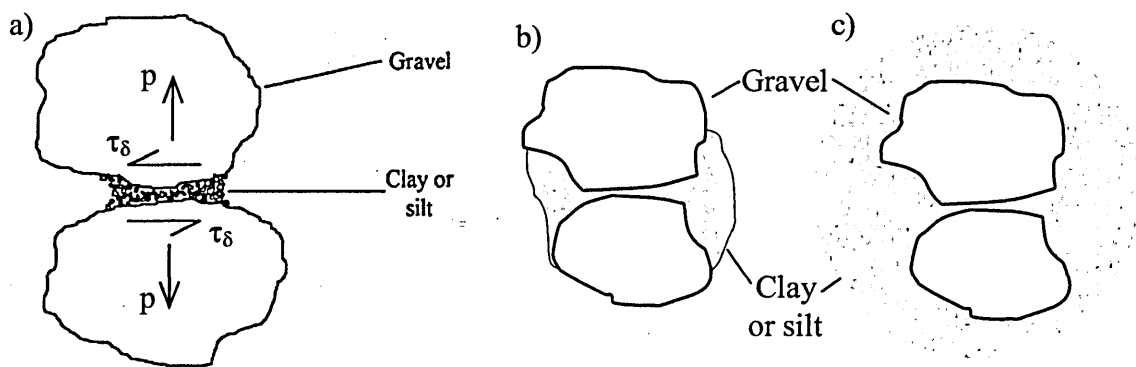


Figure 2-16: Clay and silt particles within a mass of soil.

Fine particles existing in relatively few numbers can be shown as in Figure 2-16a; thus adding two stresses to the model described in Equation 2-6. These forces, denoted as p and τ_δ , would add a tensile force between the two larger

particles (p) while also increasing the frictional force (τ_d) between the particles. Casagrande (1932) first suggested this effect for a relatively dry loaded soil. This formation of frictional bonds between larger soil particles and its subsequent collapse upon inundation was cited by Blanchfield (1998) and has been confirmed by Barden *et al.* (1973).

A soil with a larger proportion of clay and silt sized particles to large particles is such that the soil skeleton of discrete particles no longer exists and a clay matrix is predominant (Figure 2-16c). The implications of this type of soil are discussed with particular reference to compaction by Day (1989) and by Barnes and Staple (1988) with reference to acceptability.

A number of intermediate stages, between few silt and clay particles existing at contact points and a clay matrix, may exist within an opencast coal mine backfill. Such an intermediate stage is illustrated in Figure 2-16b.

There is an intermediate stage at which sufficient clay and silt sizes material exists at the particle contacts such that the shear forces within it become significant but not controlling. Once the proportion of clay and silt to large particles is so great that the shear strength of the clay and silt controls settlement the situation of the clay matrix existing is reached, Figure 2-16c.

2.2.10.3 Effect of Water on Soil Structure

Thus far, the discrete particle soil model has been considered only in the dry state, which is the least likely of the three possible states of saturation. The two remaining states of saturation are the saturated state and the unsaturated state.

With the addition of water to totally expel any air present in the voids of the soil the soil becomes totally saturated. Total saturation is most likely to occur in a soil below the water table.

The theory of partially saturated soils should first be outlined before continuing into the discussion of its possible effects on the soil structure. A partially saturated soil constitutes three phases (soil, water and air) as shown in Figure 2-17 (Fredlund, 1995). A fourth phase is sometimes argued to exist: where the air/water interface forms a tensile surface or contractile skin.

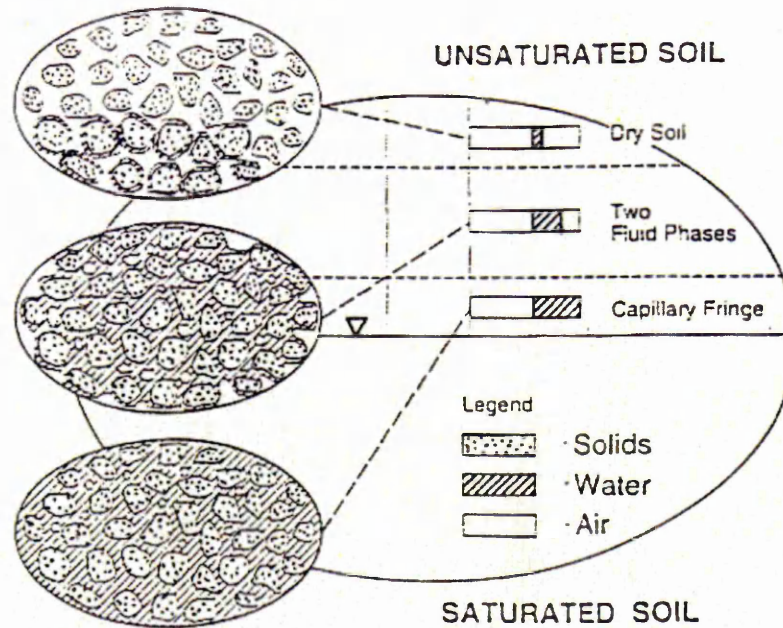


Figure 2-17: Categorisation of partially saturated soils based on various degrees of saturation (Fredlund, 1995).

The three stages of saturation shown in Figure 2-17 are all likely to exist in an opencast coal mine material undergoing compaction and groundwater recharge (Blanchfield, 1998). In the UK, opencast coal mine backfills are usually compacted dry of optimum moisture content and will, therefore, be in the two fluid phases stage, if not the dry soil stage (Blanchfield, 1998).

2.2.10.5 Effect of Water on Soil Stresses

In a partially saturated soil with a low volume of water held within it, the water will be located at the contacts between particles. The water will form a meniscus as shown in Figure 2-18 and a tensile force between the two soil

particles will be created. A lower pressure will develop in the water than in the air, the difference between the porewater pressure, u_w , and the pore-air pressure, u_a , is known as the suction or matrix suction:-

$$\text{Matrix Suction} = u_a - u_w$$

Equation 2-7

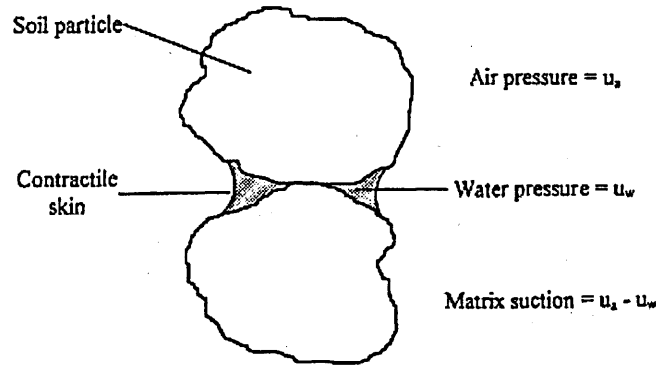


Figure 2-18: Air/water interface forming a meniscus.

This type of suction is termed “capillary” or “matrix” suction. “Osmotic” suction is the suction generated by the hydration of certain minerals or by the differing concentration of dissolved salts partially in a soil. The combined effect of matrix and osmotic suction is termed the total suction.

2.2.10.6 Stress analysis in saturated soils

The theory of effective stress allows the effect of pore water pressure, u_w , to be taken into account when stressed soil problems occur. The effective stress, σ' , is taken to be the total stress, σ , less the pore water pressure.

$$\sigma' = \sigma - u_w$$

Equation 2-8

Further, any change in volume can also be related to changes in pore water and total stress by the unique equation:

—

Equation 2-9

The specific function will vary upon the soil type.

2.2.10.7 Stress Analysis of Unsaturated Soils

It has been attempted, by a number of authors to incorporate the theory of partially saturated soils into the theory of effective stress. Fredlund and Rahardjo (1993) cited Bishop's (1959) proposed equation:

$$\sigma' = \sigma - u_w + X(u_a - u_w)$$

Equation 2-10

Where X is a coefficient between 0 and 1 which is dependent on degree of saturation, S_r , (for a fully saturated soil, $S_r = 1$ and $X = 1$ and for a completely dry soil, $S_r = 0$ and $X = 0$) and soil type (to a lesser extent). Fredlund and Rahardjo (1993) also state that similar expressions were suggested by Croney *et al.* (1958).

A number of researchers experienced difficulty in applying Bishop's equation (Jennings and Burland, 1962; Blight, 1965). It was discovered that under certain conditions, behaviour varied independently of applied stress, $(\sigma - u_a)$, and the suction, $(u_a - u_w)$. Burland (1965) concluded that the mechanical properties of partially saturated soils should be related independently to these two independent stress state variables where ever possible.

2.2.10.8 Consolidation

The time dependence of effective stress is a function of the soil's permeability. In highly permeable soils an increase in pore water pressure can dissipate almost instantly, whereas in soils of low permeability the pore water pressures may take several decades, or longer, to dissipate fully, causing a gradual strength reduction in the soil which may show itself as a gradual volume change.

It is assumed that pore water pressure is constant until a load is applied to the soil and that the confining pressure is zero, then on the application of a load the soil particle will try to rearrange and compress. However, the pore water in a

soil of low permeability will increase in pressure and resist the particle rearrangement. Then as the pore water dissipates the rearrangement of the soil particles gradually becomes possible resulting in a compressive volume change within the soil.

2.3 Mechanisms of Creep

The phenomenon of creep settlement has been generally attributed to the re-orientation and the crushing of contact points of the particles within a soil mass (Sowers *et al.*, 1965 and Marsal, 1973). It is further reasoned that this crushing must be accompanied by a re-orientation of the particles.

Consideration should be given to the material types within the fill material so as to identify correctly the mechanisms at work. The existence of a clay matrix in which the larger particles are present may provide a number of other time-dependent mechanisms, such as change in effective stress, thixotropy and viscosity.

2.3.1 Effect of Water on Behaviour

Volume changes may take place in a soil on the addition of water to the soil these are listed here:

- Consolidation
- Change in effective stress
- Variation of inter-particle friction due to local moisture content variations (Pigeon, 1969)
- Clay and silt sized particles acting as lubrication (Barden *et al.*, 1973)
- Possible effects of thixotropy in the clay/silt portion of the soil (Mitchell, 1960)
- Elimination of any suction forces
- Change of soil particle structure:
 - Softening
 - Slaking
 - Expansion

- Weathering - physical
- Weathering - chemical

One or more of these effects, with the exception of consolidation, may be used to explain (in part or in full) the phenomenon of collapse and inundation settlement of a fill following post-compaction inundation of water, as discussed below.

2.3.1.1 Suction

With the introduction of large volumes of water to a relatively dry soil the isolation of the water trapped - by the relative air and water pressures - around a particle contact point is removed. With the removal of the tensile force and suction supplied by the trapped water, the strength of the particle contact is reduced. It is this sudden reduction of strength that has been attributed, at least in part, as a mechanism of sudden volume change (Blight, 1965; Goodwin, 1991).

2.3.1.2 Clay/Silt Sized Particle Lubrication

Clay/silt sized particle acting as lubrication to larger soil particles was first suggested by Casagrande (1932). On inundation the wetted smaller particles will lubricate the larger particles, allowing them to rotate and slide past each other thus reducing the void space.

2.3.1.3 Thixotropy

Mitchell (1960) discussed the effects of thixotropy with reference to soils. The term thixotropy was first introduced by Peterfi (1927). A useful definition was written by Burgers and Scott-Blair (1948) as the “process of softening caused by remoulding, followed by a time-dependent return to the original harder state”.

The typical behaviour of a thixotropic material can be seen in Figure 2-19. The increase in strength with time may offer an explanation of creep within

some soils.

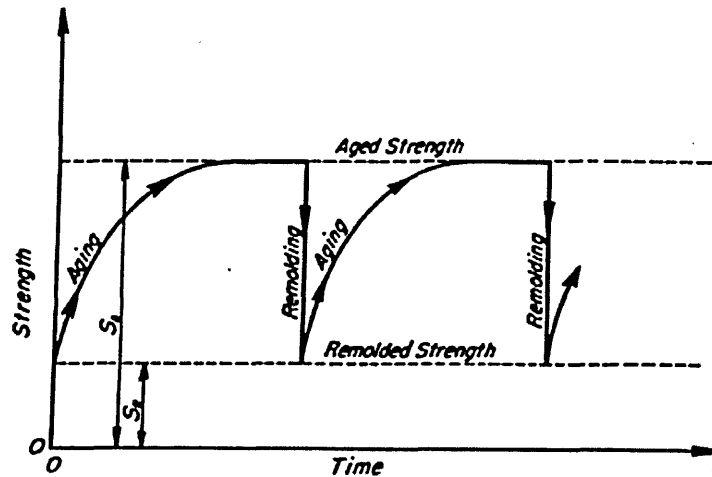


Figure 2-19: Properties of a purely thixotropic material, after Mitchell (1960).

Thixotropic effects in fine grained soils have been shown to result from rheological particle reorientation, water structure changes and accompanying increases in the effect stress (Mitchell, 1960). The role of thixotropy is thought to be minor since thixotropic phenomena have only been observed in moist or saturated soils, whereas the creep behaviour of dry soil is similar to that of soils containing water (Kuhn and Mitchell, 1993).

2.3.1.4 Change of soil particle structure

This is related to the behaviour of the parent rock upon weathering and exhumation, which was discussed in Section 2.1.6.

A time lapse will occur once a partially saturated soil is wetted, before the effects manifest themselves, be they collapse or swell. Although the water is present around soil particles, a certain amount of time is required for it to soak into the micropores, soften the material and fail the points of contact (Bally, 1988). This time lapse was recorded as being of the order of a couple of hours by Lawton *et al.* (1992). This time delay is therefore unlikely to directly affect the creep settlement, which is usually measured in years.

Naderian and Williams (1996), employing a computer based model, found that

the initial collapse of an opencast coal mine backfill reduced the permeability to such an extent that the settlement behaviour changed from collapse settlement to consolidation.

2.3.2 Brittle Fracture

Brittle fracture occurs when the maximum tensile stress in the surface of a particle is large enough to initiate fracture propagation from surface flaws.

2.3.3 Particle Crushing.

Marsal (1967) stated:

"Apparently, the most important factor affecting both shear strength and compressibility is the phenomenon of fragmentation undergone by a granular body when subjected to changes in its state of stresses, both during the uniform compression stage and during deviator load application. A similar fact is observed in one-dimensional compression tests."

Marsal (1973) gave evidence in support of this statement where it was shown that after compression the grading of the fill had changed, to that containing a larger percentage of fine material.

It is important, in an attempt to devise a mathematical model for this behaviour, to define the degree to which the particles of an element of soil are crushed or broken (Hardin, 1985). Hardin identified the following parameters upon which the degree of crushing will be dependent:

- particle size distribution
- particle shape
- state of effective stress
- effective stress path
- void ratio
- particle hardness (hardness of cementing material or weakest constituent of a particle and weakest particle of an element)

- presents or absents of water.

Other evidence of the crushing of particles has been observed by other investigators into the compression of granular fill, some of this is shown in Figure 2-20.

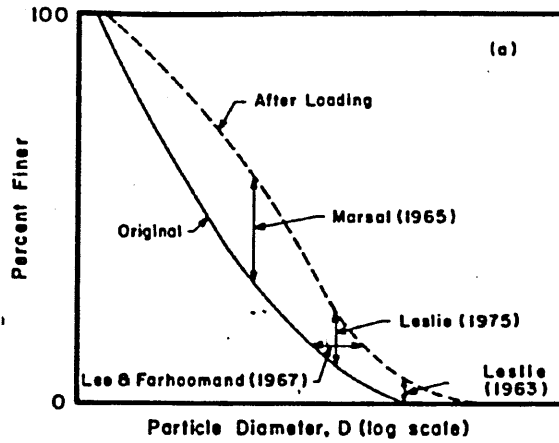


Figure 2-20: Previous measures of particle breakage, after Hardin (1985).

Marsal (1965) used a system of measuring the particle breakage that consisted of measuring the percentage of material passing a single sieve size.

2.3.3.1 Particle crushing and void ratio

Marsal (1973) introduced a dimensionless breakage parameter, B_g , which is the sum of the positive differences between the percentage of total sample contained in a grain size fraction before and after a test, expressed as a percentage. A relationship that includes the void ratio, e , can then be defined:

—

Equation 2-11

Where: — —

Marsal (1973) performed particle crushing tests using the apparatus shown in Figure 2-21.

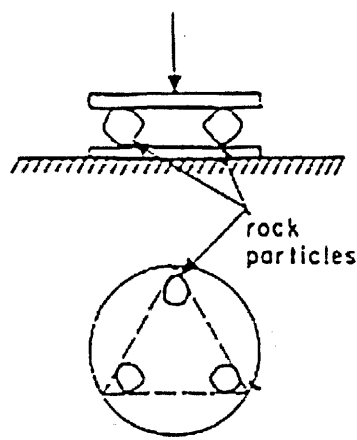


Figure 2-21: Crushing test apparatus, after Marsal (1973).

2.3.3.2 Investigation into particle point crushing

Sowers *et al.* (1965) observed that "popping" sounds were heard when samples of broken rock were loaded at each increment in a test. The popping noise was attributed to the crushing of highly stressed particle contacts. No evidence of particle reorientation was observed; however, this was not quantifiably measured.

Sowers *et al.*, went on to investigate the crushing of particle points by shaping the ends of cylindrical samples of rock into cones or pyramids. These samples were loaded with the point in contact with various surfaces (metal and rock). The results of these tests showed a \log_{10} time relationship similar to those found from the analysis of the dam data. The points were observed to crush rapidly on loading and continued to settle at a reduced rate as the area in contact with the test surface was increased. The increase in contact surface came from the increased size of the contact point and from the cushioning effect of the crushed and spalled material surrounding the contact area.

2.3.4 Asperity Indentation and Ploughing in Rock Friction

Scholz and Engelder (1976a) and Scholz and Engelder (1976b) carried out an investigation into the frictional phenomenon of stick and slip in rock sliding. The phenomenon was investigated, in Scholz and Engelder (1976a), using a bi-axial loading frame. In this a rock sample (a 30° - 60° - 90° prism) was set

opposing a frictional surface, a 2.5cm diameter disc inset into a piece of steel the same size and shape as the rock sample, see Figure 2-22. In Scholz and Engelder (1976b) the relative hardness of the rock sample was also considered using a piece of equipment which would slide a polished rock sample under the hard asperity, as shown in Figure 2-23. In Scholz and Engelder (1976a) the rock samples were of silicate rocks (natural quartz crystal and a crystal of Olivine). Where as, in Scholz and Engelder (1976b) the rock samples used as asperities were apatite, quartz, topaz, corundum, orthoclase and diamond. The samples used for the flat surfaces were quartz, orthoclase, fused silica, synthetic diamond and limestone in both cases.

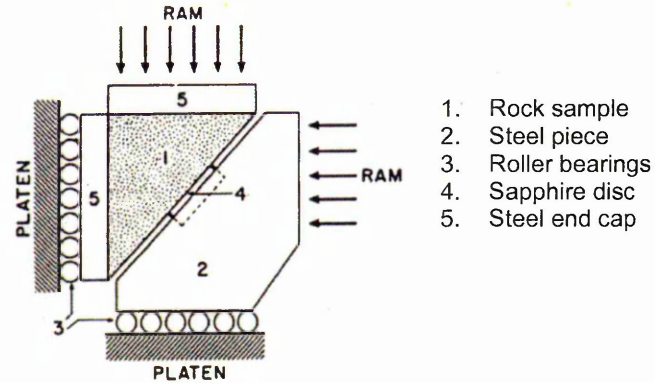


Figure 2-22: Bi-axial loading frame as used in Scholz and Engelder (1976a).

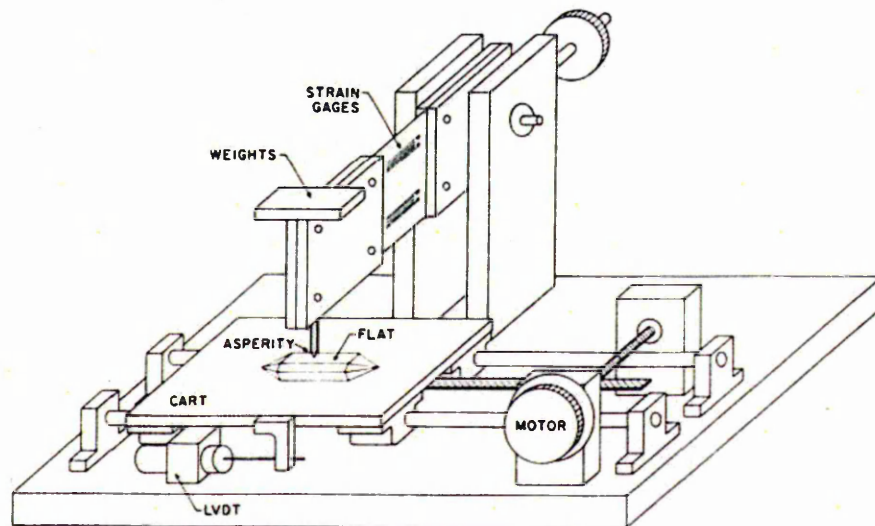


Figure 2-23: Experimental equipment used in Scholz and Engelder (1976a).

Stick and slip has been observed over a broad range of pressures and temperatures and is thought to be the cause of earthquakes when it occurs in faults. The stick and slip motion occurs as a result of instability in which frictional resistance drops rapidly at the onset of sliding or during sliding. If the drop in friction is more rapid than the unloading curve of the system loading the frictional element, stick-slip will occur (Scholz and Engelder, 1976a).

The investigation, referenced here, looked at the relationship of asperity indentation and ploughing in the stick and slip phenomenon. The models within Scholz and Engelder (1976a and b) could be applied to the indentation of an asperity of a particle into an adjacent particle followed by the ploughing of that asperity along the surface of the adjacent particle.

2.3.4.1 Asperity indentation

Within the investigation Scholz and Engelder demonstrated that asperity creep occurs. This showed that, for the two materials tested, the area of indentation increased with the duration of loading of the indenter. Figure 2-24 shows the results of this demonstration.

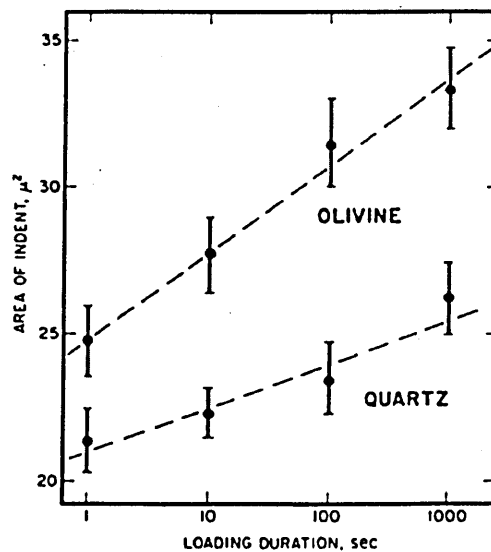


Figure 2-24: Area of indent as a function of loading duration for quartz and olivine, after Scholz and Engelder (1976a).

These results suggest that when two surfaces are placed in frictional contact under a normal force, N , the asperities of the harder materials will gradually penetrate the softer surface through indentation creep. The real area of contact, A , will thus increase with time as, from Figure 2-24.

$$A = (1 + \alpha \log t) \frac{N}{P_1}$$

Equation 2-12

where, α is an empirically derived constant, t is time in contact and P_1 is the penetration hardness measured at unit time. Frictional sliding will then occur when:

$$F = (1 + \alpha \log t) \frac{S}{P_1} N$$

Equation 2-13

where, S is the shear strength of the softer material and, F is the shear force. Therefore the static coefficient of friction, μ_s , will be time dependent, where:

$$\mu_s = (1 + \alpha \log t) \overline{\mu_s}$$

Equation 2-14

$\overline{\mu_s}$ is the frictional coefficient at unit time of contact. Scholz and Engelder (1976a) stated that Equation 2-14 satisfactorily agrees with the observed time dependence of friction in rock materials.

2.3.4.2 Asperity ploughing

A similar equation those above were derived for the phenomenon of asperity ploughing, in terms of the sliding velocity, v :

$$A = (1 - \beta \log v) \frac{N}{P_1}$$

Equation 2-15

where β is a constant that depends on α and the asperity geometry. Therefore the force to cause sliding, F , will be given by:

$$F = (1 - \beta \log v) \frac{S}{P_1} N$$

Equation 2-16

and the dynamic coefficient of friction defined as:

$$\mu_d = (1 - \beta \log v) \bar{\mu}_d$$

Equation 2-17

where $\mu_d = (1 - \beta \log \bar{v}) \bar{\mu}_d$, where \bar{v} is the average sliding velocity during stick and slip. According to Equation 2-16, friction will be constant at a constant sliding velocity and a stick and slip instability will not occur.

2.3.4.3 Stick and slip

If sliding is halted and the surfaces held in contact for a time (t) at a normal force N , an additional area of contact, A' , will be produced by indentation creep, where:

$$A' = (1 - \beta \log v) \frac{N}{P_1}$$

Equation 2-18

If loading is resumed, ploughing must occur over the area $A + A'$, which will drop to A as sliding commences, resulting in a sudden reduction in friction causing stick and slip behaviour. The force necessary to initiate slip is therefore:

$$F = \mu_d N + A' S$$

Equation 2-19

2.3.4.4 Other conditions

The model briefly described above relates to situations where a hard asperity indents/ploughs into a soft substrate. The same model, however, could probably be applied to situations where a soft asperity is in contact with a hard substrate. For example, the soft asperity is likely to flatten by creep, thus similarly increasing the contact area.

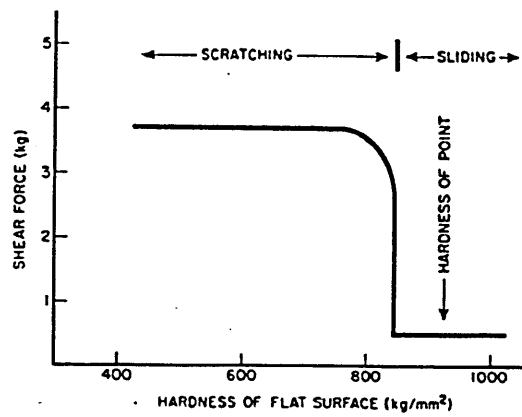


Figure 2-25: Friction between a metal sheet of varying hardness, after Scholz and Engelder (1976b).

2.3.5 Potential for Particle Breakage

A detailed review of particle breakage is provided in Hardin (1985) and a brief summary of is given here. It is clear that to break or crush a silt sized particle would require much higher stress states than would be need to induce such failure in a larger sized particle. Therefore, the potential of a particle to fail could be determined based upon its size. The potential for breakage of a particle of a given size, D , may be represented by:

$$b_p = \log_{10} \left[\frac{D \text{ in mm}}{0.074 \text{ mm}} \right] \text{ for } D \geq 0.074 \text{ mm}$$

Equation 2-20

Thus $b_p = 0$ for $D < 0.074 \text{ mm}$

This equation can be integrated for a soil element for which b_p is representative of the potential breakage significant to the soils behaviour:

$$B_p = \int_0^1 b_p df$$

Equation 2-21

where df is the differential of "percentage passing" divided by 100 and B_p is termed the breakage potential.

As shown in Equation 2-21, B_p is equal to the area between the line defining the upper limit, $D = 0.074 \text{ mm}$, and the part of the distribution curve for which

$D > 0.074\text{mm}$, where the unit area is the area of one \log_{10} cycle. B_p is easy to determine graphically or by numerical integration, if enough points on the distribution curve are digitised.

2.4 Creep Theories, Analysis and Prediction

2.4.1 Introduction

A number of theories have been developed, by analysis of data from various sources, which can be used to predict the likely amount of creep settlement of a fill. The theories can be broadly divided into two groups, those that apply to cohesive soils and those that apply to soils that are non-cohesive in nature. A third group of theories can also be identified, those that can be applied to both cohesive and non-cohesive soils, but these are few in number and are often, upon consideration, only applicable in very specific circumstances.

The theories that are reviewed here were developed in various fields of geotechnics including those directly related to opencast mining.

2.4.2 Creep Settlement Definitions

Creep has been defined as the long-term settlement of a soil under conditions of constant load and moisture content (Hills, 1994; Blanchfield, 1998). Sowers *et al.* (1965) gave a slightly more simplistic definition in which creep settlement took place under conditions of constant effective stress.

Neither of these definitions can easily be applied to opencast coal mine backfill. This is due to the length of time over which increasing load is applied to the soil and the moisture content variability subsequent to the beginning of behaviour that can be identified as creep settlement.

2.4.3 Alpha (α) Coefficient

Based on the observations from 14 rock fill dams Sowers *et al.* (1965) were able to define an empirical relationship for the creep deformation of the dams.

The observations made in the field were supported by a number of confined compression tests on broken rock completed under laboratory conditions. The settlements observed by Sowers *et al.* (1965) were of the order of 0.25% to 1.00% of the height of the dam in the first ten years following completion of the dam's construction.

The observations made, when plotted on a semi-logarithmic scale, showed an approximately linear relationship. The resulting settlement- \log_{10} time plot is a familiar figure (see Figure 2-26) in papers discussing the creep settlement of soils, indicating the wide acceptance and ease of use of the approach.

Although the settlement- \log_{10} time data shown in Figure 2-26 (cited in Sowers *et al.*, 1965) shows some irregularities - that are attributed to varying water loadings from the retained water - they can be approximated to straight lines. Thus the following equation can be found:

$$\Delta H = \alpha(\log t_2 - \log t_1)$$

Equation 2-22

Where, ΔH is the settlement in percent of the fill height (referred to in general by the symbol s) that occurred between times t_1 and t_2 from the beginning of the period of settlement. Sowers *et al.* (1965) took the beginning of the settlement period to be when 50% of the rockfill was placed and compacted. Difficulties arise when this is applied to creep settlement problems in which the point in time when creep begins is not when 50% of the fill is placed, and when fill is placed erratically, as can happen with opencast coal mine backfills, or when fill is placed over a long period.

The laboratory data gathered by Sowers *et al.* (1965) while investigating the creep settlement behaviour of the rockfill materials indicated a rapid initial compression. The initial compression was followed by continuing settlement that approximates to a straight line on the semi- \log_{10} plot, similar to that observed in the field data.

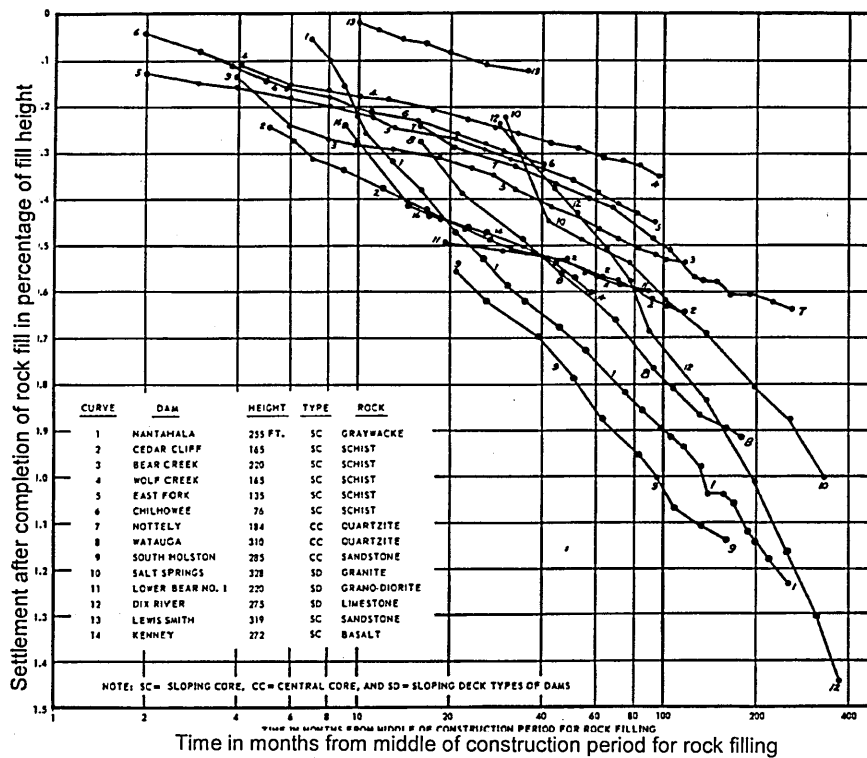


Figure 2-26: Observed settlements of rockfill dams after completion of construction, as cited in Sowers *et al.* (1965).

2.4.4 Typical Values of the α Parameter

Various studies that report both site specific and typical values of the creep rate parameter α have been published. Notably, these publications include the Charles and Watts (2001) and SARCOB (1993). Generally, average α values are of the order of 0.45% to more than 1.00% for uncontrolled fills and 0.10% to 0.25% for controlled fills. Once an mean average value has been selected or determined an additional range is also considered to account for deviation from the select α value. These additional ranges are typically $\pm 75\%$ to $\pm 125\%$ for uncontrolled fills and $\pm 50\%$ for controlled fill.

The large spread of the values taken for α for fills placed in an uncontrolled manner is indicative of the degree of compaction they may have seen during their placement. For example, a fill placed by end tipping by dumper trucks will be more compact than that placed by dragline because of the load applied to the fill by the dumper trucks travelling to dump their subsequent loads of fill. Similarly, the ranges applied to account for deviations from the average values

reflect the nature of the filling. In a controlled fill the inherent variability of the fill would be much less than in an uncontrolled fill. Consequentially, the range of likely deviation is reduced.

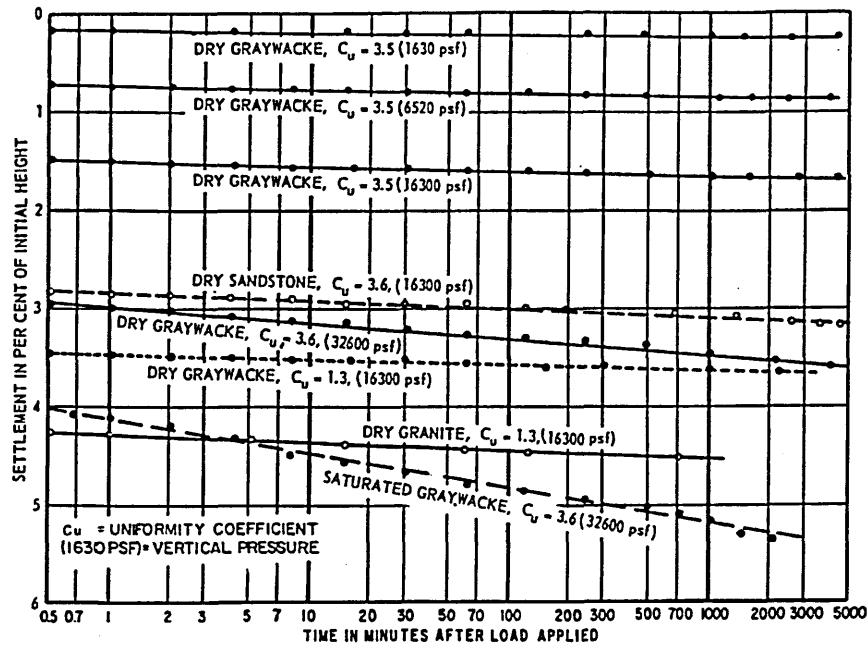


Figure 2-27: Settlement- \log_{10} time curves for laboratory confined compression tests of broken rock for constant vertical pressures applied in increments, after Sowers *et al.* (1965).

2.4.5 Theory of Rate Processes

Rate process theory claims that atoms and other entities, termed flow units, are separated by energy barriers, which fix their equilibrium positions at the minimum potential energy. In order to overcome these barriers the particles must acquire free energy, termed activation energy. The activation energy usually comes from the applied stress energy which yields thermal and acoustic energy (or vibrations). After crossing the energy barriers the flow units would occupy the holes left by other (displaced) flow units or by defects of the crystalline lattice. The deformation of liquid and solids then may be viewed as the sequence of displacements of flow units, made possible by the presence of various defects in the structure of materials.

In the general form, the secondary creep strain rate can be expressed by the relationship (Schoeck, 1961):

$$\dot{\epsilon} = \sum_{i=1}^n f_i(\sigma, T, s_i) e^{-U_i(\sigma, s_i)/RT}$$

Equation 2-23

This relationship shows that there exist different thermally activated processes with various activation energies U_i and frequencies f_i . Both U_i and f_i depend on the stress, σ , and structure, s_i , additionally f_i depends upon absolute temperature, T . R is the universal gas constant.

Figure 2-28 shows the rate process theory in geometrical terms; while only a brief definition of terms used is given here a full description and explanation of terms can be found in Feda (1989).

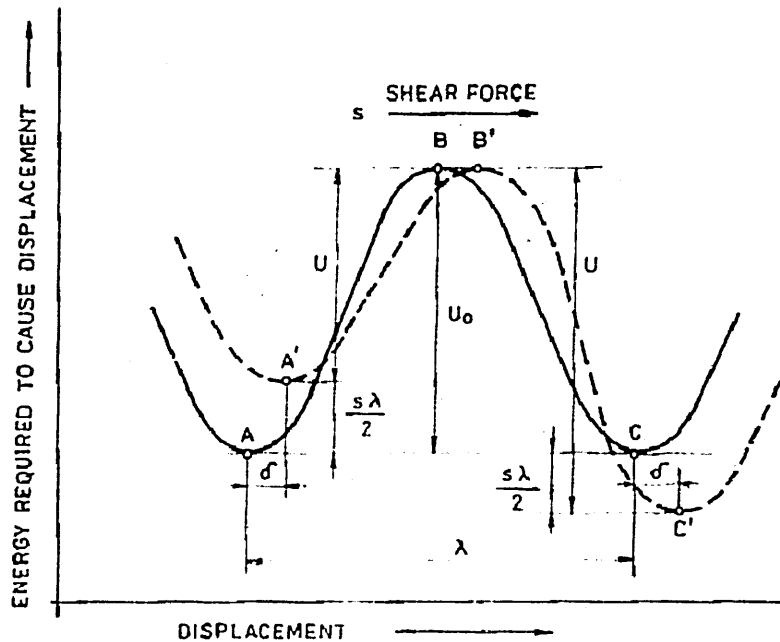


Figure 2-28: Energy barriers in rate process theory, after Feda (1989).

A and C represent stable, equilibrium positions of flow units separated by distance γ . U_0 is the height of the energy barrier to be surmounted if deformation is to occur. If a shear force, s , is applied to each flow unit the original barrier (ABC) becomes distorted ($A'B'C'$) and the movement for A' to

C' is preferred because crossing the barrier in this direction calls for the energy $U < U_0$.

2.4.5.1 Parkin (1977) Creep prediction

An alternative method to that of Sowers *et al.* (1965) was proposed by Parkin (1977), which utilised the rate process theory. The rate of displacement is determined by the probability of any particle acquiring the necessary energy to overcome an energy barrier. There is a gradual re-distribution of energy through the system, so that the probability of particles acquiring critical energy decreases with displacement and therefore time. If this is accepted, then the creep strain rate \dot{s} can be expected to follow the exponential decay function as shown:

$$\dot{s} = a(t - t_0)^{-m}$$

Equation 2-24

where a and m are constants and t_0 is the point of initiation of creep.

Expressing this in a logarithmic form:

$$\log \dot{s} = \log a - \log(t - t_0) \cdot m$$

Equation 2-25

This allows double logarithmic plotting to give the values of a and m provided that the initial time t_0 is known. In most cases, it is found that m is close to 1 with some fluctuations. In the case when $m = 1$ the above creep strain rate relationship integrates to the logarithmic relationship of Sowers *et al.* (1965) (Hills, 1994).

$$\dot{s} = \frac{ds}{dt} = a(t - t_0)^{-1}$$

Equation 2-26

Integrating between the limits of time T_2 to T_1 gives:

$$s = \int_{T_1}^{T_2} a(t - t_0)^{-1} \cdot dt$$

Equation 2-27

$$s = a[\ln(t - t_0)]_{T_1}^{T_2}$$

Equation 2-28

$(T_2 - t_0)$ and $(T_1 - t_0)$ become the times t_2 and t_1 , respectively as in the relationship of Sowers *et al.* (1965). Thus:

$$s = \frac{a}{\log_{10} e} (\log_{10} t_2 - \log_{10} t_1)$$

Equation 2-29

$$s = \alpha (\log_{10} t_2 - \log_{10} t_1)$$

Equation 2-30

This method can be used to predict creep settlement by identifying the values of a , m and t_0 , then integrating Equation 2-24 over the limits of the period of prediction as referenced from t_0 .

This method, as with the method of Sowers *et al.* (1965), has the problem of identifying when creep behaviour commences, *i.e.* the point at which t_0 occurs. Parkin (1971) proposed a method for estimating t_0 by writing Equation 2-26 as:

$$(t - t_0)^m = a/\dot{s}$$

Equation 2-31

From this it can be seen that since $m > 0$, a graph of t against $1/\dot{s}$ must then indicate when $1/\dot{s}$ becomes zero, *i.e.* as $1/\dot{s}$ tends towards zero t tends to t_0 (Parkin, 1971). This method, however, requires a considerable amount of interpretation (Hills, 1994).

Hills (1994) gives an example of the comparison of the Sowers *et al.* (1965) and the Parkin (1977) methods for data gathered from the Ceder Cliff Dam. The example indicates a good correlation between the two prediction methods, which indicated strains of 0.17% and 0.20% respectively.

2.4.5.2 Other creep prediction theories

From observations made at 23 rockfill dams Soydemir and Kjaernsli (1979) attempted to combine the relationships of displacement/time and displacement/dam height. Equations were produced for the displacement/dam height relationship for different time periods of the form:

$$S = \beta H^\delta$$

Equation 2-32

where S is the crest settlement and β and δ are constants dependent upon the time period for which settlement is to be estimated.

Clements (1984) observed that the use of the methods for predicting settlement of Parkin (1977), Sowers *et al.* (1965) and Soydemir and Kjaernsli (1979), in rockfill dams, led to significant errors. Clements used the data published for 68 rockfill dams to make a comparison upon which this statement is based. The significant errors were attributed to the empirical / quasi-empirical nature of the relationships.

A further noteworthy mathematical summary into the micromechanics of creep was given by McDowell and Khan (2003). McDowell and Khan concluded that, using established relationships of the strength of ceramics, creep of granular materials at high stress levels on the normal compression line can be explained in terms of time dependence of particle strength.

2.4.6 Secondary Compression in Clay

Terzaghi's classical theory of one-dimensional consolidation considers only primary consolidation, or the compression due to hydro-consolidation (i.e. the dissipation of pore water pressures). However, it is recognised that there is a

small but significant compression* which is due to the secondary compression effects (Taylor, 1948).

Many authors have investigated the secondary compression of clays and have given various possible mechanisms for its occurrence. Below is a brief summary of these:

- Bolt (1956) suggested that the compression under load was a combination of deformations of the particle structure due to the mechanical interaction forces in the relatively coarse grained part and those due to the physio-chemical interaction force between the double layers in the fine grained part.
- Newland and Allely (1957) showed that the slope of the secondary compression curve *log-time* plot $\left(\frac{\Delta s}{\Delta \log t}\right)$ was essentially independent of sample thickness, t , load increment ratio, $\frac{\Delta p}{p}$, and the duration of the previous load increment. The duration of the load increment after the primary consolidation appeared to be the only factor to affect the secondary compression void ratio, e .
- Wahls (1962) assumed that the secondary compression resulted from a viscous yielding of the grain structure and consequent reorientation of the grains, and this occurred so slowly that the pore pressures that were produced were negligible.
- Leonards and Girault (1961) reasoned that secondary compression could not be attributed to viscous drag or other mechanisms associated with the orientation of polarised molecules in the vicinity of clay particles. They noted that the secondary compression was influenced largely by the load increment ratio.

* It should be note that in some cases it is the effects of primary consolidation that are small and secondary compression and initial settlement together account for most of the total settlement.

- Mesri (1973) listed the following factors to be of the most significance in influencing the secondary compression:
 - absorbed water
 - mineralogical composition
 - precompression
 - sustained loading
 - effect stress ratio.

2.4.6.1 Coefficient of secondary compression

Mesri (1973) defined the secondary compression coefficient in terms of settlement (s_α), as a dimensionless coefficient (c_α) and as a rate function (ε_α):

$$s_\alpha = \frac{\Delta s}{\Delta \log t}$$

Equation 2-33

$$c_\alpha = \frac{\Delta e}{\Delta \log t}$$

Equation 2-34

$$\varepsilon_\alpha = \frac{c_\alpha}{\Delta \log t}$$

Equation 2-35

Where, s is the settlement, e is the void ratio and t is the time.

2.4.6.2 Modification to one-dimensional consolidation theory

Sridharan and Roa (1982) discussed the mechanisms governing the volume change and shear strength behaviour of clays and discussed the role of the modified effective stress concept expressed as:

$$c = \sigma \cdot a_m = \sigma - \bar{u}_w - \bar{u}_a - R + A$$

Equation 2-36

where σ' is the effective contact stress, \bar{c} defined as the modified effective stress, $\bar{\sigma}$ is the mineral contact stress, a_m is the ratio of mineral/mineral contact area to total interparticle area, σ is the externally applied stress, \bar{u}_a is the

effective pore air pressure, R is the ratio of total electrical interparticle repulsion to the total interparticle area and A is the ratio of total electrical interparticle attraction to total interparticle area. Equation 2-36 can be written as:

$$\bar{c} = \sigma' + \sigma''$$

Equation 2-37

where σ' is the conventional effective stress, σ'' is the intrinsic effective stress, equal to $A - R$ which is the net electrical attractive pressures.

2.5 Discussion and Summary

2.5.1 Creep Definition

Probably the largest problem when using the methods available for the prediction of creep settlement is that of determining the point at which creep settlement begins. A possible reason for this difficulty is that the most common and widely accepted definition for creep settlement when applied to a fill is incorrect. Creep settlement in opencast mine backfills, occurs under varying conditions of both stress and moisture content. This is opposed to the definition of creep commonly used by authors such as Terzaghi (1943) and Sowers *et al.* (1965):

"Long-term settlement occurring under conditions of constant stress and moisture content"

The possible redefinition of creep for opencast mine backfills is given consideration in this research. Further, consideration is also given to plastic failure of the soil structure. Plastic failure of the soil structure could be defined as in Kolbuszewski and Frederick (1963), as the deformation that takes place after no further reorientation of the soil particles can take place, *i.e.* when fill particles are forced to be crushed. This simplistic definition of "plastic creep" does not differentiate though between particle crushing and particle asperity crushing at highly stressed contact points, as described by Sowers *et al.* (1965).

2.5.2 Stress Path Development

Assuming that the opencast coal mine backfill is a discrete particle material transmission of stress through the fill will follow time-dependent paths. These stress paths will move as one or more particles in the path fails, either in rotation, fracture or crushing. The stresses will then be transmitted through another 'string' of particles. This constant reorganisation of the stress paths will gradually reach a state where all the stress paths that have formed are strong enough to sustain the loading upon them for the given stress deformation state.

Where the soil is made up of clay as well as discrete particles, discrete stress paths may form in isolated zones where only suitable discrete particle pathways exist. Elsewhere in zones where a clay matrix is predominant, the stress may be transmitted in a more even manner. Where clay lumps are present with the discrete particles, the discrete particles may first indent into the clay and reach equilibrium before being loaded so heavily that the stress path fails and a stronger path is found. Alternatively the clay lump may form a reinforcing cushion around the points of discrete particles on the stress path.

The identification of these paths, their variation and their effect on creep is considered as part of this research.

2.5.3 Primary, Secondary and Component Mechanisms

The mechanisms of creep as described in this review may be ordered to form a standard hierarchy of these mechanisms. For example, if, as suggested by Sowers *et al.* (1965) – and restated by Hills & Denby (1996) who probably represent the consensus view of industry – crushing of the particle contact points is the main cause of creep settlement in rock fill then the subsequent rotation and reorientation of the particles would be a secondary mechanism. .

Equally, a hierarchy may not exist or may prove difficult to define. In this case creep behaviour may be seen as being made up of component mechanisms. For example, as a particle rotates its rate of rotation will be determined by the

friction and ploughing against and into adjacent particles, the ploughing and friction would be termed component mechanisms.

The relative proportion of 'primary' and 'secondary' mechanisms, if such exist, may yield important information and relationships that will aid the understanding of creep settlement both in opencast backfilling and in other materials.

2.5.4 Fill Composition

The composition of an opencast backfill has been assumed to be a discrete particle material for the purposes of prediction of creep settlement, as exemplified by the fact that the most widely utilised method for creep prediction was developed from observations made of rockfill dams by Sowers *et al.* (1965). The application of the equation developed by Sowers *et al.* has not been hailed as a success, rather it has been used in place of any other more suitable method available.

The use of the creep equation suggested by Sowers *et al.* probably owes its continued use to its simple empirical form. The empirical constant, α , allows many of the differences in behaviour of a rockfill and an opencast backfill to be accounted for and thus enables its application to the prediction of creep settlement in opencast backfill. However, if the use of the α constant in this equation does provide for the usefulness of the equation, it also fails to provide an explanation of the behaviour of the soil. It was also stated by Clements (1984) that significant errors arose from the use of the Sowers *et al.* equation and that these errors were due to the semi-empirical nature of the equation.

The existence of clay in lumps, at particle contacts and as a matrix in the opencast backfill, is rarely addressed when discussing the creep settlement of such fill. This is despite the fact that after a number of years some, possibly much, of the backfill will have deteriorated into clay. Behaviour of the clay, no matter to what degree its content of the overall volume of the fill, will have some effect on the creep settlement. The possibility is that it provides the controlling factor of creep within certain zones of the fill where it is

concentrated to the extent that it forms a matrix. Alternatively, it may provide a secondary mechanism where it is found in lumps within the fill, with these lumps acting in a similar fashion to a soft rock with harder rock asperities indenting into them, as described in Sholz and Enger (1976a and b). Clay particles reinforcing the contacts of larger particles may be gradually broken down and removed by slow infiltration or recharging of the fill with water. Alternatively, these particle contact reinforcements may act as a factor that further complicates the creep settlement process where they exist.

The precise nature of backfill needs clarification, such that the creep theory may be put on a rational footing.

2.5.5 Changes in Material after Compaction

The backfill can be seen to undergo three phases of change:

- excavation and transportation
- placement and compaction
- settlement.

The stress and weathering that the backfill undergoes during excavation and transportation has been discussed within this review, particularly in Sections 2.1.5.2 and 2.1.6.3. One aspect of this, considered of importance, is that of the expansion of the mudrock. On exhumation, the reduction in stress on the mudrock from its overburden will be re-applied, to some greater or lesser degree, in the backfill. In theory, this re-application of stress will cause, over time, the mudrock fragments to compress towards a state similar to that in which it was found in. However, this would not be completed in an engineering timescale.

This general situation does not preclude the behaviour of fragments of rock within the backfill that are not orientated in the same plane as they occupied in their strata formation, which may experience even greater degrees of compression. Similarly, as fragments rotate into different orientations, they may become subject to larger degrees of compression thus adding to the creep settlement phenomena.

The placement and subsequent compaction of the fill may cause various changes in the particles and/or particle arrangement. Different placement/compaction methods would effect the amount of settlement likely to occur and, possibly, the relative importance of different settlement components. This could be extended to the differing of compaction methods affecting what mechanisms of settlement provided the largest proportion of settlement.

Changes in the particles/particle arrangements after the placement and compaction processes have been completed may also effect the creep settlement of the fill, as discussed in 2.5.3. These changes may be due to the ongoing creep and/or collapse/inundation settlement that takes place. The changes may affect which mechanisms are predominant and which are secondary in the creep process.

Changes in backfill compaction with time need to be investigated in addition to the classification of the fill initially.

2.5.6 Suction

Suctions are generally assumed not to effect creep. However, mechanisms that could affect creep and involve the water required to provide suction forces are conceivable.

Suctions occur where two particles are in contact with each other and this contact is reinforced by the presents of water which exists at pressure below atmospheric. If the two particles of low-permeability are in contact with each other they will be 'reinforced' by the effects of suction, then the particles will draw in some (or possibly all) of the water over a long period. This removal of the water may cause a gradual reduction in the stress reinforcing the particle contacts. Conversely, this weathering may affect the potential for weathering of individual particles, particularly at the contacts.

3 Methodology

The methodology described in this chapter was developed to achieve the aims and objectives of the research as outlined in Chapter 1. It exploits the equipment detailed in Chapter 4 and accommodates the limitations of the equipment encountered through out the testing programme.

This investigation into the mechanisms of creep settlement utilised large scale laboratory based testing and a non-destructive technique to image the internal structure of the specimens. As revealed through the literature review (Chapter 2) the micro mechanics of creep settlement are understood to be numerous and complex.

This research employs both high quality large scale testing carried out the laboratory environment supplemented with non-destructive three-dimensional imaging. The multi-pronged approach adopted in the methodology described helps address the inherent complexity of the phenomena being investigated. Specifically, it was considered that the analysis of imaging of the samples would reveal the behaviour exhibited by individual particles in the sample under compression.

3.1 Laboratory based testing

The laboratory testing undertaken as part of this research forms one of the two-pronged approached described herein. The laboratory testing uses the large scale testing equipment described in detail in the Chapter 4. The equipment is made up of 'large' and 'small' compression cells, which are capable of compressing specimens, of approximately 600mm and 250mm in diameter, respectively, with a pressure of 400kPa. The maximum size of the specimens' constituent particles in compared to the size of the specimens and compared to those typical in the field it is possible to see why the testing is considered large scale. The testing has produced the high quality data which is presented in Chapter 6.

The use of large scale testing in geo-mechanical investigations is not new and many examples can be identified in the literature (e.g. Kjaernsli and Sande, 1963 and Brady and Kirk, 1990). The increase potential for the collection of high quality data from such testing, in which precise control can be exerted, provides the justification for its use over, say, field observations. Also the use of testing at this such scaled means the variables excluded in micro-scale testing can be examined.

Notwithstanding the above, it was necessary to limit the scope of the testing for two reasons:

- **Time.** The nature of the phenomenon being investigated (creep compression) is such that it occurs over relatively long periods. Further, the phenomenon occurs along side others that mask it or, at least, make it very difficult to identify.
- **Expense.** Large scale testing is expensive in terms of money and space. The size of the equipment and samples required meant that the costs of equipment manufacture, raw materials and transport all had to be met.

3.1.1 Schedule of testing

The schedule of testing used in this research is shown in Table 3-1. Further Table 3-1 provides details of the variables for each of the tests carried out as part of the research.

The test variables were:

- **Cell Size – Specimen size** was shown to be a factor in influencing settlement behaviour of compacted mudstone by Blanchfield and Anderson (2001). As such the two cell sizes used in this research mean that two different specimen sizes can be tested.
- **Compaction treatment – either heavy or light.** This refers to the method of compaction and the amount of energy impacted to the specimen in compacting it. The details of the energy levels are

given in the specimen preparation summary for each test.

Details of the compaction equipment are given in Section 4.1.6.

- **Inundation condition** – either inundated or not. This refers to the degree of saturation of a specimen. Where a specimen was inundated the details are given in the testing summary for each test. The inundation of specimens is detailed in 3.1.3.2.
- **Material source.** Details about the material sources and the properties of the material are given in Chapter 5.
- **Applied stress.** Generally the cell pressure and, therefore, the vertical stress applied were kept constant during an individual test and through out the testing schedule. However, cycles of loading, unloading and loading were carried out for a few of the tests. Details are given in Section 3.1.3.1.

It was originally envisaged that testing would be undertaken over a range of applied stresses; however this was reduced to one stress level. This was primarily due to limitation of the equipment; specifically, the reliability of the hydraulic loading arrangement. It was found that this failed relatively frequently at higher pressures; more details are given in Section 4.1.7. This had a considerable effect on what testing could be achieved due to the time required to set up and run each test, see Table 3-2.

3.1.2 Test Preparation (Cell and Specimen)

Prior to the initiation of testing programme it was necessary to investigate the properties and characteristics of the soils to be used in the research programme. Details of this initial testing are provided in Chapter 5.

Chapter 4 gives a detailed description of the equipment used in this research and details its commissioning.

The preparation of each test specimen was a time consuming element of the research. It was completed in four stages:

- Disassembly of the cell following the completion of any preceding testing, removal and disposal of specimen.
- Cleaning and checking, for damage etc., of the cell components.
- Preparation of the new test specimen.
- Assembly/reassembly of the cell.

| Test number | Variables | | | | |
|-------------|-----------|------------------------------------|-----------|----------------------|-------------------------|
| | Source | Compaction treatment* ¹ | Cell type | Applied stress (kPa) | Inundation condition |
| 1 | Houghton | heavy | large | 400* ² | Not inundated |
| 2 | Orgreave | heavy | large | 400 | Inundated* ³ |
| 3 | Orgreave | light | large | 400 | Inundated |
| 4 | Houghton | light | large | 400 | Inundated |
| 5 | Houghton | light | small | 400* ² | Not inundated |
| 6 | Orgreave | light | small | 400 | Not inundated |
| 7 | Houghton | light | small | 400* ² | Not inundated |
| 8 | Orgreave | light | small | 400 | Not inundated |
| 9 | Houghton | light | small | 400 | Not inundated |
| 10 | Orgreave | heavy | small | 400 | Not inundated |
| 11 | Orgreave | heavy | small | 400 | Not inundated |
| 12 | Houghton | heavy | small | 400 | Not inundated |
| 13 | Orgreave | light | small | 400 | Not inundated |
| 14 | Houghton | heavy | small | 400 | Not inundated |
| 15 | Orgreave | light | small | 400 | Not inundated |

Notes

*1. Compaction treatment refers to the level of compactive energy imparted to the specimen during preparation. Details are given in Section 3.1.2.1.

*2. Tests in which two short unload / reload cycles were undertaken.

*3. Due to a diaphragm failure the specimen was inundated during initial loading; after the diaphragm was replaced the specimen was loaded in its wet state.

Table 3-1: Summary list of the testing producing a complete set of results.

3.1.2.1 Specimen preparation

The specimen preparation took place once the cell components had been checked. The cell walls were positioned and temporarily clamped in position on to the cell bottom plate.

The material of the specimen was then put through a sieve to remove oversized particles. A sieve with apertures of 120 mm by 120 mm was used for the large cells and one with apertures of 37.5 mm by 37.5 mm for the small cells, see Section 5.3.

The specimen was then placed in to the cells and compacted in either 3 or 5 layers for 4 minutes per layer in the large cells and in either 2 or 4 layers for 3 or 5 minutes respectively in the small cells. The compaction equipment used in the large and small cells is described in Section 4.1.6.

A sample from each of the test specimens was taken at the time of compaction for determination of the specimen's moisture content.

3.1.2.2 Cell assembly

Given the size and weight of the various cell components it was necessary to employ mechanical assistance when assembling the various cell pieces. The fixing of each cell component to the assembly was undertaken in a prescriptive manner dictated by the cell's design. Where the tightening of screw and nuts was necessary it was undertaken over a period of several hours; first tightening fixings opposite each other at, say, 12 o'clock and 6 o'clock. The fixings at 3 and 9 o'clock would then be tightened, and then those at 1 and 7 o'clock, and then those at 4 and 10 o'clock before returning to those at 12 and 6 o'clock and so on until all of the fixings were tight. It was necessary to follow this process to achieve an even distribution of the clamping load for the diaphragms and of load in each of the cell's tie bars.

Typical times to accomplish each of the stages above are shown in Table 3-2.

| Stage | Typical time to complete (days) | |
|-------|---------------------------------|-------------|
| | Large cells | Small cells |
| 1 | 2.0 | 1.0 |
| 2 | <1.0 | <1.0 |
| 3 | 2.0 | 0.5 |
| 4 | 4.0 | 4.0 |
| Total | >8.0 | >5.5 |

Table 3-2: Typical cell and test specimen preparation times.

A number of equipment failures were experienced, the most significant of these was the rupture of a diaphragm. A more detailed commentary of these failures is given in Section 4. The repeated occurrences of diaphragm failure lead to a number of modifications to the diaphragm manufacture. These are

included for in the commissioning testing and equipment descriptions given here.

Where such a failure of the equipment was encountered, the duration of stage 4 was considerably extended. Ignoring the time required to manufacture a diaphragm, the time required to assemble a cell including a diaphragm would increase, typically, by 10 days for the large cells and 8 days for the small cells. The process of attaching the diaphragm load plate and the top plate had to be carried out in series.

3.1.3 Testing Procedure

The procedures relating to the laboratory based work are outlined below, whilst those for the CT scanning are included in Section 3.2.2.2.

3.1.3.1 Loading / Unloading

Following the successful assembly of a cell, it was connected to the loading system. The loading of the specimen within the cell was undertaken. The cell pressure was increased in increments, the increments used are shown in Table 3-3.

In between the application of each increment a period of time of not less than 12 hours was allowed to elapse before the next load increment was applied.

| Increment | Cell Pressure Increase (kPa) | Idealised Load Increase (kN) | | |
|-----------|------------------------------|------------------------------|-------------|---------------|
| | | Small Cells | Large Cells | |
| Loading | 1 | 0 to 50 | 0.0 to 1.3 | 0.0 to 13.9 |
| | 2 | 50 to 100 | 1.3 to 3.5 | 13.9 to 27.8 |
| | 3 | 100 to 200 | 3.5 to 7.1 | 27.8 to 55.6 |
| | 4 | 200 to 400 | 7.1 to 14.1 | 55.6 to 111.2 |
| Unloading | 5 | 200 to 400 | 7.1 to 14.1 | 55.6 to 111.2 |
| | 6 | 100 to 200 | 3.5 to 7.1 | 27.8 to 55.6 |
| | 7 | 50 to 100 | 1.3 to 3.5 | 13.9 to 27.8 |
| | 8 | 0 to 50 | 0.0 to 1.3 | 0.0 to 13.9 |

Table 3-3: Specimen loading regime

In a number of tests (numbers: 1, 5 and 7) after the load was fully applied a cycle of unloading and reloading was carried out. The purpose of this was to investigate the effect of such an event under controlled conditions, following similar uncontrolled events caused by power failures. Two unloading/reloading cycles were carried out over two periods of approximately 8 hours. The period between the two unload/reload cycles was 48 days.

The unload/reload testing carried out within Test 1 consisted of:

- first unloading the specimen from a cell pressure of 400kPa to 90kPa, before reloading it,
- followed by unloading it from 400kPa to 180kPa, before reloading it.

The unload/reload testing carried out within Tests 5 and 7 consisted of:

- first unloading the specimen from a cell pressure of 400kPa to 100kPa, before reloading it,
- followed by unloading it from 400kPa to 0kPa, before reloading it.

The results of these tests are included with those of the other tests in Chapter 6.

Unloading of the specimens was generally undertaken in a controlled fashion, the load on the specimen being reduced in increments. The increments used are as shown in Table 3-3. Again, a period of at least 12 hours was allowed to pass between each increment of unload.

3.1.3.2 Sample inundation

The controlled inundation of samples was undertaken through the sample inundation ports located in the bottom plates of each cell (see Section 4.1.2.2). The samples were vented through the drainage hole extending through and along the length of the piston rod (see Sections 4.1.2.4 and 4.1.2.6).

The samples were inundated with water under a constant head of 3.5m, measured from the bottom of the sample. The water was sourced from a series of tanks that allowed the water to be stored at ambient temperature.

A number of samples were inundated by the rupture of diaphragms, this mode of inundation is described in Section 4.1.7.

3.1.3.3 Data recording

Data recording was carried out automatically using the equipment described in Section 4.1.5. The frequency of the recording of reading was tailored to the phase of the test. A recording interval of 30 seconds was used where the specimens were being loaded and the magnitude of movements likely to be observed was large over a given period. Similarly, when the loading was constant and the movements were observed to be small over a similar period the frequency of recordings was reduced to every 30 minutes.

3.2 Non-destructive Testing

The programme of large-scale laboratory work was supplemented by a programme of data gathering that utilised non-destructive testing techniques. The data gathered was in the form of three-dimensional reconstructed images (multi-planar reformats) obtained using x-ray computered tomography equipment. The details of this equipment are given in Section 4.2.

The non-destructive testing was carried out as part of the testing undertaken using the small cells.

3.2.1 Methodology Development

3.2.1.1 Two-dimensional Imaging

It was initially thought that the two-dimensional imaging (photography) of the samples could be achieved by manufacturing windows in the walls of the compression cells. However, this was quickly ruled out due to the likely effects of side wall friction. Effects of which could be significant potentially masking or cancelling out those of creep compression. It was also thought that the transparent material used for the windows would be susceptible to

scratching, inhibiting the quality of any image taken through it. Further the possibility of compromising the testing through weakening the cells' walls.

3.2.1.2 Plain Film Radiography

Other ways of imaging the samples were sought and the non-destructive techniques of plain film radiography offered some potential. Plain film radiography works in a similar way to that of photography with the image being in the same plane as the film. The exception being that instead of the film used being sensitive to light reflected from an object, the film used in radiography is sensitive to the radiation that has passed through an object. As the radiation passes through an object its intensity is attenuated. The amount by which the intensity is attenuated depends on the density of the object (the denser the object the more attenuation). The radiographic film is sensitive to the varying intensity of the radiation just as photographic film is sensitive to light and thus when processed a permanent image is formed on the radiographic film. Alternative digital radiographic equipment is available and becoming common in use in the field of medical diagnostic radiography as well as non-destructive materials testing. This process uses radio-sensitive detectors to collect the radio-attenuation information and convert it into a digital image. Digital radiography is akin to digital photography.

Due to the relatively easy access to x-ray radiography, provided by its wide spread use as a medical diagnostic tool, it was the first source to be investigated. A sample was prepared in an uPVC tube of approximate dimensions of 150 mm long by 100 mm external diameter and a wall thickness of 4 mm. The sample was made up of mudstone derived particles taken from the Houghton Main sample (see Chapter 5), ranging in size from fine (clay sized) to a maximum particle size of those passing a 28 mm sieve.

This sample was x-rayed in the Sheffield Hallam University radiography suite and a radiograph taken; this is shown in Figure 3-1.

As can be seen (Figure 3-1), it is possible to obtain images based on density variation through a soil sample. However, with this method it is not possible to

distinguish single particles located away from the sides of the sample using this method. Further, the samples geometry is shown deformed in the image and the cell walls are not clearly visible. The reason for this relates to the high intensity of the x-ray radiation required to pass through the sample. This meant that the collimation of the x-ray beam was narrow causing the areas of the image away from its centre to be stretched. Also, the intensity of the radiation was such that the density of the uPVC of the sample container did not sufficiently attenuate it to show a difference in density on the radiograph.

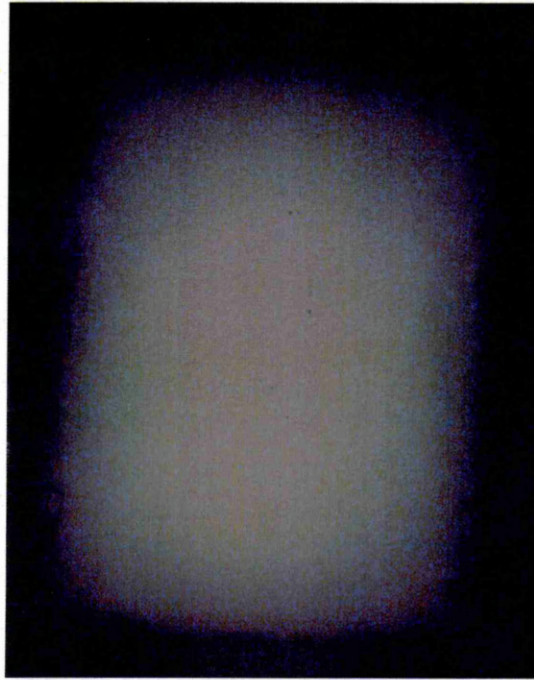


Figure 3-1 Radiograph of sample, taken as part of the investigations into suitable non-destructive imaging techniques.

Given that the samples to be used in the main testing were much larger than that used in this preliminary investigation, and as a result the radiation intensity required would have to be similarly greater, it was decided that plain film x-ray based radiography was not suitable in this case.

3.2.1.3 γ -ray and Isotope Radiography

The source of the radiation detected further defines the radiographic technique. In order of increasing penetration (analogous to intensity), the forms of

radiation sources used in non-destructive imaging are: x-ray, γ -ray (gamma) and isotopic.

Investigations in to the use of these techniques were carried out. The School of Faculty of Health and Wellbeing at Sheffield Hallam University in conjunction the Royal Hallamshire Hospital provided assistance in investigating the viability of gamma source radiation based techniques. NDT Ltd.* of Sheffield provided assistance in to the investigation of the viability of isotopic source techniques. These investigations found that the use of these techniques for the purposes of this research did not offer a practicable method.

3.2.1.4 Three-dimensional Imaging

The two primary methods of generating three-dimensional images of the internal structure of a specimen used in non-destructive testing (particularly medical diagnostics) are: Magnetic Resonance Imaging (MRI) and Computed Tomography (CT). The use of these two methods was investigated for this study.

The images from MRI are generated by detecting the radiofrequencies emitted by the effects of two magnetic fields, generated by the MRI equipment, on the proton contained at the nucleus hydrogen atoms within the subject being imaged. A sample was prepared for the investigation by compacting soil material into a cylindrical container (as described in Section 3.2.1.2) and fully saturating it. Fully saturating the sample would provide as many hydrogen atoms to be contained in the sample as practicably possible for the equipment to detect.

The investigation into the use of MRI was undertaken at the Jessops Hospital for Women[†] in Sheffield. It was found that the signal generated by placing the

* <http://www.ndt.ltd.uk/>

[†] The Jessop Hospital for Women has now been incorporated in to the Royal Hallamshire Hospital in Sheffield.

sample into the MRI scanner was not sufficiently distinct for the scanner to generate an image.

The investigation in to the use of CT proved more successful, with the CT equipment being able to generate good quality images of the small samples used in the plain film and MRI investigation. The use of this technique also proved successful when the size of the scan subject was increased to the size to that of the specimens contained in the small cells used in this research. The incorporation of the technique in to the testing programme is described below.

3.2.2 Computered Tomography Procedures

The use of computered tomography is not wide spread outside the fields of medical diagnosis and research. This is primarily due to the expense of the equipment. Its use in this research was arrived at, following review of a number of techniques and a brief feasibility study of each. An account of this process is given in Sections above.

3.2.2.1 Laboratory based and transport arrangements

On completion of the loading phase of the testing carried out using the small cells the valves, through which pressure was applied, were closed; thus locking in the load into the cell. The cell was then disconnected from laboratory's loading system and the displacement monitoring equipment.

The pressure gauge mounted to the top plate of each cell provided a direct read out of the cell's pressure and allowed monitoring of any change. Should any change in pressure have been noted, an alternative pressure system was available. Though this was not need at any time during the research.

The cell was then transported, by car, the short distance from Sheffield Hallam University to the Royal Hallamshire Hospital. On arrival at the hospital the cell was lifted on to a trolley and wheeled to the CT suite where it was lifted on to CT bed.

Following scanning the cell was transported back to Sheffield Hallam University and reconnected to the loading system and displacement monitoring equipment.

This procedure was repeated prior to unloading of the specimen by depressuring the cell at the end of each test.

Displacement monitoring was not carried out during the transporting or scanning of the cell. However, only negligible pressure loss was noted in the cells where any pressure loss was observed at all.

3.2.2.2 CT Scanning Protocol

A study was undertaken to establish the most appropriate scanning protocol.

The variables that had to be set were:

- the level of X-ray energy used in kV,
- the exposure to this energy in mA-s,
- the method of scanning (axial or helical), and
- the exposure.

The variables had to be set such that scans produced were sufficiently defined and detailed images that were usable within the project. This need had to be balanced against ensuring that the scanner's main purpose, *i.e.* as a medical diagnostic tool, was not compromised.

This essentially meant that the protocol should be set at the maximum possible compromise of energy and exposure whilst ensuring the scanner did not overheat. Through a series of trials it was found that using a scanning protocol that utilised a scanning pitch (see Equation 3-1) of 0.7 to 1, an energy level of 120kV at an exposure of 100mA with a rotation time of 3 seconds (300mA-s) was found to produce satisfactory results.

$$\text{Pitch} = \frac{\text{distance table travels during one } 360^\circ \text{ revolution}}{\text{Slice Thickness}}$$

Equation 3-1

A pitch of less than or equal to one provides the best image quality as the reconstruction software has less interpolation of data to perform. Further, each voxel will be near to isotropic, meaning that reconstructions in another plane should be of equal quality to the plane in which the cell and specimen were scanned.

These settings pushed the scanner to its working limits and required periods of up to 20 minutes in which the scanner was allowed to cool. The frequency of these breaks increased with the number of scans undertaken. Typically the first break was required after 50 minutes of scanning (i.e. approximately one and a half full specimen scans). More typical to the scanners main purpose, the scanner may be set to 120kV and 200mA with a 0.8 second rotation (i.e. 160mA-s) when scanning the abdominal area (which would include the pelvic region) of a patient of average size.

The scans were then viewed as a 3mm thick reconstruction to reduce the amount of image noise. The field of view was planned to be as small as possible in order to utilise most of the scan's matrix and therefore each fragment will be made up of more voxels improving their resolution.

Further discussion is given in Section 7.2.2.

4 Equipment

Various items of equipment were used in this investigation into soil behaviour. In order to remain concise, the only equipment described is that which is considered to be either non-standard or whose use is non-typical in geotechnical research. Descriptions of standard equipment can be found in various publications including: national and international standards, standard texts, and research papers; for example BS 1377:1990:Parts 1-9. Where it is considered useful or necessary reference is made to the specific published source.

The equipment used in this research has been devised specifically to meet the stated aims and objectives. It is recognised, however, that the uniqueness of the equipment is founded on developments made by others. Their efforts are acknowledged and where appropriate referenced.

The equipment used in this research includes both laboratory based equipment (much of which is shown in Figure 4-1), which includes the laboratory itself. As well as a computed tomography scanner used as a diagnostic tool at the Royal Hallamshire Hospital, Sheffield.

4.1 Laboratory Equipment



Figure 4-1: Photograph showing much of the laboratory equipment.

4.1.1 The Laboratory

Located at Sheffield Hallam University, the laboratory was part of the dedicated geotechnics laboratory facilities. The temperature of the laboratory was maintained between 19° and 23° and this was monitored throughout the duration of the laboratory based work. Sample data for the periods 14th to 20th July and 30th October to 5th November 2001 are presented as Figure 4-2. For July, October and November the average external temperatures were 17.0°C, 12.4°C and 7.5°C, respectively.

4.1.2 Compression Cells

The primary purpose of the compression cells was to provide a means of compressing a prepared specimen under a controlled level of stress whilst allowing the measurement of specimen strain. Various secondary features of the cells were also identified during the development of the experimental methodology. Because the design of the cells was undertaken along side the

development of experimental methodology some of these features were built into the cells but were not fully utilised within this research.

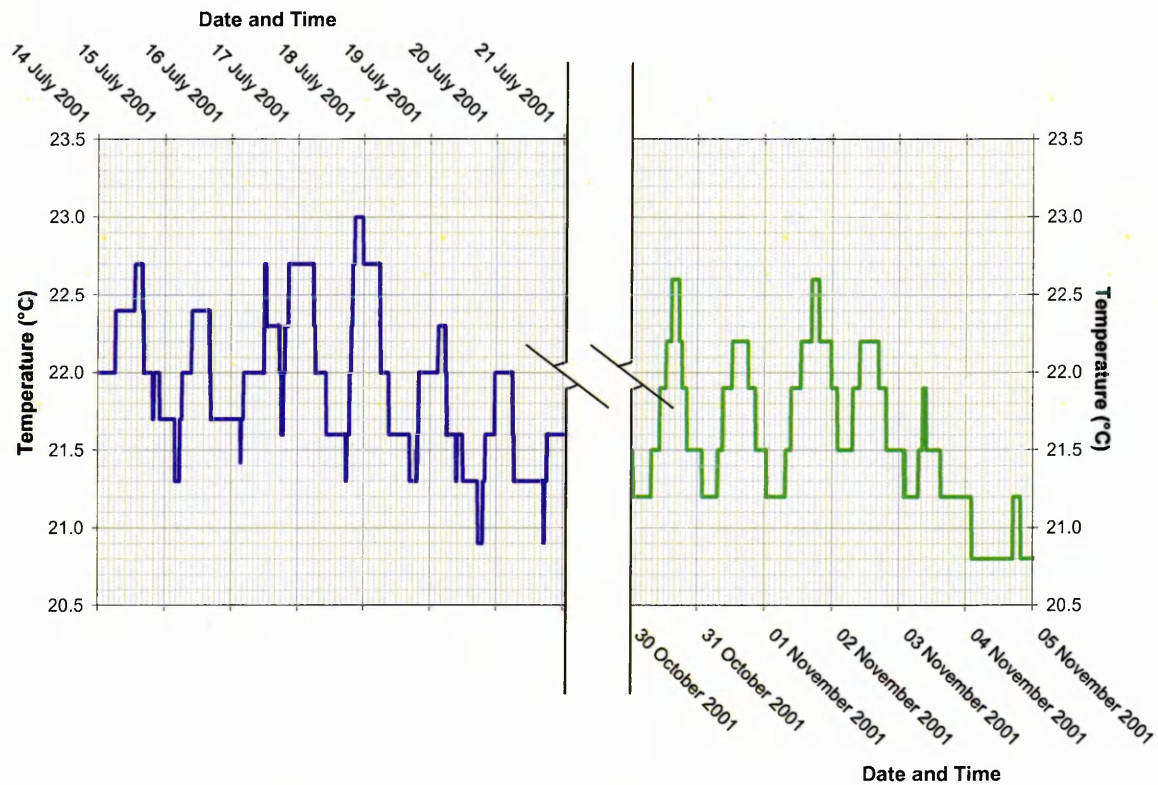


Figure 4-2: Sample laboratory temperature monitoring data.

To enable scanning in a CT scanner and still satisfy the aim of undertaking large scale testing two sizes of cell were manufactured; detailed dimensions are shown in Figure 4-3. . The large cells were capable of housing a specimen of 595mm in diameter and approximately 640mm in height. The small cells were capable of housing a specimen of 235mm in diameter and approximately 300mm in height. As far as was practicable the two sizes of cells were in all other aspects kept as similar to one another as possible.

The main features of the compression cells are shown in Figure 4-3. They include:

- Stiff construction of cell components within the pressure range 0 to 8 bar - to ensure the integrity of the testing methodology and specimen deformation measurements.
- Limited ferrous (large cells) and non-ferrous (small cells) construction - to enable and aid the use of non-destructive testing techniques.

- Hydraulic loading system - to provide control of the stress conditions.
- Upper and lower drainage – to allow the control of the specimen’s drainage condition.

| Dimensions for cells (mm) | | |
|---------------------------|----------------|----------------|
| | Large | Small |
| a | 12 | 9 |
| b | 595 | 235 |
| c | 620 typical | 280 typical |
| d | 150 to 600 | 100 to 300 |

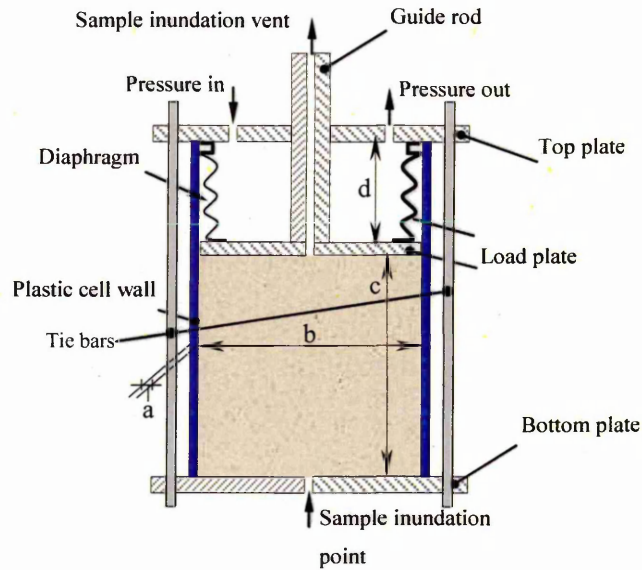


Figure 4-3: Schematic of the compression cells used in this project.

4.1.2.1 Cell components – walls

After some investigation into available materials and products that could be used to form the walls of the cells, the use of plastic pipe was identified. This meant the need to exclude magnetic materials from the cell construction was met, thus enabling the possible use of Magnetic Resonance Imaging (MRI). Further, the relatively low density of the plastic compared to that of steel, brass or even aluminium served to ensure the possibility of the use of radiological based techniques by reducing the radiological energy required to penetrate a typical specimen. Whilst the use of a denser material may not have prohibited the use of a radiological based non-destructive testing technique it would have reduced its effectiveness, particularly of the relatively low energy medical scanner available.

Two types of plastic pipe were used in the research. The pipe for the small cells was supplied by Hepworth Industrial Plastics from the Hepworth “Hep30 Trunk” range of products. The pipe for the large cells was supplied by Uponor Ltd, from MOndail range of products. Both of these ranges are manufactured

for the water supply industry and are formed by extrusion methods. The plastic forming the pipe used for the large cells' walls was a molecular orientated polyvinyl-chloride (PVC) plastic, whilst that for the small cells was a PVC alloy.

Given the unique and non-standard use of the pipe additional information, to the standard technical data sheets, was sought. It was considered that the pipes' behaviour under extended periods of stress should be determined. Given the nature of the pipes' use in this research it was reasoned that if the pipe itself was to undergo creep expansion under the stress from inside the cell then the magnitude of this movement could compromise the research.

It was considered that the stress on the cell walls (the pipe) caused by the testing would be complex. The stress above the loading piston would be a relatively simple hydraulic pressure acting outwards. The stress below the piston, from the sample, was unlikely to be so uniform, with more highly stressed areas and point loads being imposed by the sample. However, given the particle size distributions of the samples to be tested, it was considered that the stress on the cell walls would not significantly exceed the loading pressure, if at all. Thus, it was reasoned that the stress on the cell walls due to the testing could be considered to be uniform.

The internal pressure acting on the cell would be resisted by the walls of the cells acting in tension, causing a 'hoop stress' to develop within the walls. The relationship between the hoop stress and the applied pressure is described by Equation 4-1.

$$s = \frac{P(D-e)}{20e} \qquad \text{Equation 4-1}$$

where: s is the hoop stress in MPa,
 P is the applied stress (as a pressure in bar),
 D is the external diameter, and
 e is the minimum wall thickness.

Data from creep tests carried out on the pipes manufactured from PVC and modified PVC (mPVC) as used in the water industry are widely available.

Data from testing carried out on the behalf of North West Water by materials engineers is presented in Figure 4-4 (J. D'Souza, *pers. comm*). The materials used in the products supplied by Hepworth and Uponor are mPVC (J. D'Souza, *pers. comm* & T. Stevens, *pers. comm*).

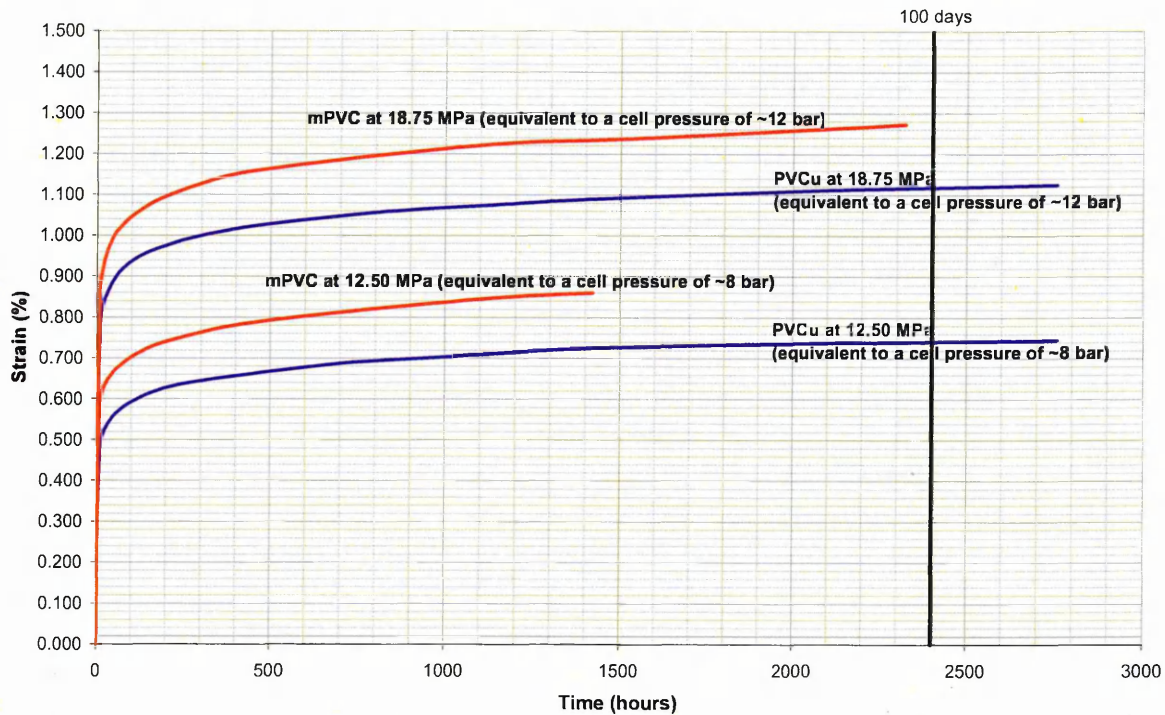


Figure 4-4: Creep data from testing carried out on behalf of North West Water (natural scale).

As indicated by the presented data the creep rate of the cell walls under stress reduces significantly with time. The reducing relationship is linear with the decadic logarithm of time as shown in Figure 4-5.

This behaviour of the pipe was of some concern particularly given the nature of the testing for which the cells were to be used. This concern was dealt with by first calculating the amount of creep for the cell walls over any given period. The effect on the internal volume of the cell was then calculated. This volume change would effectively mean a shortening of the specimen within the cell. It was then reasoned that by pre-stressing the cells a situation could be achieved whereby the possible shortening of a specimen caused by the potential creep of the cell walls could be considered negligible.

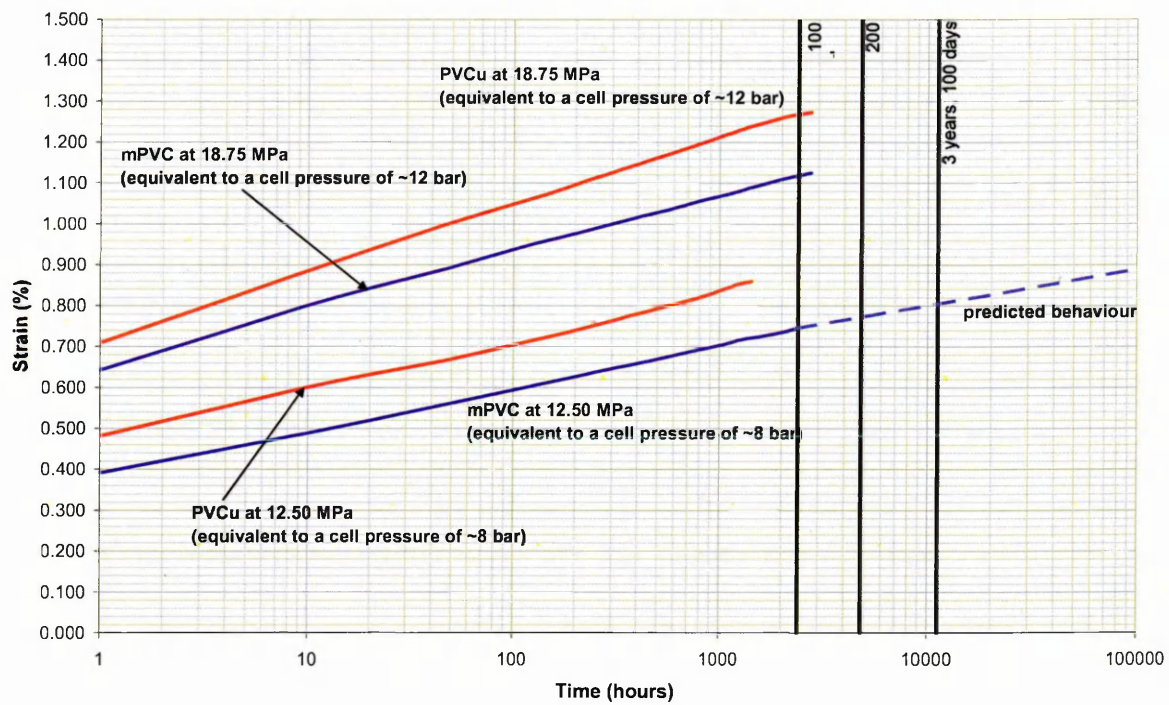


Figure 4-5: Creep data from testing carried out on behalf of North West Water (\log_{10} scale).

As a further precaution, metal banding (stainless steel in the case of the large cells and aluminium for the small cells) was placed around the cell walls following the pre-stressing period.

Confirmation of the effectiveness of these mitigation measures was provided by the implementation of a system of monitoring to check for and measure any deformation of the cell walls. The results of this monitoring demonstrated that the cell wall did not undergo any significant straining during the testing periods. Thus, there was no need to apply a calibration constant to account for cell wall deformation.

4.1.2.2 Cell components – top and bottom platens

The top and bottom platens of the large and small cells were manufactured from aluminium. Aluminium was selected in response to the needs to exclude ferrous and relatively dense materials from the cells' construction, thus enabling and promoting the likelihood of success in non-destructive testing. Also, aluminium's resilience to corrosion in wet environments was

advantageous as was the relative ease with which aluminium can be precision machined, which considerably eased the cells' manufacture.

Figure 4-6 shows the top platen assembly. The top platen provides for the passage of the piston rod of the piston assembly (see Section 4.1.2.4). The hole through the top platen had to allow the piston to move with as little frictional resistance as possible whilst maintaining a seal against the hydraulic pressure within the cell. A bush housing containing a nylon bush that incorporated grooves for o-rings, which maintained the seal, was manufactured.

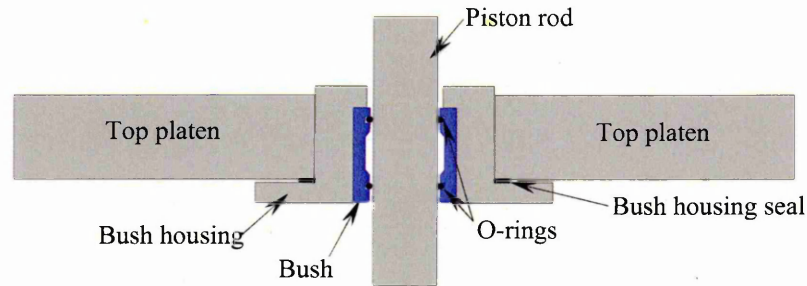


Figure 4-6: Top plate, piston bush, housing, o-ring and piston rod section.

The design of the cells was such that their deformation under load would be negligible. This was particularly pertinent with the top platens as they were used as the reference datum for the deformation measurements. The design calculations for the platens are presented in Appendix A.

A further feature of the bottom platen of the cells was the drainage grooves machined into their surface that are in contact with the test specimen. These match those similarly machined into the loading plate (part of the piston assembly).

4.1.2.3 Cell components – tie bars

Two material types were used to form the tie bars: on the small cells aluminium was selected, whilst the large cells' tie bars were made of high strength steel. The use of steel as the tie bar material for the large cells was not

prejudicial to the non-destructive testing technique, which was previously planned for use in conjunction with them. However, the use of computed tomography would have been made more difficult if steel was used on the small cells. This difference was due to the planned use of the small cells in a computed tomography scanner.

The tie bars were sized such that the imposed loading was within their elastic range. A factor of safety on this requirement of 1.75 was imposed. The calculations relating to the tie bar design can be found in Appendix A.

4.1.2.4 Cell components – piston assembly

The piston assembly (includes a diaphragm which is described in detail separately in 4.1.2.5) fulfils two functions: firstly it provides a means of loading the test specimen in the cell and it facilitates the measurement of any deformations.

The assembly is made up of three elements: the diaphragm, the aluminium piston and loading plate. The reasons for choosing aluminium are the same as for the choice of aluminium for the top and bottom platens, see Section 4.1.2.2.

A further feature of the piston assembly's loading plates are the drainage grooves machined into the surface of the load plates in contact with the test specimen.

4.1.2.5 Cell components – diaphragms and diaphragm assemblies

The diaphragms and their assemblies were manufactured from latex rubber with a polyurethane waterproof coating. The diaphragms were reinforced with synthetic fibres incorporated into the rubber bodies at highly stressed locations. These locations were the clamping areas and the bottom (closest to the loading plate) convolution. The diaphragms were attached to the piston assemblies and top platens by clamping with the clamping rings fixed with through screws into the loading plate or top platen. Due to several equipment failures the

diaphragm construction was modified several times. This is discussed in Section 4.1.7.

4.1.2.6 Cell components – associated plumbing

The ‘associated plumbing’ refers to the valves and other connections which were used to isolate the cells from the loading and load control system. On the small cells these components were selected from a standard range plastic plumbing fittings. Whilst on the large cells they were selected from a standard range of metal fittings. Again, this difference was due to the planned use of the small cells in a computed tomography scanner.

In addition to the plumbing fittings, a small pressure gauge was attached to the cells, such that the pressure within the cell (and therefore the stress on the specimen) could be monitored independently of the load control system. This was of particular use on the small cells when they were remote from the load / control system during CT scanning sessions.

4.1.3 Cell Commissioning

As part of the commissioning of the cells the cell walls were pre-stressed and their behaviour under load was investigated.

4.1.3.1 Cell wall pre-stressing

In order to pre-stress of the cell walls and reduce any increase in the diameter of the cells due to the plastic behaviour of the cell walls, see Section 4.1.2.1, the cells were assembled without the diaphragm and filled with water. A pressure of 8 bar was then applied for a minimum of 100 days, though this was typically extended to more than 6 months.

4.1.3.2 Side wall friction

In order to establish the behaviour of the cells under stress, an investigation of the load transfer from the diaphragm and from a specimen to the cells’ walls

was carried out. This investigation took place in four stages for each cell size. Figure 4-7 shows a cross-section through each of these different stages of the investigation. The stages were:

- Stage one: the load cells* were placed between the loading plate and the bottom platen, to measure the load lost to side wall friction between the cell walls and the diaphragm under static conditions. Steel bearing plates were placed between the load cells and the aluminium cell components, protecting them.
- Stage two: as stage one but with a 7mm thick rubber packer of known deformation behaviour inserted beneath the load cells. The packers provided for some extension of the diaphragm as the load was applied.
- Stage three: as stage one but with a specimen (compacted to an average dry density of 1.75Mg/m^3 at natural moisture content, using the method outlined in Section 4.1.6) included in the test cell.
 - The specimen thickness in the large cell was approximately 225 mm.
 - The specimen thickness in the small cell was approximately 150 mm.
- Stage four: as stage three but with a 7mm thick rubber packer of known deformation behaviour inserted beneath the load cells.

The idealised load from the pressurisation of the diaphragm was calculated and the results from each stage of the investigation were compared against it. An example of the testing results and their comparison against the calculated idealised load is given in Figure 4-8. The results of this investigation are given in Table 4-1.

* Load cells were Sensotec precision pancake thin load cells, model 41, with a quoted accuracy of 0.1% full-scale.

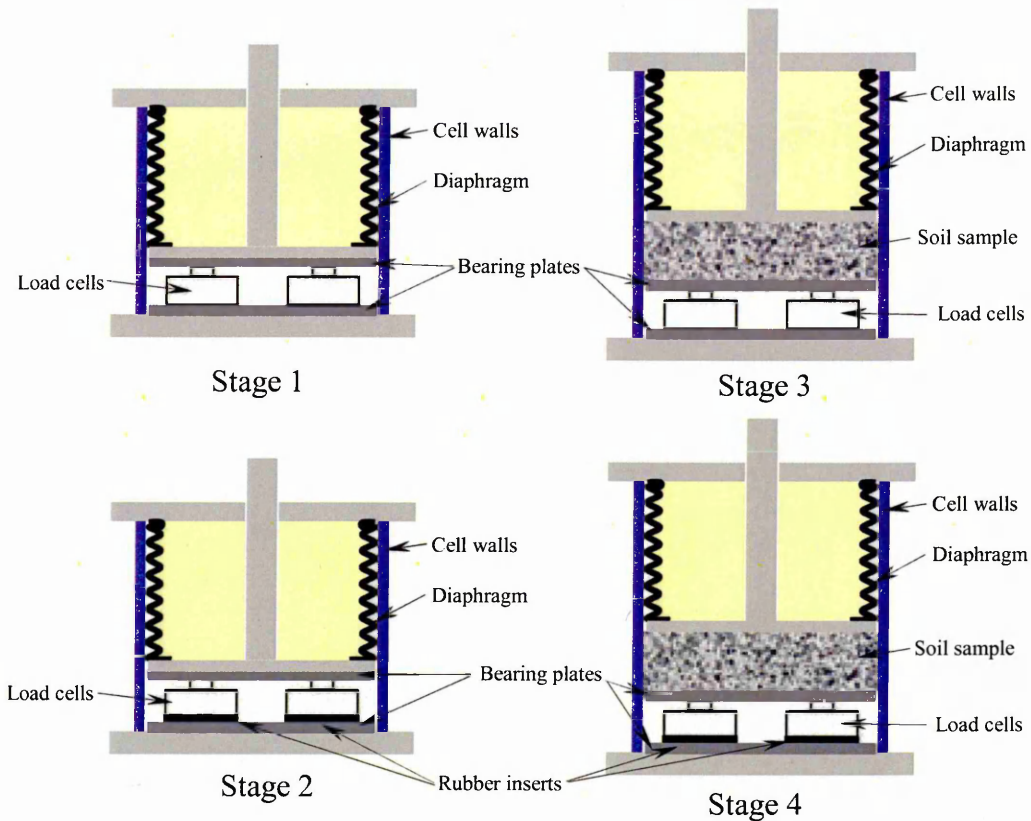


Figure 4-7: Side wall friction investigation, cell set ups.

As can be seen from the results in Figure 4-8 and Table 4-1 the loss of load to friction was proportional to the applied stress. Also, that with increased frictional resistance, provided by the inclusion of a sample, the load losses to friction increases. The results do not show a significant difference between the loss of load in the static condition (Stages 1 and 3) and the dynamic conditions (Stages 2 and 4), *i.e.* greater than 1%. This testing should not be considered as a comprehensive investigation into side wall friction but as reconnoitre testing carried out to better understand the behaviour of the cells under test conditions.

| Applied pressure (bar) | Small Cells | | Large Cells* | |
|-----------------------------|-------------|------|--------------|-------|
| | 4 | 8 | 4 | 8 |
| Idealised load (kN) | 14.1 | 28.2 | 111.2 | 222.4 |
| Reduction in load (stage 1) | 0.1% | 0.2% | 3.2% | 5.2% |
| Reduction in load (stage 2) | 0.2% | 0.3% | 3.1% | 5.6% |
| Reduction in load (stage 3) | 1.0% | 0.8% | 4.6% | 7.0% |
| Reduction in load (stage 4) | 0.9% | 1.0% | 5.0% | 6.7% |

* in the large cells load measurements were made using three load cells in parallel, with the total load being the sum of the loads measured by each load cell.

Table 4-1: Results of side wall friction investigation.

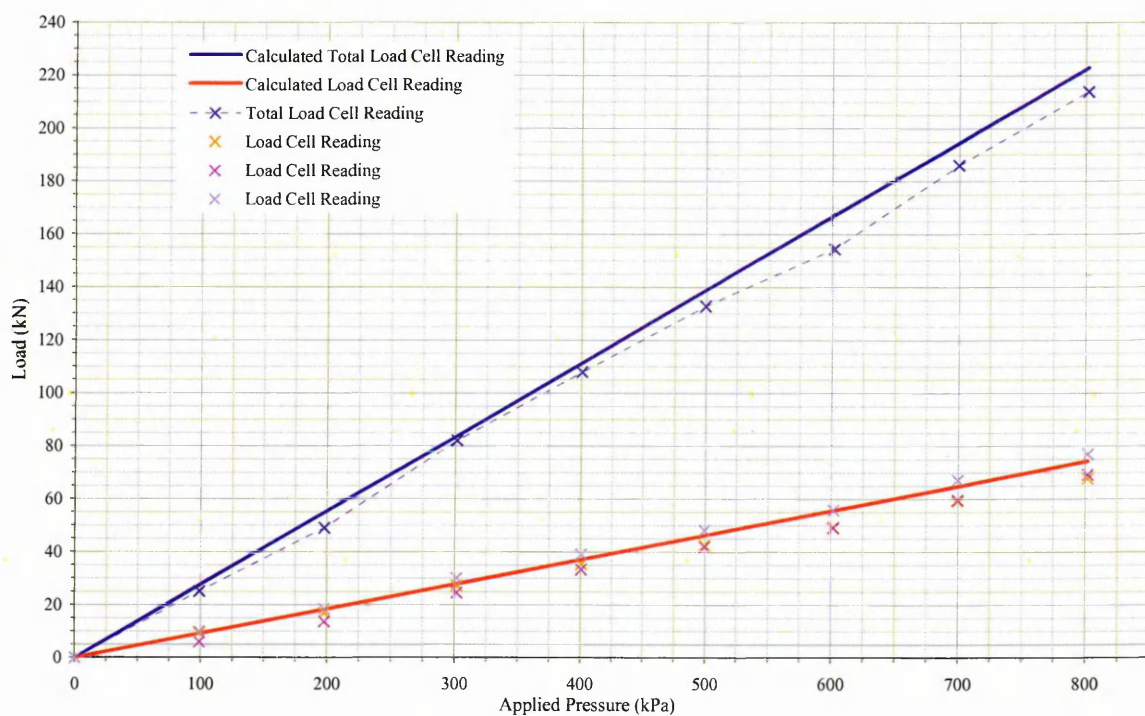


Figure 4-8: Side wall friction investigation, detailed results of the Stage 2 testing for the large cells.

4.1.4 Loading and Load Control System

A schematic of the loading and load control system is given Figure 4-9. The loading and control system for the main testing was made up of two parallel arrangements, allowing for two different loads to be applied to different cells, each made up of the following components:

- Compressed air feed (providing the pressure in the loading system)
- Air pressure regulator (to regulate the supply pressure)
- Air/water cylinder (to convert the pneumatic pressure to hydraulic)
- Bourdon Gauge (to give an accurate visual reading ($\pm 0.5\%$ full scale) of the system pressure,)
- Control manifold (allowing the isolation of one or more cells, the connection of a different load system, or the bleeding of the system)

The level of the water in the air/water cylinders could be monitored via a clear plastic tube attached to a scale. The volume of the air/water cylinder was calibrated such that the water level readings could be used to manually check specimen volume changes.

4.1.5 Data Acquisition Equipment and Systems

4.1.5.1 Cell pressure (load) measurements

The cell pressure to each cell was monitored using a pressure transducer located within the loading and load control system. The pressure transducers used were supplied by R.D.P Electronics Ltd, model number A5 (mid range). These transducers had a quoted accurate of $\pm 0.5\%$ full scale and the capability of measuring pressure ranges from ± 3.5 bar to ± 50.0 bar. These transducers were calibrated and the results of the calibration confirmed their quotes accuracy.

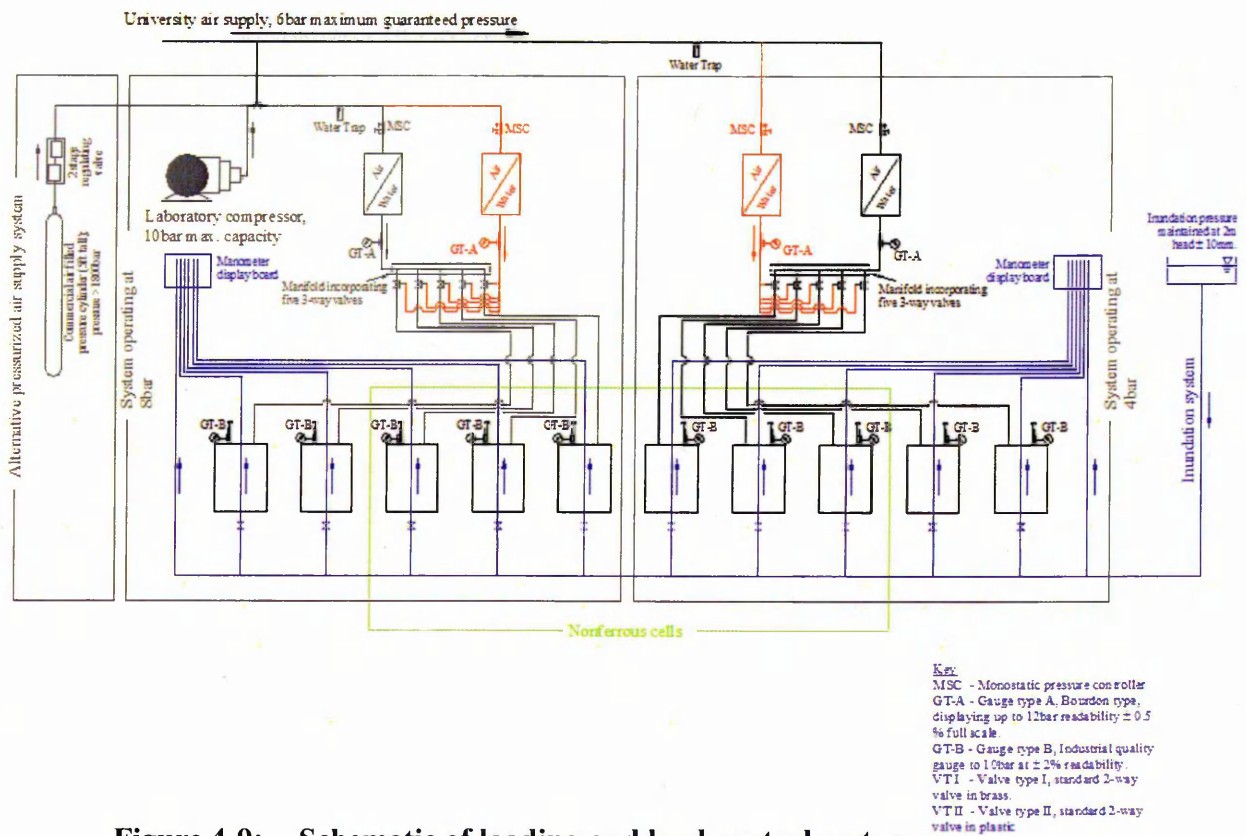


Figure 4-9: Schematic of loading and load control system.

4.1.5.2 Specimen deformation measurements

Measurement of the vertical deformations were made via the piston guide rod and measured in relation to the top platen. Each cell had a dedicated linear variable differential transformer (LVDT) displacement transducer attached to the cells, held within a purpose made clamp, in order to measure deformations. The transducers used were DCTH LVDT transducers, manufactured by R.D.P. Electronics Ltd; they had an accuracy of $\pm 0.25\%$ over a travel range of ± 5 mm. These transducers were supplied with calibration certificates; however, further calibration checks were carried out on them and the results calibration confirmed their quotes accuracy.

4.1.5.3 Data recording arrangement

The primary data recording arrangements were based around the electronic transducers and a personal computer (PC) used as a dedicated logger. The transducers were connected to a control box from where the transducers drew their power. From the control box the data signal from the transducers were connected to an input card in the PC. These signals were recorded using a data acquisition program written using the HP VEE (Visual Engineering Environment) visual programming language, from Hewlett Packard.

4.1.5.4 Specimen inundation measurements

Inundation of the specimens (both controlled and uncontrolled, see Section 4.1.7) was monitored by manometers in conductivity with the specimen through the cell plumbing which was open to the atmosphere. The manometers were connected through the cells' bottom plate and through the guide rod allowing direct connection with the top and bottom surfaces of the specimens.

4.1.6 Specimen Compaction Equipment

The specimen compaction equipment comprised purpose made plates each of a diameter to fit into the large and small cells to which an electric vibrating

“Kango” hammer could be attached. Two plates were made to match the internal diameters of the cells, with approximately 3 mm of clearance. The Kango hammer complied with the specification for such a piece of equipment given in BS 1377:1990:Part 4.

4.1.7 Laboratory Equipment Failures

Despite the building on the experience of other researchers, for example Rowe and Barden (1966) and Blanchfield (1998), failures in the equipment meant that only a reduced programme of testing was possible. The implications of this are seen in the Chapter 6, in that the amount of data available is less than that planned for. This is discussed, where appropriate, in the Chapter 7.

The predominant failure of the equipment was the rupturing of diaphragms under load. It was found that the large diaphragms were particularly subject to rupture during the loading phase of the testing, though some small cells suffered the same failure.

After some investigation two mechanisms explaining the rupture were inductively identified following examination of the diaphragms. These were the deformation of the diaphragm under pressure into the gap between the loading plate and the cell walls and either locally overstressing the diaphragm or trapping it and pinching it such that it ruptured. The other mechanism of rupture identified was the local overstressing of the diaphragm against the screws fixing the upper clamping ring to the top plate. A further contributing factor to the likelihood of diaphragm rupture was the frequency and location of any imperfections in the diaphragm originating in the manufacturing process.

These mechanisms were mitigated by:

- increasing the thickness of the diaphragm construction
- increasing the number of layers of reinforcing material within the diaphragm construction.
- improving quality control during the manufacturing procedure,
- including a rubber skirt over the gap between the loading plate and the cell walls,

- including a rubber cover over the heads of the screws fixing the upper clamping ring to the top plate.

Whilst these precautions did reduce the frequency of diaphragm ruptures they did not eliminate them.

Another significant obstacle to planned programme of laboratory work was a power failure that occurred during the Christmas Break 2001. The power failure was compounded by the University's backup systems also failing. The results of this double failure were to increase the occurrence in diaphragm rupture.

A number of other failures were encountered during the testing though these were relatively minor (such as the failure of valves during commissioning). It is considered that these minor failures did not have a significant impact on the testing programme or the testing itself.

4.2 *Computed Tomography*

4.2.1 Introduction

The computed tomography (CT) equipment used within the research programme was a commercially available medical scanner; however, its description here is warranted due to its novel application. Further, an explanation of the principles of this non-destructive testing technique is given below.

The procedures for the successful use of the scanner were developed around the equipment's physical limitations and those imposed by its use as a diagnostic tool in a busy modern hospital, they are described in Section 3.2.2.2.

4.2.2 CT, An Overview

Computed tomography (CT) is the utilisation of X-ray technology and computer processing power to produce digital sectional images of an object, in

medical CT the object is the patient. A schematic sketch of the equipment use for CT scanning is shown in Figure 4-10.

The scanning process involves the patient being moved, on a precision controlled table, through the aperture in the gantry. As this is happening the X-ray tube and opposing array of detectors are rotated. The information gathered at the detectors thus provides a three dimensional data set of density information.

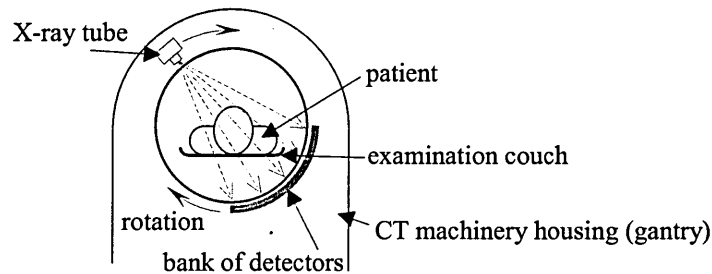


Figure 4-10: Schematic sketch of a CT scanner and its components.

The information gathered from the bank of X-ray detectors is then processed using a number of mathematical procedures in order to form the digital image. The procedures are known as the iterative least square technique (ILST), the algebraic reconstructive technique (ART) and the simultaneous iterative reconstruction techniques (SIRT). Details on these can be found in standard texts on the subject of Computed Tomography, such as Kalender (2000).

4.2.2.1 Attenuation

In CT imaging the information gathered is that of X-ray transmission attenuation, *i.e.* the amount of degradation in the strength of the X-ray beam due to transmission through the object.

An X-ray beam is made up of many photons of various energies, *i.e.* the beam is heterogeneous, and the utilisation of a filter will remove the photons of lower energies from the beam. This is similar to the effect of passing white light (a heterogeneous beam) through a piece of coloured glass (a filter), with the result

that only the light within a narrow band of photon energies remain and emerge from the filter in a beam which is monochromatic (homogeneous).

The passing of a homogeneous X-ray beam through a medium causes the photons in the beam to lose energy, thus the beam is attenuated. The degree to which the beam is attenuated is dependent upon the thickness and type of the attenuating medium and is proportional to the intensity of the X-ray beam, *i.e.*:

$$I \propto e^{-\mu x}$$

Equation 4-2

where I is the intensity of X-ray beam, μ is the linear attenuation constant and x is the thickness of the attenuation medium.

4.2.2.2 Causes of Attenuation

Attenuation of an X-ray beam occurs due to the absorption and scattering of the photons that make up the beam. As a beam passes through a medium some of its energy is absorbed by the medium, that is some of the energy is transferred to the matter, thus causing harmful changes to living organisms (Figure 4-11a). Other photons collide with atomic particles and are forced to change course and are thus scattered. The scattered photon beams may emerge from the attenuating medium travelling in different direction from that of the incident beam (Figure 4-11b).

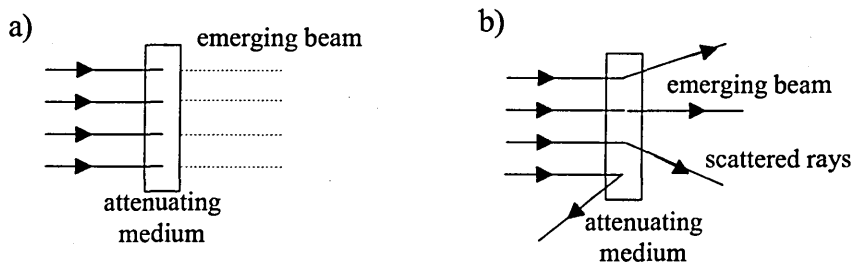


Figure 4-11: a) Energy absorption, b) Scattering of rays.

The term linear attenuation coefficient is derived from the coefficient of attenuation's relationship with the linear thickness of the attenuating medium, Equation 4-2 can be rearranged:

$$\mu = -\frac{1}{x} \ln \frac{I}{I_0}$$

Equation 4-3

The expression represents the factor by which the incident beam (I_0) is reduced in intensity to I . The SI unit of linear attenuation is m^{-1} ; however it is common to see them quoted in cm^{-1} .

4.2.2.4 Computed Tomography

Attenuation coefficient measurement is fundamental to CT scanning, the calculation of the attenuation coefficient of each voxel determines the shade of grey that is displayed in each pixel on the digital display. A voxel is one of the three dimensional elements of the object being scanned that corresponds to the two dimensional pixel (or picture element) on the screen.

The development of CT technology primarily took place in the 1970's by Godfrey Hounsfield's team in Hayes, United Kingdom, at EMI Central Research Laboratories. It was common for this team to express linear attenuation coefficients as arbitrary measures which are known today as Hounsfield Numbers or CT numbers. Hounsfield numbers (H) are measures of the attenuation coefficient as values based upon the comparison between an attenuation medium and water as an attenuation medium.

$$H = 1000 \left(\frac{\mu_{\text{medium}}}{\mu_{\text{water}}} \right)$$

Equation 4-4

During axial scanning the X-ray tube/detector arrangement rotates around the object being scanned, on completion of one revolution the object is advanced a set distance before another revolution is begun. Thus the object is stationary during each data acquisition stage (or revolution).

During helical scanning the object is moved at a constant velocity through the X-ray tube/detector arrangement while the arrangement is in motion. This produces an image that is made up of a volume of information gathered through out the entire object with no planes of interface.

4.2.3 CT, Applications in Soil Mechanics

Non-destructive testing techniques are used in various fields of the geosciences. Early applications of plain film X-ray technology* were pioneered by Slobod and Caudle (1952) in work analysing rock cores for the oil and gas industry.

The application of computed tomography (CT) in the geosciences has largely been restricted to the use of medical CT scanners. Such applications were investigated as early as 1987 by Vinegar (1987) who looked into the imaging of rocks; again, this work was driven by the interests of the oil and gas industry. The use of medical CT scanners in the geosciences has continued since these initial investigations. Workers such as Swennen *et al.* (1990), Boespflug *et al.* (1995) have continued to use CT imaging in looking at the petrology and the behaviour of rocks. Shi *et al.* (1999) applied the technique in an investigation into the shear behaviour of soils and its use on soils with large particles was demonstrated by Goodwin *et al.* (2001) and O'Neill *et al.* (2003).

* Plain film x-ray technology refers to technique of passing a collimated x-ray beam through an object on to a film sensitive to x-radiation. The film is then processed such that resulting changes to the film are fixed producing a radiograph, common in medical diagnostics particularly relating to broken bones. The technique is akin to that of photography where a film, sensitive to light is used and the resulting processing produces a photograph.

Industrial CT scanners have become available and researchers such as Steudi (1994) and Otani *et al.* (2000) have used them to research soil behaviour.

Micro-focus CT scanning has also been developed from the early work by Vinegar (1987). This involves placing a sample (typically restricted in size to about 75mm by 75mm by 75mm) on to a precision controlled rotating table between a X-ray source and detector. This technique can resolve information to voxels as small as 10 μ m. Nakashima *et al.* (1997) and Van Geet *et al.* (2001) reported work largely dependent on the use of micro-focus CT scanning investigating the internal structure of rock cores. Oda *et al.* (2004) also used micro-focus CT to exam the shear behaviour of a sand soil.

An overview of the techniques and their application in the geosciences is given by Mees *et al.* (2003).

4.2.4 CT Equipment Used

The scanner used was a GE Medical Systems Ltd. HiSpeed CT/i Pro. It is made up of three parts: the table, the gantry and the workstation. The table and gantry are shown in Figure 4-12. The table supports the cell and is passed through the gantry at a controlled rate using inbuilt servo controlled motors. The gantry contains the X-ray tube and detector array, which collects the base data from which the three-dimensional image is constructed.

The workstation part of the scanner is shown in Figure 4-13. It is this element of the scanner in which the scanner's settings are controlled, most of the data processing is done, and the data is reconstructed and manipulated.



Figure 4-12: GE Medical Systems HiSpeed CT/i Pro CT Scanner, gantry and table.



Figure 4-13: GE Medical Systems Advantage Windows Workstation.

5 Test Materials

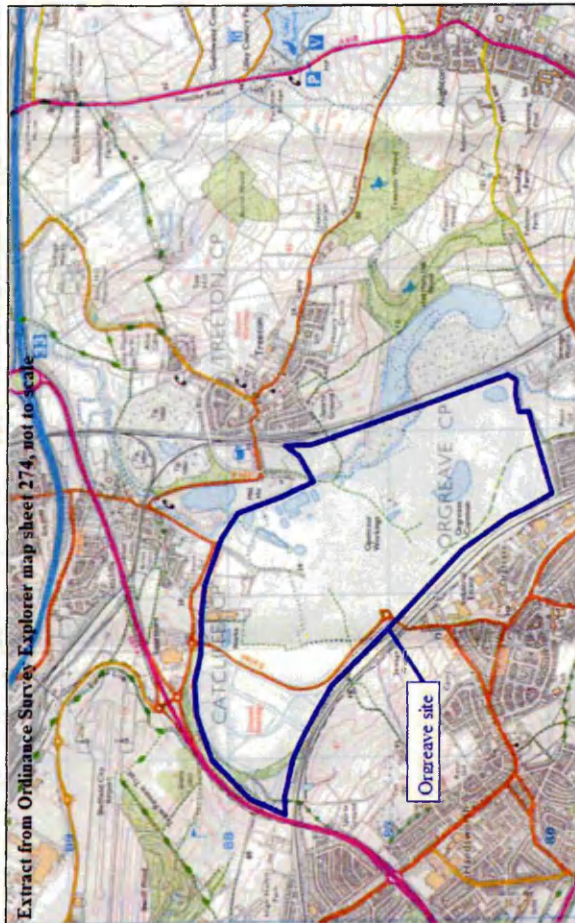
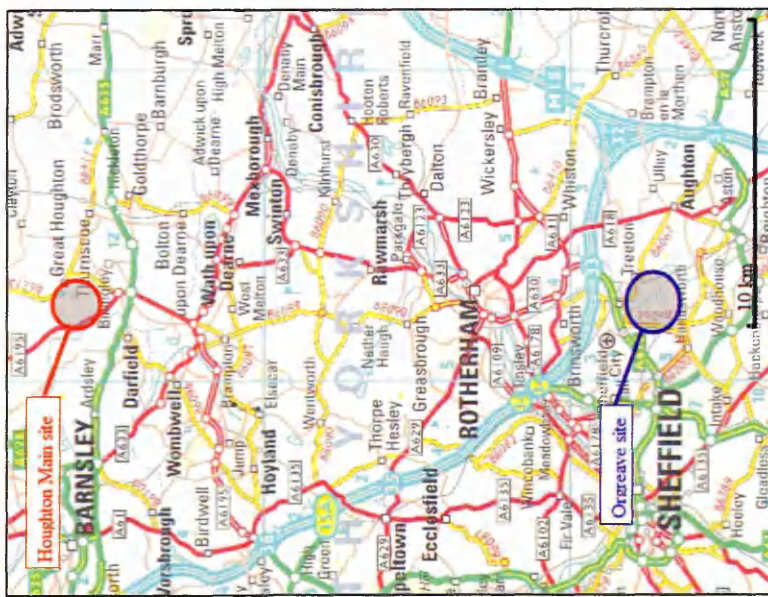
The two opencast backfill materials used in the testing programme were sourced from opencast coal mine sites in South Yorkshire: Houghton Main opencast site and Orgreave opencast site. Both of these sites were licensed for coal extraction to RJB Mining.

In order to provide a means of assessing and comparing the two materials against each other and other published data the following standard classification and compaction tests were carried out. The testing reported in this chapter was generally completed in accordance with BS 1377:1990 and the National Coal Board (NCB) Technical Memorandum (1971). Details of specific methods and any departures from these standards are described in subsequent sections.

5.1 Origin and Description of Samples

Three samples were collected. The first two were collected from the Houghton Main opencast coal mine in early 2000. The third sample was collected from the Orgreave opencast coal mine in September 2002.

Both sites are in South Yorkshire in the United Kingdom and the Houghton Main opencast coal site lies approximately 20 km to the north of the Orgreave opencast coal site. (The Ordnance Survey Land Ranger grid references for the centre of the Houghton Main and Orgreave sites are: SE 424 063 and SK 423 871, respectively). Annotated extracts of maps at various scales and showing the site location are presented as Figure 5-1.



© Crown copyright Ordnance Survey. All rights reserved.

Figure 5-1: Locations of Houghton Main and Orgreave Opencast Coal Mine sites.

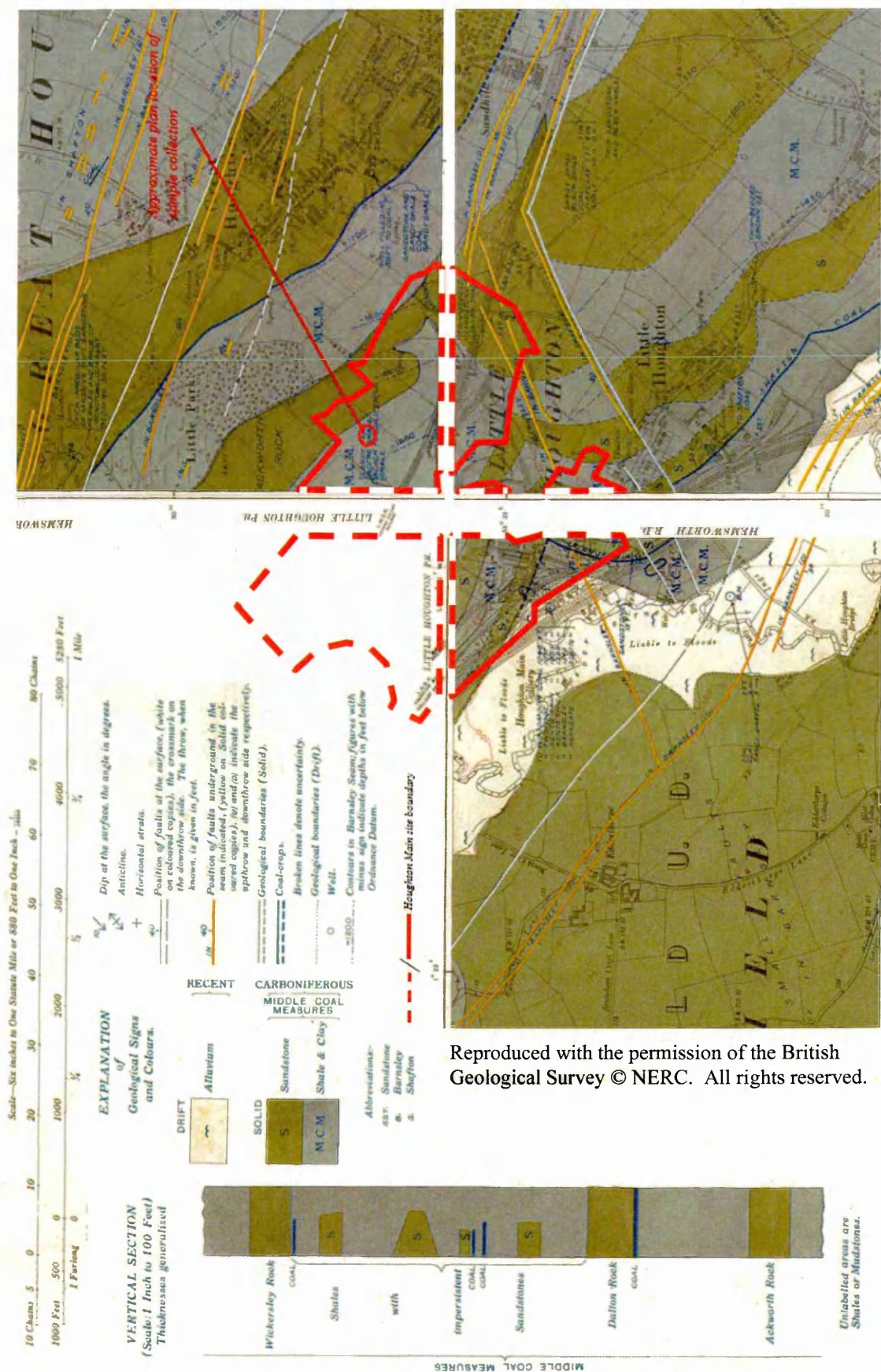
Coal extraction began at the Houghton Main opencast mine site in early 1997 with coal extraction from the Shafton and Highgate seams. The maximum planned depth of the excavation was 65 m over a plan area of some 88.2 hectares. Figure 5-2 shows the geology in the vicinity of the site comprising mudrocks, with inferior sandstones, of the Middle Coal Measures.

The sample was taken from the western end of the site where it was excavated by 15 tonne tracked excavator from a single stratum of freshly exposed material in a 15 m low-wall during coal overburden removal. This stratum was of a typically massive and near structureless mudrock. On this site it was usual that the removal of the coal overburden would be completed using an RH-120 excavator. Approximately 2.0 tonnes of the excavated material was then placed in a trailer for transport to the laboratory. The excavated material contained occasional particles that were greater than 300 mm in nominal diameter. These were visually identified and excluded from the sample.

At the laboratory the sample was removed from the trailer onto a clean surface, quartered and thoroughly mixed. Particles greater than 100 mm nominal size were removed and their total mass recorded for use in the particle size distribution analysis. The remainder of the sample was also weighed and placed in storage drums, with tight fitting lids, until required for testing.

The following description of the sample to BS 5930:1999 was made at the time of storage at the laboratory:

“Blue grey, slightly clayey, sandy, fine to coarse GRAVEL with frequent cobbles. Gravel and cobbles are subangular to angular of weak mudrock. (CARBONIFEROUS MUDROCK)”



Reproduced with the permission of the British Geological Survey © NERC. All rights reserved.

Figure 5-2: Houghton Main Opencast Site Geology.

5.1.2 Orgreave Sample

Coal extraction began at the Orgreave opencast mine site in April 1995 with coal extraction from several shallow seams including the Wathwood and Two-Foot seams. The maximum planned depth of the excavation was above 90 m over a plan area of some 294.4 hectares. Figure 5-3 shows the geology in the vicinity of the site to comprise of mudrocks and sandstones of the Middle Coal Measures.

The sample was taken from below the Houghton Marine Band in an area to the east of the centre of the site, where the coal overburden had recently been blasted in preparation for its removal. This blasted material was excavated by 15 tonne tracked excavator from a single stratum. This stratum was of a typically massive and near structureless mudrock. Approximately 2.0 tonnes of the excavated material was then placed in a trailer for transport to the laboratory. The excavated material contained occasional particles that were greater than 300 mm in nominal diameter. These were visually identified and excluded from the sample, similarly to the Houghton Main samples.

At the laboratory the sample was removed from the trailer onto a clean surface, quartered and thoroughly mixed, particles greater than 100 mm nominal size were removed and their total mass recorded for use in the particle size distribution analysis. The remained of the sample was also weighed and placed in large bulk storage bags, each containing approximately 1 tonne of material for short-term storage. Where longer term storage was necessary the material was transferred into storage drums, with tight fitting lids.

The following description of the sample to BS 5930:1999 was made at the time of storage at the laboratory:

“Grey, slightly clayey, very sandy, fine to coarse GRAVEL with frequent cobbles. Gravel and cobbles are subangular to angular of weak mudrock. (CARBONIFEROUS MUDROCK)”

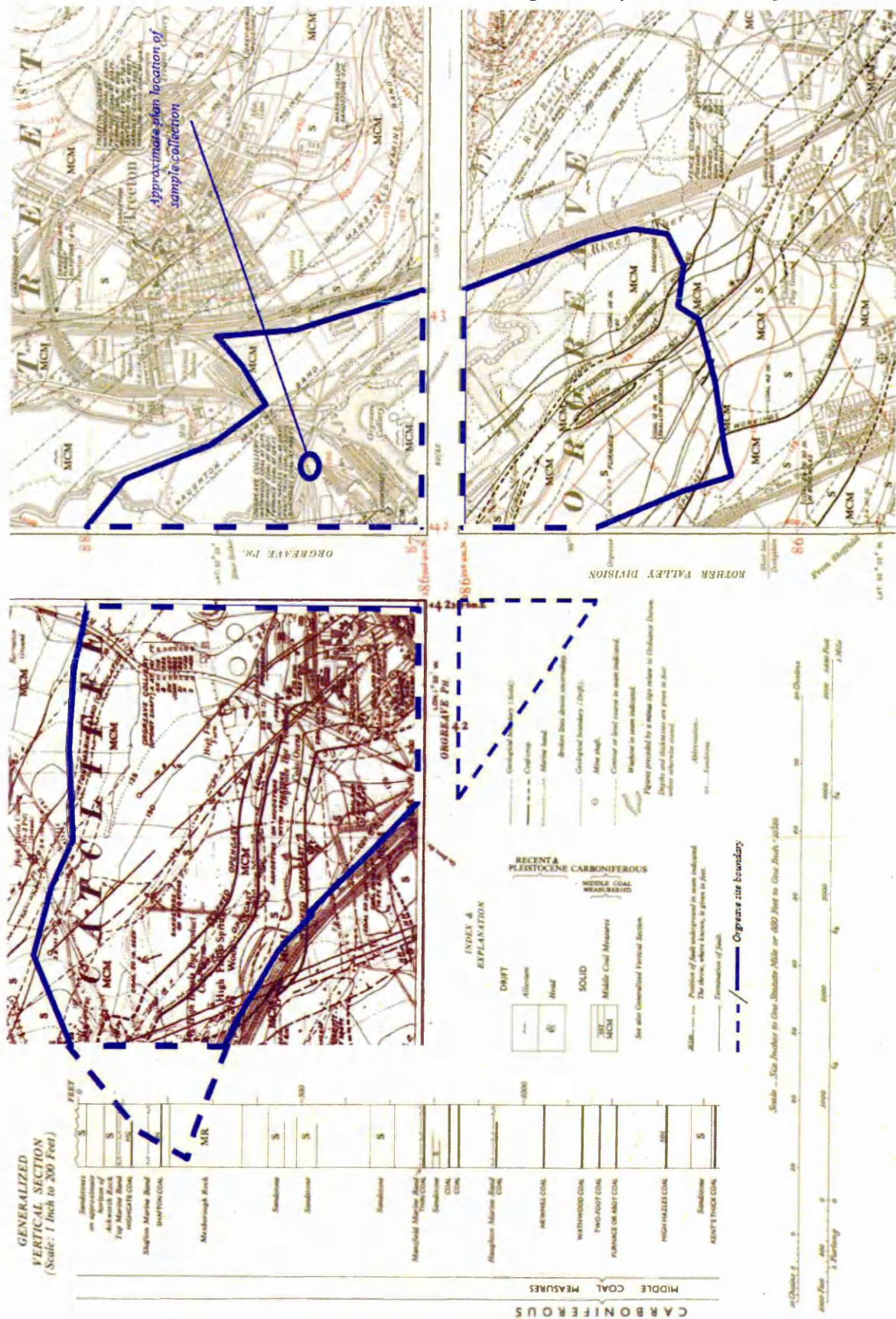


Figure 5-3: OGREAVE OPENCAST SITE Geology.

5.2 Particle Density

Particle density determinations to BS 1377:Part 2:1990 using the gas jar method were carried out on 4 no. sub-samples. A summary of the results are presented in Table 5-1.

| | Mean average particle density, Mg/m ³ | Upper limit Mg/m ³ | Lower limit Mg/m ³ |
|-----------------------|--|-------------------------------|-------------------------------|
| Houghton Main Samples | 2.75 | 2.78 (+1.2%) | 2.73 (-0.7%) |
| Orgreave Sample | 2.73 | 2.78 (+2.1%) | 2.67 (-2.2%) |

Table 5-1: Summary of particle density results.

5.3 Particle Size Distribution (PSD)

Particle size distributions were determined for each sample in accordance with the wet sieving method of BS 1377:Part 2:1990 amended as suggested in the NCB Technical Memorandum (1971). As part of the preparation of the specimens into the compression cells large particles were removed. Where a specimen was prepared for use in a large cell, particles that were greater than 120 mm in nominal diameter were removed. In the case of the small cells particles greater in size than 37.5 mm in nominal diameter were removed. The particle size distributions for the specimens used in the testing are shown in Figure 5-4.

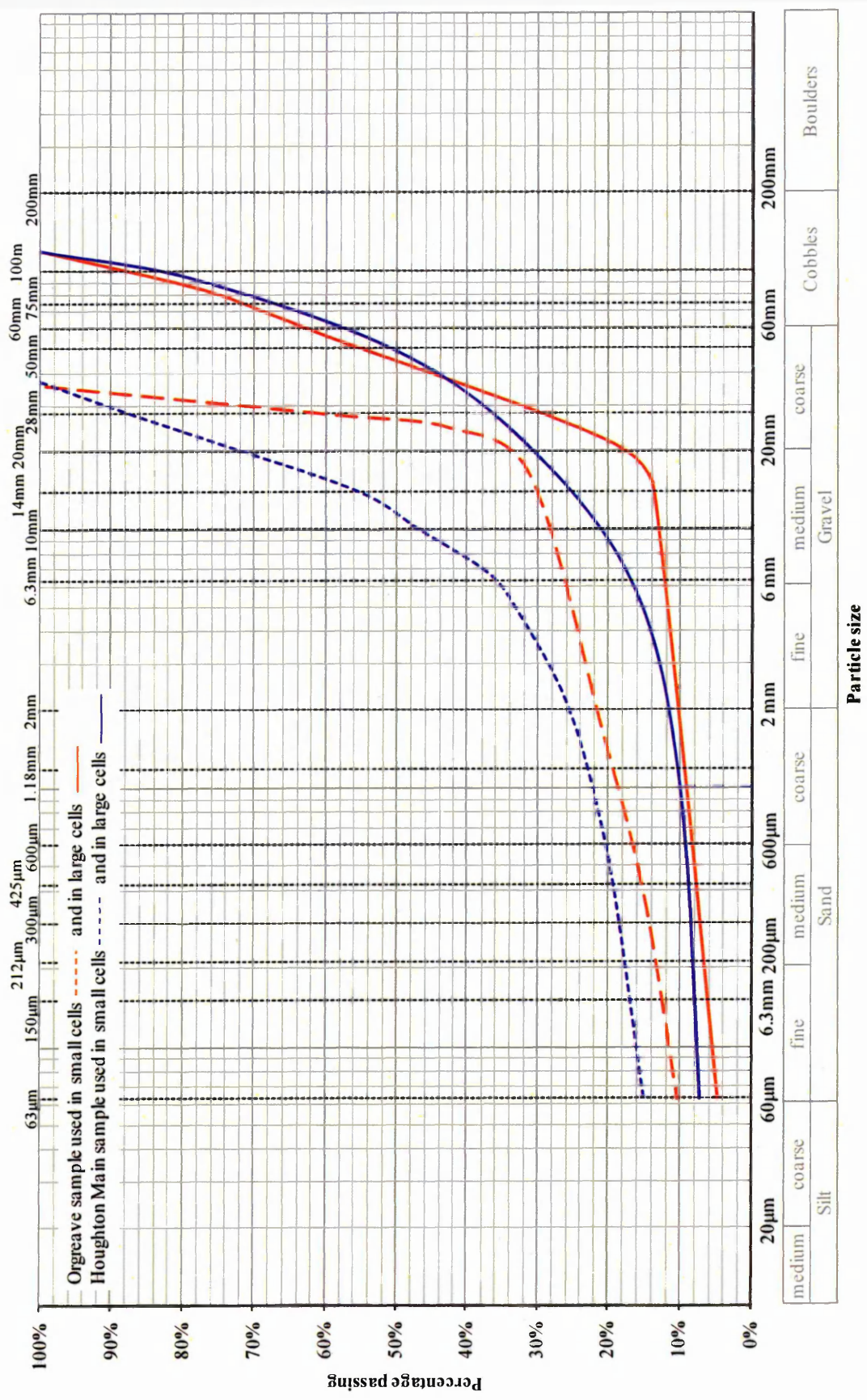


Figure 5-4: Graph of particle size distributions for the specimens used in the testing.

5.4 Particle Shape Analysis

Samples were taken and photographed from the material retained on the 75 mm, 50 mm, 37.5 mm, 28 mm and 20 mm aperture sieves; these are shown as Figure 5-6 and Figure 5-8. A particle shape analysis has been completed for each sample and is reported in Sections 5.4.1 and 5.4.2. The analysis employed the quantitative shape descriptors proposed by Lee (1964) and by Krumbein (1941), see Figure 2-8 and Figure 2-10, respectively. The nomenclature used is that described in Chapter 2.



Figure 5-5: Photographs of particles (20mm, 28mm, 37.5mm & 50mm) taken from the Houghton Main specimens.



Figure 5-6: Photographs of particles (75mm) taken from the Houghton Main specimens.

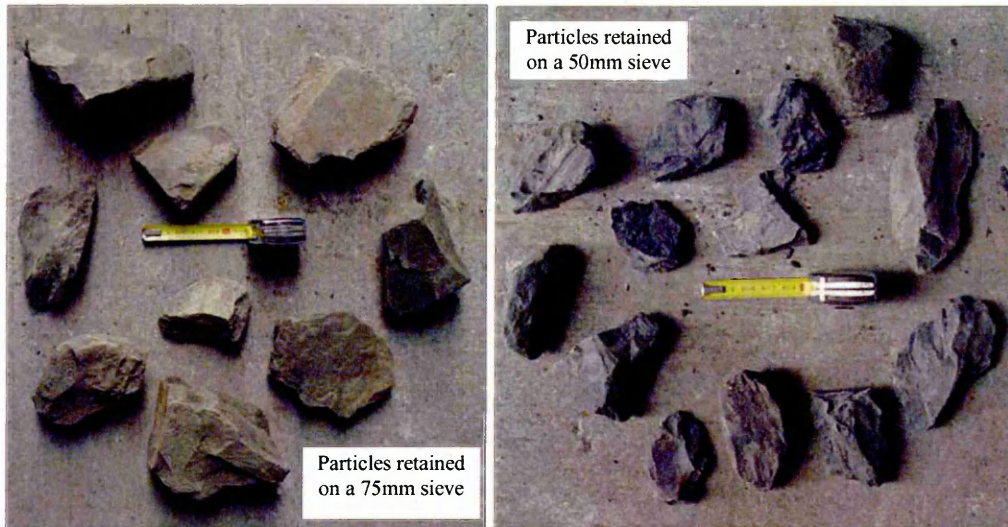


Figure 5-7: Photograph of particles (75mm & 50mm) taken from the Orgreave specimens

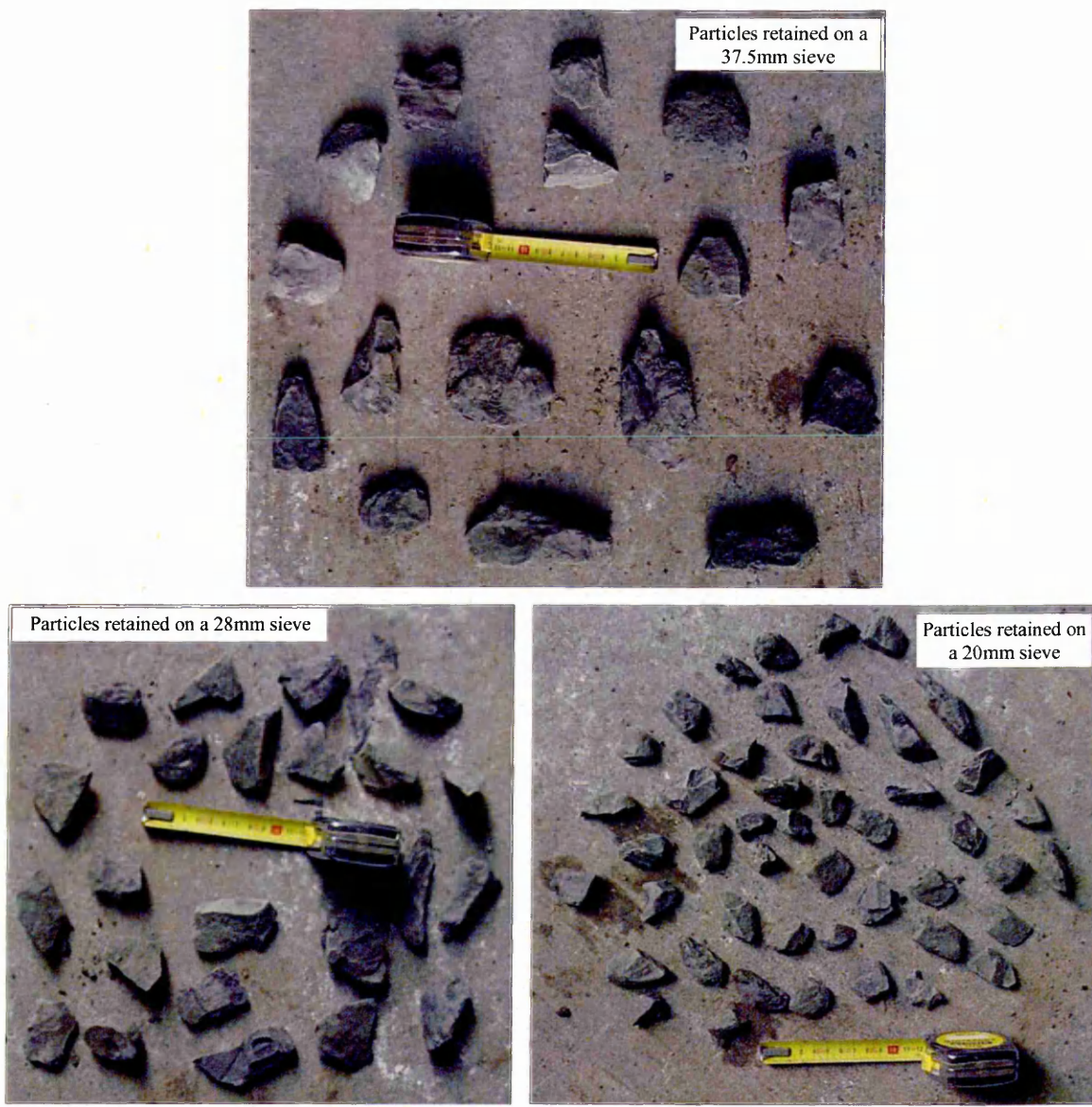


Figure 5-8: Photograph of particles taken from the Orgreave specimens.

5.4.1 Houghton Main Sample

Figure 5-9 summarises the findings of the particle shape analysis carried out for the Houghton Main specimen.

Particles of the Houghton Main material are generally equi-dimensional and occasionally disc shaped; smaller particles are often rod shaped and occasionally blade shaped.

The particles fall into the category 900 – 999 from the “roundness” chart (see Figure 2-10). This supports the particle shape description made to BS 5930:1999 in Section 5.1.1.

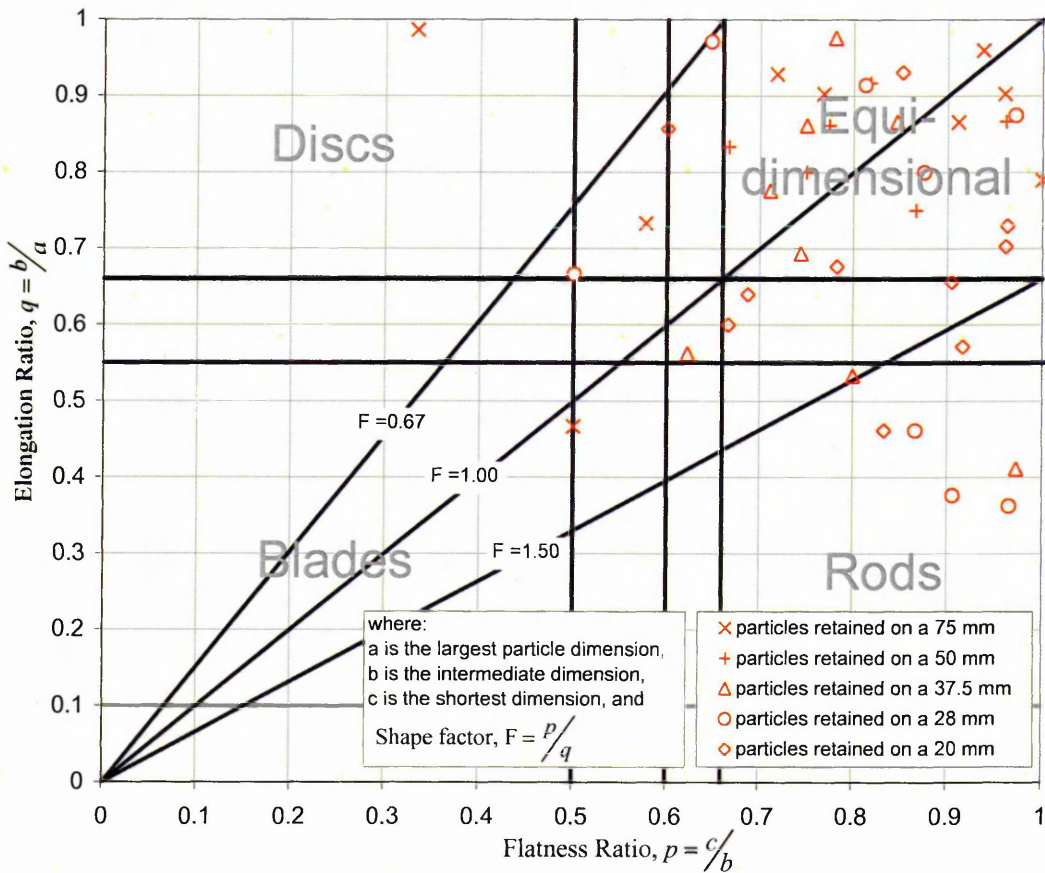


Figure 5-9: Distribution of particles from the Houghton specimen by shape factor.

5.4.2 Orgreave Sample

Figure 5-10 summarises the findings of the particle shape analysis carried out for the Houghton Main specimen.

Particles of the Orgreave material are predominately equi-dimensional and occasionally rod or blade shaped; smaller particles are often rods or blades and occasionally disc shaped.

The particles fall into the category 800 – 899 to 900 – 999 from the “roundness” chart (see Figure 2-10). This supports the particle shape description made to BS 5930:1999 in Section 5.1.2.

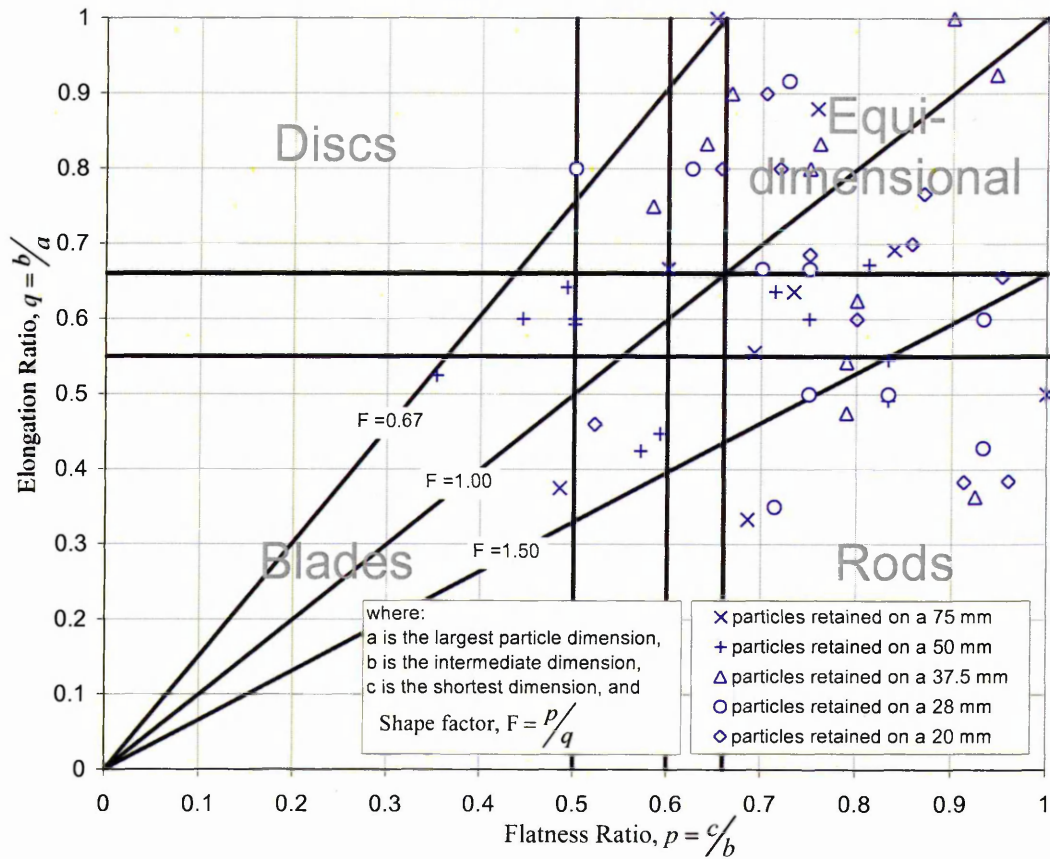


Figure 5-10: Distribution of particles from the Orgreave specimen by shape factor.

5.5 Moisture Content

Moisture content determinations for the samples from Houghton Main and Orgreave were made at the time of collection and were repeated throughout the period of storage. The oven-drying method as specified in BS 1377:Part 2:1990, as amended in the NCB Technical Memorandum (1971), was used to determine the moisture content.

The moisture content of the samples at the time of collection from Houghton Main and Orgreave were 5.7% and 6.7%, respectively.

5.6 Atterberg Limits

Atterberg limits determinations to BS 1377:Part 2:1990 were completed for the clay sized fraction of 4 sub-samples taken from the Houghton Main and Orgreave samples. The sample used in the determinations was material that had undergone size reduction during its excavation and processing. The following results were obtained:

| | Houghton Main Samples | Orgreave Samples |
|--------------------------|-------------------------------------|---------------------|
| Plastic Limit, PL | 21.3 % | 24.0 % |
| Liquid Limit, LL | 36.6 % | 37.6 % |
| Plastic Index, PI | 15.3 % | 13.6 % |
| Liquidity Index, LI | -1.3 % | -1.5 % |
| Plasticity description * | intermediate to low plasticity Clay | low plasticity Clay |

Table 5-2: Results of Atterberg limit determinations.

5.7 Standard Compaction Test

A suite of standard compaction testing was undertaken in order to provide an insight into the compaction behaviour of the materials. The 4.5 kg rammer method from BS 1377:Part 4, as amended in the NCB Technical Memorandum (1971), was employed and a summary of the results for the Houghton and Orgreave samples are presented in Figure 5-11 and Figure 5-12, respectively.

* After BS 5930:1999.

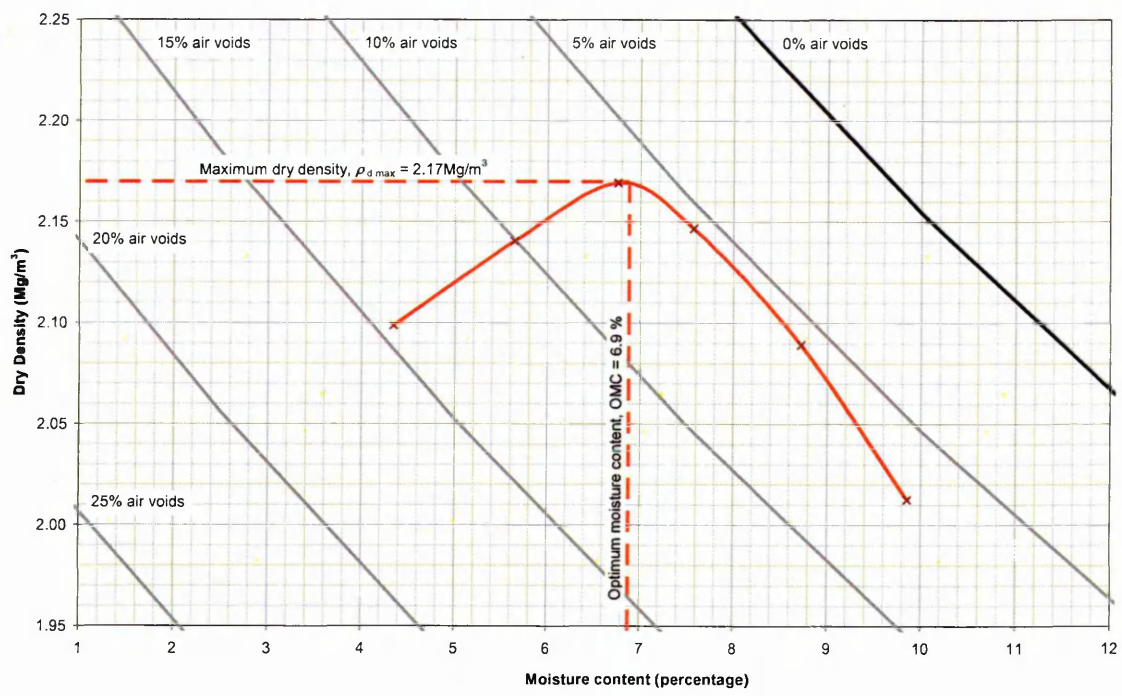


Figure 5-11: Graph of mean results from standard compaction testing of the Houghton Main Sample.

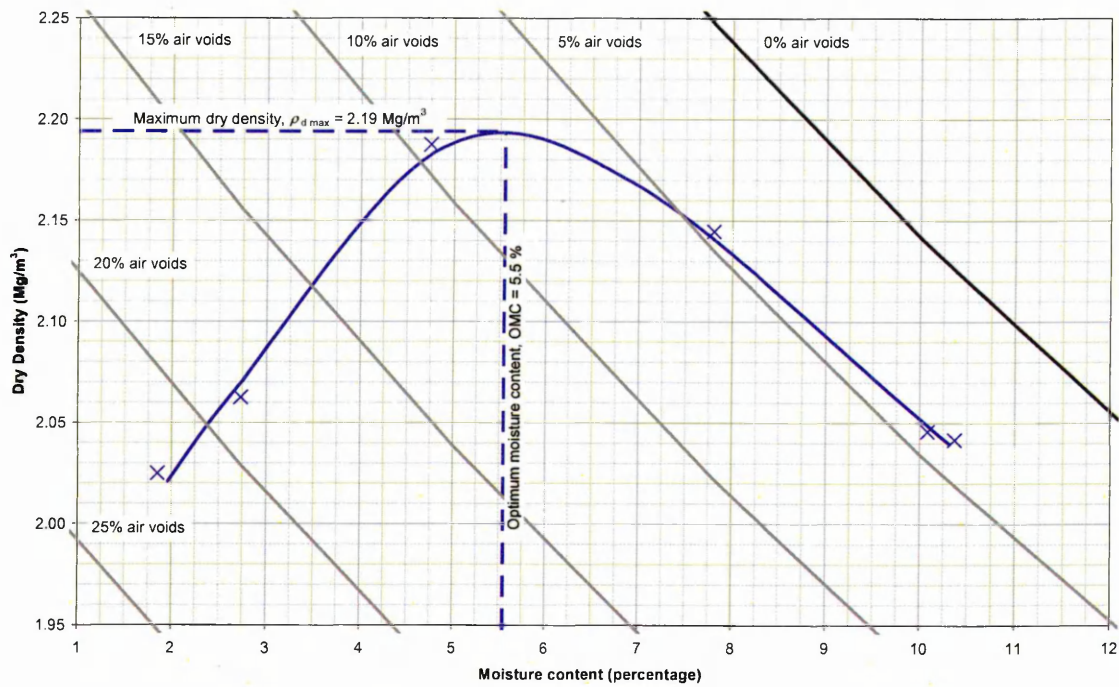


Figure 5-12: Graph of mean results from standard compaction testing of the Orgreave Sample.

6 Results and Analysis

6.1 Introduction

This chapter is split into three parts. The results of the laboratory work are presented first, along with the detailed specimen preparation data. The second part of the chapter presents selected images generated from the CT scanning and their analysis. A summary is provided at the end of each set of the detailed results. The final section is a summary and comparison of the two sets of results.

6.2 Laboratory Test Data

The detailed results for each test are presented here in their own sub-section. Each sub-section follows the same format and gives:

- a summary of the test including the specimen preparation and test variables.
- the specimen compaction details.
- a plot of measured displacement against time on a natural scale.
- a plot of measured strain against time on a decadic logarithmic scale.

The plots of displacement and strain against time present the two main pieces of information. As well as displacement or strain being plotted against time the applied stress is also plotted. The applied stress is shown in terms of the pressure of the hydraulic loading system (this information is labelled in the graph legend as “pressure”). This stress is also shown in terms of “corrected pressure” (and is labelled such in the graph legend). The “corrected pressure” refers to a correction made for losses due to side wall friction. The quantification of this correction is based on the reconnaissance investigation described in Section 4.1.3.2.

The plots of strain against the decadic logarithm of time allow the comparison of the test results with results from other studies, including field measurements.

Further, these plots provide a ready visualisation of the empirical value α , as defined by Sowers *et al.*

A summary of all of the testing results is given in Table 6-1 in Section 6.3.

6.2.1 Detailed results for Test 1

A summary of the variables used in Test 1 is shown below:

| Variables | | | | | |
|-----------|----------------------|-----------|--------------|--------------------|----------------------|
| Source | Compaction treatment | Cell type | Stress (kPa) | | Inundation condition |
| | | | Pressure | Corrected pressure | |
| Houghton | heavy | Large | 400 | 380 | Not inundated |

The displacement measured on the application of the applied pressure during the test is plotted against time on a natural scale on Figure 6-1. Figure 6-2 shows displacement as strain plotted against time on a \log_{10} scale.

During one of the Christmas holiday periods, a power failure occurred causing an unplanned unloading of the specimen. Also due the power failure, no displacement data was recorded for its duration. On the re-supply of power the specimen was automatically reloaded. However, the data recording system had been reset by the failure and so no data was collected from the period of reloading and no record of the duration of the failure was made.

So as to quantify the effects of this unplanned event an investigation into the effects of an unload / reload event was undertaken. Under controlled conditions the specimens under test were cycled through two unload / reload events and the effects on specimen volume change monitored. The results of this investigation can be seen in Figure 6-1 and Figure 6-2 for Test 1, Figure 6-9 and Figure 6-10 for Test 5, and Figure 6-13 and Figure 6-14 for Test 7.

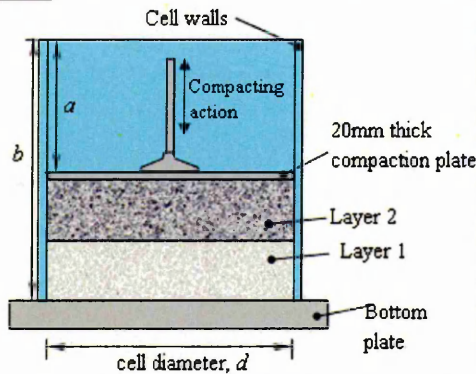
This test was terminated after 910 days of testing.

A summary of the testing results for this test and the other testing carried out is presented in Table 6-1.

Specimen compaction data

| Layer number | Layer | | Layer | | | Sample | | | |
|--------------|-----------|---------------------|----------------|------------------------------------|-----------------------------------|----------------|-----------|-----------------------------------|----------------------------------|
| | mass (kg) | dimension, a (mm) | thickness (mm) | bulk density* (Mg/m ³) | dry density* (Mg/m ³) | thickness (mm) | mass (kg) | bulk density (Mg/m ³) | dry density (Mg/m ³) |
| 1 | 67.5 | 824 | 152 | 1.60 | 1.51 | 152 | 67.5 | 1.60 | 1.51 |
| 2 | 65.9 | 709 | 116 | 2.05 | 1.94 | 267 | 133.4 | 1.79 | 1.70 |
| 3 | 66.2 | 573 | 135 | 1.76 | 1.66 | 403 | 199.7 | 1.78 | 1.68 |
| 4 | 67.6 | N/R | N/R | N/R | N/R | N/R | 267.2 | N/R | N/R |
| 5 | 72.4 | 313 | 260 | 1.94 | 1.83 | 663 | 339.6 | 1.84 | 1.74 |

NOTES:

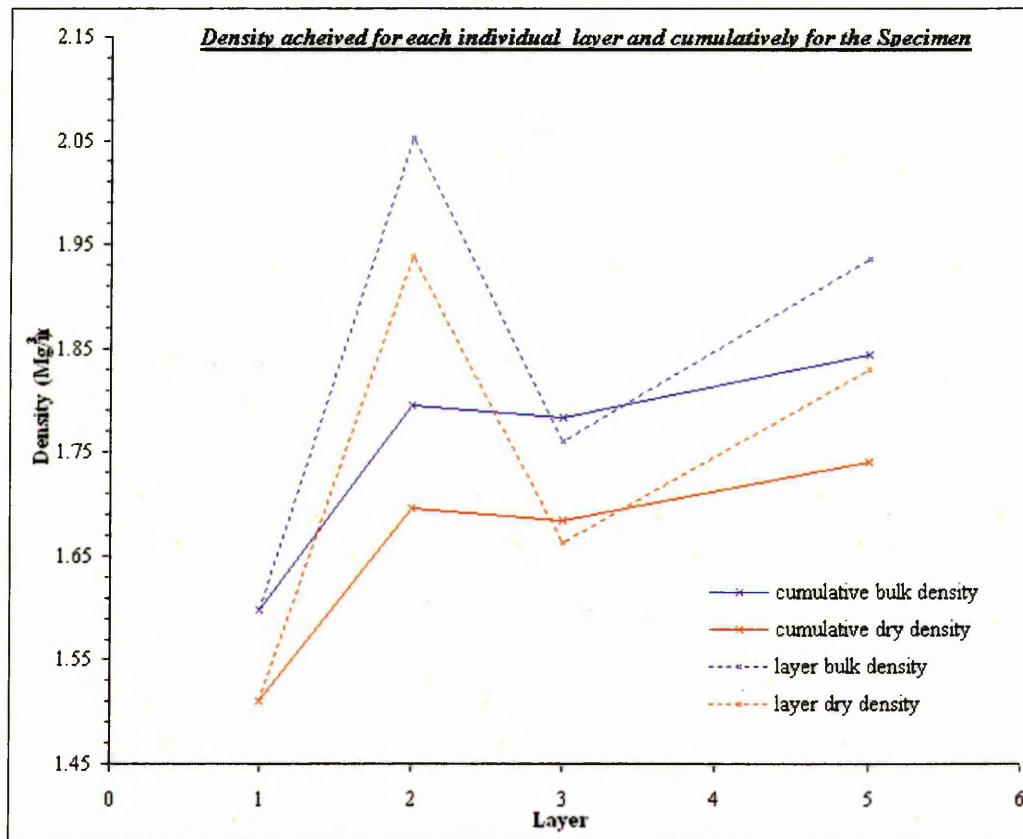


Specimen Moisture Content = 5.5%
 Cell diameter, d = 0.595 m
 Dimension, b = 996 mm

* It is assumed that the preceding layer was not further compacted in the calculation of these columns.

Compaction time - 4 minutes per layer

N/R - Not Recorded



6.2.1.2 Testing results (Test 1)

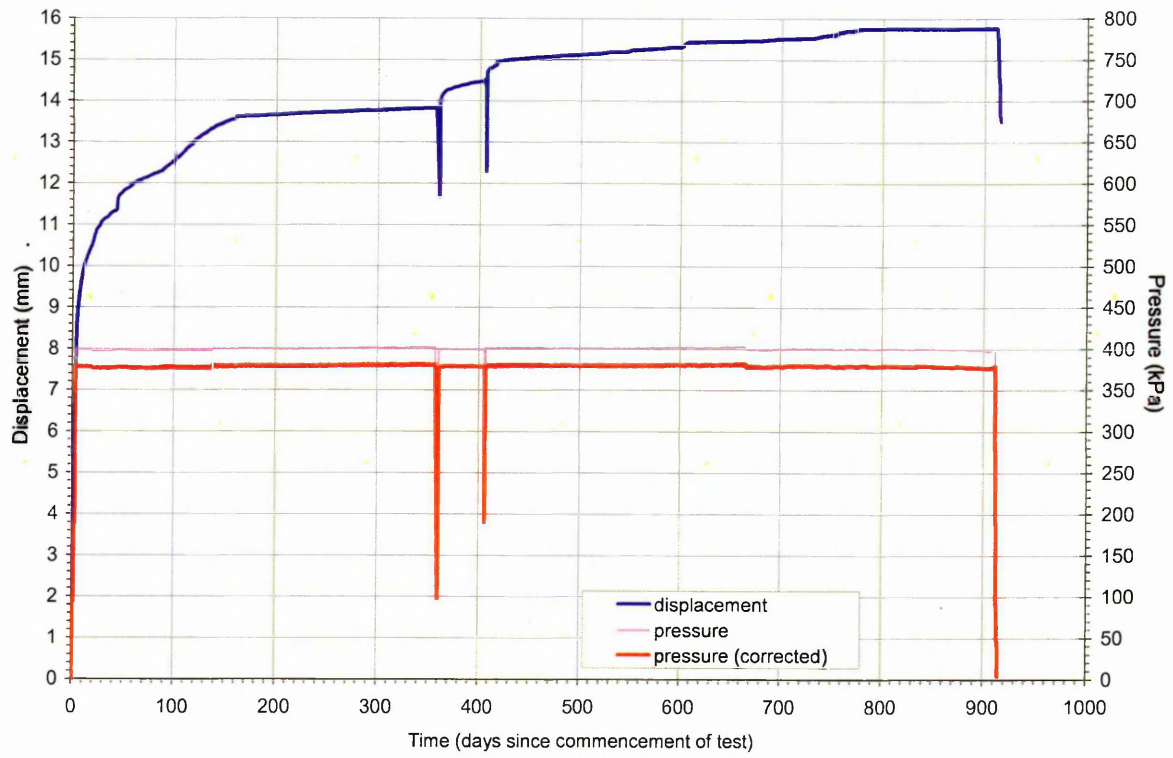


Figure 6-1: Graph of Pressure and Displacement against Time for Test 1.

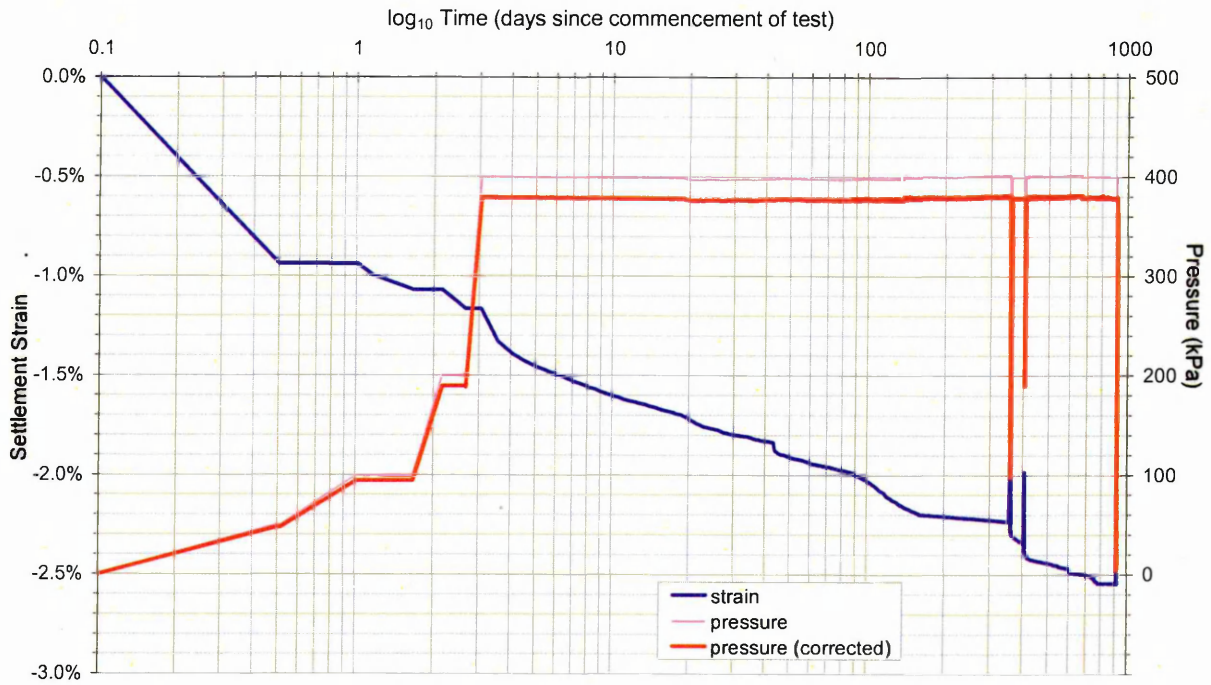


Figure 6-2: Graph of Pressure and Strain against \log_{10} Time for Test 1.

A summary of the variables used in Test 2 is shown below:

| Variables | | | | | |
|-----------|----------------------|-----------|--------------|--------------------|----------------------|
| Source | Compaction treatment | Cell type | Stress (kPa) | | Inundation condition |
| | | | Pressure | Corrected pressure | |
| Orgreave | heavy | Large | 400 | 380 | Inundated |

Following the loading of the specimen with a cell pressure of 400kPa the diaphragm failed, the water held within the diaphragm then inundated the specimen to saturation.

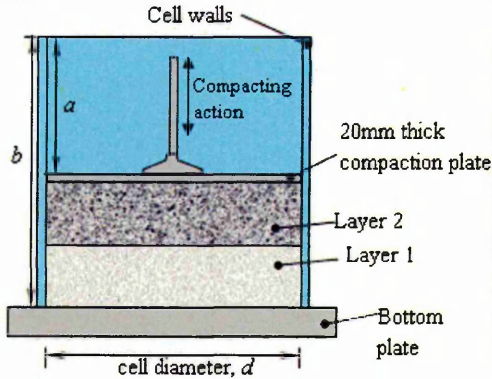
Following replacement of the failed diaphragm the inundated specimen was then reloaded. The displacement measured on the application of the applied pressure during the test is plotted against time on a natural scale on Figure 6-3. Figure 6-4 shows displacement as strain plotted against time on a \log_{10} scale. Only records of the post inundation loading are presented in Figure 6-3 and Figure 6-4.

This test was terminated after 170 days of testing.

Specimen compaction data

| Layer number | Layer | | Layer | | | Sample | | | |
|--------------|-----------|---------------------|----------------|----------------------------|---------------------------|----------------|-----------|---------------------------|--------------------------|
| | mass (kg) | dimension, a (mm) | thickness (mm) | bulk density* (Mg/m^3) | dry density* (Mg/m^3) | thickness (mm) | mass (kg) | bulk density (Mg/m^3) | dry density (Mg/m^3) |
| 1 | 70.3 | 851 | 129 | 1.96 | 1.82 | 129 | 70.3 | 1.96 | 1.82 |
| 2 | 70.9 | 715 | 136 | 1.87 | 1.74 | 265 | 141.2 | 1.91 | 1.78 |
| 3 | 69.9 | 594 | 121 | 2.07 | 1.93 | 387 | 211.1 | 1.96 | 1.82 |
| 4 | 71.4 | 468 | 126 | 2.04 | 1.89 | 513 | 282.5 | 1.98 | 1.84 |
| 5 | 70.4 | 335 | 133 | 1.91 | 1.77 | 645 | 353.0 | 1.97 | 1.83 |

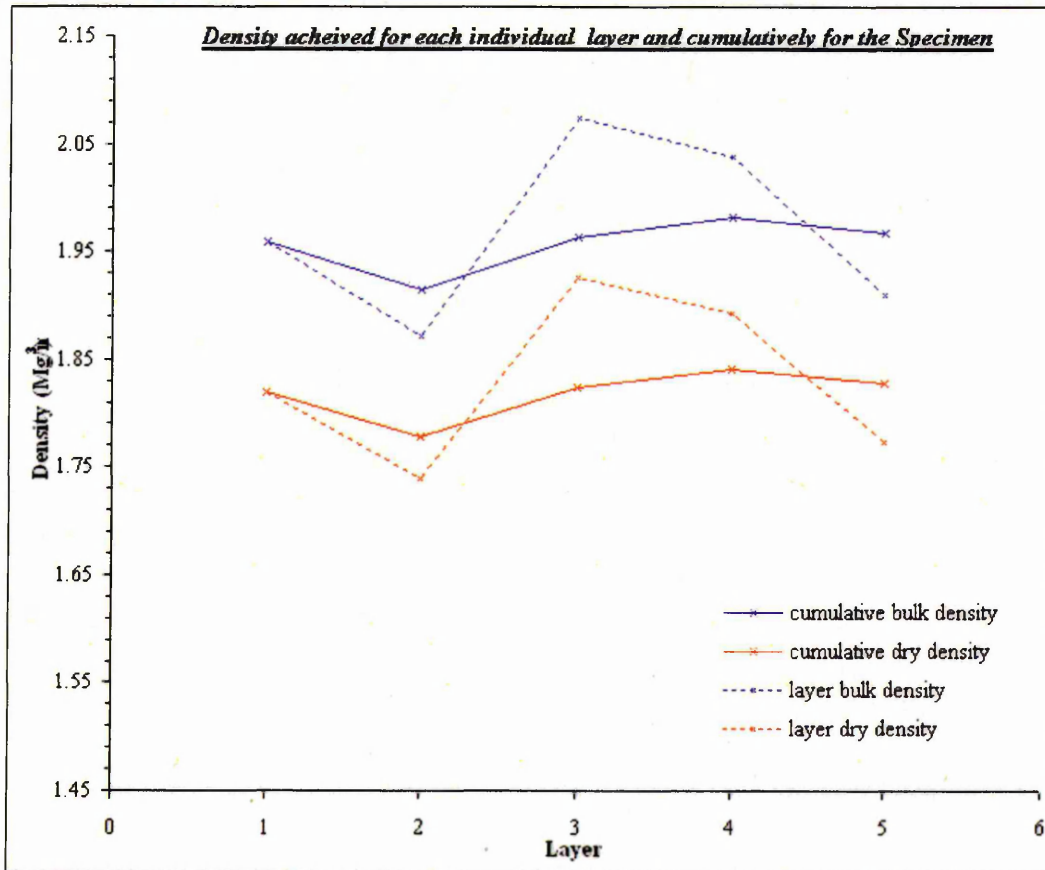
NOTES:



Specimen Moisture Content = 7.1%
 Cell diameter, d = 0.595 m
 Dimension, b = 1000 mm

* It is assumed that the preceding layer was not further compacted in the calculation of these columns.

Compaction time - 4 minutes per layer



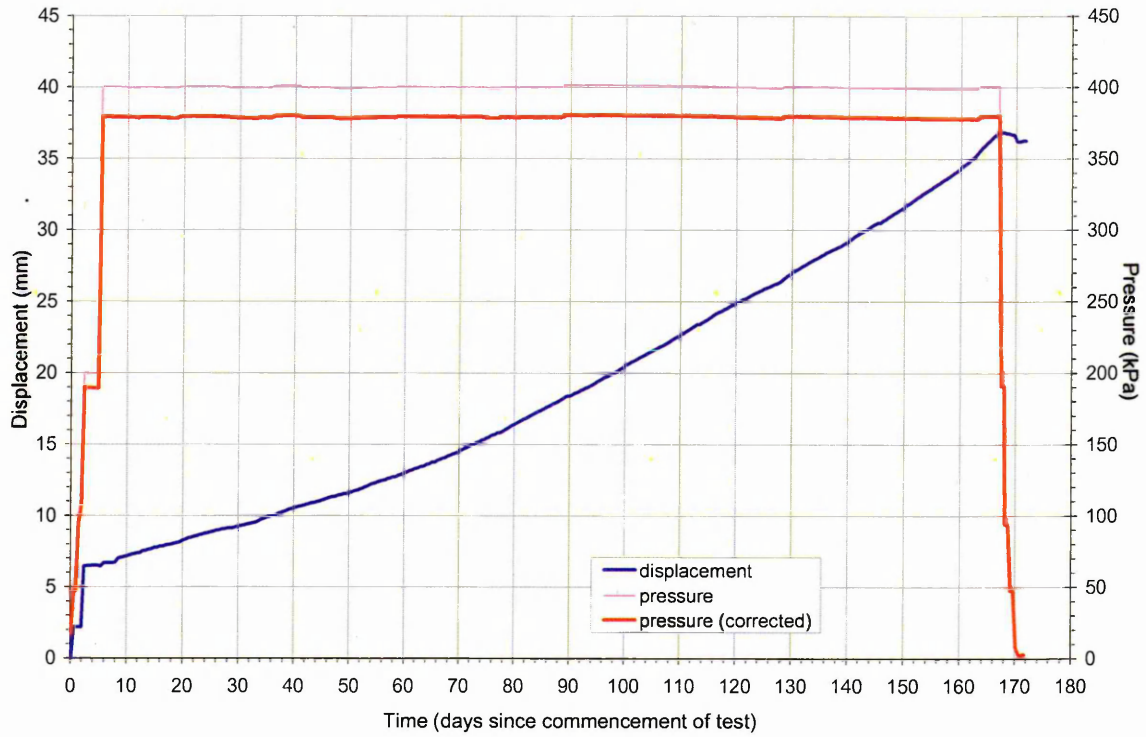


Figure 6-3: Graph of Pressure and Displacement against Time for Test 2.

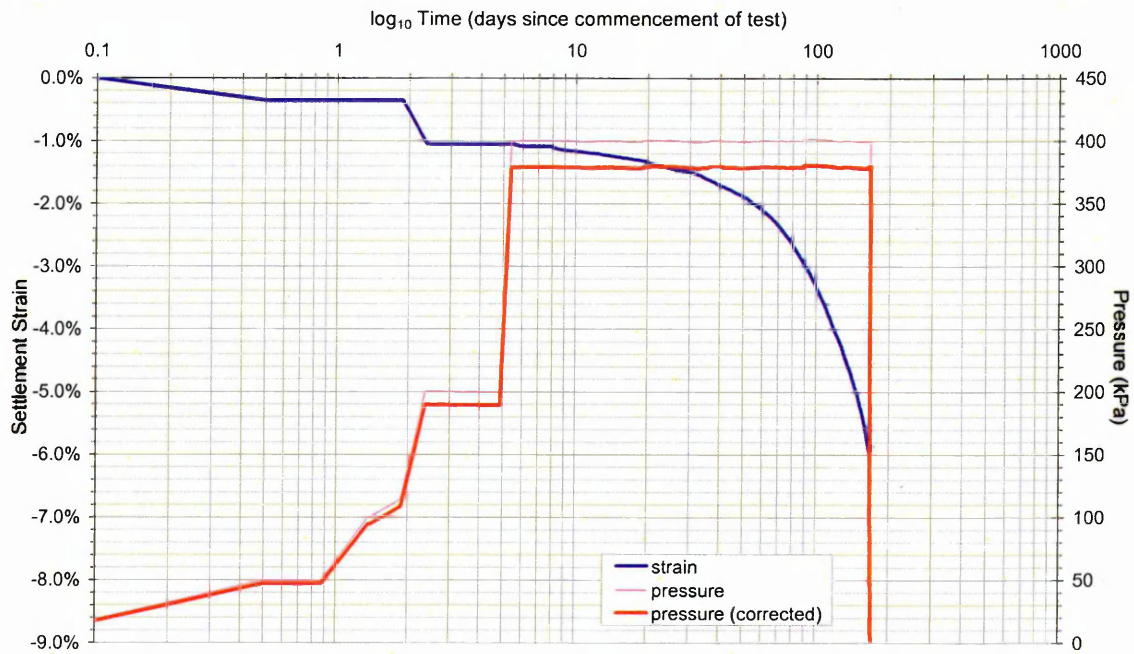


Figure 6-4: Graph of Pressure and Strain against \log_{10} Time for Test 2.

6.2.3 Detailed results for Test 3

A summary of the variables used in Test 3 is shown below:

| Variables | | | | | |
|-----------|----------------------|-----------|--------------|--------------------|-------------------------|
| Source | Compaction treatment | Cell type | Stress (kPa) | | Inundation condition |
| | | | Pressure | Corrected pressure | |
| Houghton | light | Large | 400 | 380 | Inundated after 11 days |

Following a period of 11 days of maintained loading the specimen was inundated. The procedure for this controlled inundation is outlined in Section 3.1.3.2.

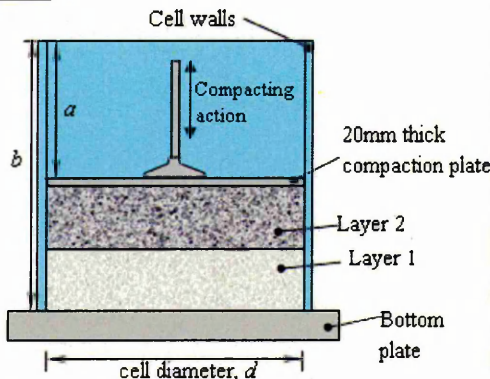
The displacement measured on the application of the applied pressure and inundation during the test is plotted against time on a natural scale on Figure 6-5. Figure 6-6 shows displacement as strain plotted against time on a \log_{10} scale.

This test was terminated after 94 days of testing.

Specimen compaction data

| Layer number | Layer | | Layer | | | Sample | | | |
|--------------|-----------|---------------------|----------------|----------------------------|---------------------------|----------------|-----------|---------------------------|--------------------------|
| | mass (kg) | dimension, a (mm) | thickness (mm) | bulk density* (Mg/m^3) | dry density* (Mg/m^3) | thickness (mm) | mass (kg) | bulk density (Mg/m^3) | dry density (Mg/m^3) |
| 1 | 104.2 | 762 | 215 | 1.74 | 1.63 | 215 | 104.2 | 1.74 | 1.63 |
| 2 | 104.9 | 556 | 206 | 1.83 | 1.71 | 421 | 209.1 | 1.79 | 1.67 |
| 3 | 107.6 | 333 | 223 | 1.73 | 1.62 | 644 | 316.6 | 1.77 | 1.65 |
| 4 | N/A | N/A | N/A | N/A | N/A | N/A | N/A | N/A | N/A |
| 5 | N/A | N/A | N/A | N/A | N/A | N/A | N/A | N/A | N/A |

NOTES:

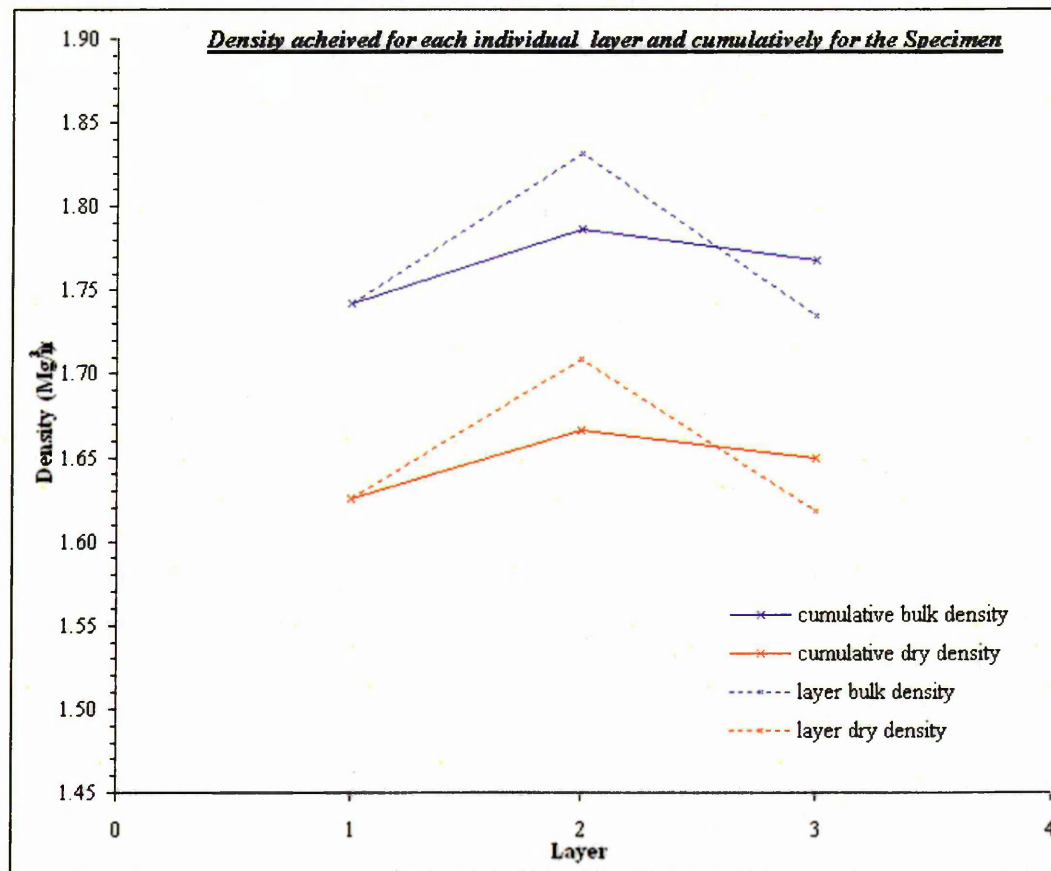


Specimen Moisture Content = 6.7%
 Cell diameter, d = 0.595 m
 Dimension, b = 997 mm

* It is assumed that the preceding layer was not further compacted in the calculation of these columns.

Compaction time - 4 minutes per layer

N/A - Not Applicable



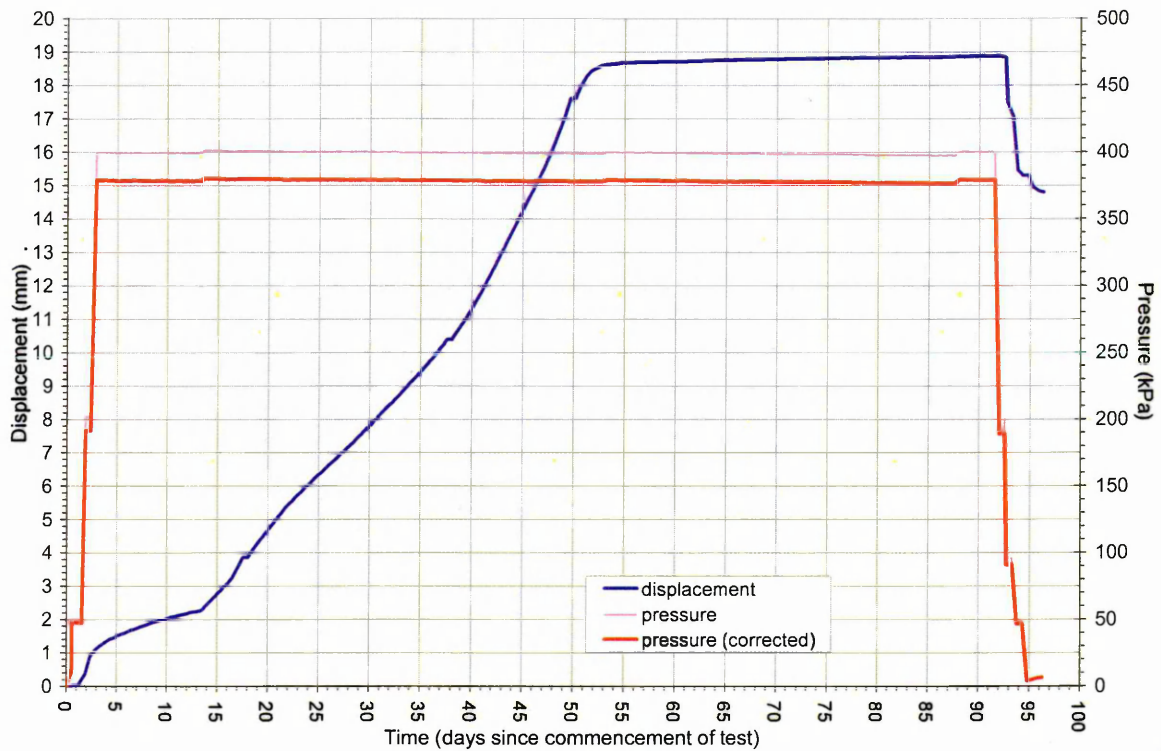


Figure 6-5: Graph of Pressure and Displacement against Time for Test 3.

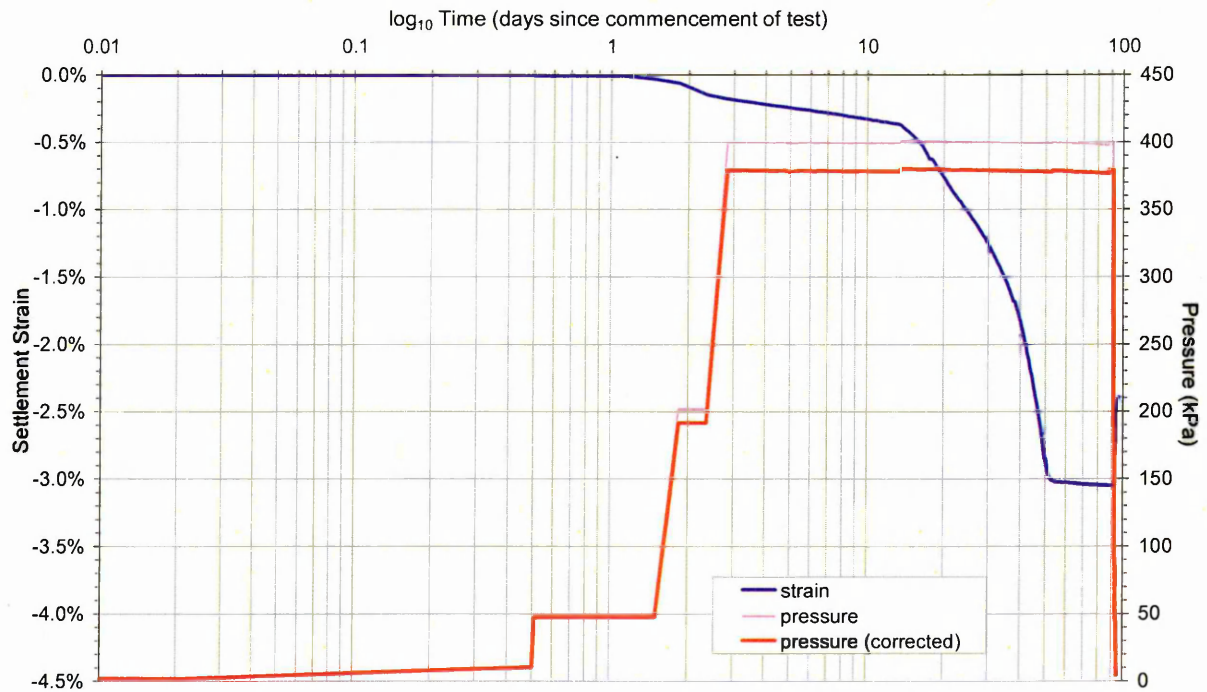


Figure 6-6: Graph of Pressure and Strain against \log_{10} Time for Test 3.

A summary of the variables used in Test 4 is shown below:

| Variables | | | | | |
|-----------|----------------------|-----------|--------------|--------------------|-------------------------|
| Source | Compaction treatment | Cell type | Stress (kPa) | | Inundation condition |
| | | | Pressure | Corrected pressure | |
| Houghton | light | Large | 400 | 380 | Inundated after 14 days |

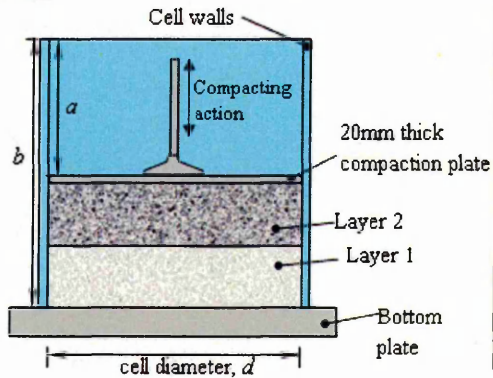
Following a period of 14 days of maintained loading the specimen was inundated. The procedure for this controlled inundation is outlined in Section 3.1.3.2.

The displacement measured on the application of the applied pressure and inundation during the test is plotted against time on a natural scale on Figure 6-7. Figure 6-8 shows displacement as strain plotted against time on a \log_{10} scale.

This test was terminated after 116 days of testing.

Specimen compaction data

| Layer | | dimension, a (mm) | Layer | | | Sample | | | |
|--------|--------------|------------------------|-------------------|---------------------------------------|--------------------------------------|-------------------|--------------|--------------------------------------|-------------------------------------|
| number | mass (kg) | | thickness (mm) | bulk density* (Mg/m ³) | dry density* (Mg/m ³) | thickness (mm) | mass (kg) | bulk density (Mg/m ³) | dry density (Mg/m ³) |
| 1 | 104.9 | 780 | 200 | 1.89 | 1.79 | 200 | 104.9 | 1.89 | 1.79 |
| 2 | 102.2 | 558 | 222 | 1.66 | 1.57 | 422 | 207.1 | 1.77 | 1.68 |
| 3 | 106.8 | 332 | 226 | 1.70 | 1.62 | 647 | 313.9 | 1.74 | 1.66 |
| 4 | N/A | N/A | N/A | N/A | N/A | N/A | N/A | N/A | N/A |
| 5 | N/A | N/A | N/A | N/A | N/A | N/A | N/A | N/A | N/A |

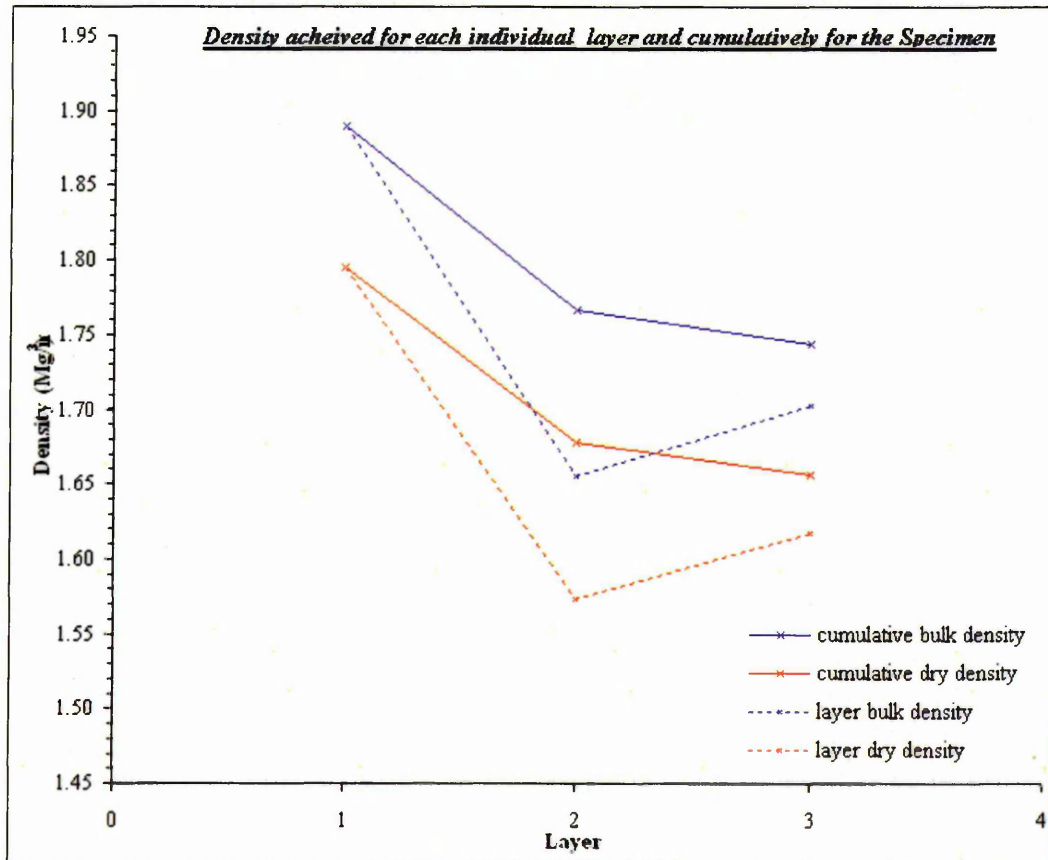
NOTES:

Specimen Moisture Content = 5.0%
 Cell diameter, d = 0.595 m
 Dimension, b = 999 mm

* It is assumed that the preceding layer was not further compacted in the calculation of these columns.

Compaction time - 4 minutes per layer

N/A - Not Applicable



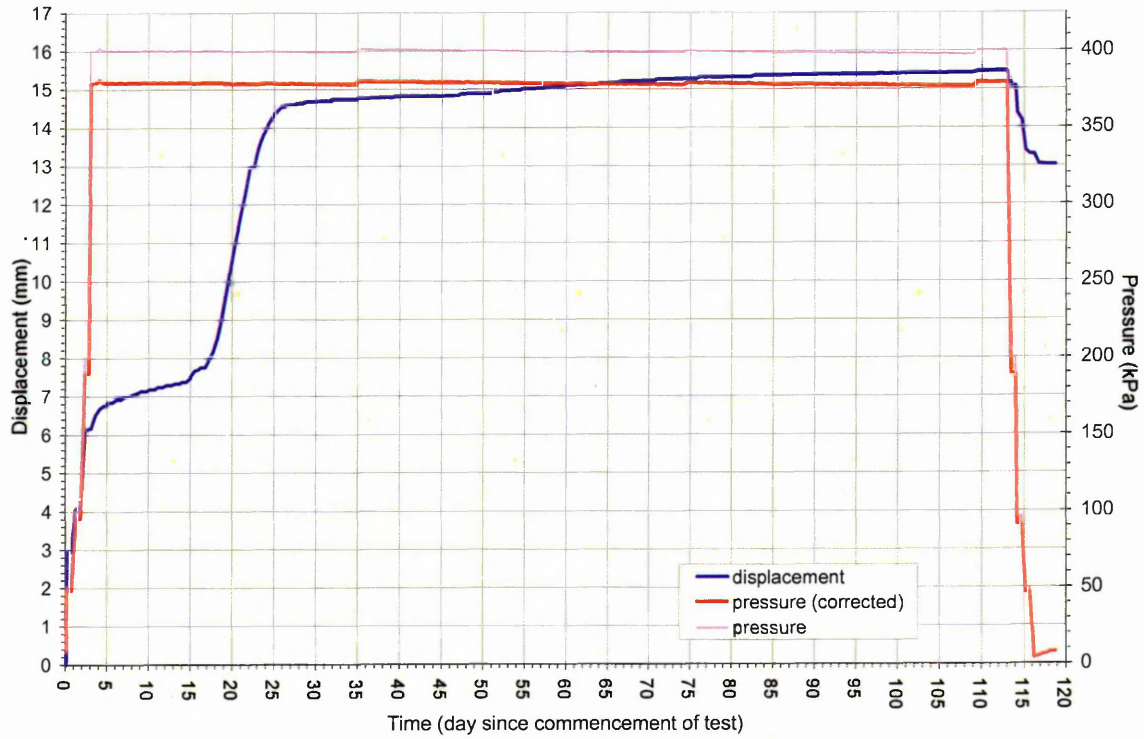


Figure 6-7: Graph of Pressure and Displacement against Time for Test 4.

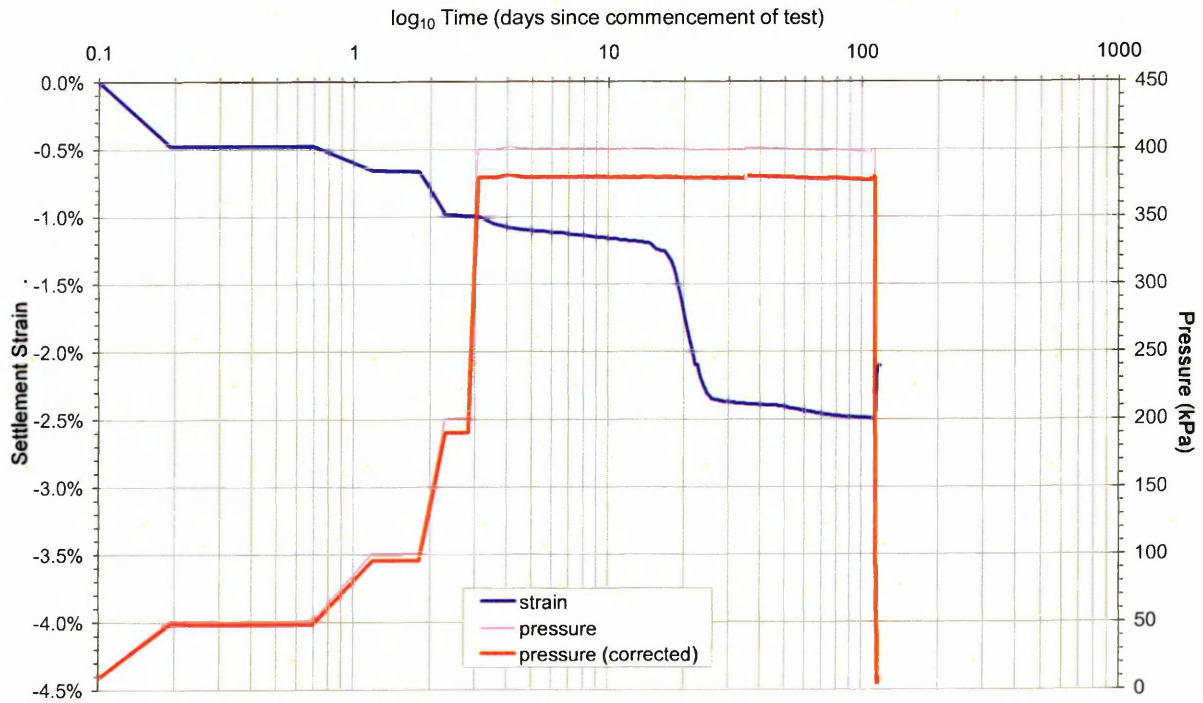


Figure 6-8: Graph of Pressure and Strain against \log_{10} Time for Test 4.

6.2.5 Detailed results for Test 5

A summary of the variables used in Test 5 is shown below:

| Variables | | | | | |
|-----------|----------------------|-----------|--------------|--------------------|----------------------|
| Source | Compaction treatment | Cell type | Stress (kPa) | | Inundation condition |
| | | | Pressure | Corrected pressure | |
| Houghton | light | Small | 400 | 395 | Not inundated |

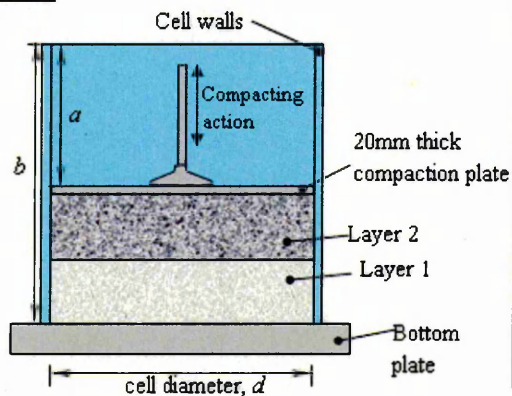
The displacement measured on the application of the applied pressure during the test is plotted against time on a natural scale on Figure 6-9. Figure 6-10 shows displacement as strain plotted against time on a \log_{10} scale.

This test was running at the same time as Test 1, and was subject to the power failure that occurred during on of the Christmas holiday periods. Further details of the failure and its effects are given in Section 6.2.1 for Test 1 and are applicable to this test.

This test was terminated after 680 days of testing.

Specimen compaction data

| Layer | | dimension, a (mm) | Layer | | | Sample | | | |
|--------|--------------|------------------------|-------------------|---------------------------------------|--------------------------------------|-------------------|--------------|--------------------------------------|-------------------------------------|
| number | mass (kg) | | thickness (mm) | bulk density* (Mg/m ³) | dry density* (Mg/m ³) | thickness (mm) | mass (kg) | bulk density (Mg/m ³) | dry density (Mg/m ³) |
| 1 | 11.3 | 273 | 149 | 1.75 | 1.67 | 149 | 11.3 | 1.75 | 1.67 |
| 2 | 10.9 | 132 | 141 | 1.78 | 1.70 | 290 | 22.2 | 1.77 | 1.68 |
| 3 | N/A | N/A | N/A | N/A | N/A | N/A | N/A | N/A | N/A |
| 4 | N/A | N/A | N/A | N/A | N/A | N/A | N/A | N/A | N/A |
| 5 | N/A | N/A | N/A | N/A | N/A | N/A | N/A | N/A | N/A |

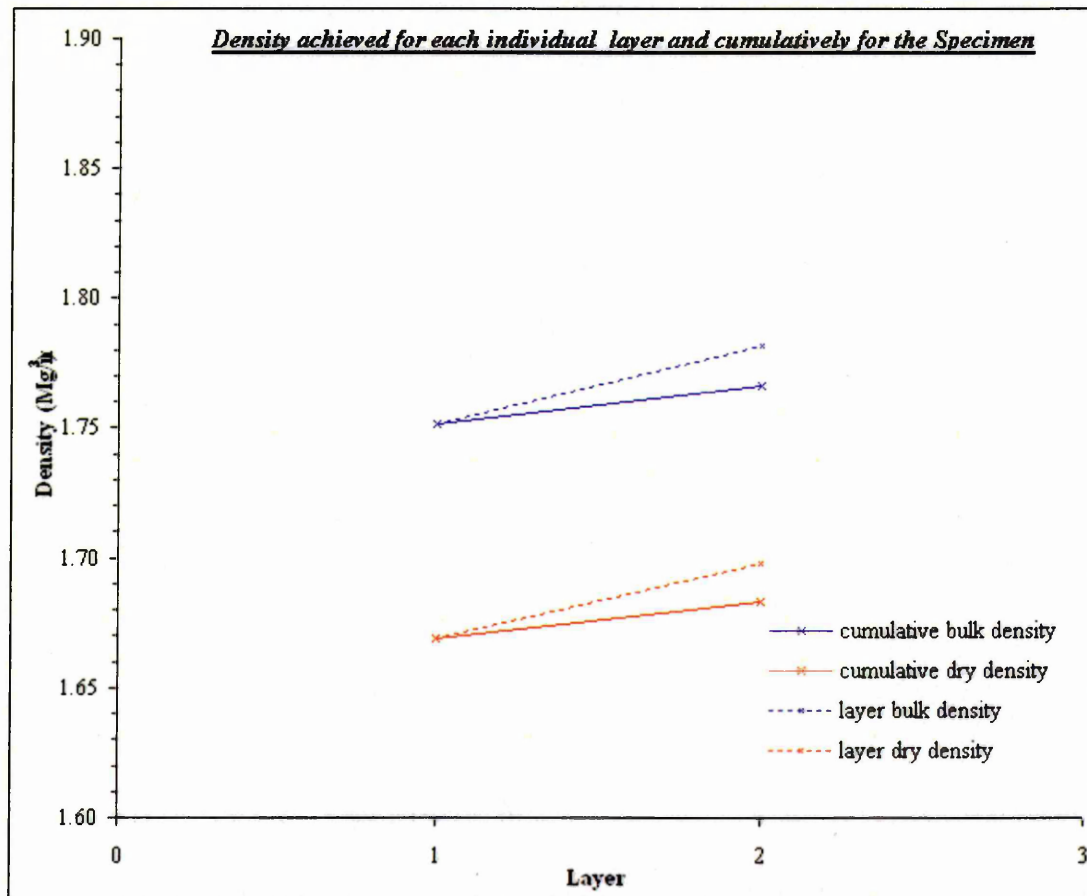
NOTES:

Specimen Moisture Content = 4.7%
 Cell diameter, d = 0.235 m
 Dimension, b = 442 mm

* It is assumed that the preceding layer was not further compacted in the calculation of these columns.

Compaction time - 3 minutes per layer

N/A - Not Applicable



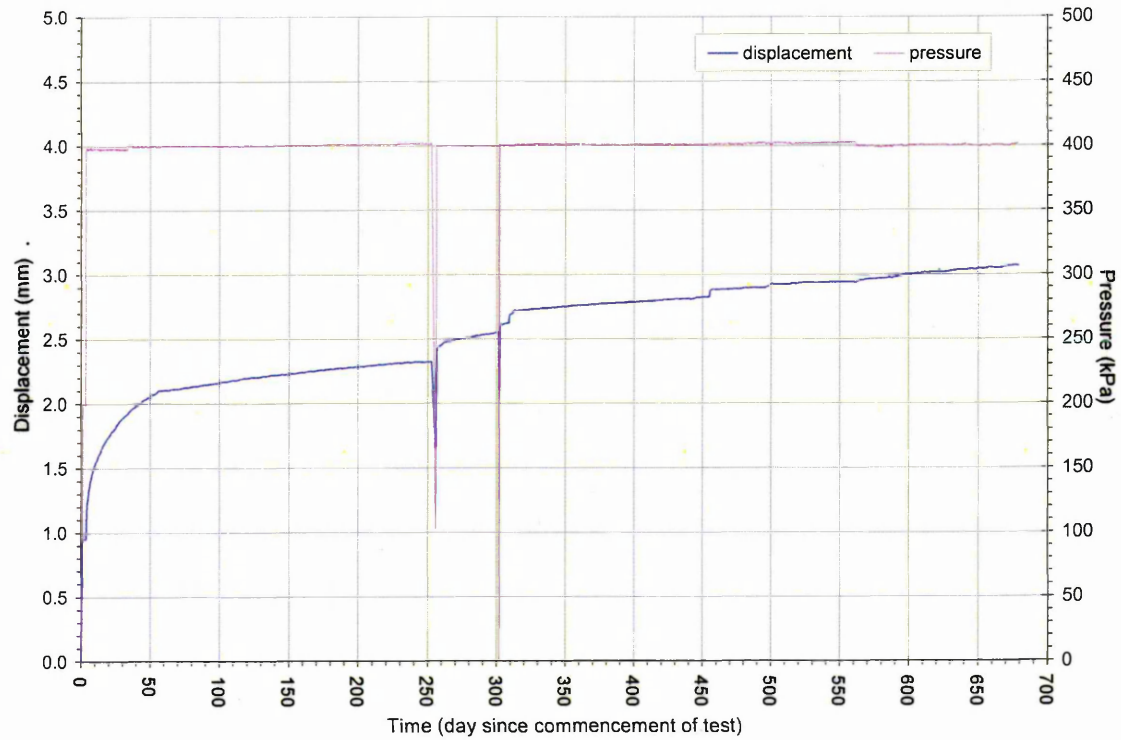


Figure 6-9: Graph of Pressure and Displacement against Time for Test 5.

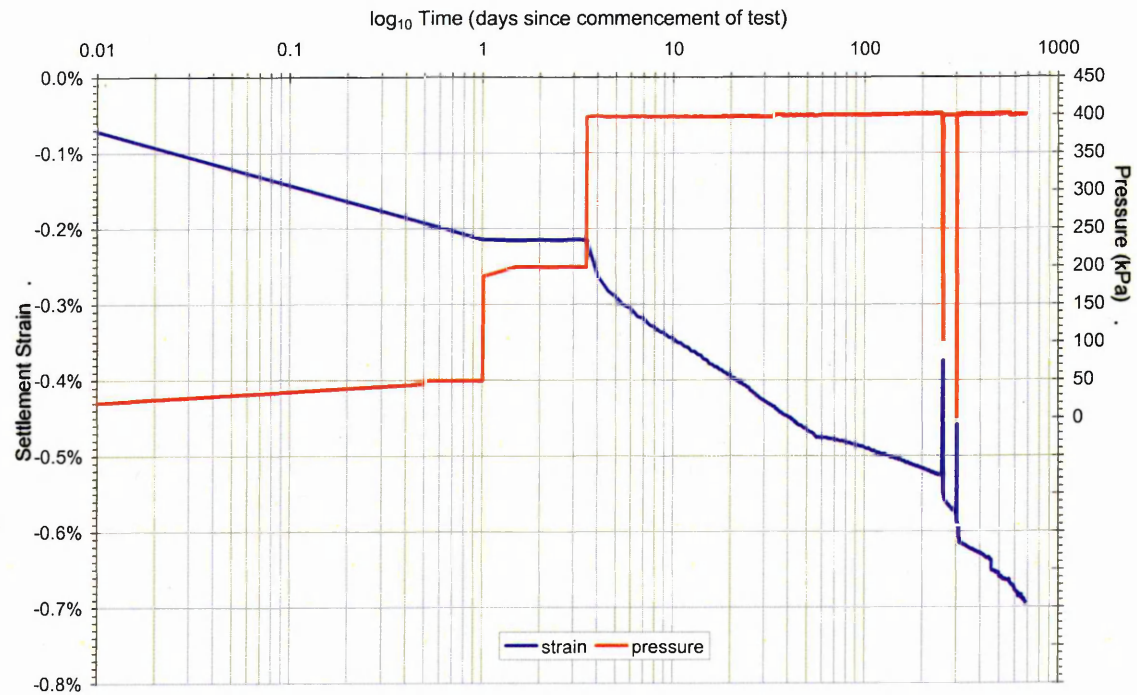


Figure 6-10: Graph of Pressure and Strain against \log_{10} Time for Test 5.

6.2.6 Detailed results for Test 6

A summary of the variables used in Test 6 is shown below:

| Variables | | | | | |
|-----------|----------------------|-----------|--------------|--------------------|----------------------|
| Source | Compaction treatment | Cell type | Stress (kPa) | | Inundation condition |
| | | | Pressure | Corrected pressure | |
| Ogreave | light | Small | 400 | 395 | Not inundated |

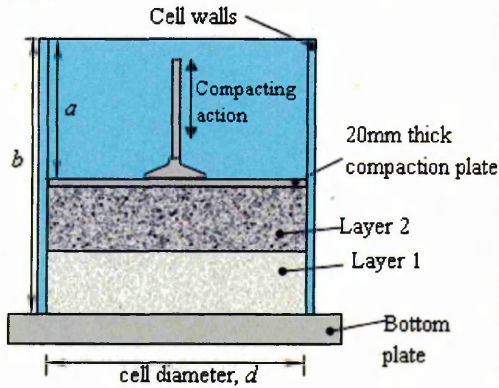
The displacement measured on the application of the applied pressure during the test is plotted against time on a natural scale on Figure 6-11. Figure 6-12 shows displacement as strain plotted against time on a \log_{10} scale.

This test was terminated after 120 days of testing.

Specimen compaction data

| Layer | | dimension, a (mm) | Layer | | | Sample | | | |
|--------|--------------|------------------------|-------------------|---------------------------------------|--------------------------------------|-------------------|--------------|--------------------------------------|-------------------------------------|
| number | mass (kg) | | thickness (mm) | bulk density* (Mg/m ³) | dry density* (Mg/m ³) | thickness (mm) | mass (kg) | bulk density (Mg/m ³) | dry density (Mg/m ³) |
| 1 | 11.0 | 280 | 141 | 1.80 | 1.68 | 141 | 11.0 | 1.80 | 1.68 |
| 2 | 11.1 | 136 | 144 | 1.78 | 1.65 | 285 | 22.1 | 1.79 | 1.67 |
| 3 | N/A | N/A | N/A | N/A | N/A | N/A | N/A | N/A | N/A |
| 4 | N/A | N/A | N/A <td N/A | N/A | N/A | N/A | N/A | N/A | |
| 5 | N/A | N/A | N/A | N/A | N/A | N/A | N/A | N/A | N/A |

NOTES:

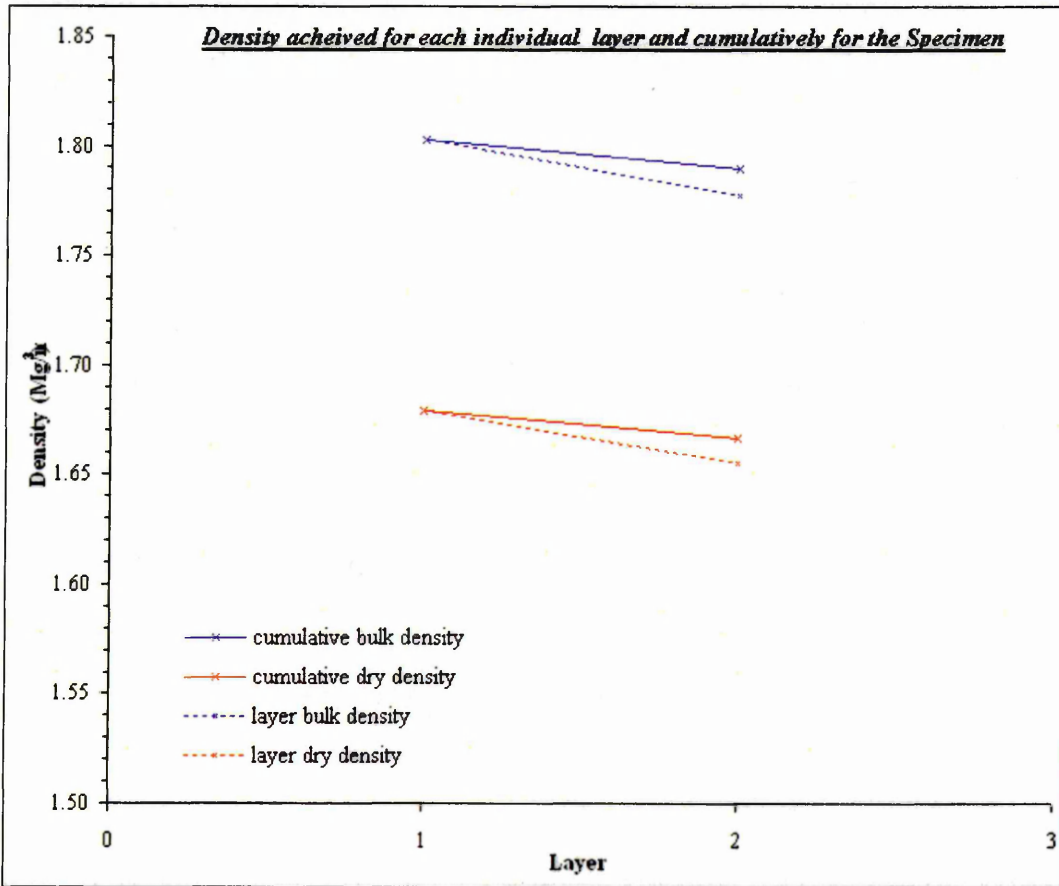


Specimen Moisture Content = 6.9%
 Cell diameter, d = 0.235 m
 Dimension, b = 441 mm

* It is assumed that the preceding layer was not further compacted in the calculation of these columns.

Compaction time - 3 minutes per layer

N/A - Not Applicable



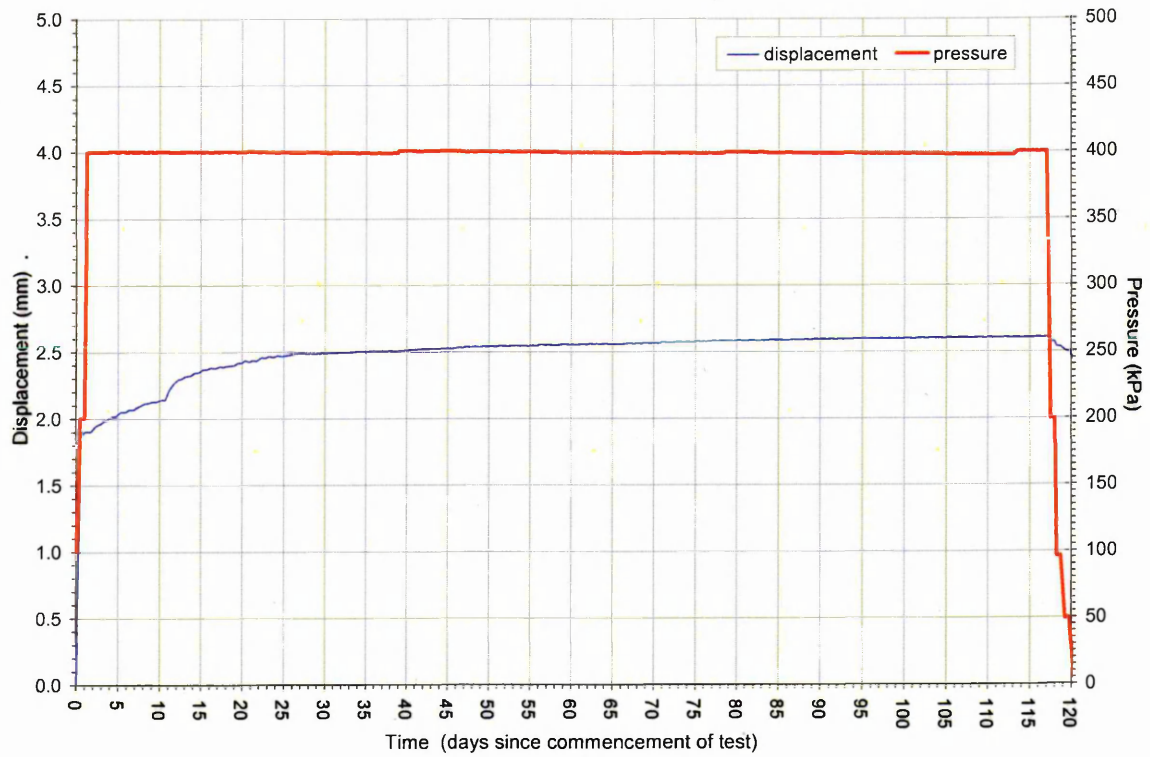


Figure 6-11: Graph of Pressure and Displacement against Time for Test 6.

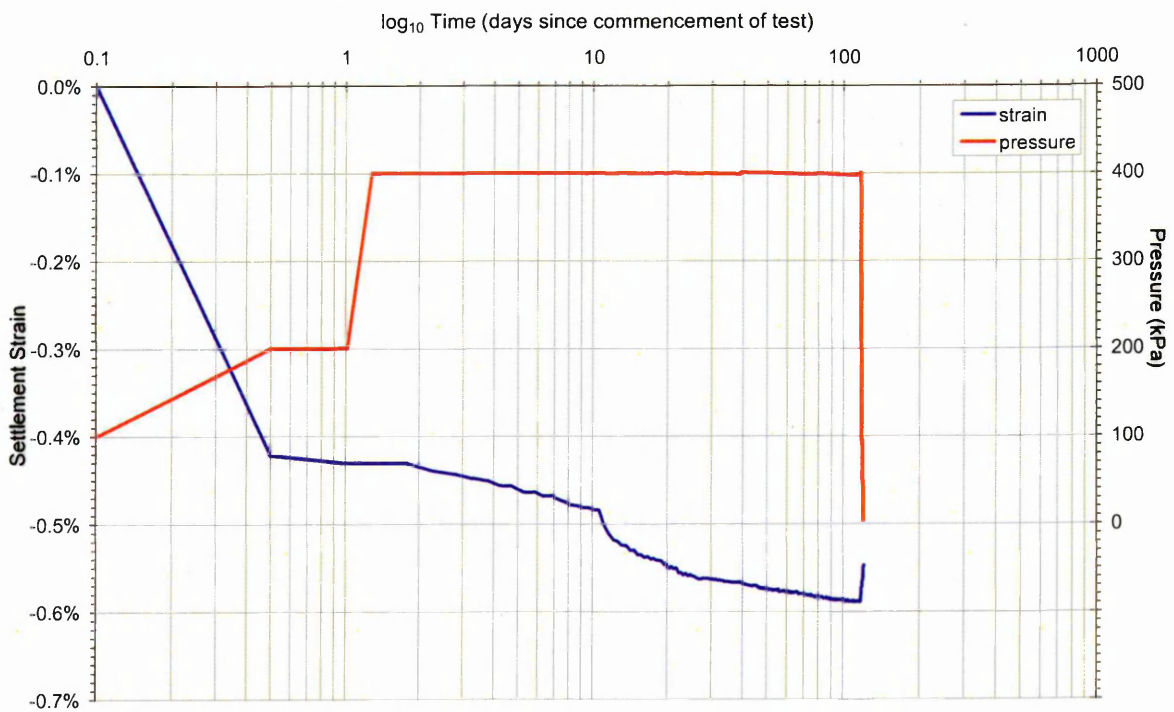


Figure 6-12: Graph of Pressure and Strain against \log_{10} Time for Test 6.

6.2.7 Detailed results for Test 7

A summary of the variables used in Test 7 is shown below:

| Variables | | | | | |
|-----------|----------------------|-----------|--------------|--------------------|----------------------|
| Source | Compaction treatment | Cell type | Stress (kPa) | | Inundation condition |
| | | | Pressure | Corrected pressure | |
| Houghton | light | Small | 400 | 395 | Not inundated |

The displacement measured on the application of the applied pressure during the test is plotted against time on a natural scale on Figure 6-13. Figure 6-14 shows displacement as strain plotted against time on a \log_{10} scale.

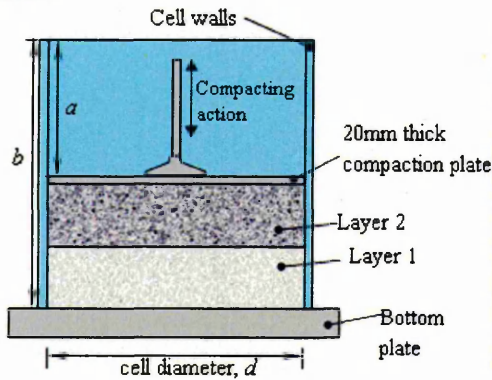
This test was running at the same time as Test 1 and Test 5, and was subject to the power failure that occurred during on of the Christmas holiday periods. Further details of the failure and its effects are given in Section 6.2.1 for Test 1 and are applicable to this test.

This test was terminated after 680 days of testing.

Specimen compaction data

| Layer | | dimension, a (mm) | Layer | | | Sample | | | |
|--------|--------------|------------------------|-------------------|---------------------------------------|--------------------------------------|-------------------|--------------|--------------------------------------|-------------------------------------|
| number | mass (kg) | | thickness (mm) | bulk density* (Mg/m ³) | dry density* (Mg/m ³) | thickness (mm) | mass (kg) | bulk density (Mg/m ³) | dry density (Mg/m ³) |
| 1 | 11.0 | 279 | 141 | 1.79 | 1.70 | 141 | 11.0 | 1.79 | 1.70 |
| 2 | 11.1 | 130 | 149 | 1.72 | 1.64 | 290 | 22.0 | 1.75 | 1.67 |
| 3 | N/A | N/A | N/A | N/A | N/A | N/A | N/A | N/A | N/A |
| 4 | N/A | N/A | N/A <td N/A | N/A | N/A | N/A | N/A | N/A | |
| 5 | N/A | N/A | N/A | N/A | N/A | N/A | N/A | N/A | N/A |

NOTES:

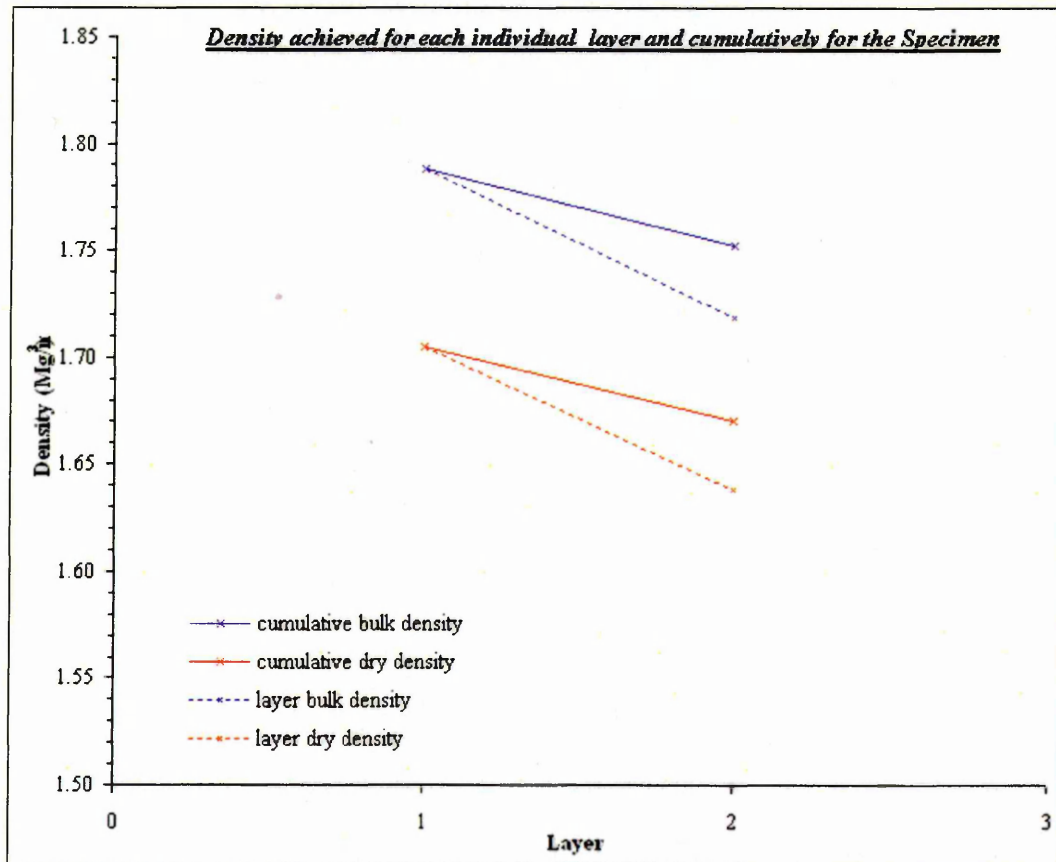


Specimen Moisture Content = 4.7%
 Cell diameter, d = 0.235 m
 Dimension, b = 440 mm

* It is assumed that the preceding layer was not further compacted in the calculation of these columns.

Compaction time - 3 minutes per layer

N/A - Not Applicable



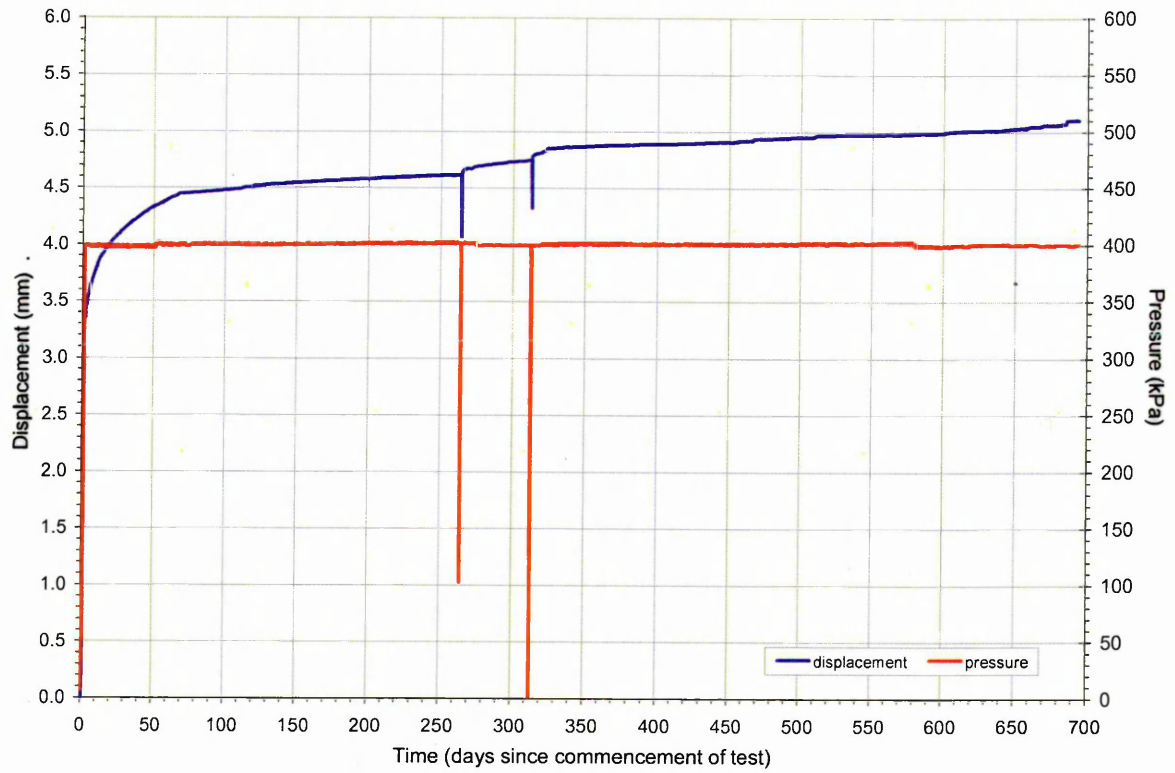


Figure 6-13: Graph of Pressure and Displacement against Time for Test 7.

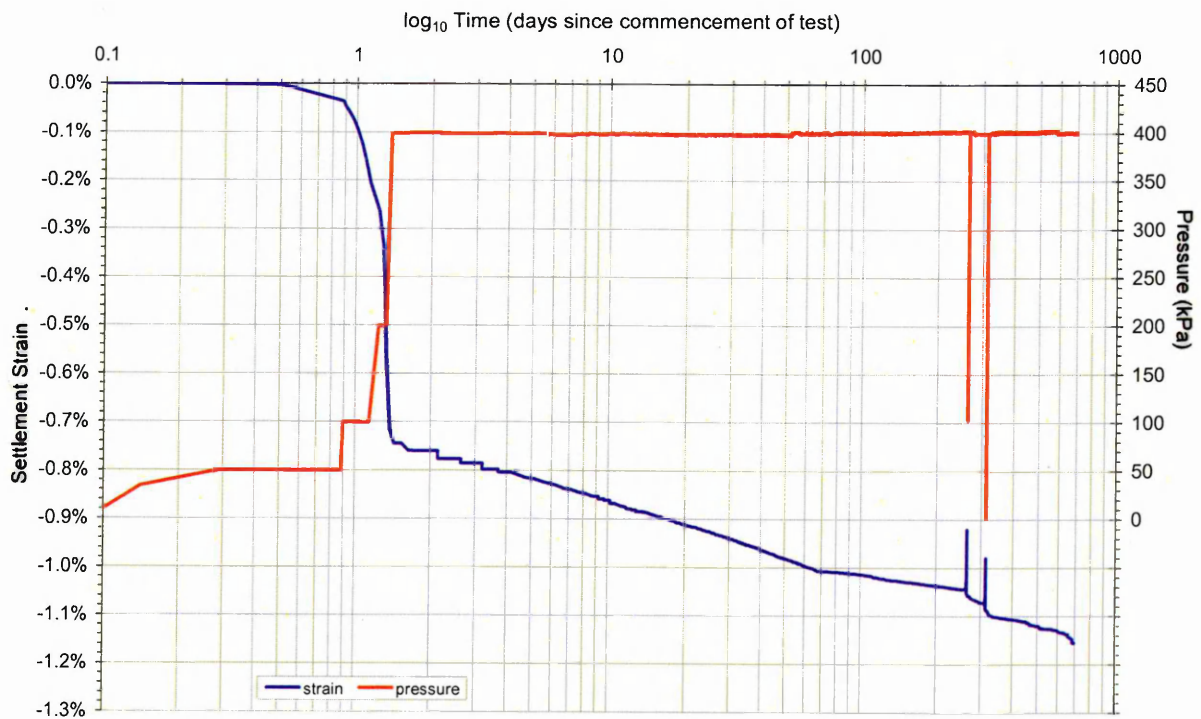


Figure 6-14: Graph of Pressure and Strain against \log_{10} Time for Test 7.

6.2.8 Detailed results for Test 8

A summary of the variables used in Test 8 is shown below:

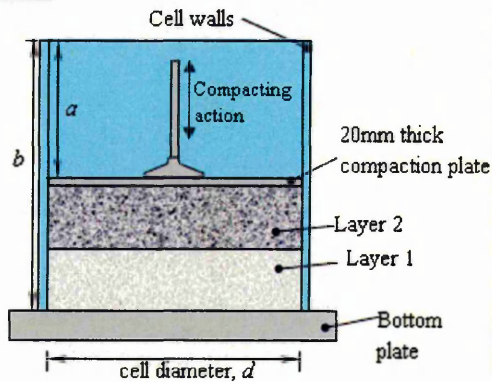
| Variables | | | | | |
|-----------|----------------------|-----------|--------------|--------------------|----------------------|
| Source | Compaction treatment | Cell type | Stress (kPa) | | Inundation condition |
| | | | Pressure | Corrected pressure | |
| Orgreave | light | Small | 400 | 395 | Not inundated |

The displacement measured on the application of the applied pressure during the test is plotted against time on a natural scale on Figure 6-15. Figure 6-16 shows displacement as strain plotted against time on a \log_{10} scale.

This test was terminated after 123 days of testing.

Specimen compaction data

| Layer | | dimension, a (mm) | Layer | | | Sample | | | |
|--------|--------------|------------------------|-------------------|---------------------------------------|--------------------------------------|-------------------|--------------|--------------------------------------|-------------------------------------|
| number | mass (kg) | | thickness (mm) | bulk density* (Mg/m ³) | dry density* (Mg/m ³) | thickness (mm) | mass (kg) | bulk density (Mg/m ³) | dry density (Mg/m ³) |
| 1 | 12.5 | 276 | 144 | 1.99 | 1.87 | 144 | 12.5 | 1.99 | 1.87 |
| 2 | 10.4 | 121 | 156 | 1.54 | 1.44 | 300 | 22.9 | 1.76 | 1.65 |
| 3 | N/A | N/A | N/A | N/A | N/A | N/A | N/A | N/A | N/A |
| 4 | N/A | N/A | N/A | N/A | N/A | N/A | N/A | N/A | N/A |
| 5 | N/A | N/A | N/A | N/A | N/A | N/A | N/A | N/A | N/A |

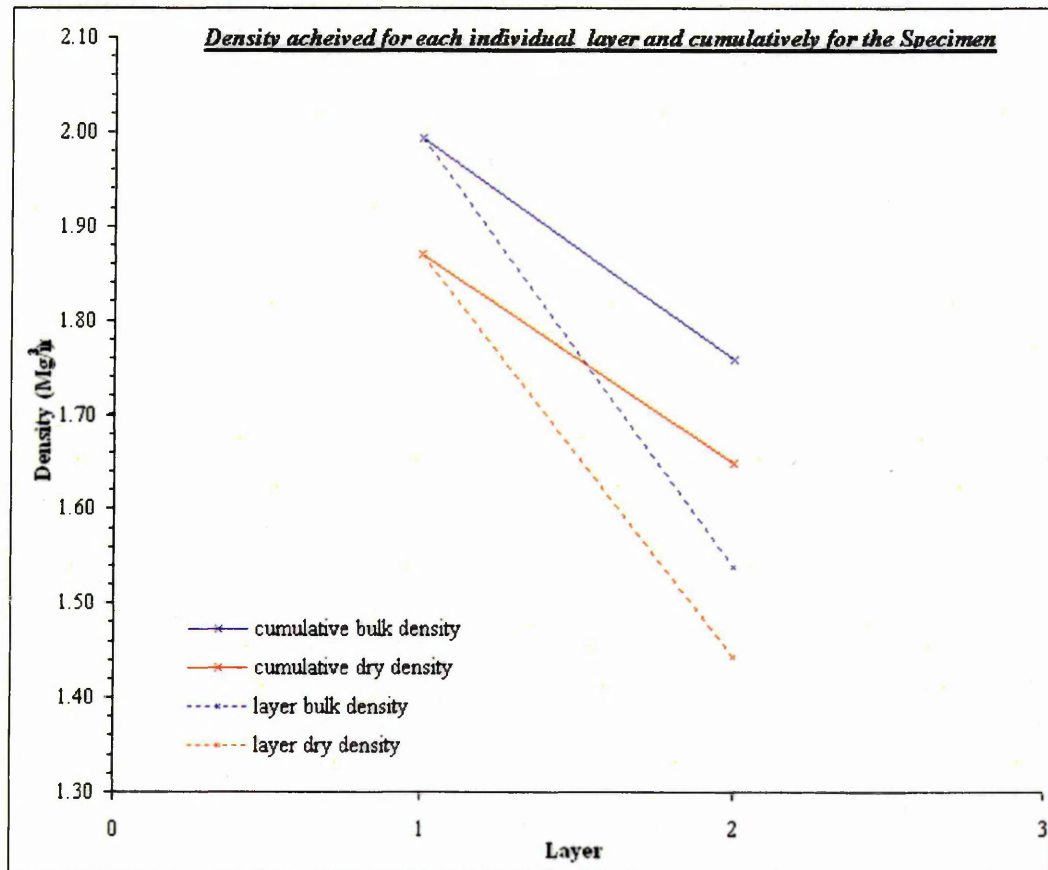
NOTES:

Specimen Moisture Content = 6.21%
 Cell diameter, d = 0.235 m
 Dimension, b = 441 mm

* It is assumed that the preceding layer was not further compacted in the calculation of these columns.

Compaction time - 3 minutes per layer

N/A - Not Applicable



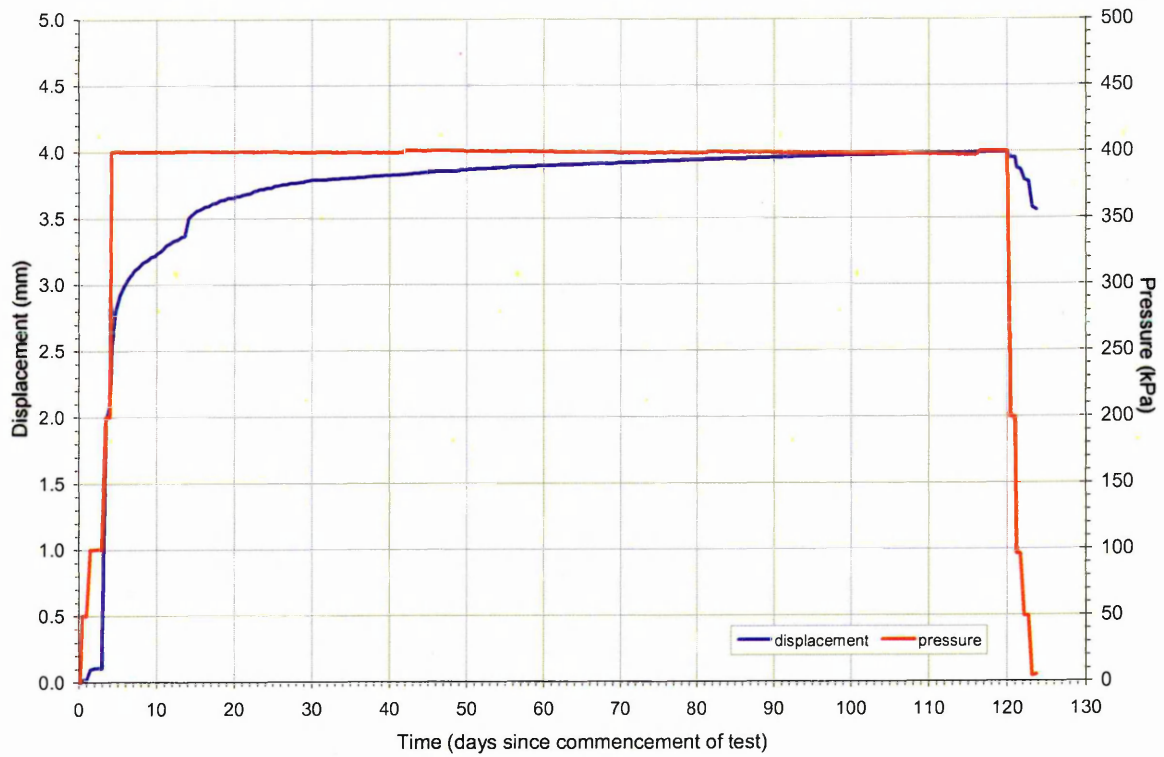


Figure 6-15: Graph of Pressure and Displacement against Time for Test 8.

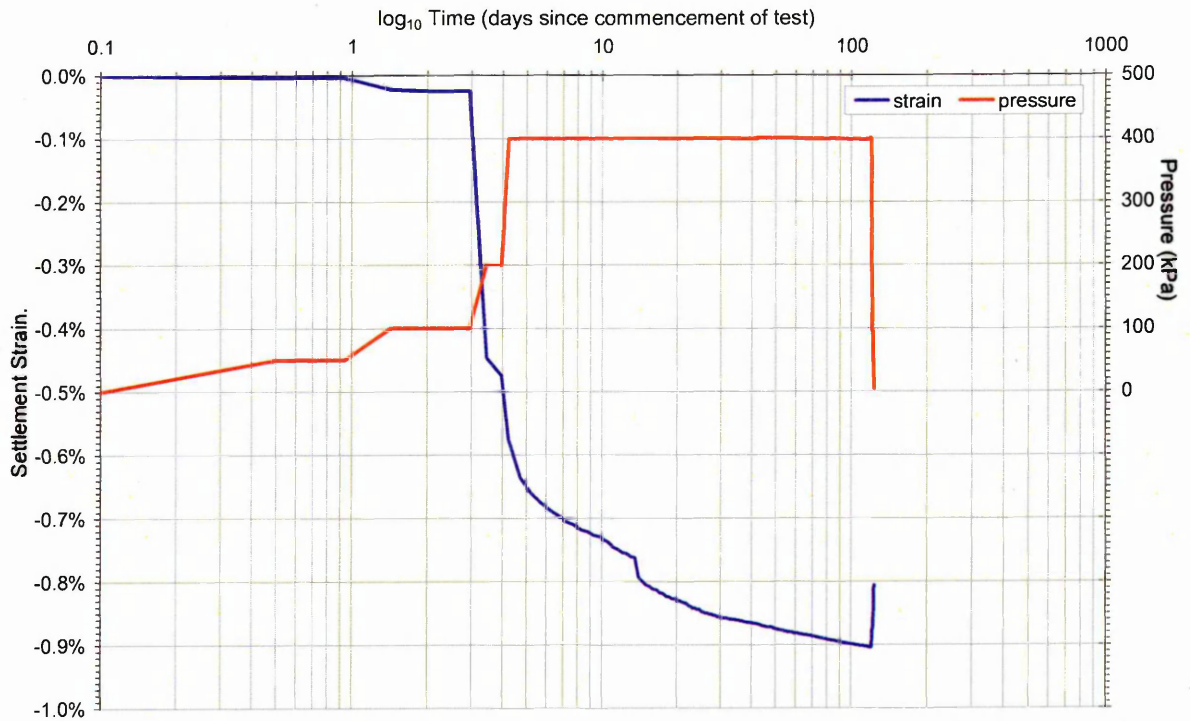


Figure 6-16: Graph of Pressure and Strain against \log_{10} Time for Test 8.

A summary of the variables used in Test 9 is shown below:

| Variables | | | | | |
|-----------|----------------------|-----------|--------------|--------------------|----------------------|
| Source | Compaction treatment | Cell type | Stress (kPa) | | Inundation condition |
| | | | Pressure | Corrected pressure | |
| Houghton | light | Small | 400 | 395 | Not inundated |

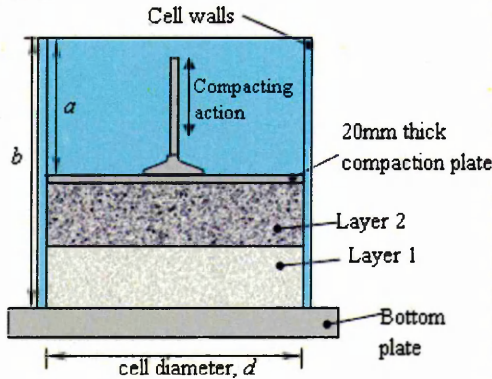
The displacement measured on the application of the applied pressure during the test is plotted against time on a natural scale on Figure 6-17. Figure 6-18 shows displacement as strain plotted against time on a \log_{10} scale.

This test was terminated after 111 days of testing.

Specimen compaction data

| Layer | | dimension, a (mm) | Layer | | | Sample | | | |
|--------|--------------|------------------------|--|---------------------------------------|--------------------------------------|-------------------|--------------|--------------------------------------|-------------------------------------|
| number | mass (kg) | | thickness (mm) | bulk density* (Mg/m ³) | dry density* (Mg/m ³) | thickness (mm) | mass (kg) | bulk density (Mg/m ³) | dry density (Mg/m ³) |
| 1 | 11.3 | 283 | 139 | 1.88 | 1.78 | 139 | 11.3 | 1.88 | 1.78 |
| 2 | 11.9 | 117 | 166 | 1.65 | 1.56 | 305 | 23.2 | 1.75 | 1.66 |
| 3 | N/A | N/A | N/A | N/A | N/A | N/A | N/A | N/A | N/A |
| 4 | N/A | N/A | N/A </td <td>N/A</td> <td>N/A</td> <td>N/A</td> <td>N/A</td> <td>N/A</td> <td>N/A</td> | N/A | N/A | N/A | N/A | N/A | N/A |
| 5 | N/A | N/A | N/A | N/A | N/A | N/A | N/A | N/A | N/A |

NOTES:

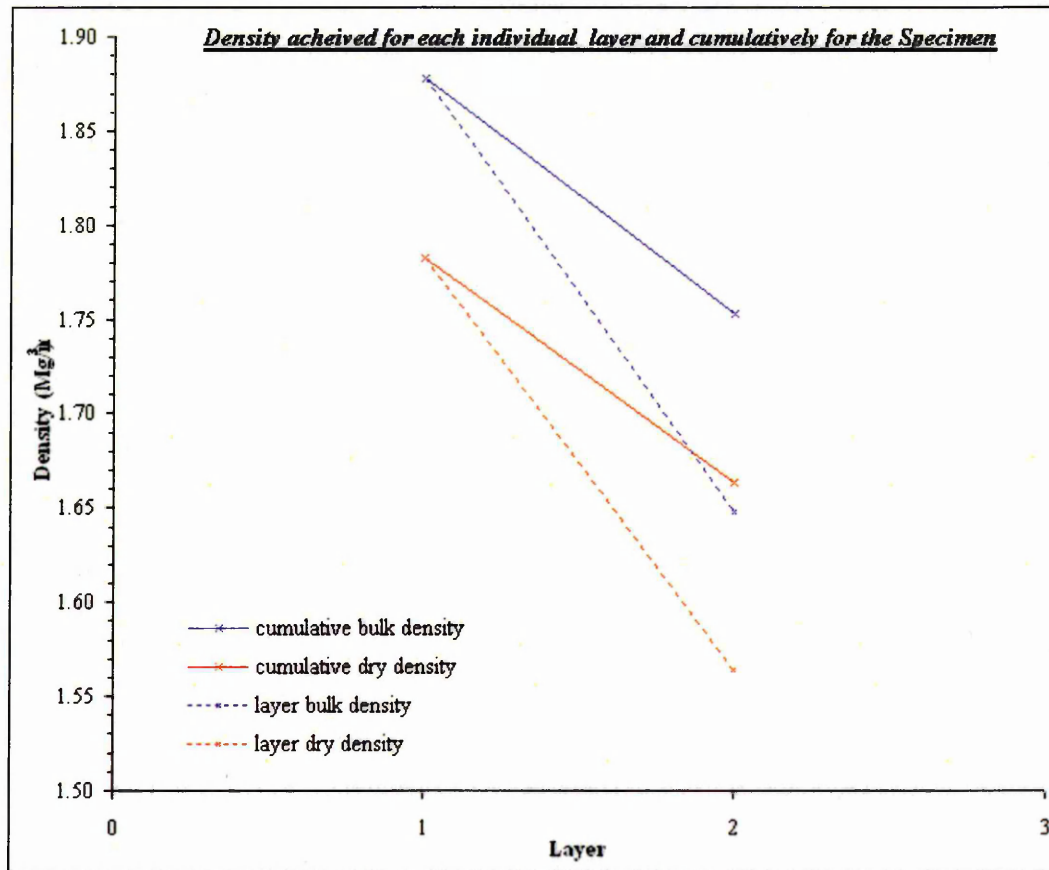


Specimen Moisture Content = 5.1%
 Cell diameter, d = 0.235 m
 Dimension, b = 442 mm

* It is assumed that the preceding layer was not further compacted in the calculation of these columns.

Compaction time - 3 minutes per layer

N/A - Not Applicable



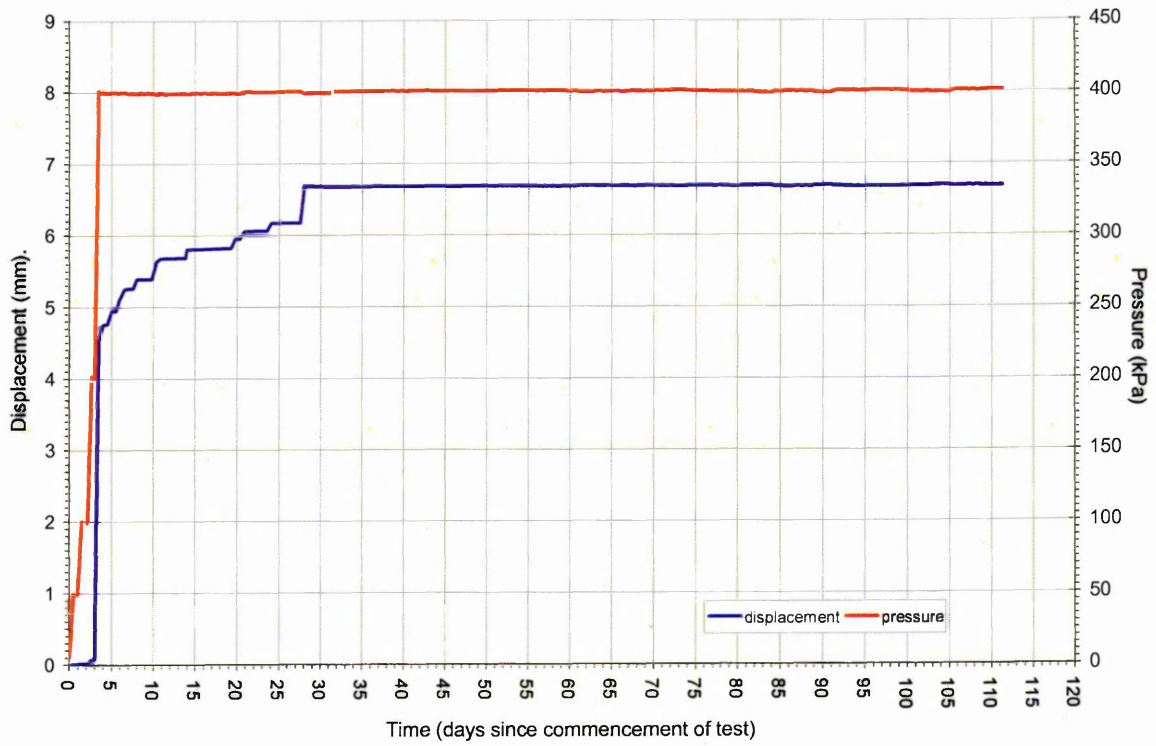


Figure 6-17: Graph of Pressure and Displacement against Time for Test 9.

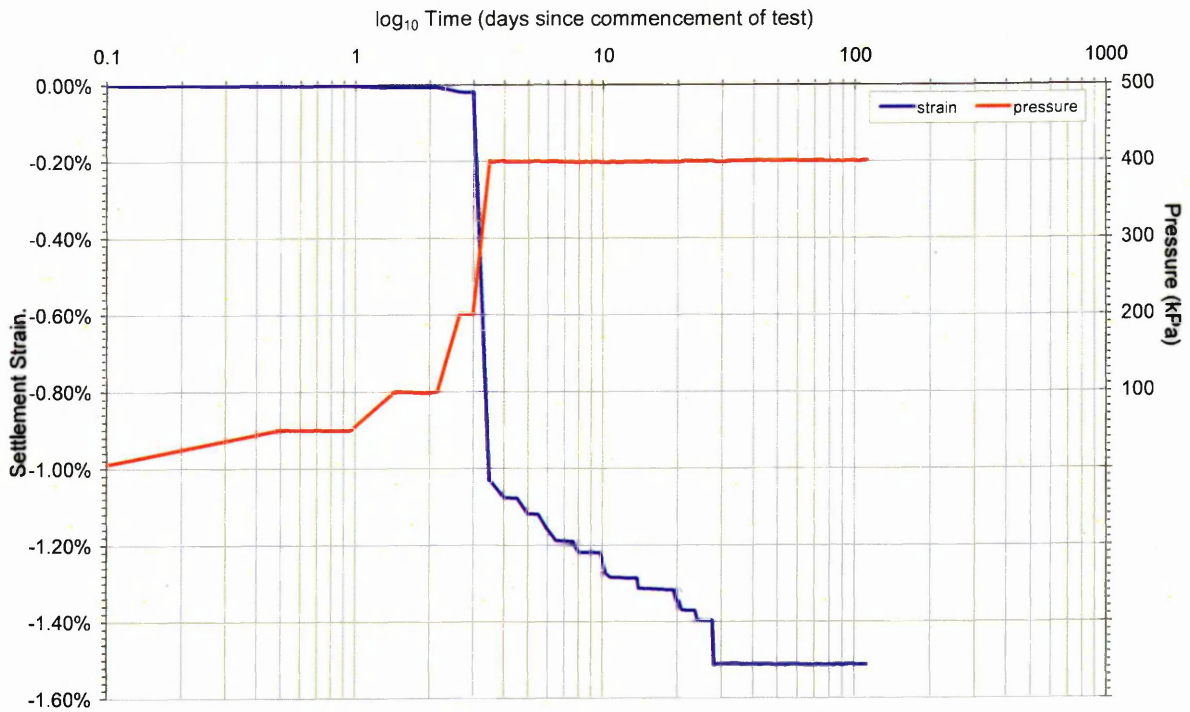


Figure 6-18: Graph of Pressure and Strain against \log_{10} Time for Test 9.

A summary of the variables used in Test 10 is shown below:

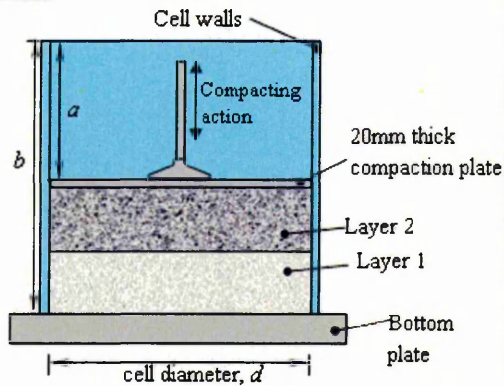
| Variables | | | | | |
|-----------|----------------------|-----------|--------------|--------------------|----------------------|
| Source | Compaction treatment | Cell type | Stress (kPa) | | Inundation condition |
| | | | Pressure | Corrected pressure | |
| Ogreave | heavy | Small | 400 | 395 | Not inundated |

The displacement measured on the application of the applied pressure during the test is plotted against time on a natural scale on Figure 6-19. Figure 6-20 shows displacement as strain plotted against time on a \log_{10} scale.

This test was terminated after 125 days of testing.

Specimen compaction data

| Layer | | | Layer | | | Sample | | | |
|--------|-----------|---------------------|----------------|-----------------------------------|----------------------------------|----------------|-----------|----------------------------------|---------------------------------|
| number | mass (kg) | dimension, a (mm) | thickness (mm) | bulk density* (Mg/m^3) | dry density* (Mg/m^3) | thickness (mm) | mass (kg) | bulk density (Mg/m^3) | dry density (Mg/m^3) |
| 1 | 6.1 | 348 | 75 | 1.88 | 1.74 | 75 | 6.1 | 1.88 | 1.74 |
| 2 | 6.3 | 267 | 81 | 1.79 | 1.66 | 156 | 12.4 | 1.83 | 1.70 |
| 3 | 6.0 | 194 | 73 | 1.90 | 1.77 | 229 | 18.4 | 1.85 | 1.72 |
| 4 | 6.1 | 118 | 76 | 1.84 | 1.71 | 305 | 24.5 | 1.85 | 1.72 |
| 5 | N/A | N/A | N/A | N/A | N/A | N/A | N/A | N/A | N/A |

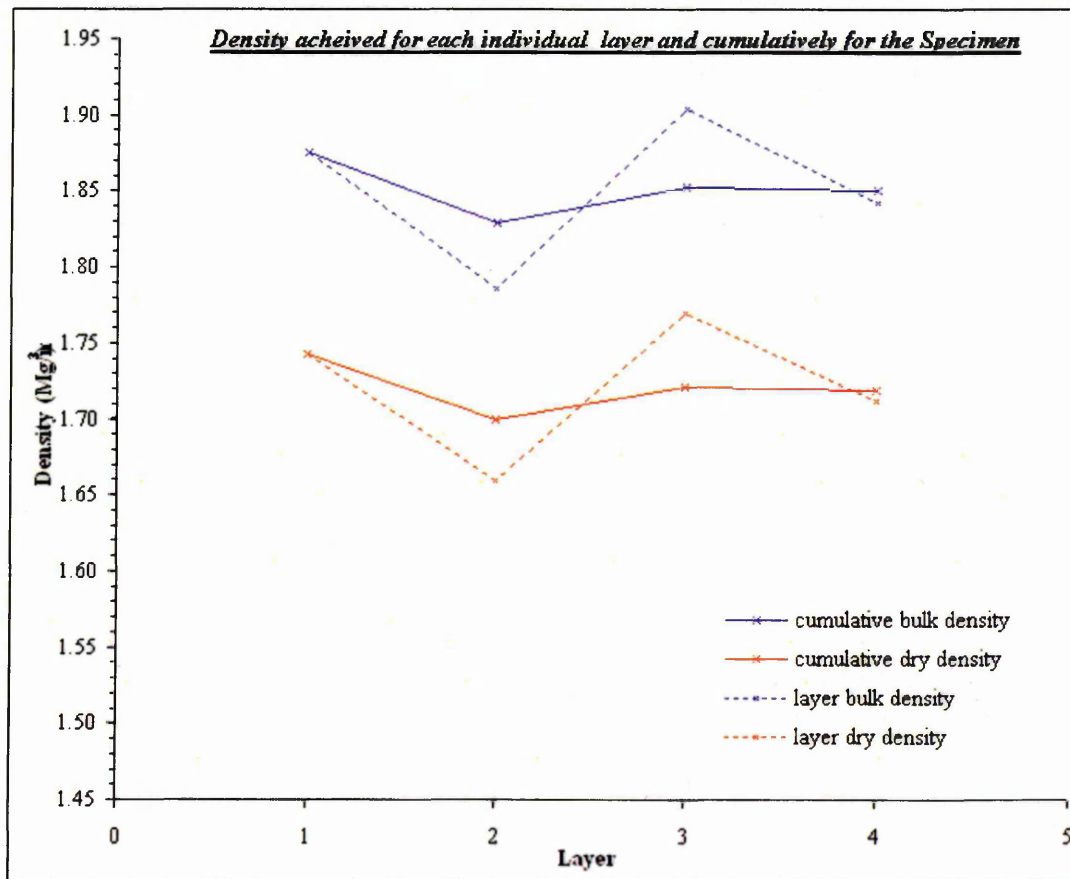
NOTES:

Specimen Moisture Content = 7.1%
 Cell diameter, d = 0.235 m
 Dimension, b = 443 mm

* It is assumed that the preceding layer was not further compacted in the calculation of these columns.

Compaction time - 5 minutes per layer

N/A - Not Applicable



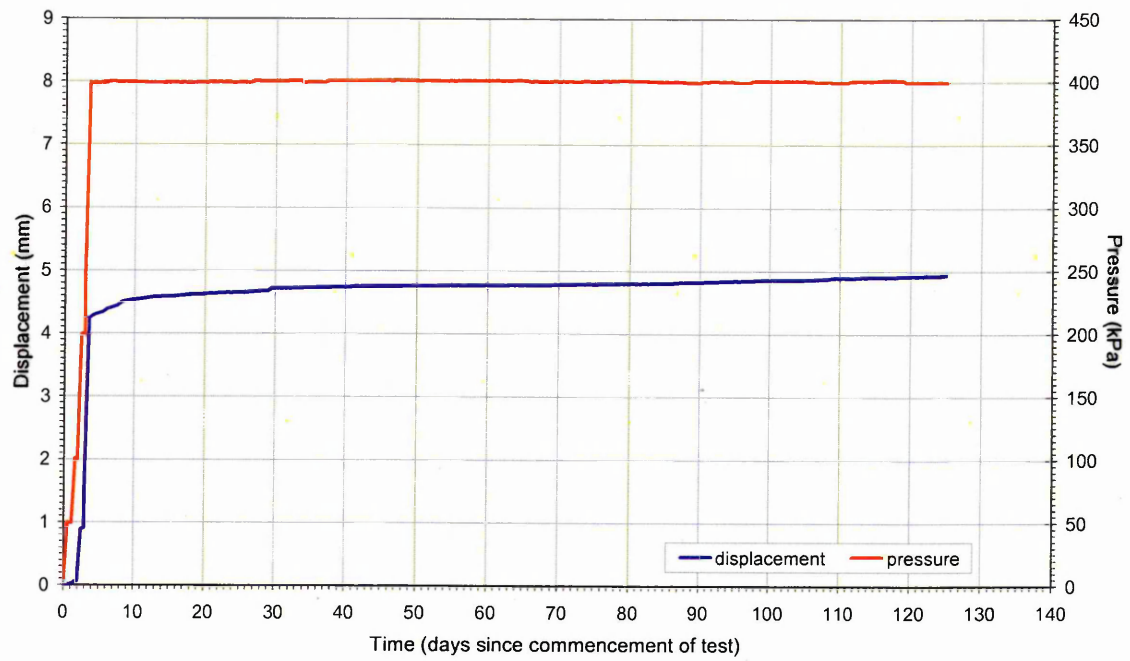


Figure 6-19: Graph of Pressure and Displacement against Time for Test 10.

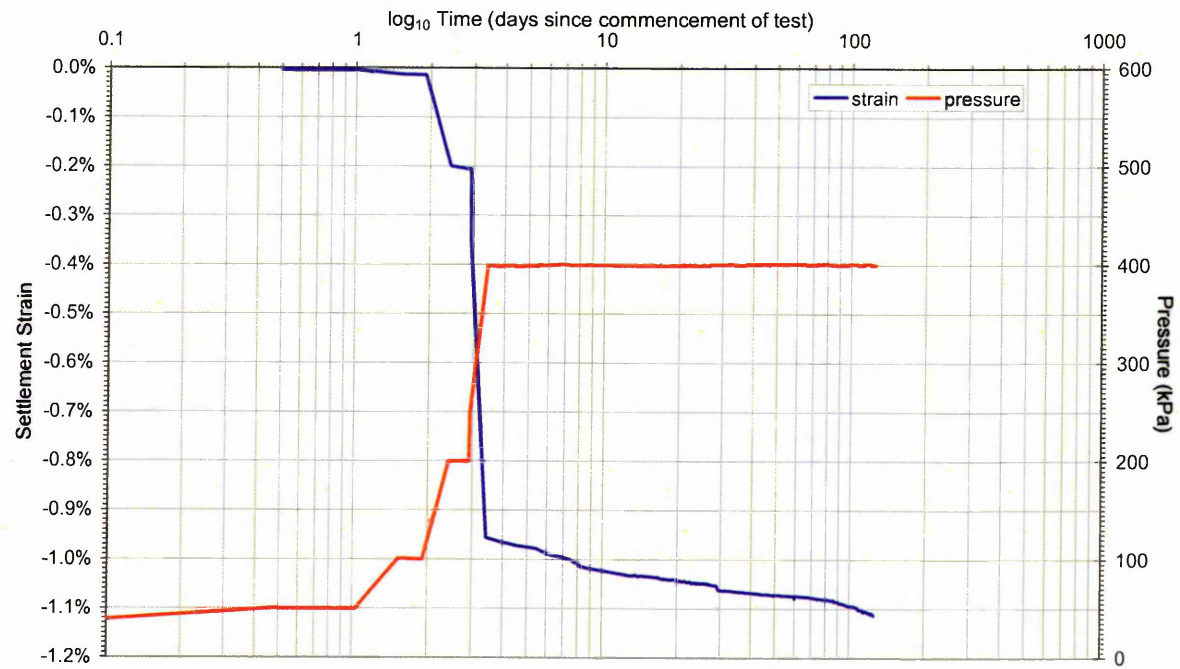


Figure 6-20: Graph of Pressure and Strain against \log_{10} Time for Test 10.

A summary of the variables used in Test 11 is shown below:

| Variables | | | | | |
|-----------|----------------------|-----------|--------------|--------------------|----------------------|
| Source | Compaction treatment | Cell type | Stress (kPa) | | Inundation condition |
| | | | Pressure | Corrected pressure | |
| Ogreave | heavy | Small | 400 | 395 | Not inundated |

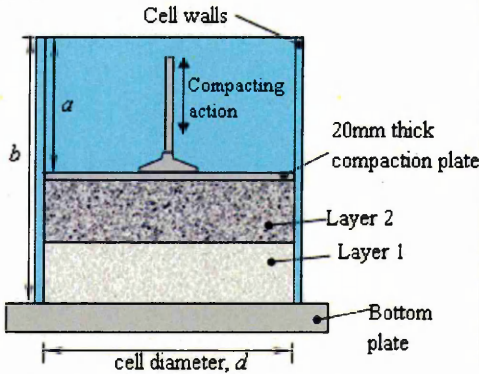
The displacement measured on the application of the applied pressure during the test is plotted against time on a natural scale on Figure 6-21. Figure 6-22 shows displacement as strain plotted against time on a \log_{10} scale.

This test was terminated after 133 days of testing.

Specimen compaction data

| Layer number | Layer | | Layer | | | Sample | | | |
|--------------|-----------|---------------------|----------------|----------------------------|---------------------------|----------------|-----------|---------------------------|--------------------------|
| | mass (kg) | dimension, a (mm) | thickness (mm) | bulk density* (Mg/m^3) | dry density* (Mg/m^3) | thickness (mm) | mass (kg) | bulk density (Mg/m^3) | dry density (Mg/m^3) |
| 1 | 6.0 | 349 | 74 | 1.87 | 1.74 | 74 | 6.0 | 1.87 | 1.74 |
| 2 | 6.0 | 274 | 75 | 1.86 | 1.73 | 148 | 12.0 | 1.87 | 1.73 |
| 3 | 6.0 | 200 | 75 | 1.85 | 1.72 | 223 | 18.0 | 1.86 | 1.73 |
| 4 | 6.0 | 125 | 75 | 1.84 | 1.71 | 298 | 24.0 | 1.86 | 1.73 |
| 5 | N/A | N/A | N/A | N/A | N/A | N/A | N/A | N/A | N/A |

NOTES:

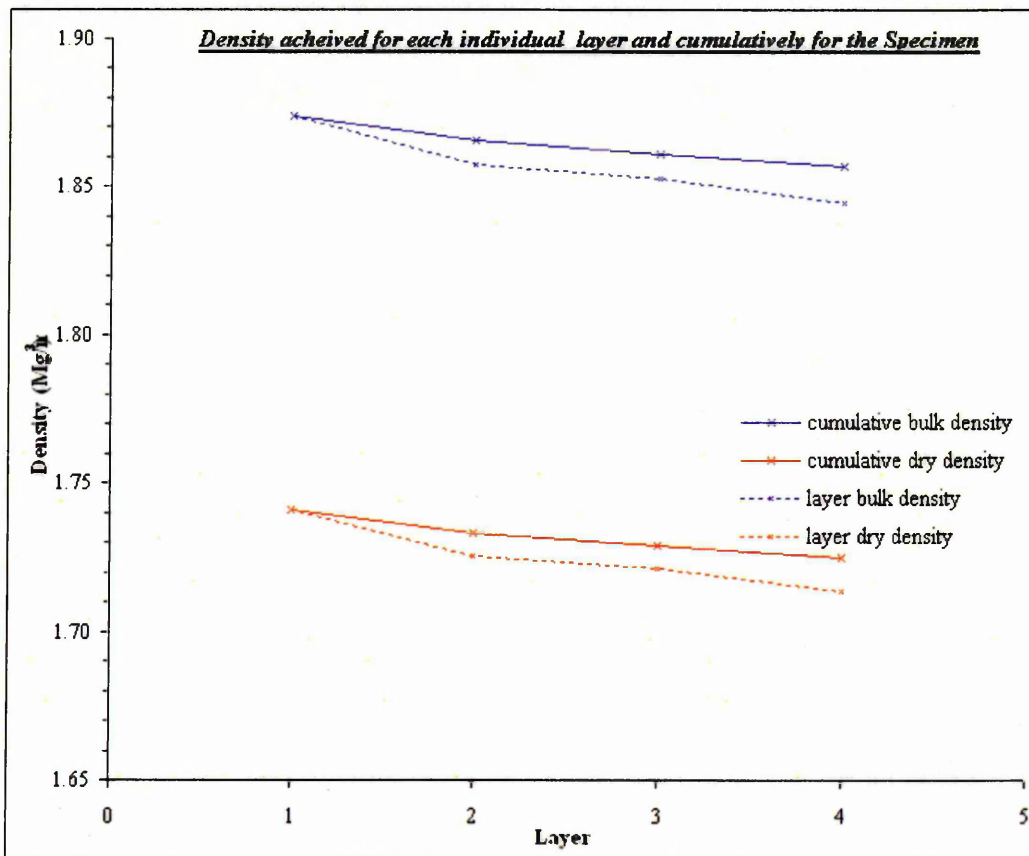


Specimen Moisture Content = 7.1%
 Cell diameter, d = 0.235 m
 Dimension, b = 443 mm

* It is assumed that the preceding layer was not further compacted in the calculation of these columns.

Compaction time - 5 minutes per layer

N/A - Not Applicable



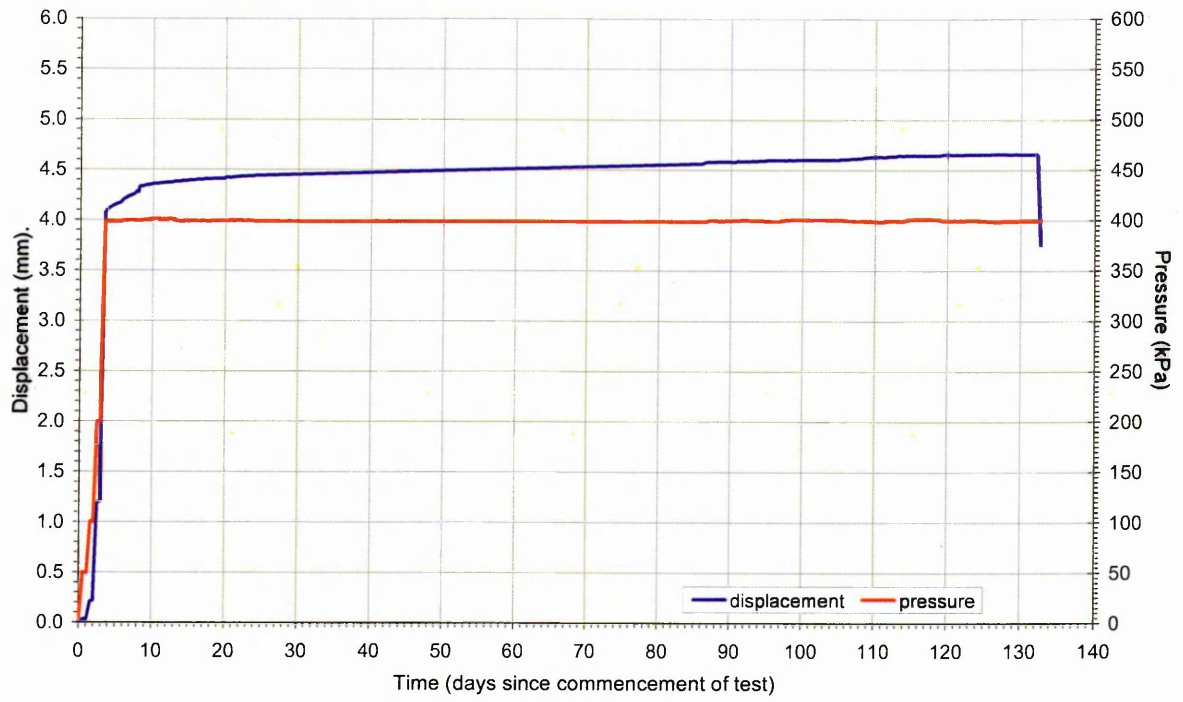


Figure 6-21: Graph of Pressure and Displacement against Time for Test 11.

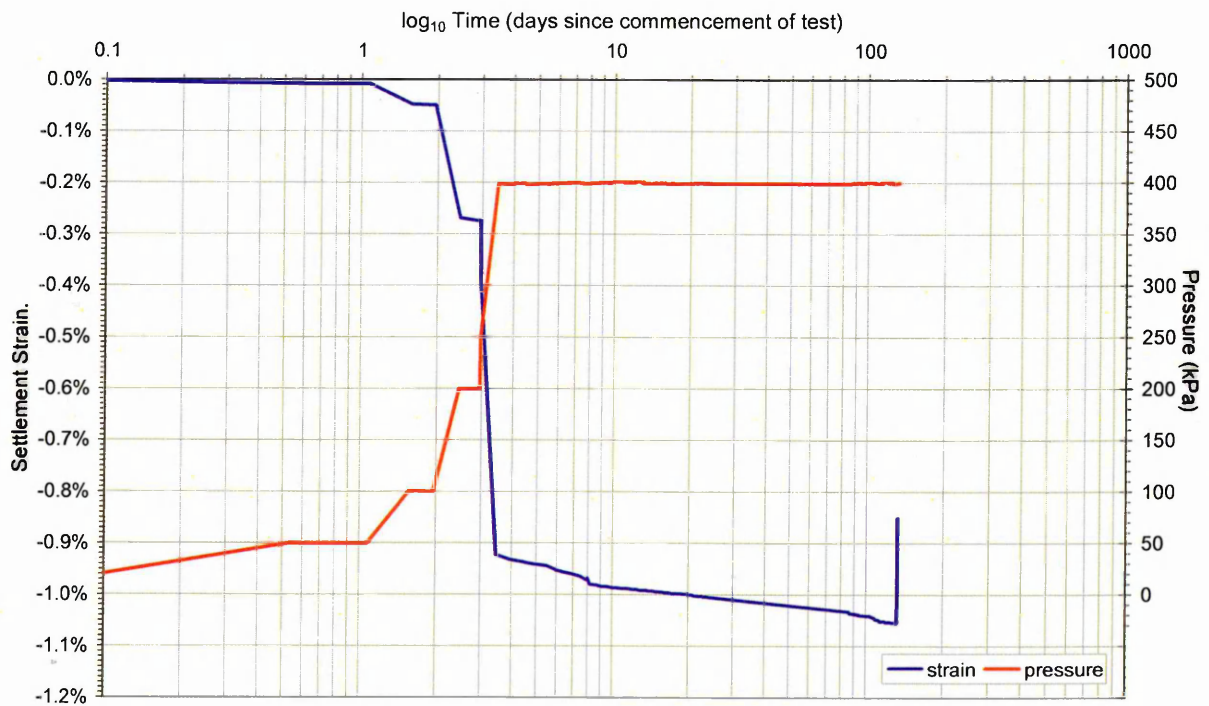


Figure 6-22: Graph of Pressure and Strain against \log_{10} Time for Test 11.

A summary of the variables used in Test 12 is shown below:

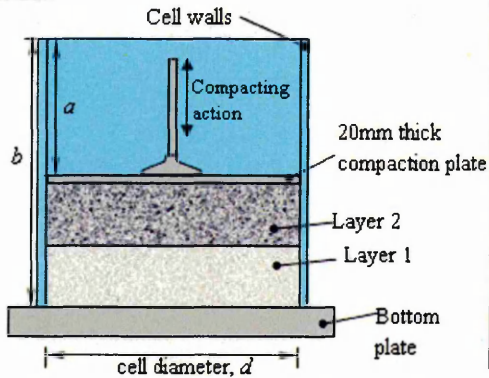
| Variables | | | | | |
|-----------|----------------------|-----------|--------------|--------------------|----------------------|
| Source | Compaction treatment | Cell type | Stress (kPa) | | Inundation condition |
| | | | Pressure | Corrected pressure | |
| Houghton | heavy | Small | 400 | 395 | Not inundated |

The displacement measured on the application of the applied pressure during the test is plotted against time on a natural scale on Figure 6-23. Figure 6-24 shows displacement as strain plotted against time on a \log_{10} scale.

This test was terminated after 116 days of testing.

Specimen compaction data

| Layer | | dimension, a (mm) | Layer | | | Sample | | | |
|--------|--------------|------------------------|-------------------|---------------------------------------|--------------------------------------|-------------------|--------------|--------------------------------------|-------------------------------------|
| number | mass (kg) | | thickness (mm) | bulk density* (Mg/m ³) | dry density* (Mg/m ³) | thickness (mm) | mass (kg) | bulk density (Mg/m ³) | dry density (Mg/m ³) |
| 1 | 6.1 | 349 | 75 | 1.87 | 1.78 | 75 | 6.1 | 1.87 | 1.78 |
| 2 | 5.9 | 275 | 74 | 1.86 | 1.77 | 149 | 12.0 | 1.87 | 1.78 |
| 3 | 6.0 | 201 | 74 | 1.87 | 1.78 | 223 | 18.0 | 1.87 | 1.78 |
| 4 | 5.9 | 127 | 74 | 1.84 | 1.75 | 297 | 23.9 | 1.86 | 1.77 |
| 5 | N/A | N/A | N/A | N/A | N/A | N/A | N/A | N/A | N/A |

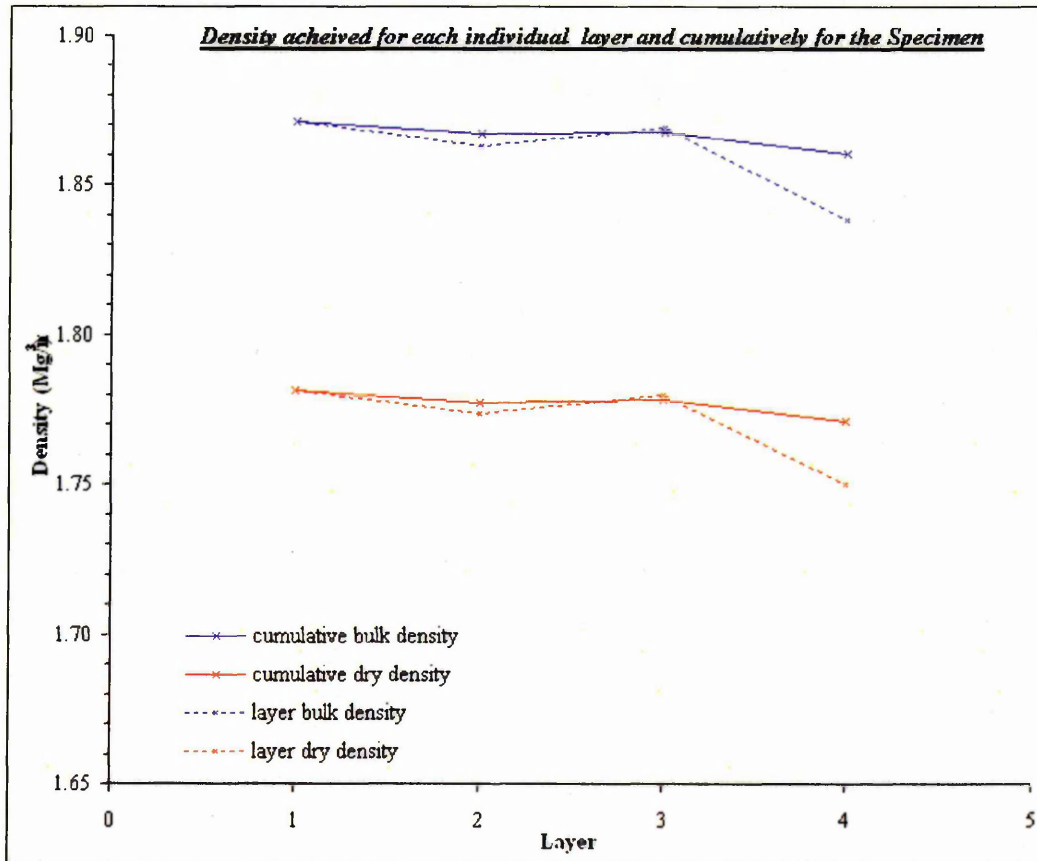
NOTES:

Specimen Moisture Content = 4.8%
 Cell diameter, d = 0.235 m
 Dimension, b = 444 mm

* It is assumed that the preceding layer was not further compacted in the calculation of these columns.

Compaction time - 5 minutes per layer

N/A - Not Applicable



6.2.12.2 Testing results (Test 12)

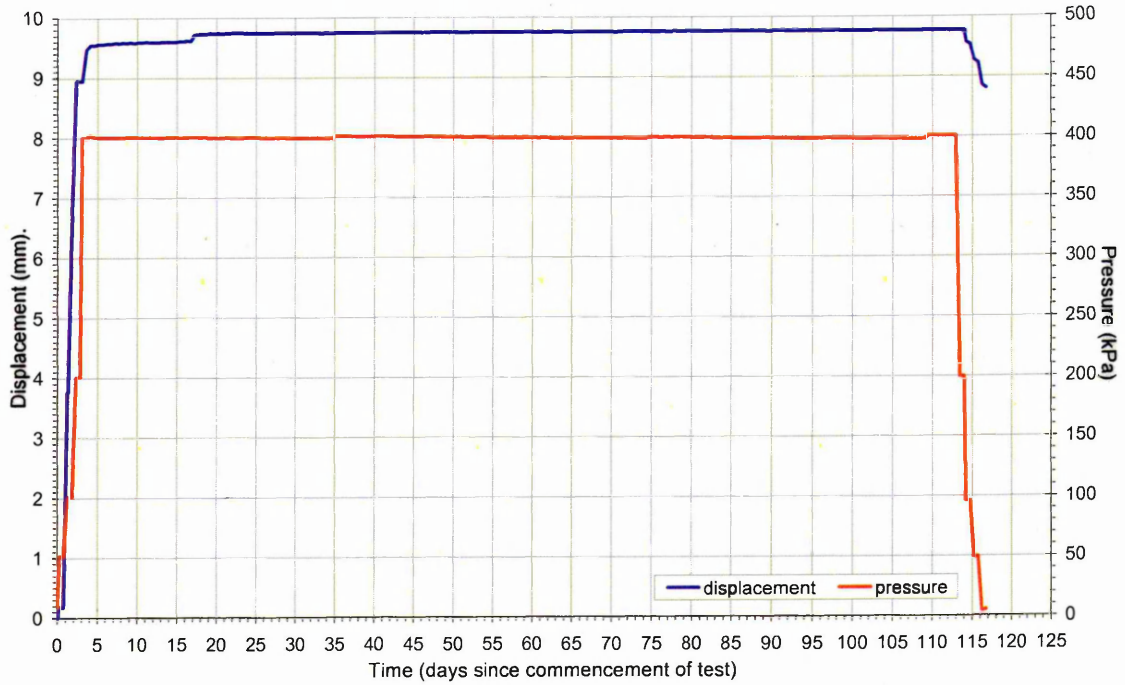


Figure 6-23: Graph of Pressure and Displacement against Time for Test 12.

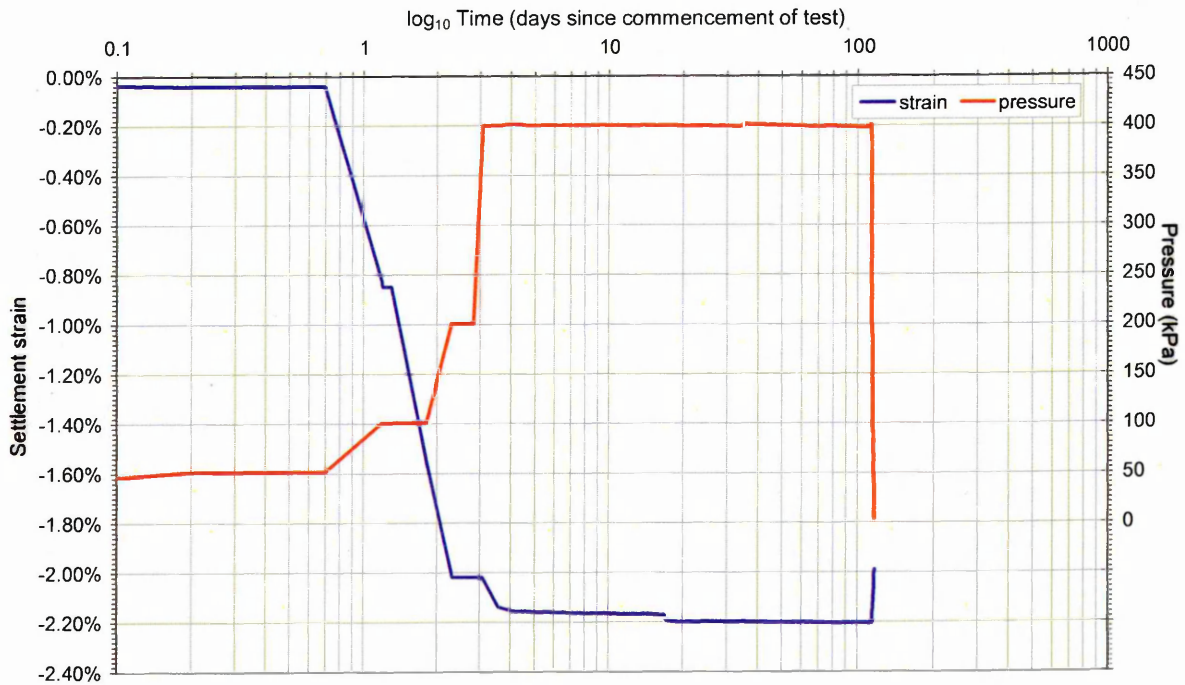


Figure 6-24: Graph of Pressure and Strain against \log_{10} Time for Test 12.

A summary of the variables used in Test 13 is shown below:

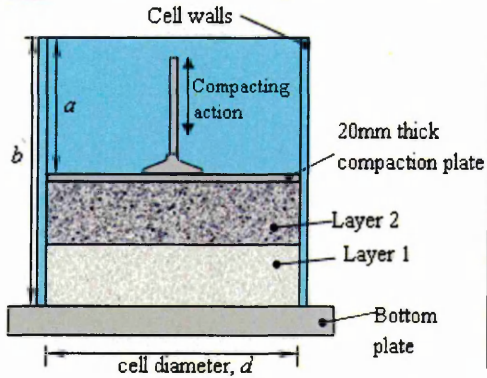
| Variables | | | | | |
|-----------|----------------------|-----------|--------------|--------------------|----------------------|
| Source | Compaction treatment | Cell type | Stress (kPa) | | Inundation condition |
| | | | Pressure | Corrected pressure | |
| Orgreave | light | Small | 400 | 395 | Not inundated |

The displacement measured on the application of the applied pressure during the test is plotted against time on a natural scale on Figure 6-25. Figure 6-26 shows displacement as strain plotted against time on a \log_{10} scale.

This test was terminated after 128 days of testing.

Specimen compaction data

| Layer | | dimension, a (mm) | Layer | | | Sample | | | | | | | |
|--------|--------------|------------------------|---|---------------------------------------|--------------------------------------|-------------------|--------------|--------------------------------------|-------------------------------------|-----|-----|-----|-----|
| number | mass (kg) | | thickness (mm) | bulk density* (Mg/m ³) | dry density* (Mg/m ³) | thickness (mm) | mass (kg) | bulk density (Mg/m ³) | dry density (Mg/m ³) | | | | |
| 1 | 11.5 | 265 | 158 | 1.68 | 1.56 | 158 | 11.5 | 1.68 | 1.56 | | | | |
| 2 | 11.3 | 112 | 153 | 1.70 | 1.58 | 311 | 22.8 | 1.69 | 1.57 | | | | |
| 3 | N/A | N/A | N/A | N/A | N/A | N/A | N/A | N/A | N/A | | | | |
| 4 | N/A | N/A | N/A </tr <tr> <td>5</td> <td>N/A</td> <td>N/A</td> <td>N/A</td> <td>N/A</td> <td>N/A</td> <td>N/A</td> <td>N/A</td> <td>N/A</td> <td>N/A</td> </tr> | 5 | N/A | N/A | N/A | N/A | N/A | N/A | N/A | N/A | N/A |
| 5 | N/A | N/A | N/A | N/A | N/A | N/A | N/A | N/A | N/A | | | | |

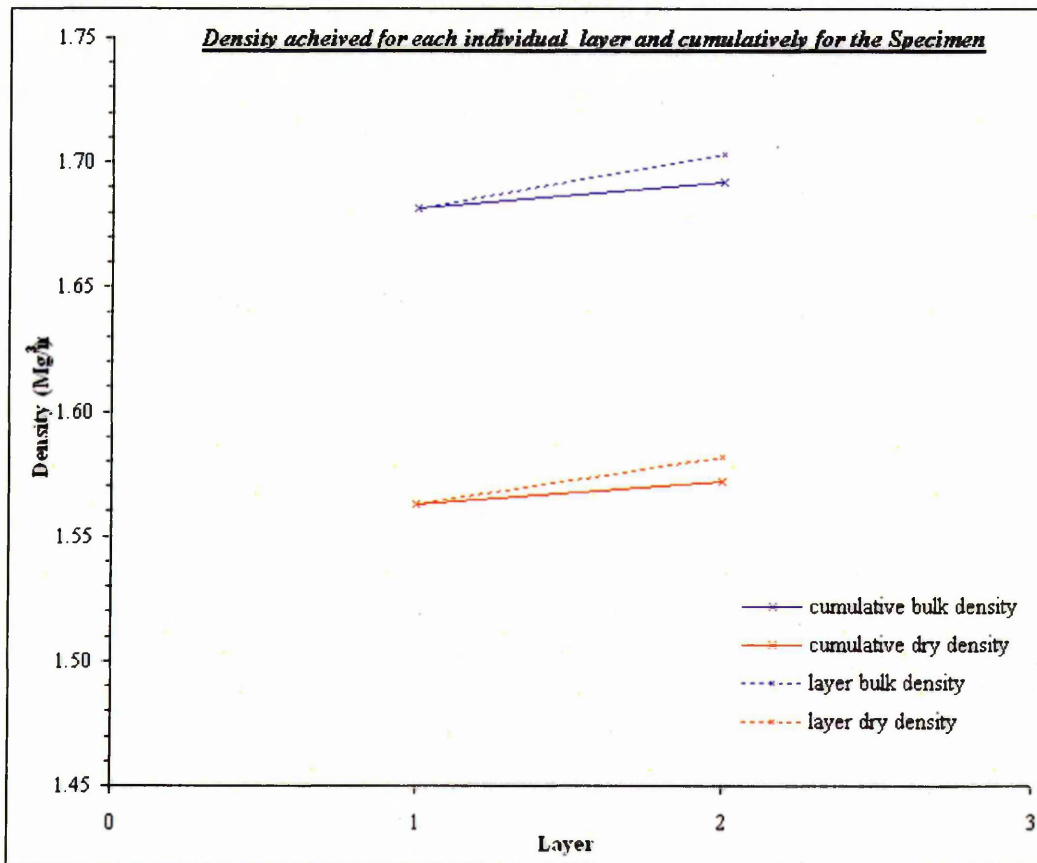
NOTES:

Specimen Moisture Content = 7.10%
 Cell diameter, d = 0.235 m
 Dimension, b = 443 mm

* It is assumed that the preceding layer was not further compacted in the calculation of these columns.

Compaction time - 3 minutes per layer

N/A - Not Applicable



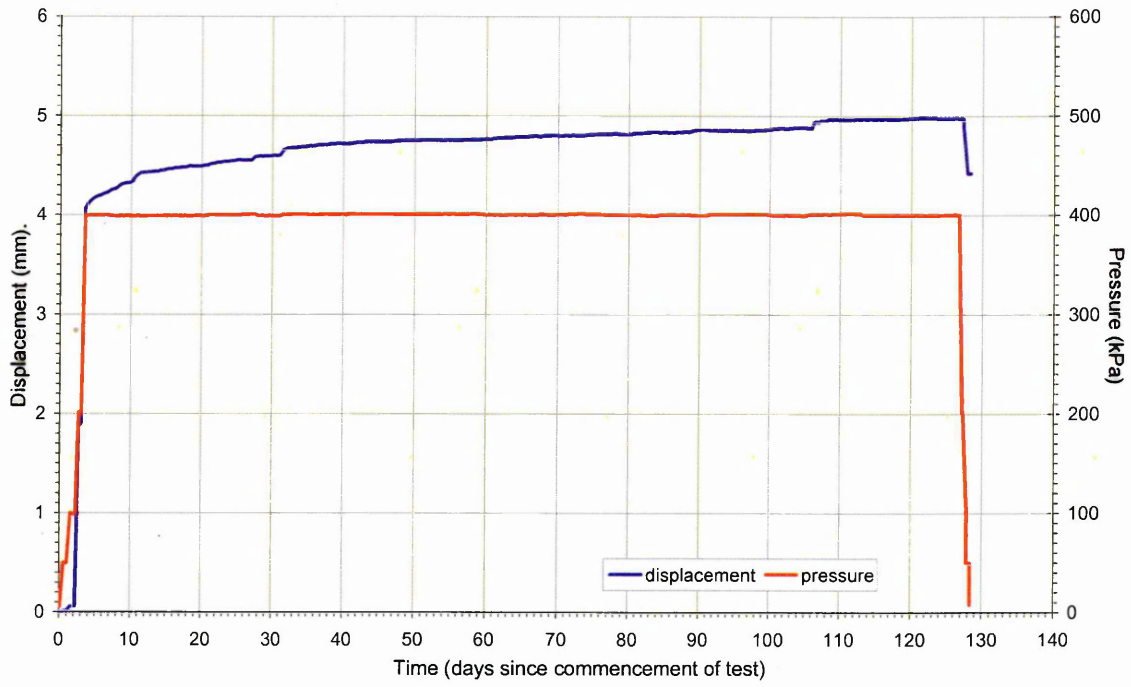


Figure 6-25: Graph of Pressure and Displacement against Time for Test 13.

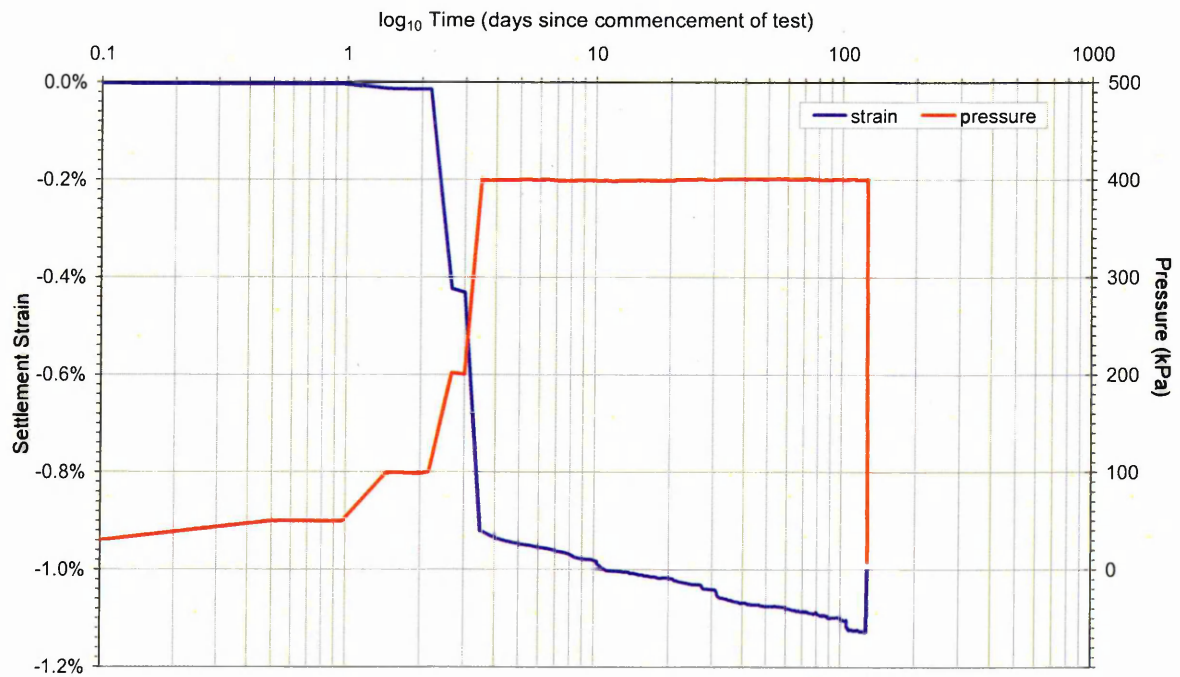


Figure 6-26: Graph of Pressure and Strain against \log_{10} Time for Test 13.

A summary of the variables used in Test 14 is shown below:

| Variables | | | | | |
|-----------|----------------------|-----------|--------------|--------------------|----------------------|
| Source | Compaction treatment | Cell type | Stress (kPa) | | Inundation condition |
| | | | Pressure | Corrected pressure | |
| Houghton | heavy | Small | 400 | 395 | Not inundated |

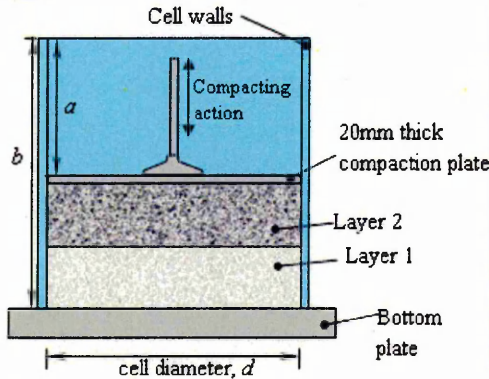
The displacement measured on the application of the applied pressure during the test is plotted against time on a natural scale on Figure 6-27. Figure 6-28 shows displacement as strain plotted against time on a \log_{10} scale.

This test was terminated after 101 days of testing.

Specimen compaction data

| Layer | | dimension, a (mm) | Layer | | | Sample | | | |
|--------|--------------|------------------------|-------------------|---------------------------------------|--------------------------------------|-------------------|--------------|--------------------------------------|-------------------------------------|
| number | mass (kg) | | thickness (mm) | bulk density* (Mg/m ³) | dry density* (Mg/m ³) | thickness (mm) | mass (kg) | bulk density (Mg/m ³) | dry density (Mg/m ³) |
| 1 | 6.1 | 349 | 76 | 1.86 | 1.78 | 76 | 6.1 | 1.86 | 1.78 |
| 2 | 5.9 | 275 | 74 | 1.85 | 1.77 | 149 | 12.0 | 1.86 | 1.77 |
| 3 | 6.0 | 198 | 76 | 1.81 | 1.73 | 226 | 18.0 | 1.84 | 1.76 |
| 4 | 5.9 | 125 | 74 | 1.85 | 1.76 | 299 | 23.9 | 1.84 | 1.76 |
| 5 | N/A | N/A | N/A | N/A | N/A | N/A | N/A | N/A | N/A |

NOTES:

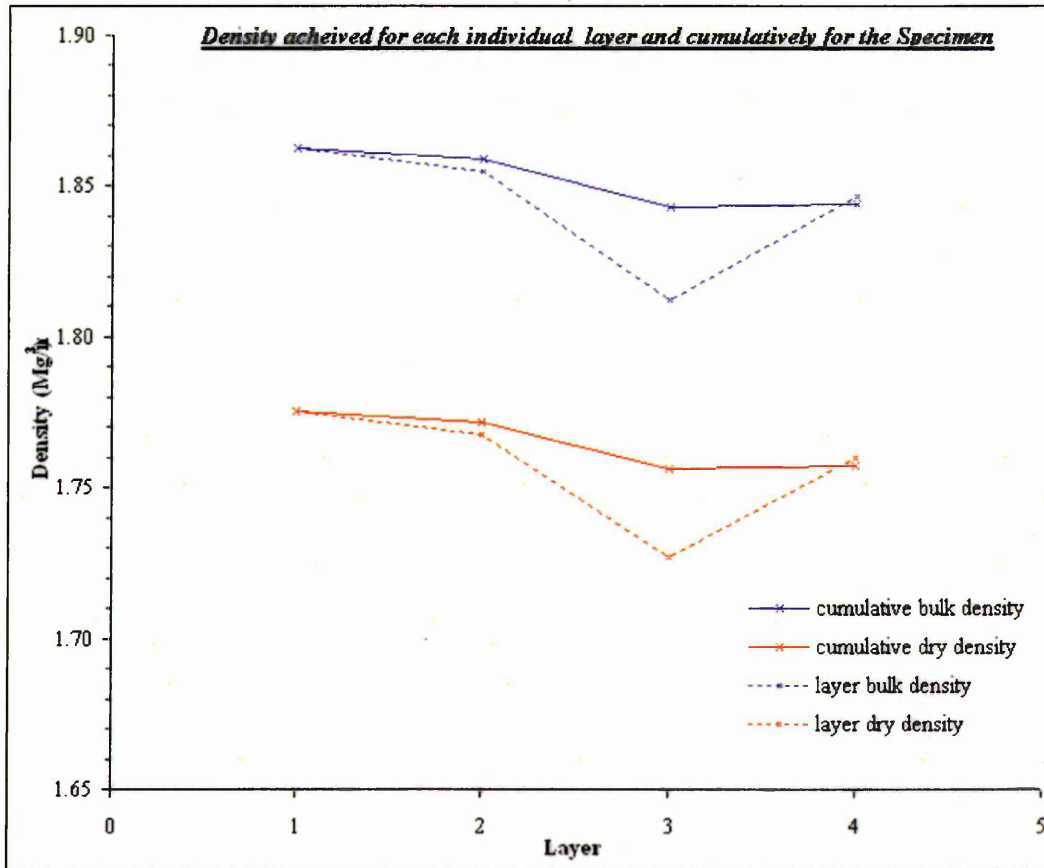


Specimen Moisture Content = 4.7%
 Cell diameter, d = 0.235 m
 Dimension, b = 444 mm

* It is assumed that the preceding layer was not further compacted in the calculation of these columns.

Compaction time - 5 minutes per layer

N/A - Not Applicable



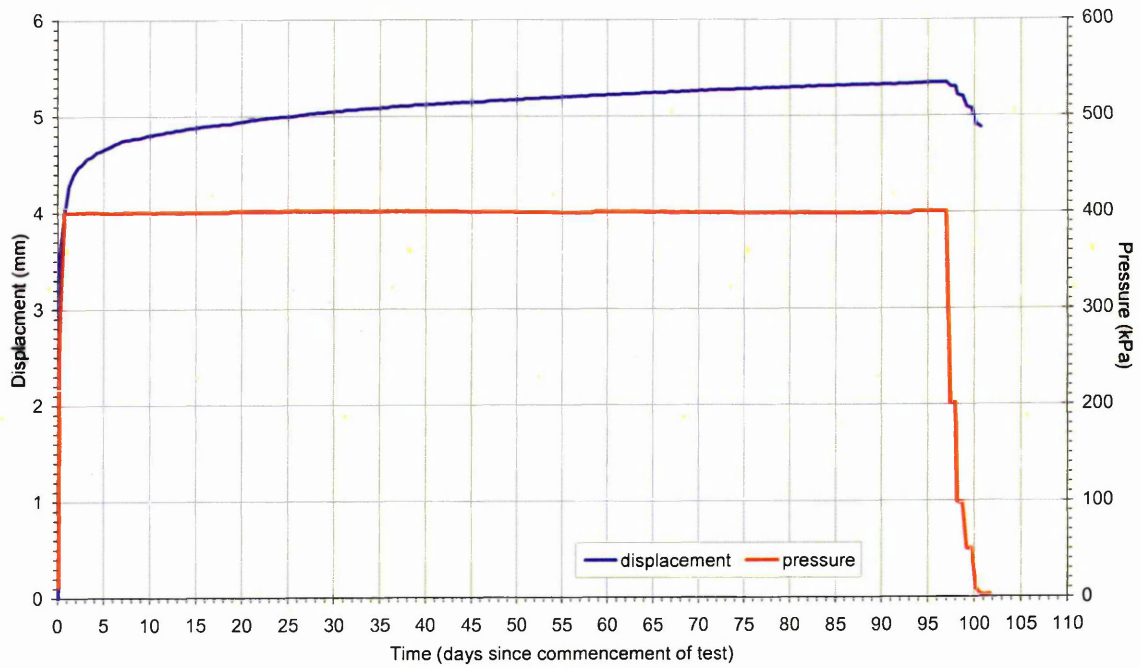


Figure 6-27: Graph of Pressure and Displacement against Time for Test 14.

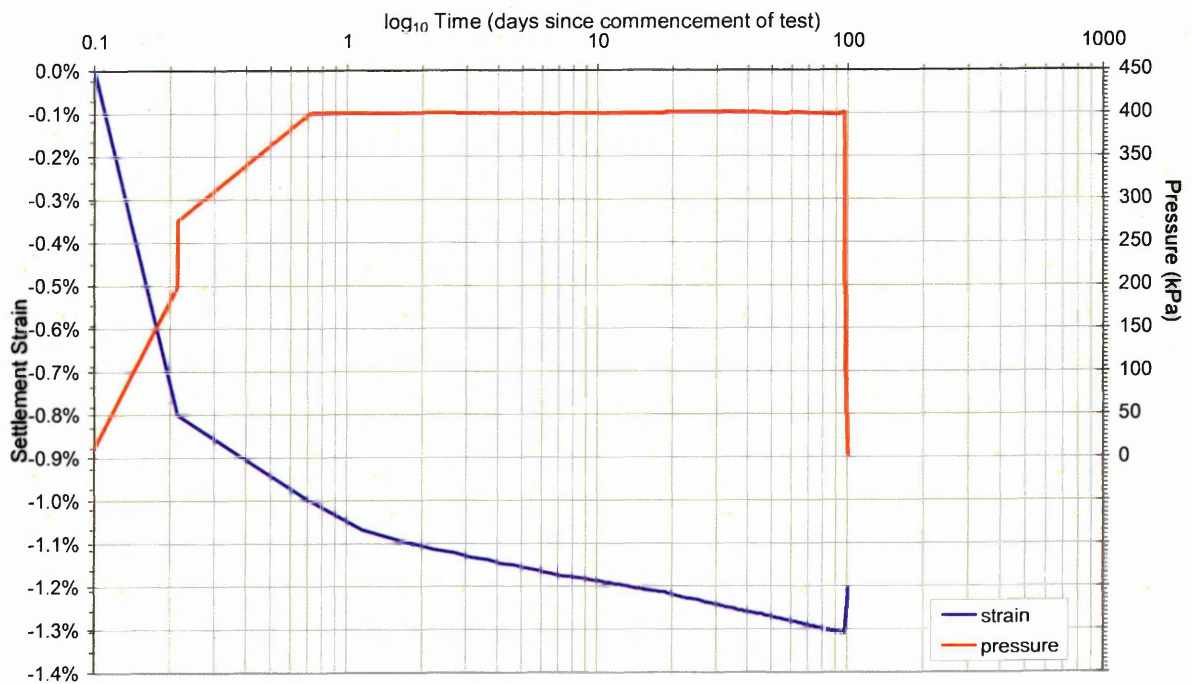


Figure 6-28: Graph of Pressure and Strain against \log_{10} Time for Test 14.

A summary of the variables used in Test 15 is shown below:

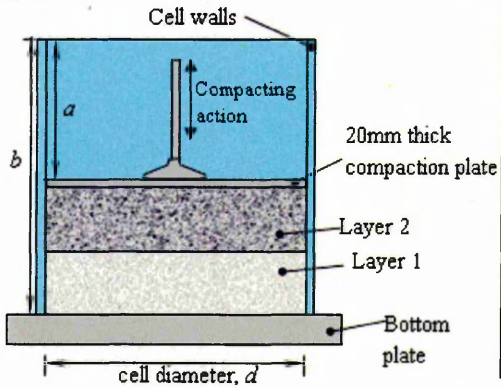
| Variables | | | | | |
|-----------|----------------------|-----------|--------------|--------------------|----------------------|
| Source | Compaction treatment | Cell type | Stress (kPa) | | Inundation condition |
| | | | Pressure | Corrected pressure | |
| Ogreave | light | Small | 400 | 395 | Not inundated |

The displacement measured on the application of the applied pressure during the test is plotted against time on a natural scale on Figure 6-29. Figure 6-30 shows displacement as strain plotted against time on a \log_{10} scale.

This test was terminated after 122 days of testing.

Specimen compaction data

| Layer | | dimension, a (mm) | Layer | | | Sample | | | |
|--------|--------------|------------------------|-------------------|---------------------------------------|--------------------------------------|-------------------|--------------|--------------------------------------|-------------------------------------|
| number | mass (kg) | | thickness (mm) | bulk density* (Mg/m ³) | dry density* (Mg/m ³) | thickness (mm) | mass (kg) | bulk density (Mg/m ³) | dry density (Mg/m ³) |
| 1 | 11.8 | 267 | 156 | 1.74 | 1.62 | 156 | 11.8 | 1.74 | 1.62 |
| 2 | 11.4 | 119 | 148 | 1.77 | 1.64 | 304 | 23.2 | 1.76 | 1.63 |
| 3 | N/A | - | - | - | - | - | - | - | - |
| 4 | - | - | - | - | - | - | - | - | - |
| 5 | - | - | - | - | - | - | - | - | - |

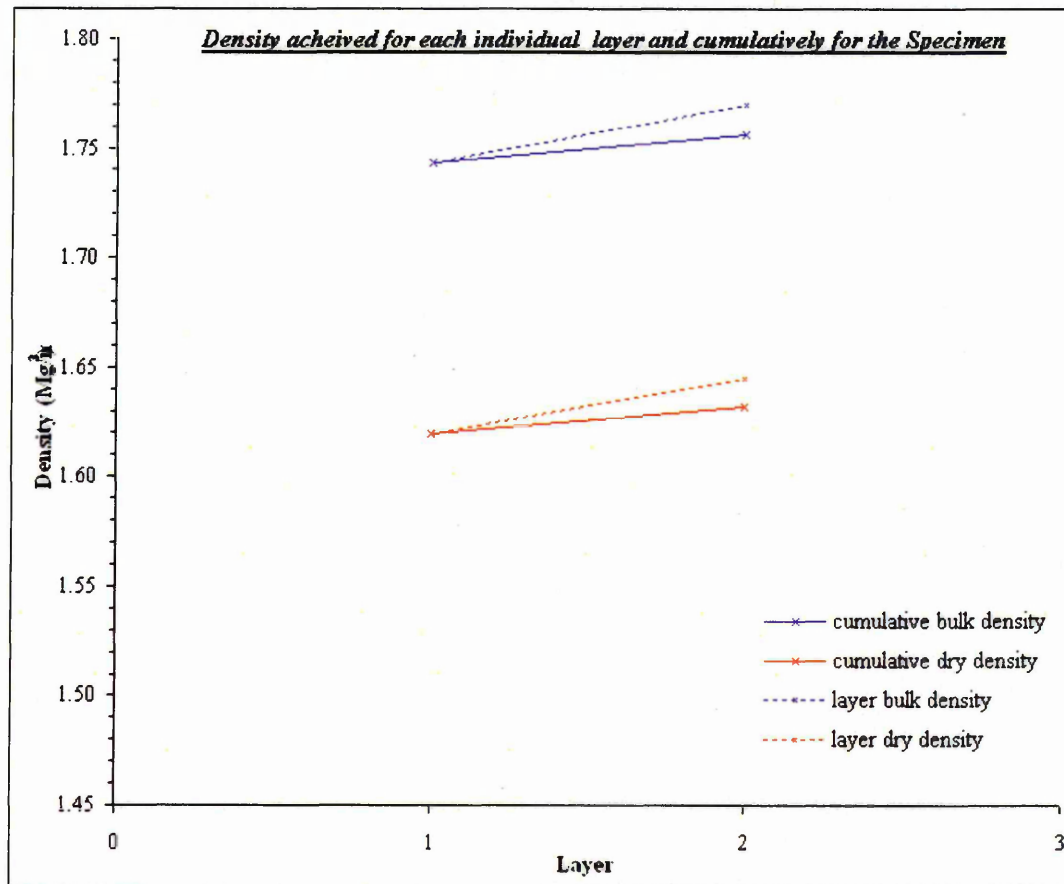
NOTES:

Specimen Moisture Content = 7.1%
 Cell diameter, d = 0.235 m
 Dimension, b = 444 mm

* It is assumed that the preceding layer was not further compacted in the calculation of these columns.

Compaction time - 3 minutes per layer

N/A - Not Applicable



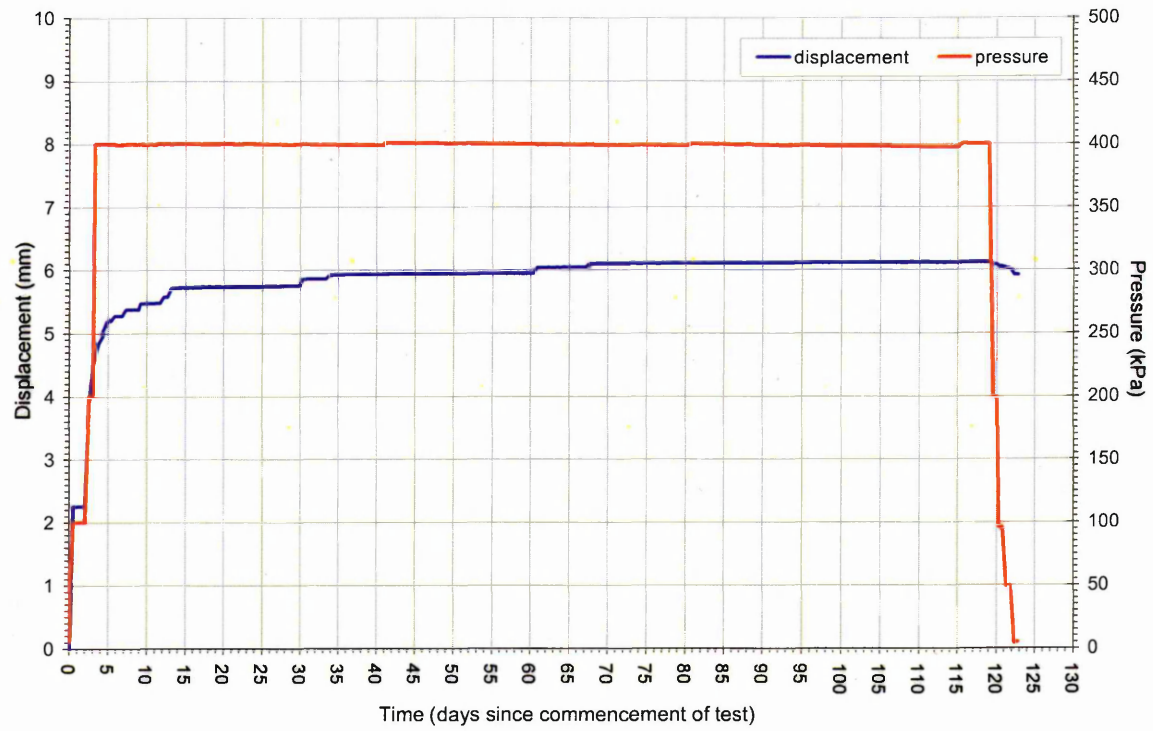


Figure 6-29: Graph of Pressure and Displacement against Time for Test 15.

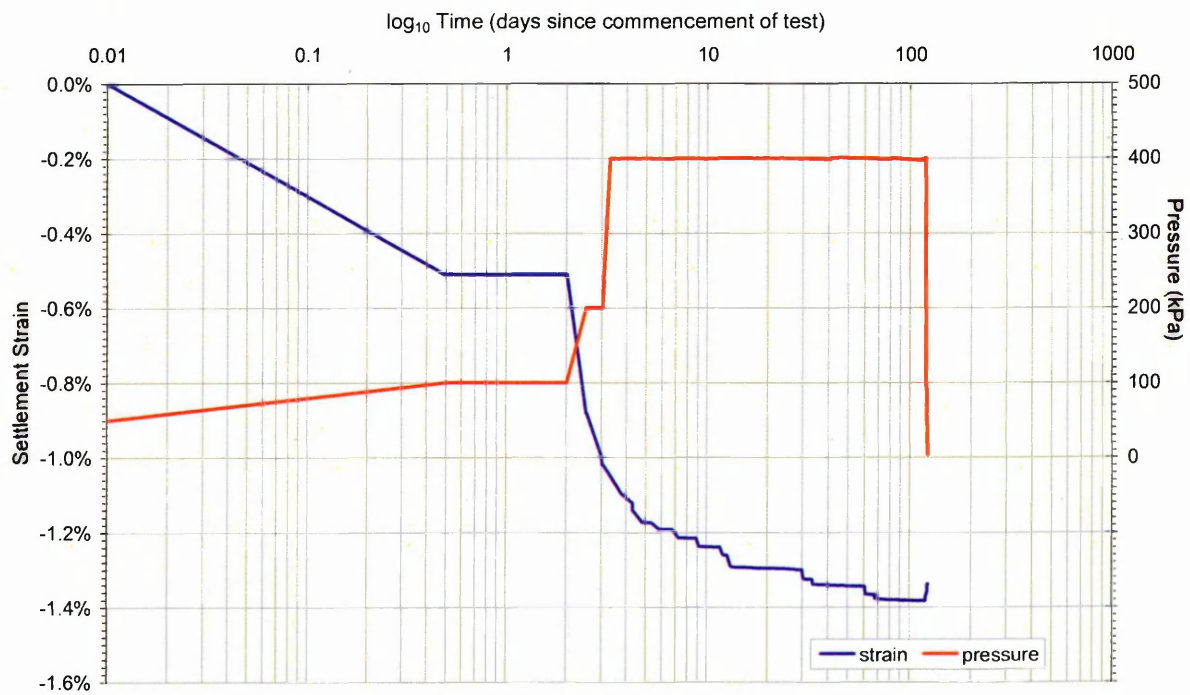


Figure 6-30: Graph of Pressure and Strain against \log_{10} Time for Test 15.

6.3 Laboratory Test Data – Summary

| Test number | Specimen info | | | | Test details | | | | Testing results | | | |
|-------------|---------------|----------------------|--|----------------------|--------------|--------------|-----|----------------------|---------------------|----------------------|------------------|----------------|
| | Source | Moisture content (%) | Dry density, ρ_d (Mg/m ³) | Compaction treatment | Cell type | Stress (kPa) | | Inundation condition | Strain measured (%) | | Creep | |
| | | | | | Applied | Corrected*1 | | Maximum | Permanent | measured over (days) | average rate (%) | |
| 1 | Houghton | 5.5 | 1.74 | Heavy | Large | 400*2 | 379 | Not inundated | 2.54 | 2.04 | ~900 | 0.5 |
| 2 | Orgreave | 7.1 | 1.83 | heavy | large | 400 | 379 | Inundated*3 | 5.95 | 5.88 | n/a | n/a*4 |
| 3 | Orgreave | 6.7 | 1.65 | light | large | 400 | 379 | Inundated | 3.05 | 2.4 | 11 / 39 *6 | 0.34 / 0.12 *6 |
| 4 | Houghton | 5 | 1.66 | light | large | 400 | 379 | Inundated | 2.5 | 2.1 | 9 / 85 *5 | 0.20 / 0.27 *5 |
| 5 | Houghton | 4.7 | 1.68 | light | small | 400*2 | 396 | Not inundated | 0.69 | - | ~650 | 0.48 |
| 6 | Orgreave | 6.9 | 1.67 | light | small | 400 | 396 | Not inundated | >0.58 | >0.54 | 118 | 0.19 |
| 7 | Houghton | 4.7 | 1.67 | light | small | 400*2 | 396 | Not inundated | 1.15 | - | ~698 | 0.25 |
| 8 | Orgreave | 6.2 | 1.65 | light | small | 400 | 396 | Not inundated | 0.9 | 0.81 | 116 | 0.15 |
| 9 | Houghton | 5.1 | 1.66 | light | small | 400 | 396 | Not inundated | 1.5 | - | 112 | 0.21 |
| 10 | Orgreave | 7.1 | 1.72 | heavy | small | 400 | 396 | Not inundated | 1.11 | - | 123 | 0.08 |
| 11 | Orgreave | 7.1 | 1.73 | heavy | small | 400 | 396 | Not inundated | 1.06 | 0.84 | 129 | 0.07 |
| 12 | Houghton | 4.8 | 1.77 | heavy | small | 400 | 396 | Not inundated | 2.2 | 1.99 | 110 | 0.12 |
| 13 | Orgreave | 7.1 | 1.57 | light | small | 400 | 396 | Not inundated | 1.13 | 1 | 123 | 0.1 |
| 14 | Houghton | 4.7 | 1.76 | heavy | small | 400 | 396 | Not inundated | >1.11 | >1.00 | 96 | 0.13 |
| 15 | Orgreave | 7.1 | 1.63 | light | small | 400 | 396 | Not inundated | 1.38 | 1.34 | 116 | 0.1 |

Notes

- Corrected pressure is that seen mid-height of the specimen and assumes that load lost to side wall friction is that given in Table 4-1.
- Generally, the load was kept constant; however, in order to assess the effects of stress variation two short unload / reload cycles were undertaken.
- Due to a diaphragm failure the specimen was inundated during initial loading, after the diaphragm was replaced the specimen was loading in its wet state.
- A constant creep rate was not measured; the specimen demonstrated a linear deformation with time at a rate of approximately 0.20%.
- The specimen was loaded and the stress kept constant, creep rate of 0.20% was prevalent. The specimen was then inundated and the applied stress kept constant, following inundation a creep rate of 0.27% was observed.
- The specimen was loaded and the stress kept constant, creep rate of 0.34% was prevalent. The specimen was then inundated and the applied stress kept constant, following inundation a creep rate of 0.12% was observed.

Table 6-1: Summary of Laboratory Testing Results.

6.4 Computed Tomography Data

6.4.1 Introduction

Of the testing detailed above carried out in a small cell, two sets of cross-sectional images through the specimens were taken using the CT scanner at the Royal Hallamshire Hospital. One set immediately following the completion of the specimen loading phase and a second set taken prior to unloading.

From these cross-sectional images three dimensional images can be generated as can longitudinal sections. In order to render the volume of this data manageable, two similar longitudinal and two similar cross sections for each scan of each test are presented and analysed here.

The section locations are shown in Figure 6-31. Similar sections taken from the scans immediately following loading are presented next to the similar section generated from the scans taken prior to unloading for each scanned specimen.

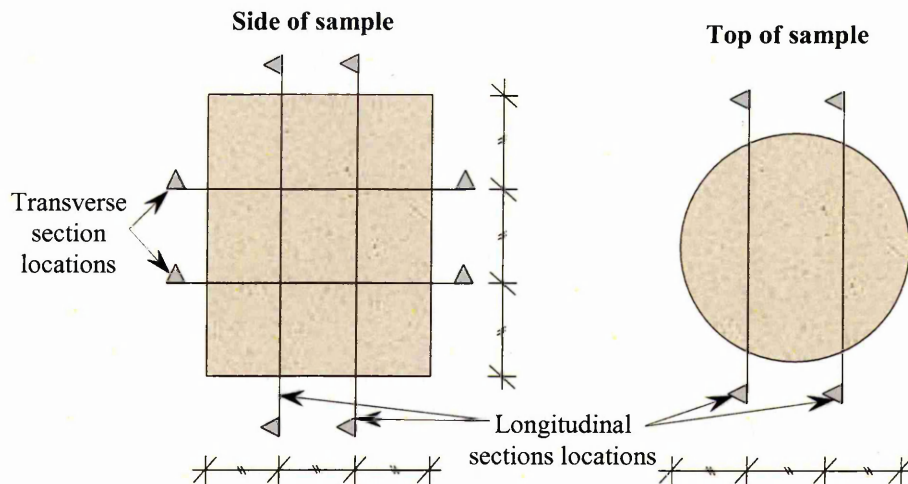


Figure 6-31: CT section locations.

6.4.2 Analysis of CT Scans

Analysis of the scans is essentially qualitative and has been made by comparing similar sections and identifying differences between them. Each

section was generated on the CT scanners workstation (see Figure 4-13). The sectional images were then compared visually on the screens of the workstation and the differences noted.

Print outs of these images are presented in the subsequent sections.

The differences noted between images were graded using the scale detailed Table 6-2. These categories are purposefully kept simple to make observations significant and to remove, as much as possible, subjectivity. The areas of difference are highlighted the images presented in subsequent sections using the colour coding also shown Table 6-2.




| Scale | Colour code | Degree of difference |
|-------|---|-------------------------|
| 1 |  | Minor difference. |
| 3 |  | Significant difference. |
| 5 |  | Major difference. |

Table 6-2: Scale of differences used in the analysis of the CT results.

As can be seen in Table 6-2, a numerical value is ascribed to a difference dependent up on how greater a difference is apparent. The numerical values selected provide a simple linear scale of 1, 3 and 5 grading the differences as minor, significant and major respectively. Herein, this scale is referred to as the ‘differences scale’.

The criteria for each for locating a noted difference on the scale are:

- 1 - Minor differences – are those where an area of the image shows apparent slight differences. It is recognised that these differences may be due to errors in reconstruction of the similar section, *i.e.* that the sections are not perfectly in the same plane or same location. It is not possible with the available CT image viewing software to select an absolute location.

2 - Significant differences – are those areas of the images which show clear differences between the two similar sections. They are not attributable to errors due to the limitations of the image viewing software.

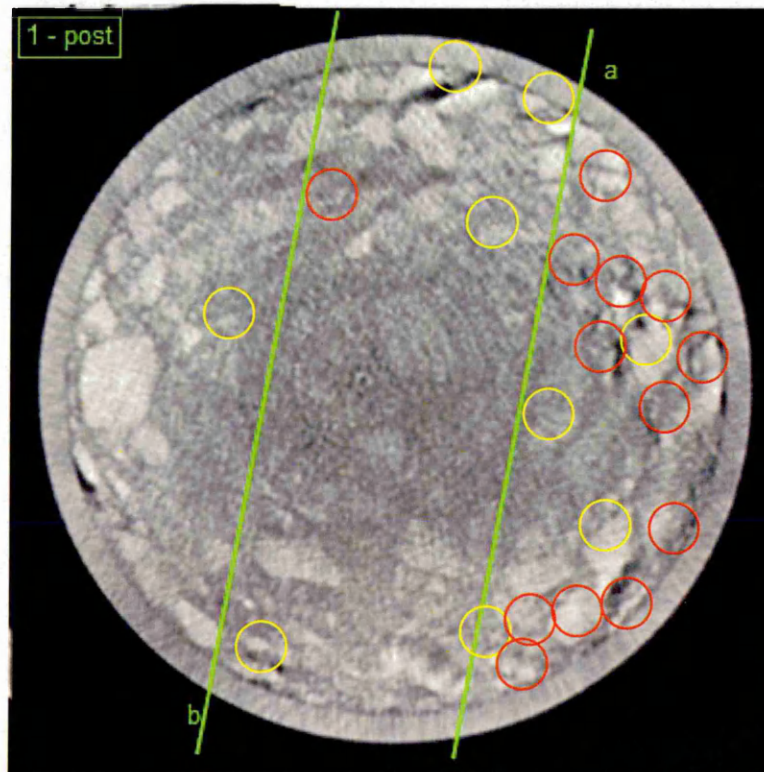
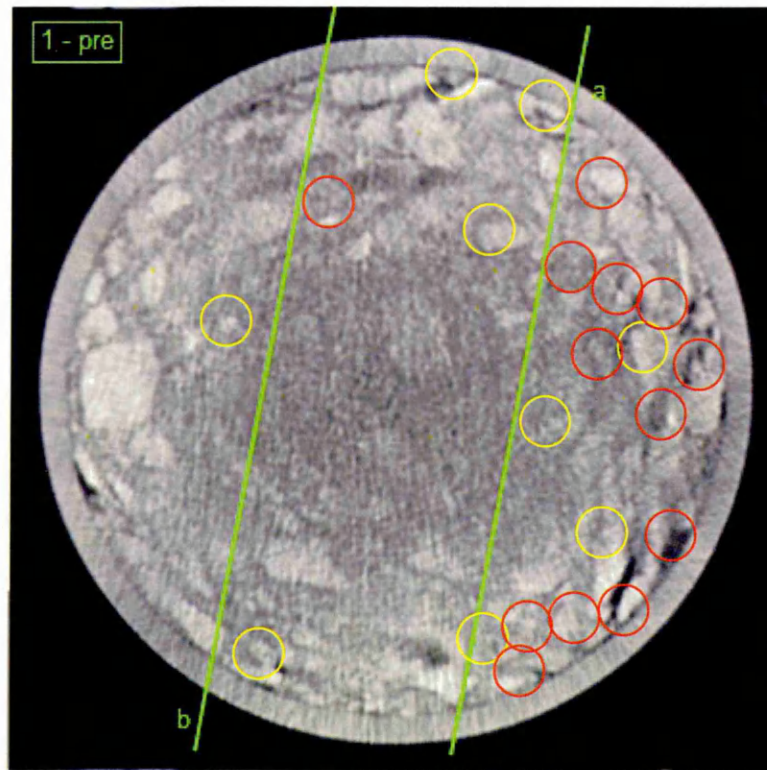
3 - Major difference – are those areas of the images which show clear differences between the two similar sections to such an extent that the images are no longer easily comparable. They are not attributable to errors due to the limitations of the image viewing software.

This method is a simplification of that proposed by Fair (2003) for quantifying the breakage of railway ballast. This more complex method subdivides breakage into ‘asperity breakage’, ‘flaking’, ‘small breakage’, ‘medium breakage’, ‘large breakage’ and ‘crushing’. Here the simplified method does not have so many sub-divisions but is expanded to include particle rotations and other re-orientations.

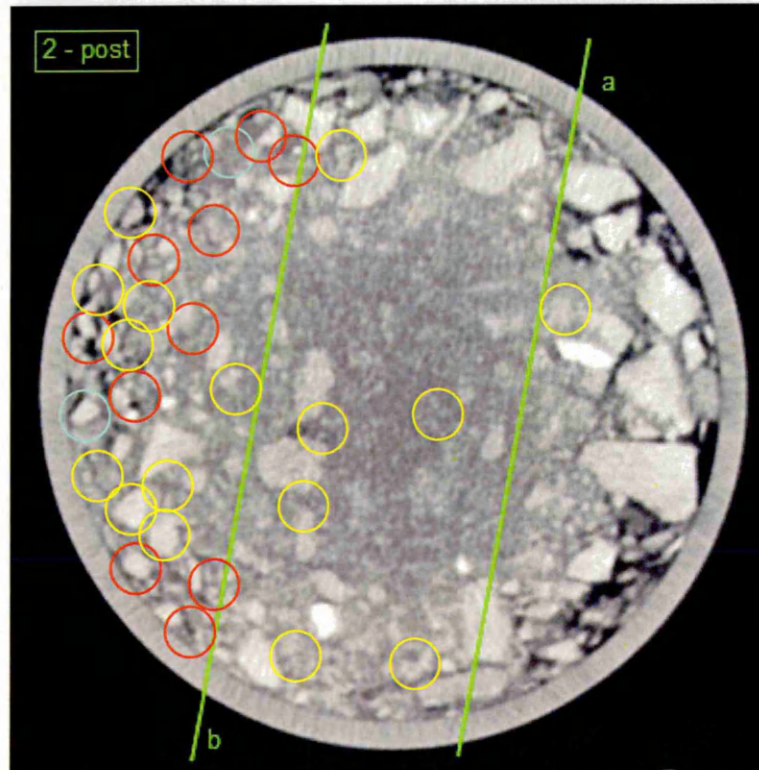
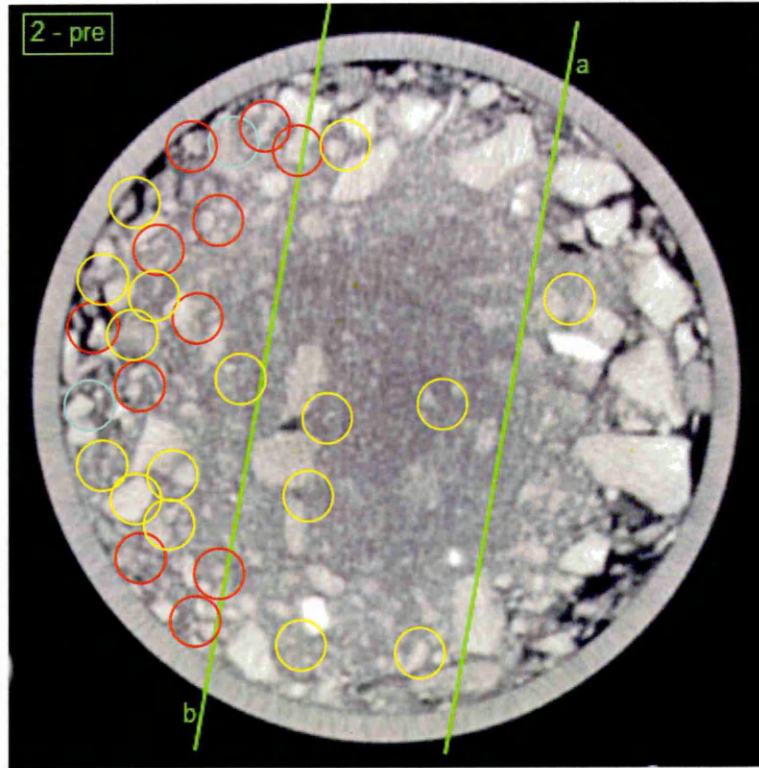
The analysis of the pairs of images yields the number of differences within each degree of the differences scale (i.e. minor, significant and major). The aggregate number of occurrences of each of these degrees is then multiplied by the numeric value from the scale. This product is, herein, termed the ‘image differences score’. Summing all of the images differences scores for each sample gives the ‘test differences score’. An example of these calculations is given in Table 6-3.

| Difference | Scale | Number of differences | Image difference score | test differences score |
|-------------|-------|-----------------------|------------------------|------------------------|
| | | | | |
| Minor | 1 | 12 | 12 | 28 |
| Significant | 3 | 2 | 6 | |
| Major | 5 | 2 | 10 | |

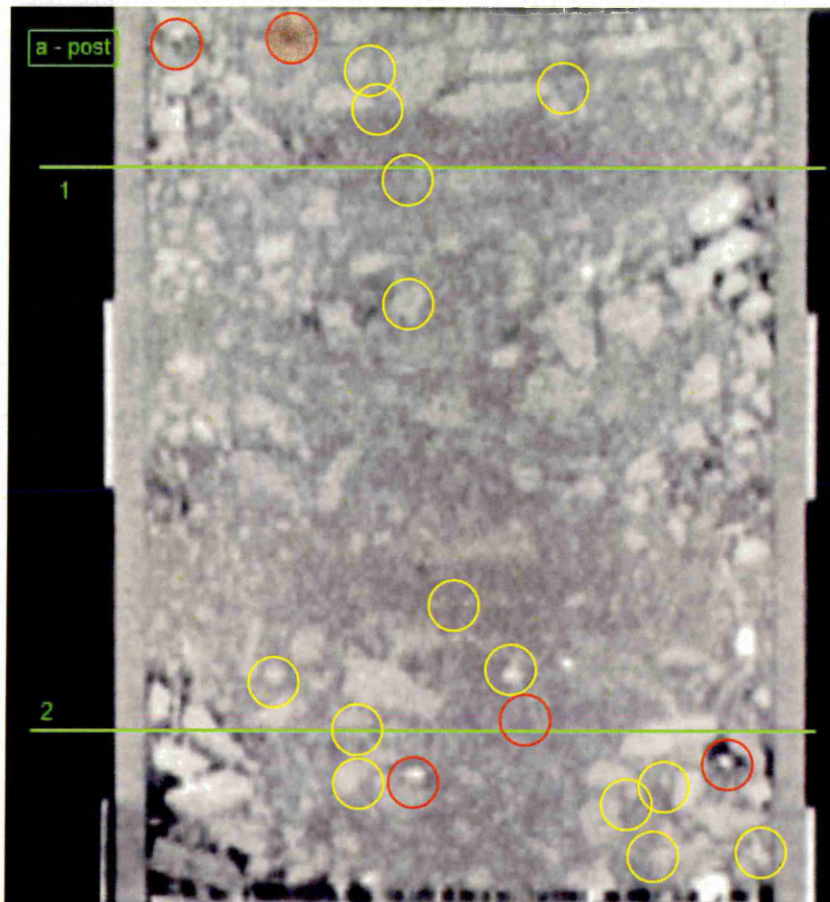
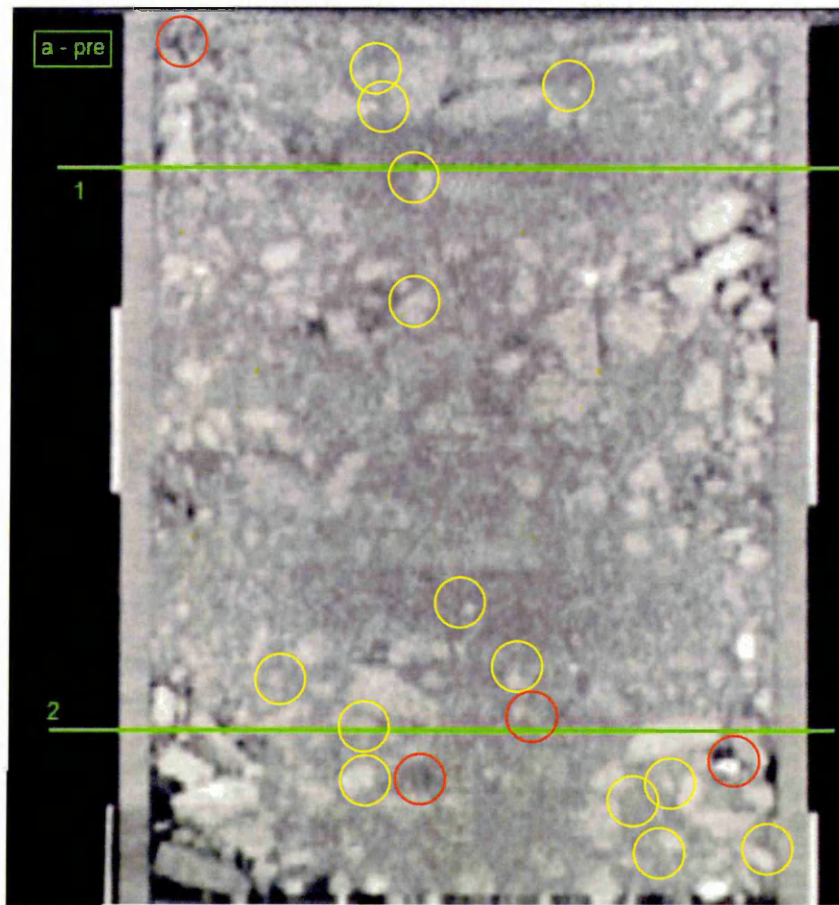
Table 6-3: Example of calculation of ‘differences score’.



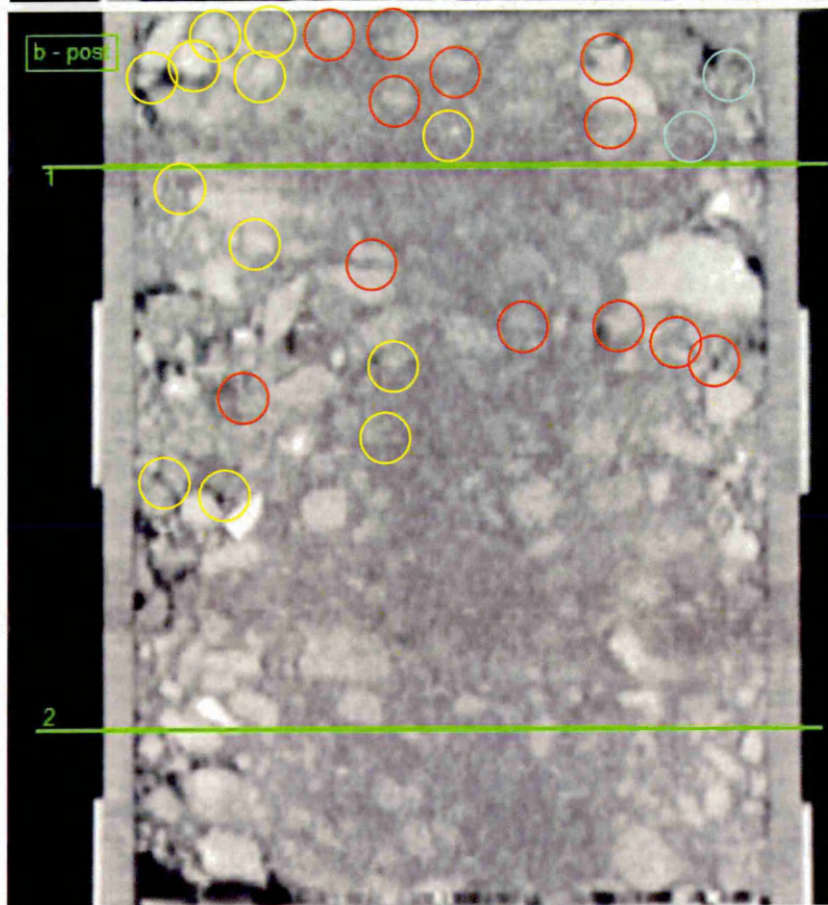
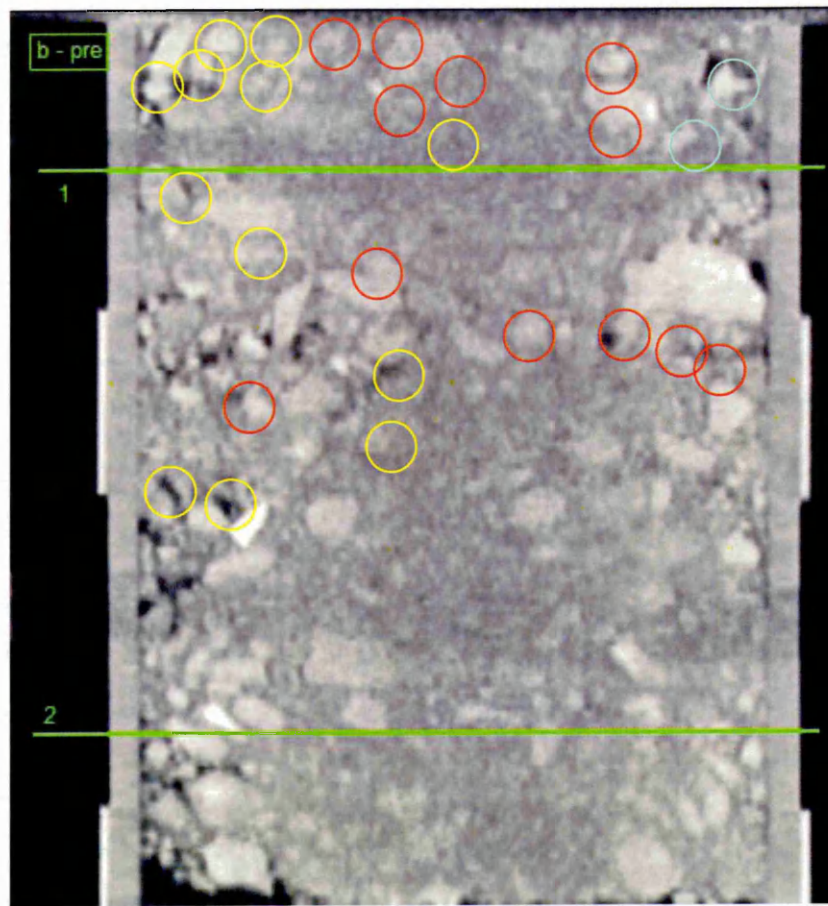
CT Scans of
Test 5

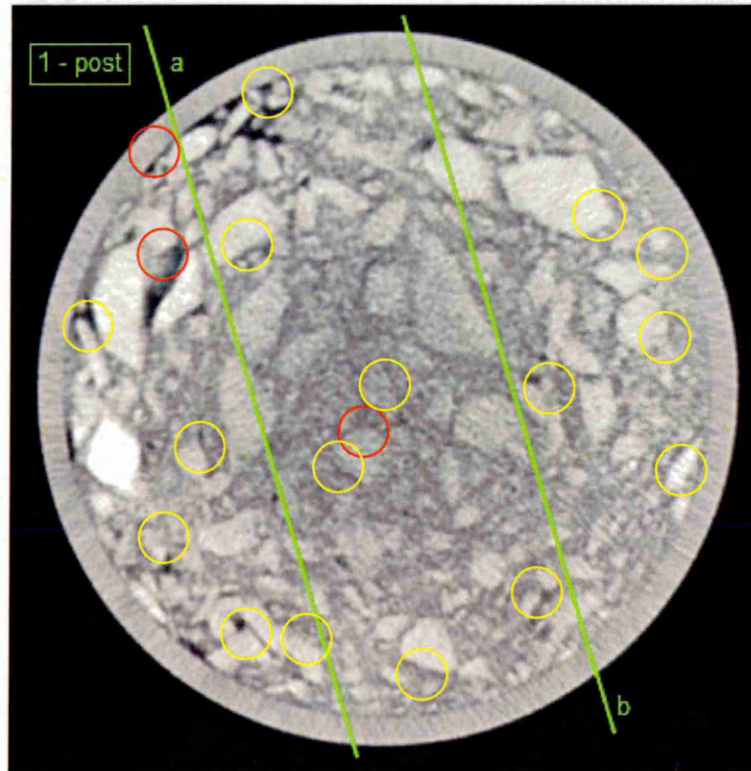
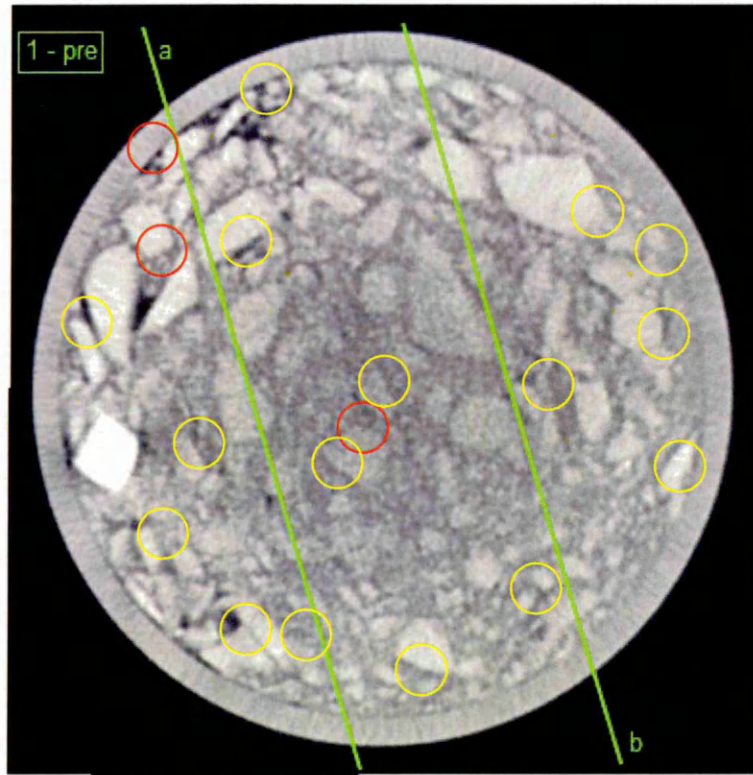


CT Scans of
Test 5

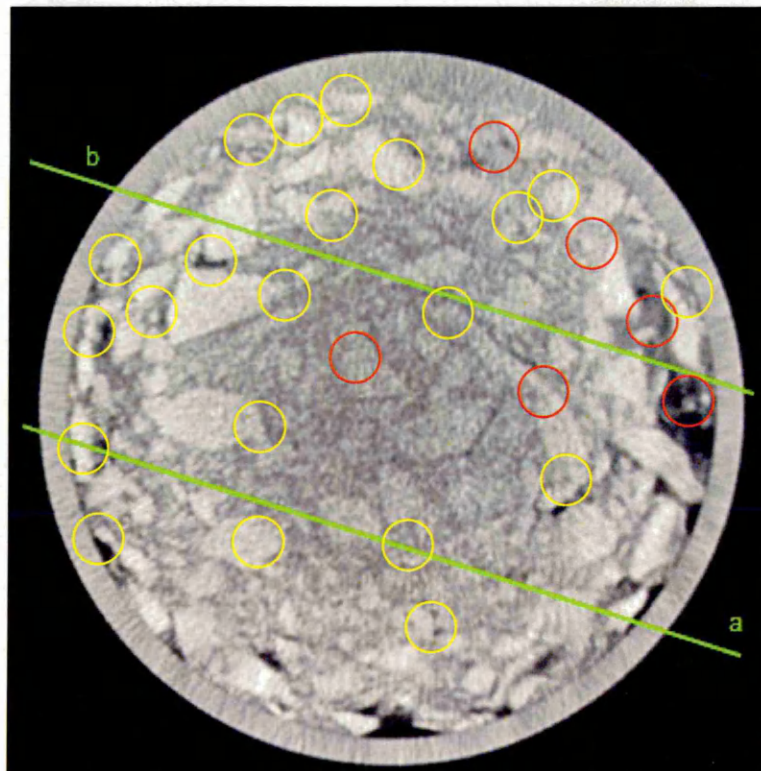
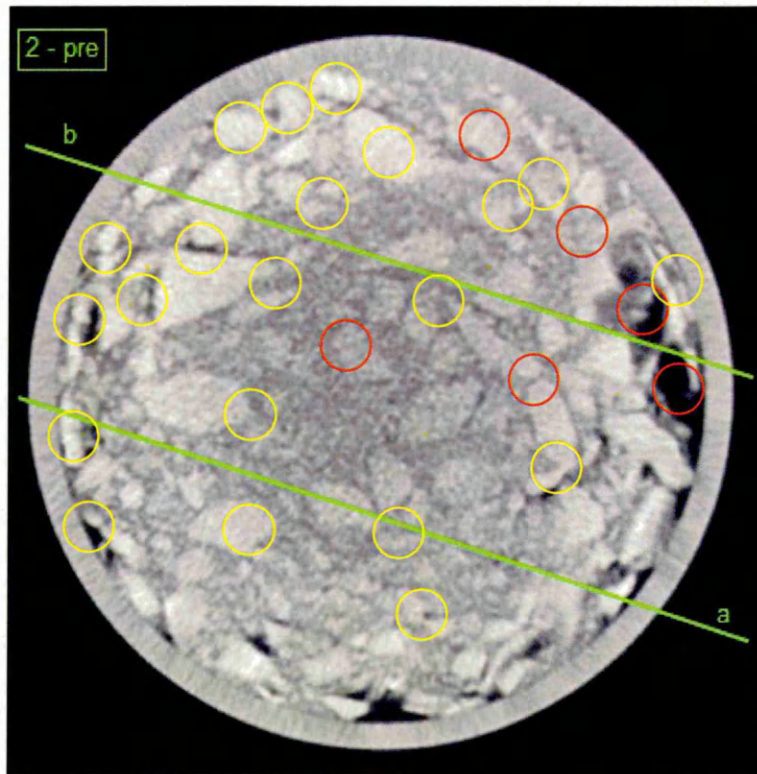


CT Scans of
Test 5

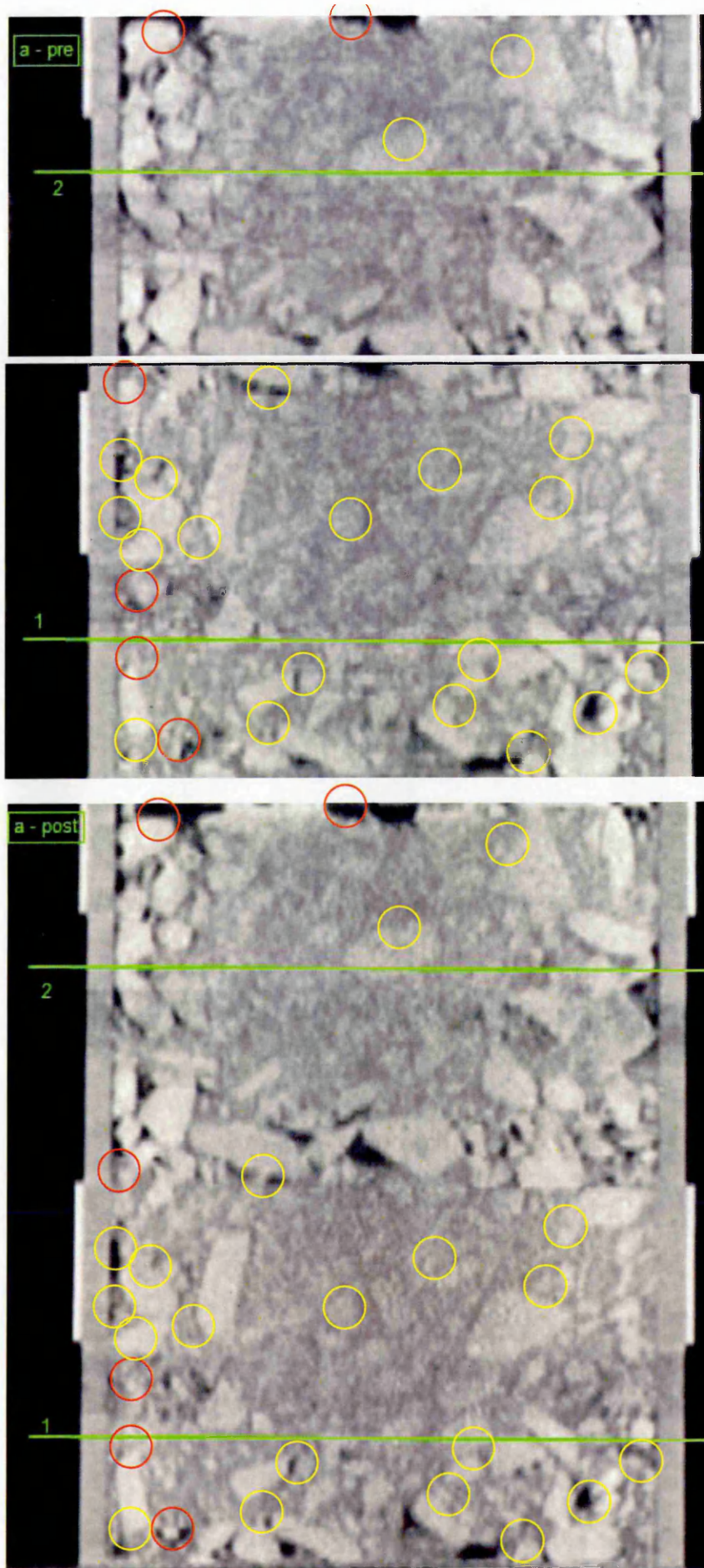




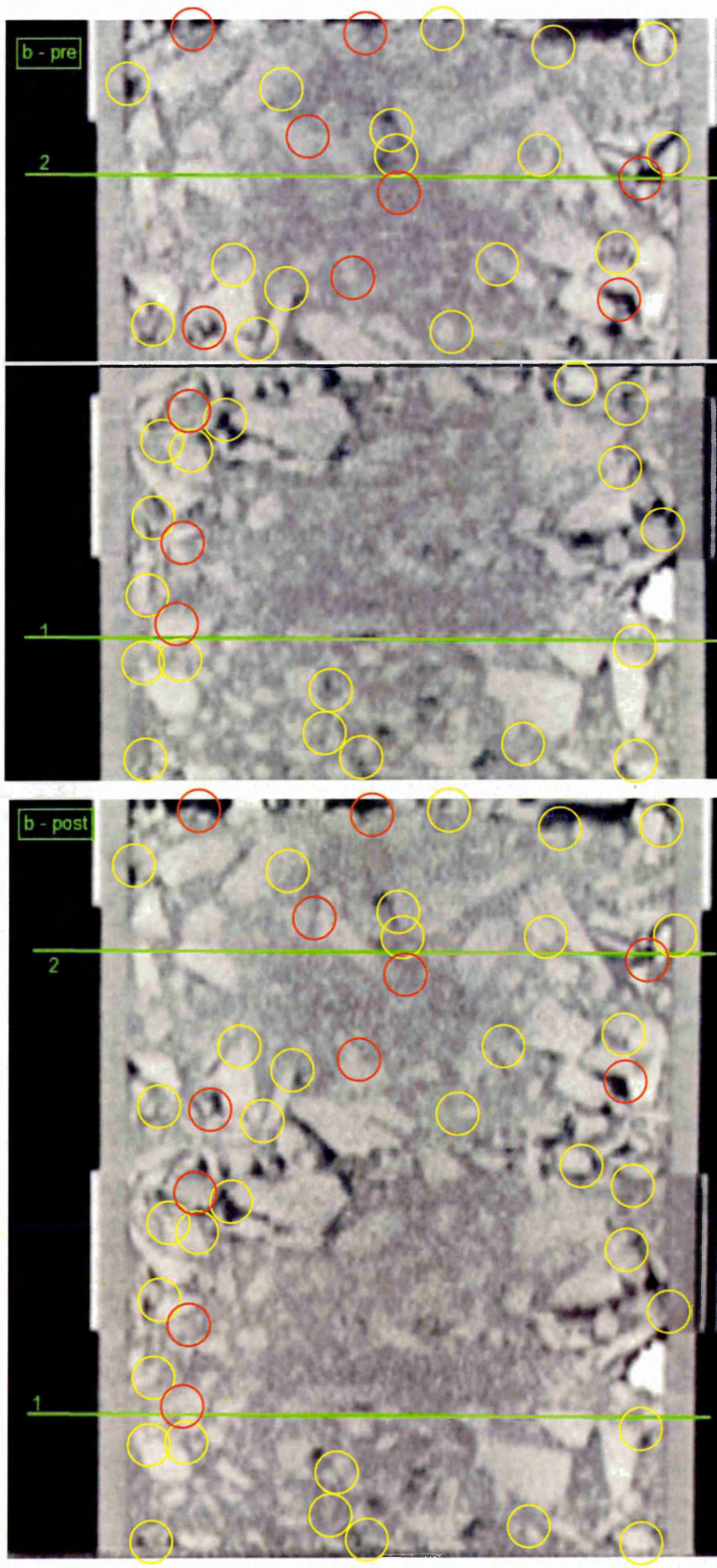
CT Scans of
Test 6

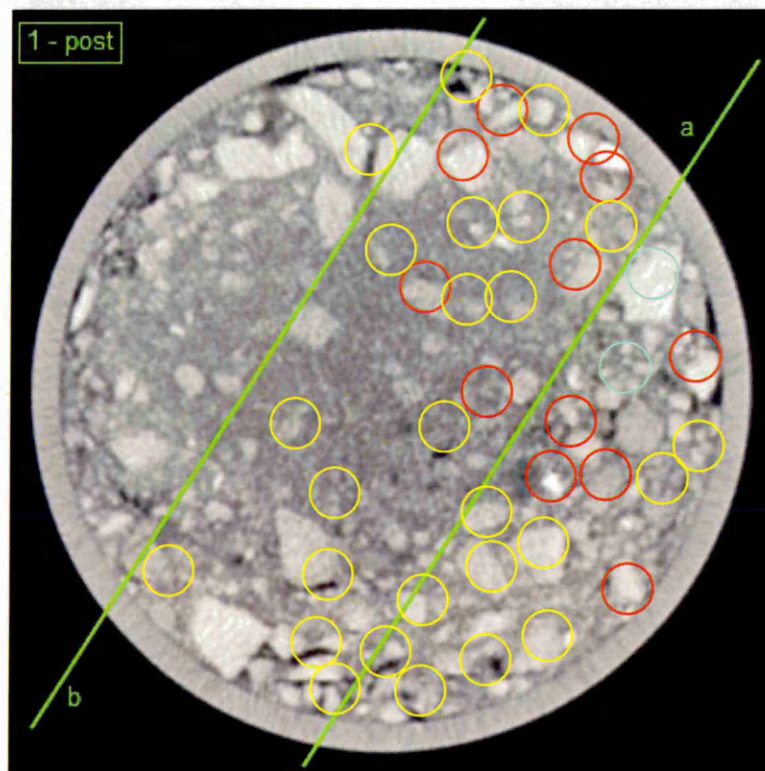
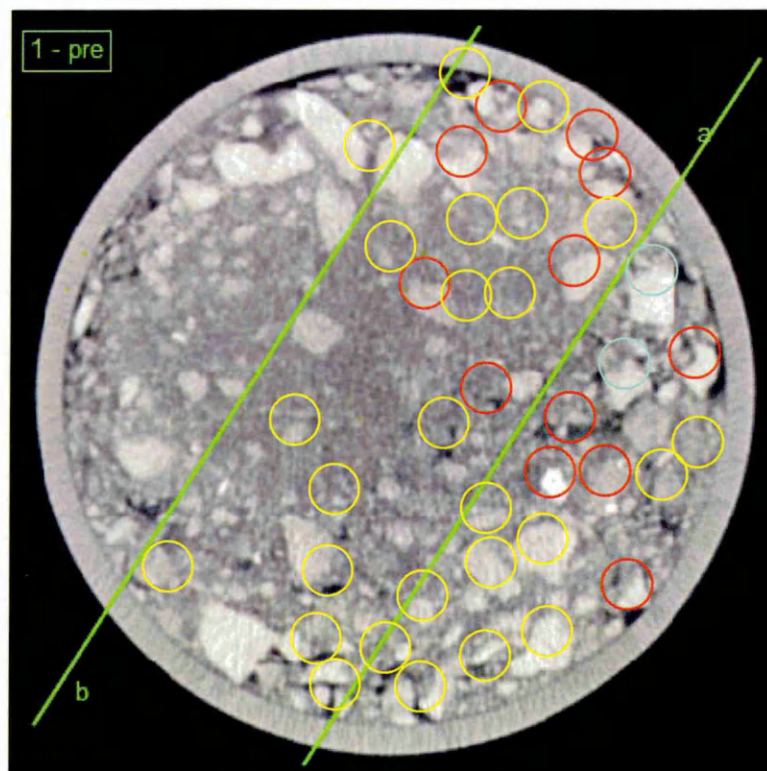


CT Scans of
Test 6

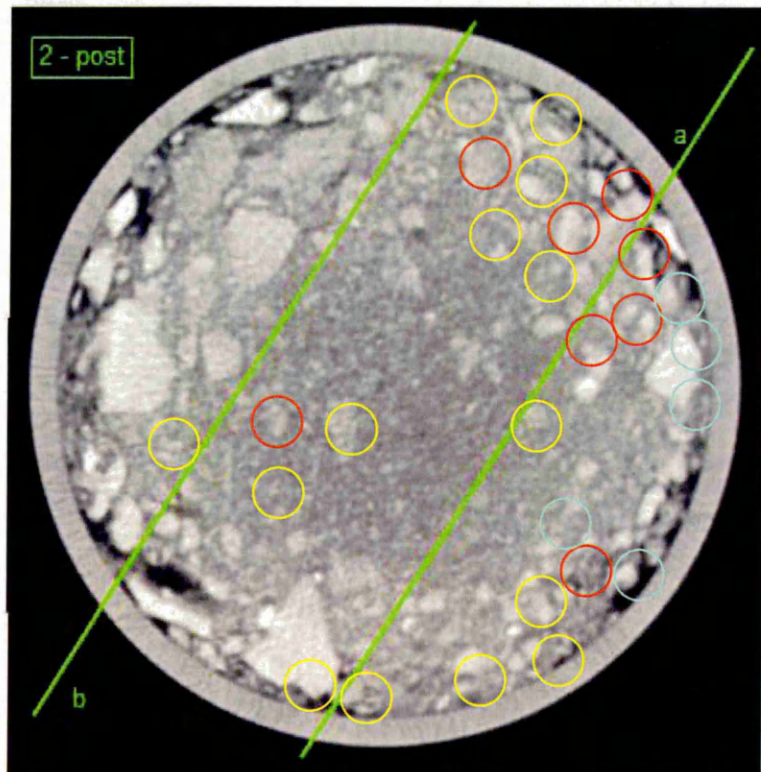
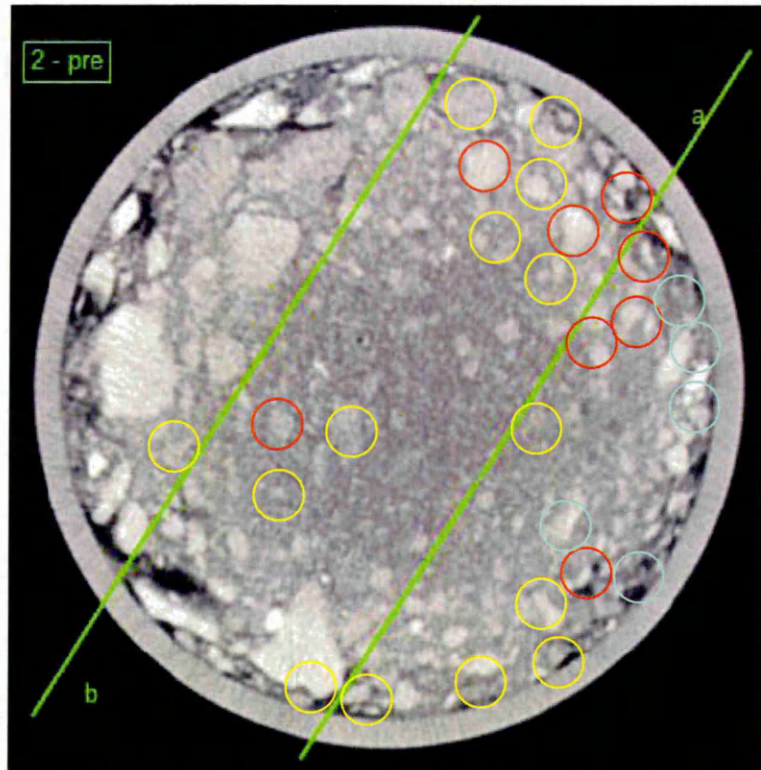


CT Scans of
Test 6

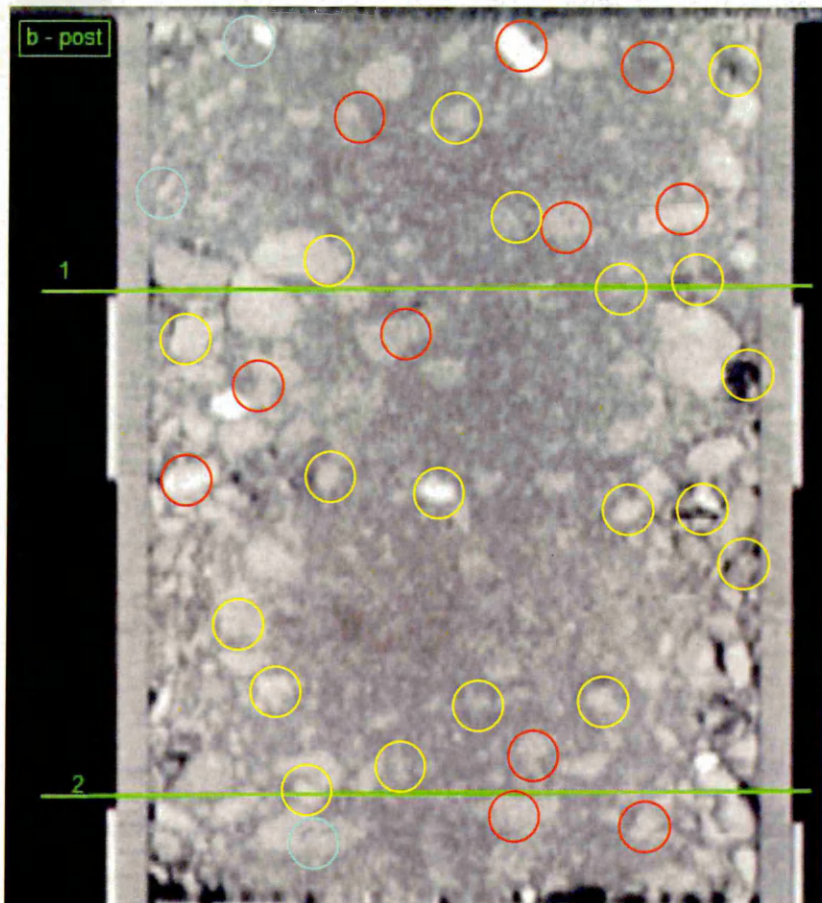
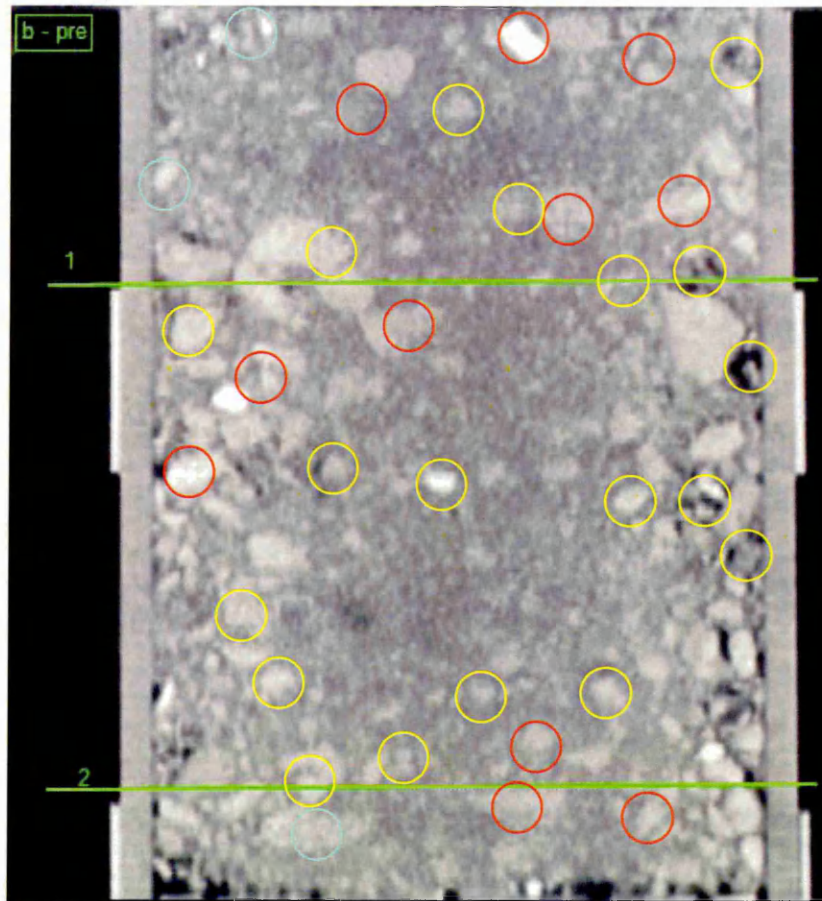




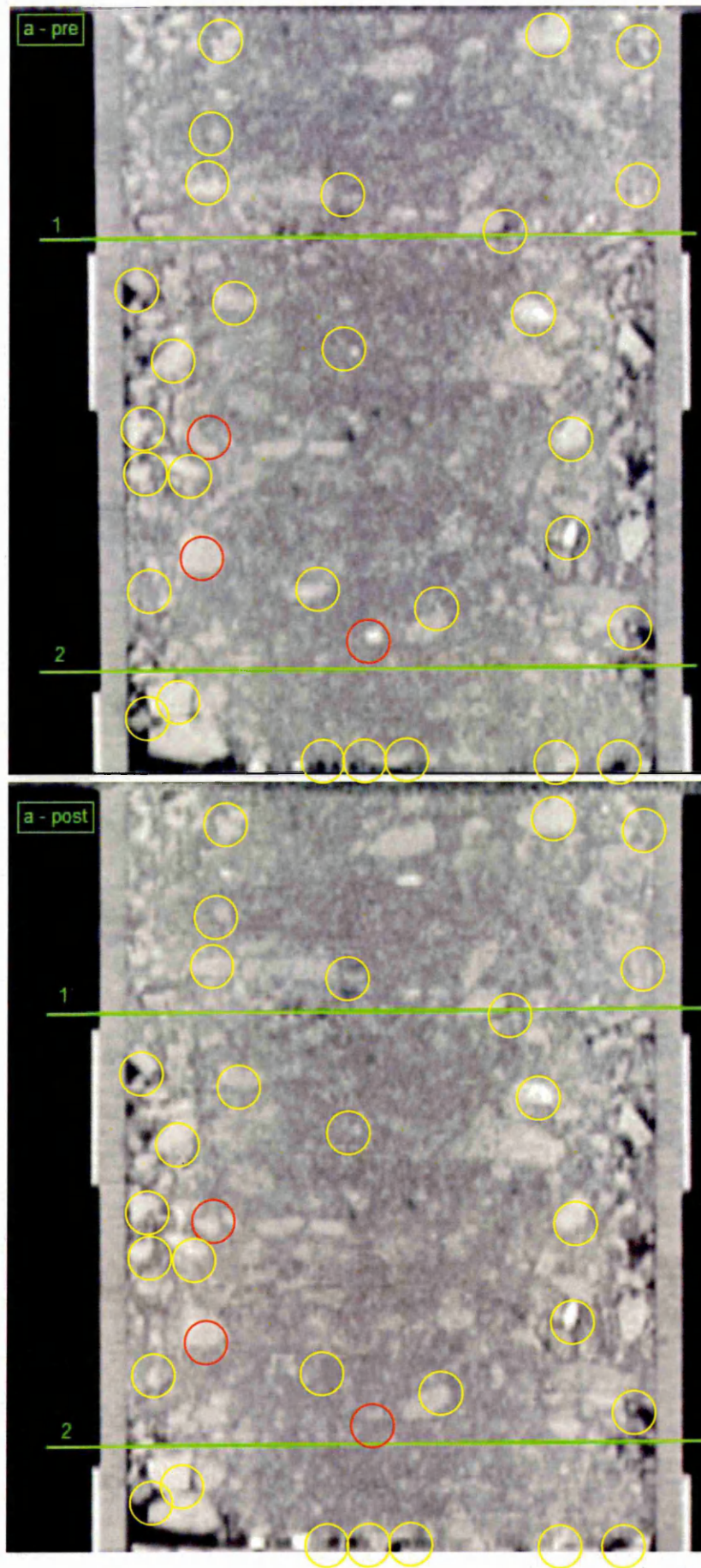
CT Scans of
Test 8

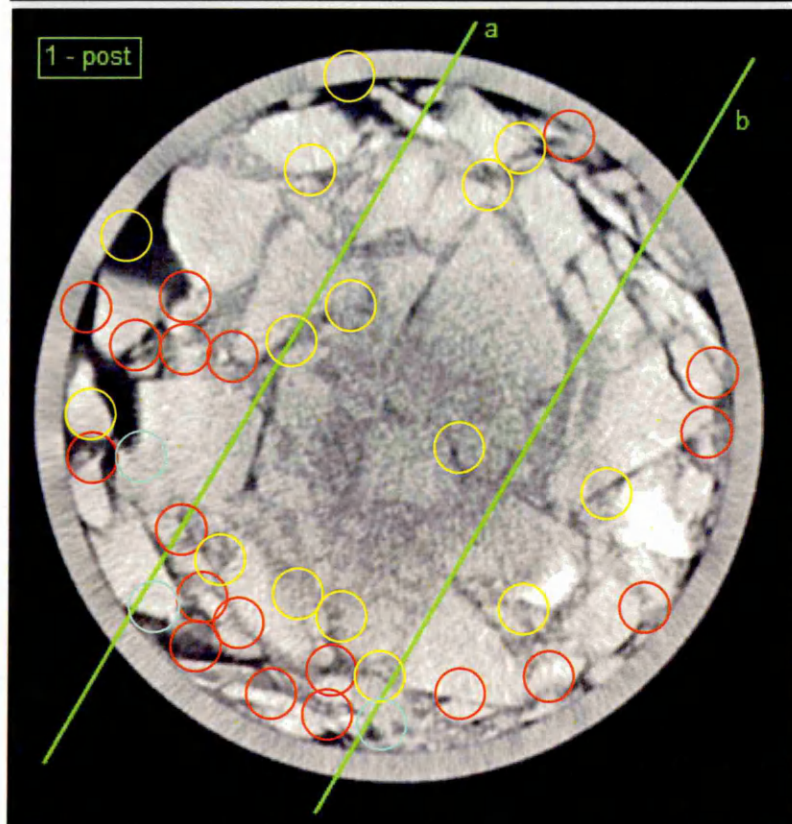
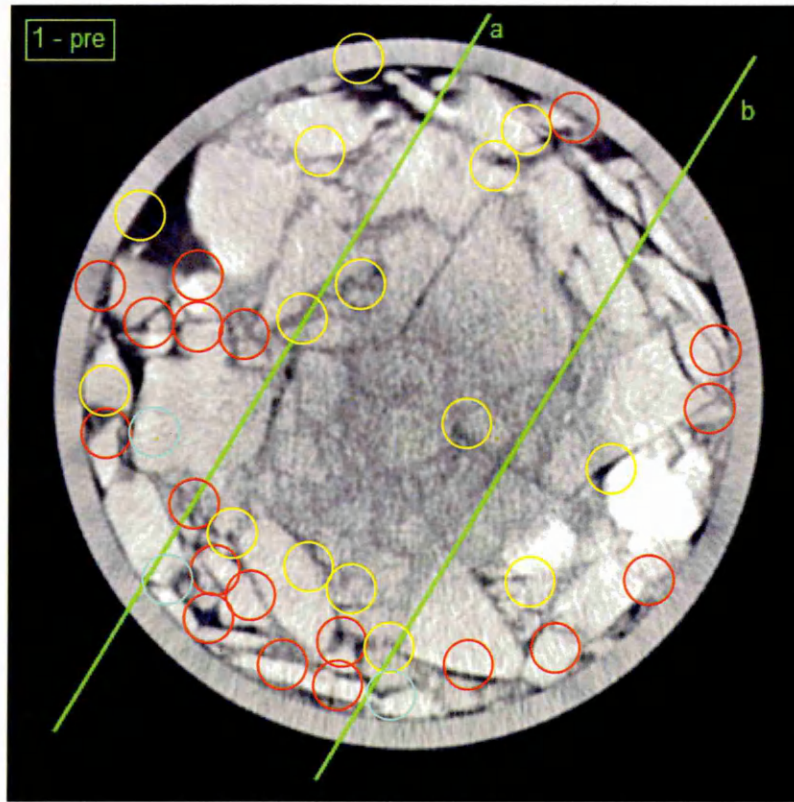


CT Scans of
Test 8

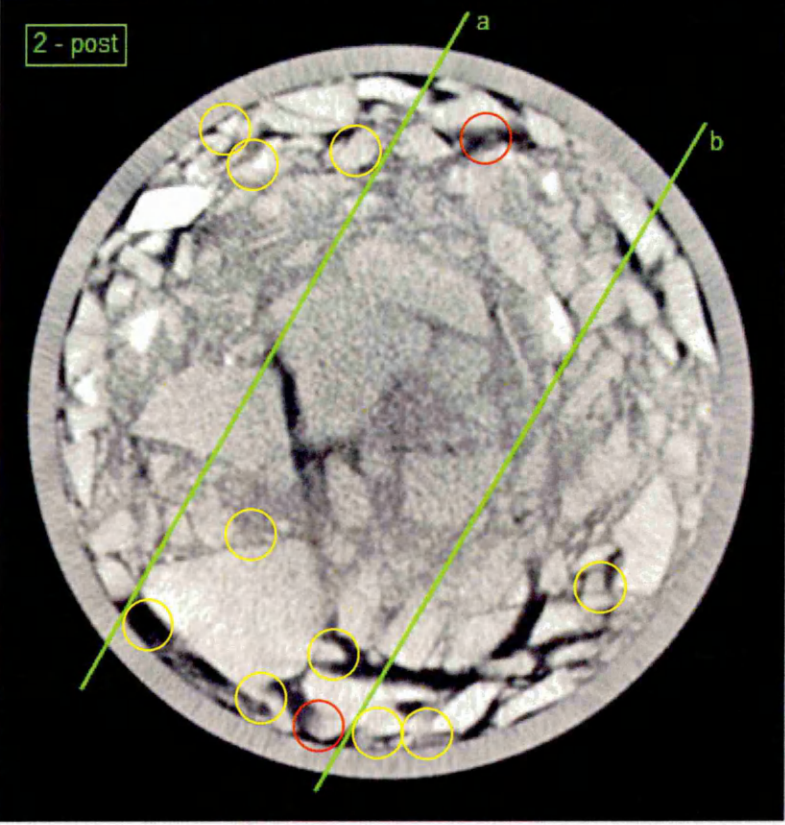
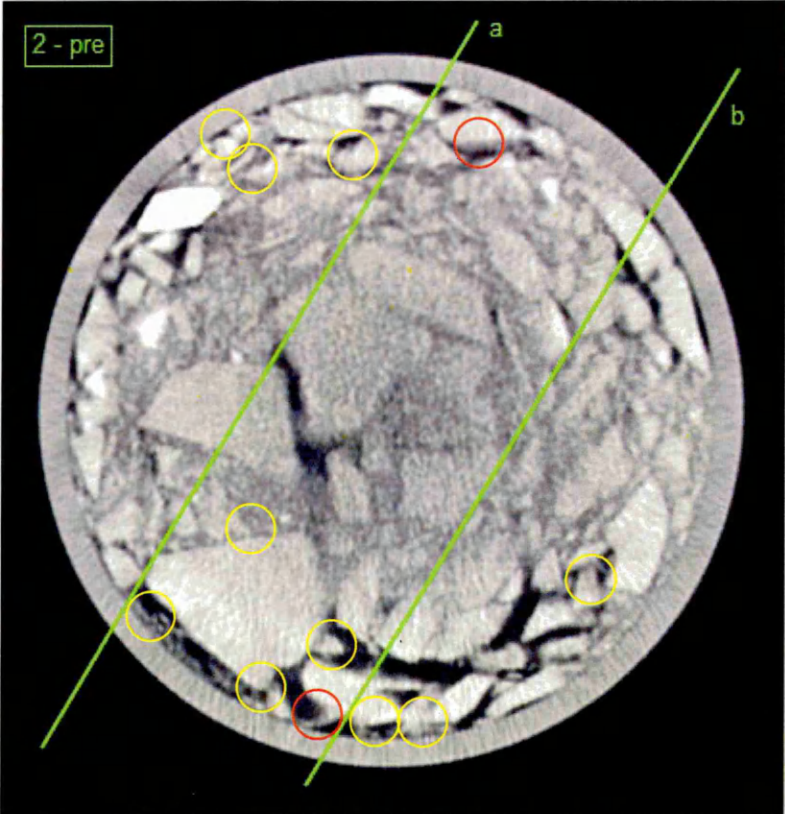


CT Scans of
Test 8

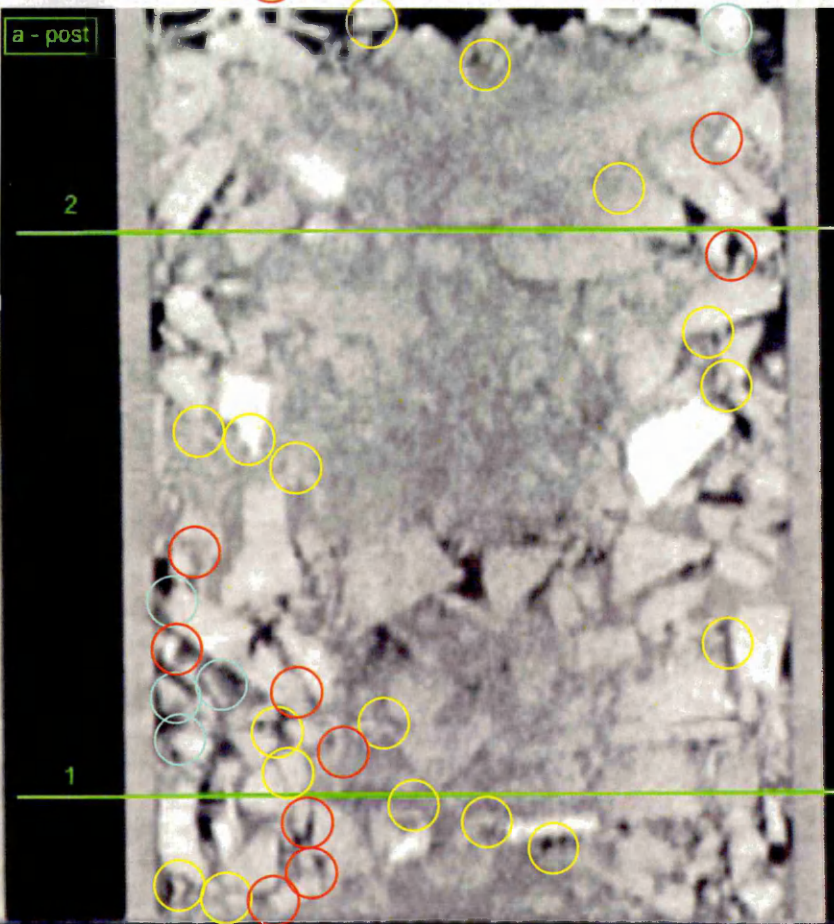
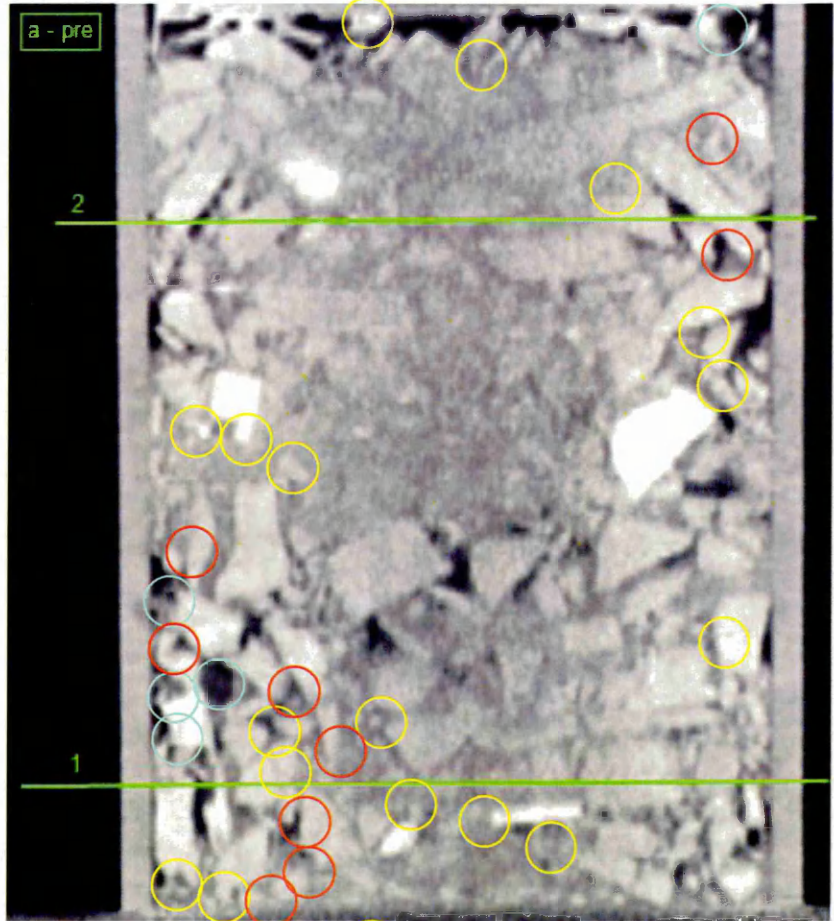




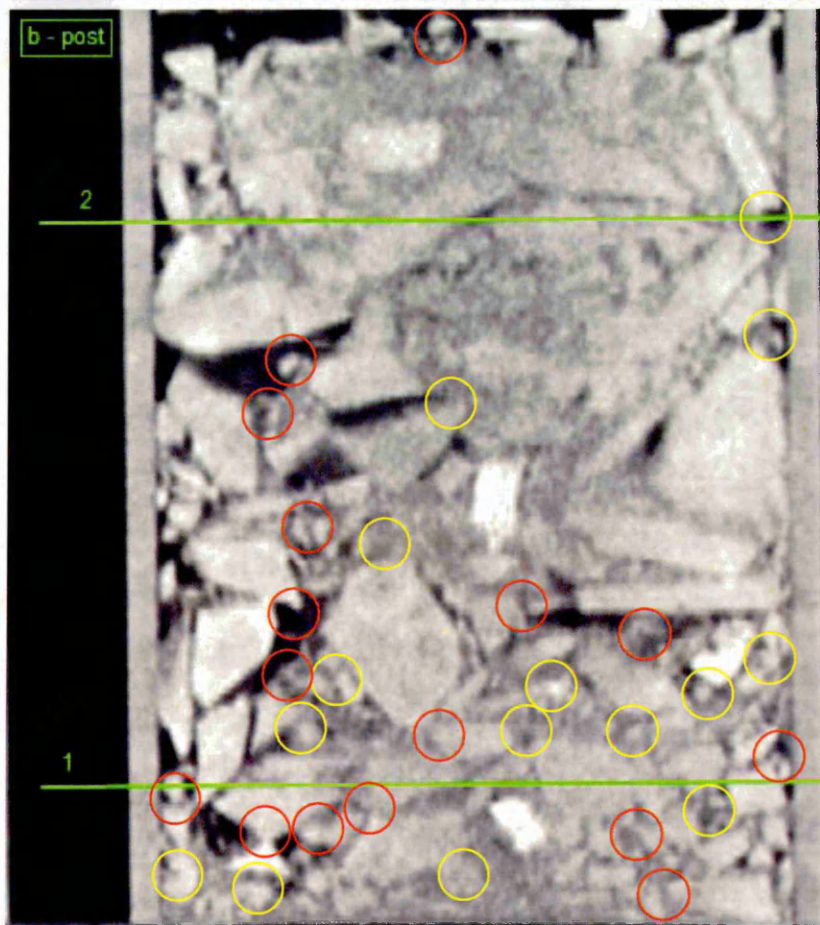
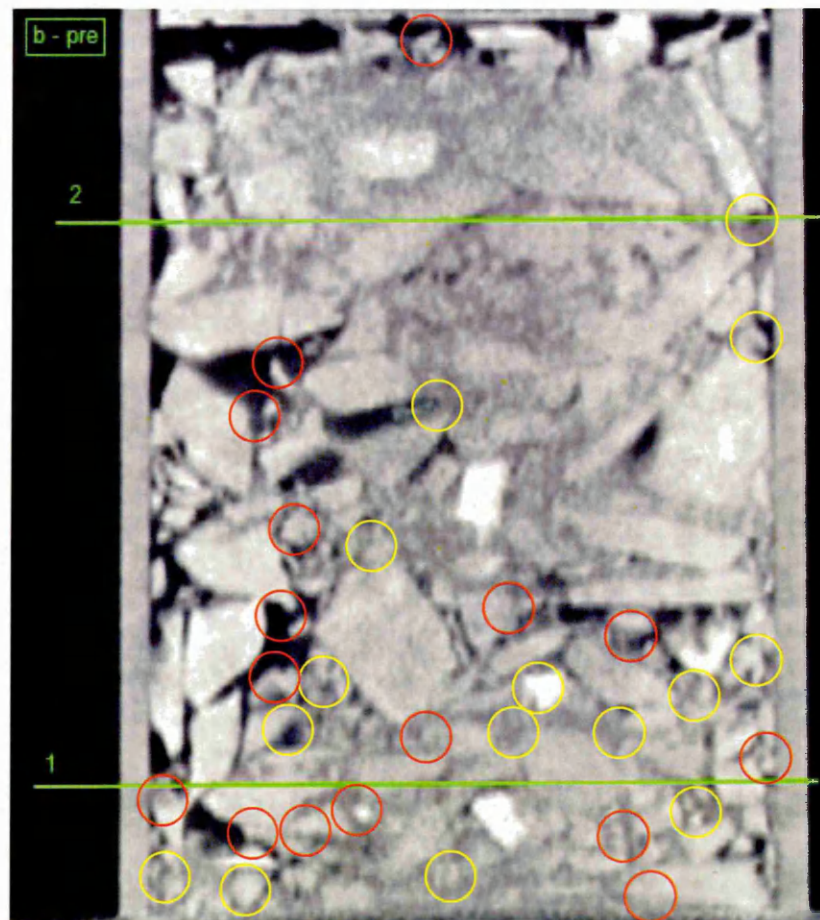
CT Scans of
Test 9

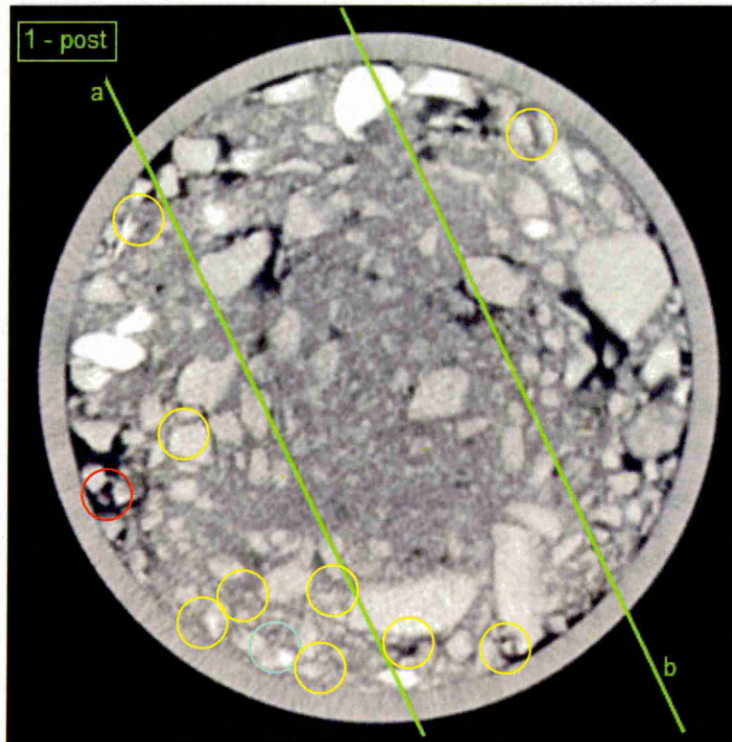
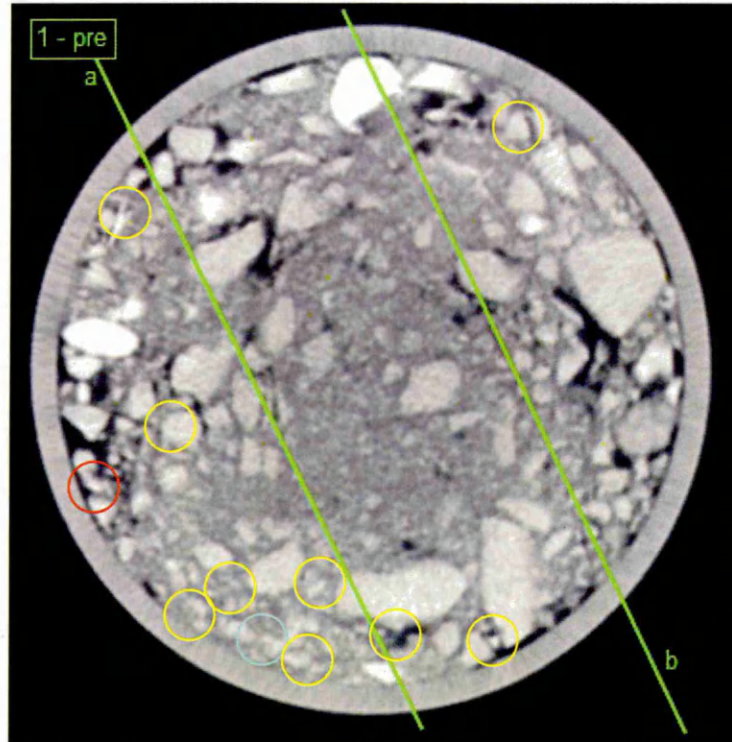


CT Scans of
Test 9

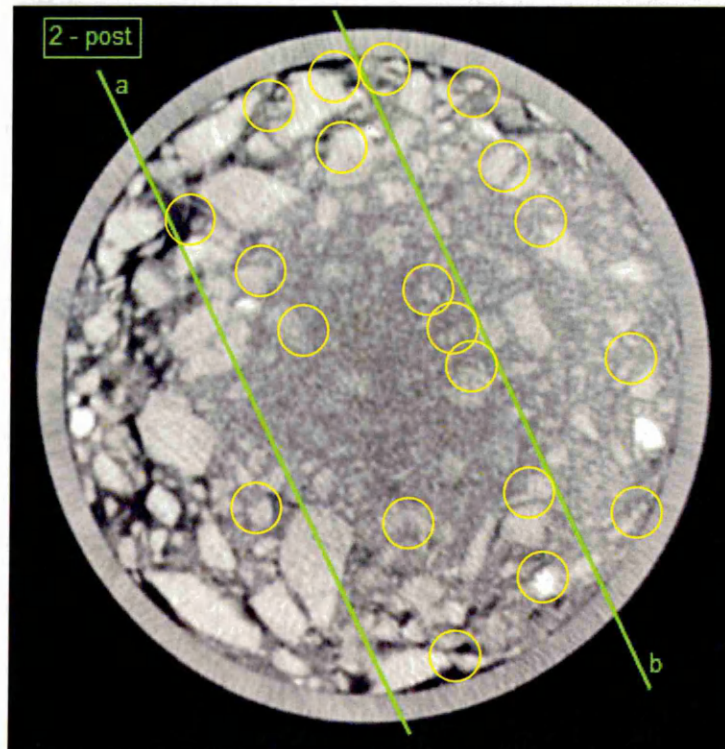
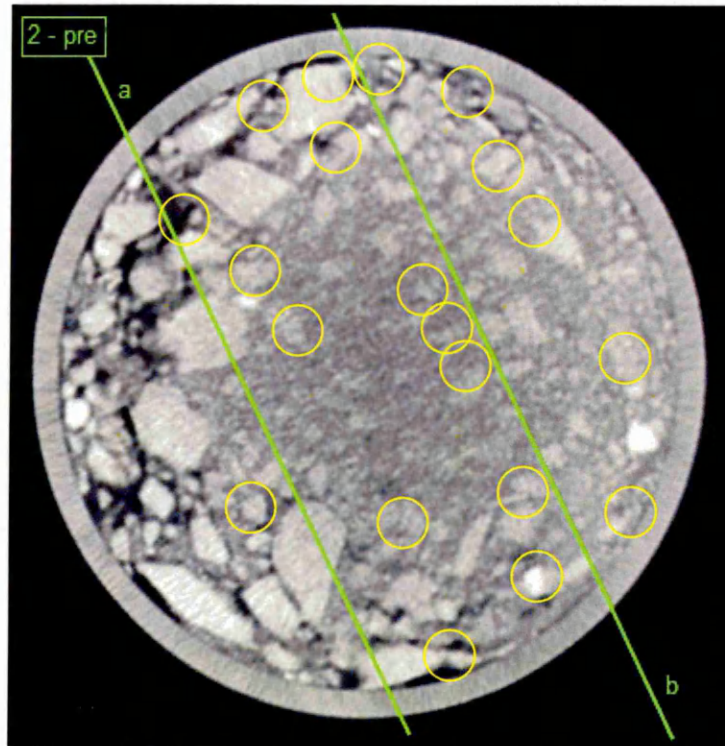


CT Scans of
Test 9

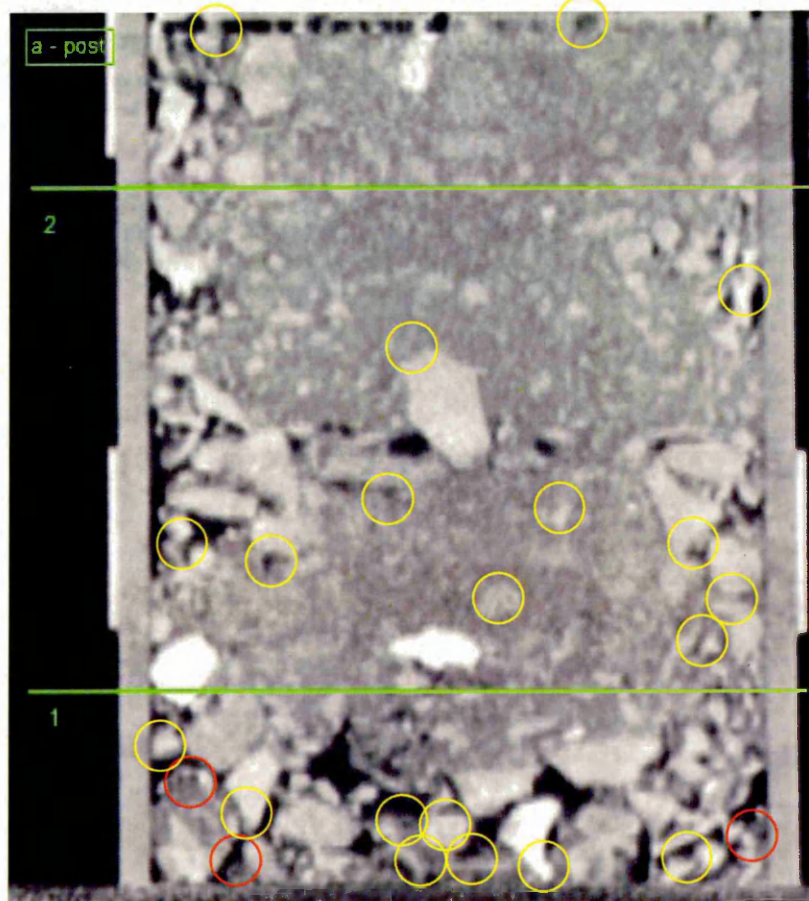
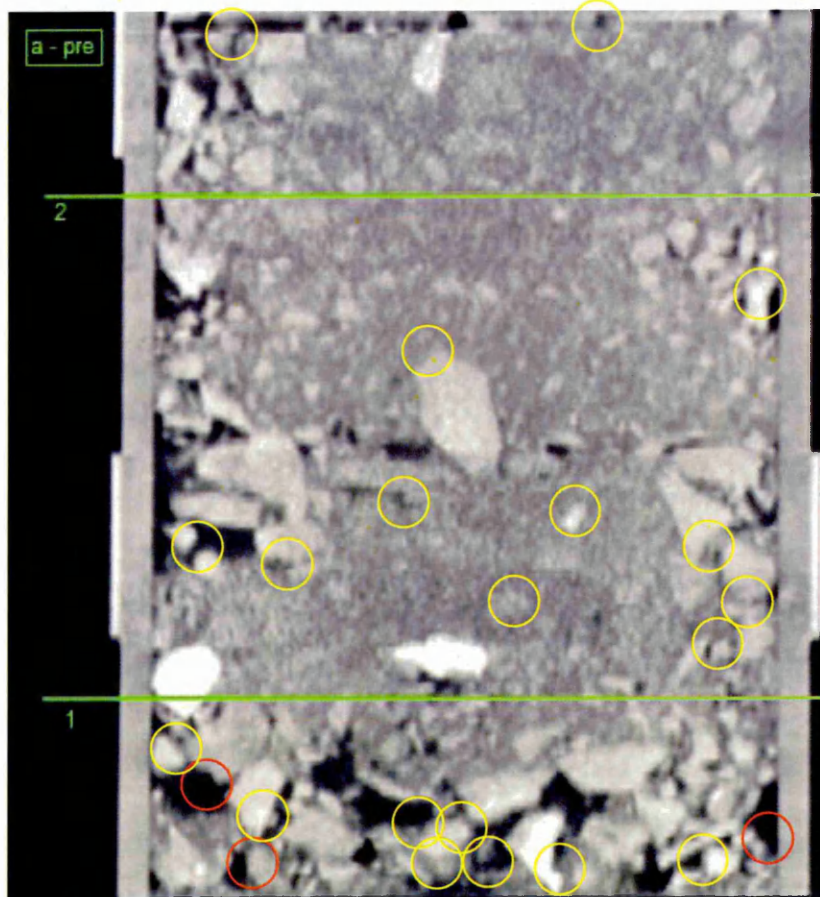




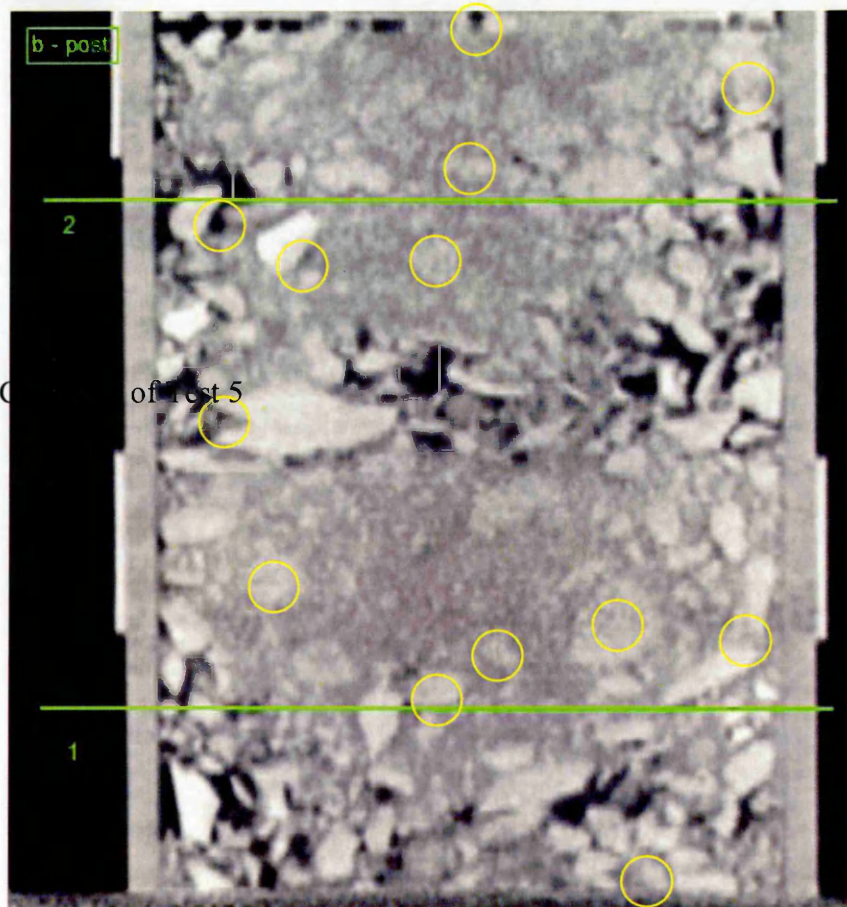
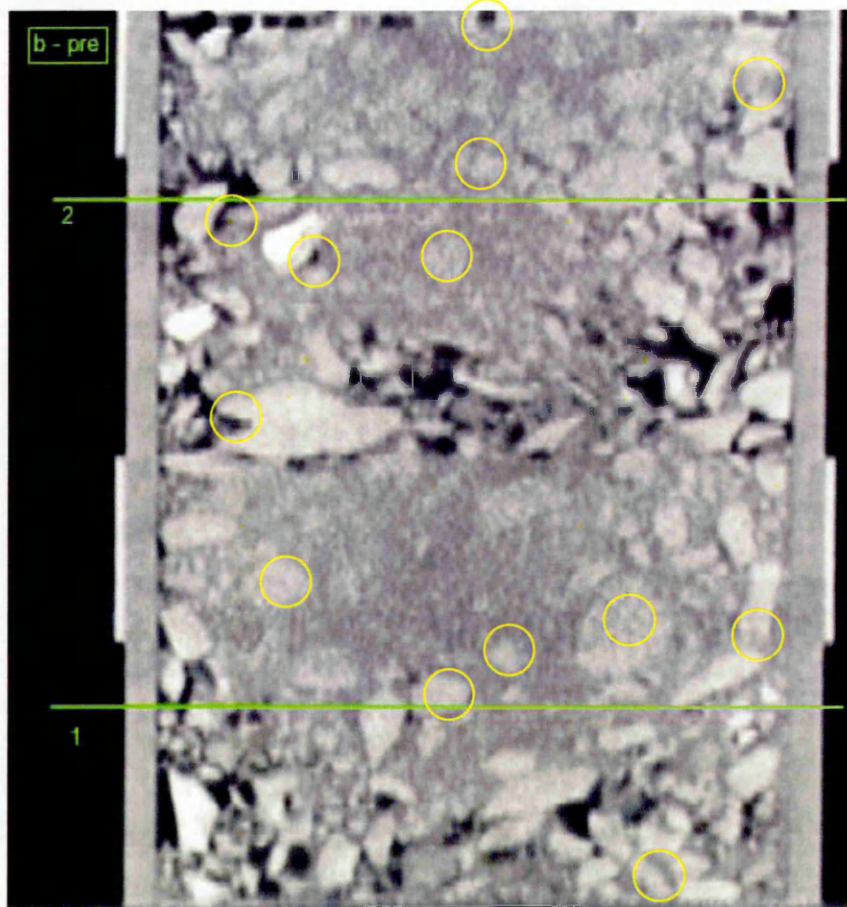
CT Scans of
Test 10



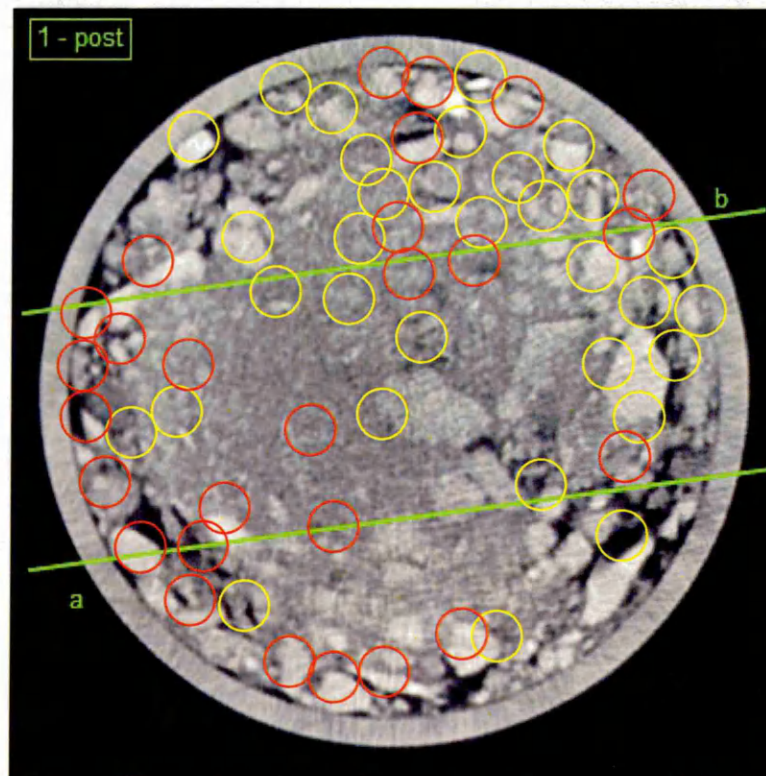
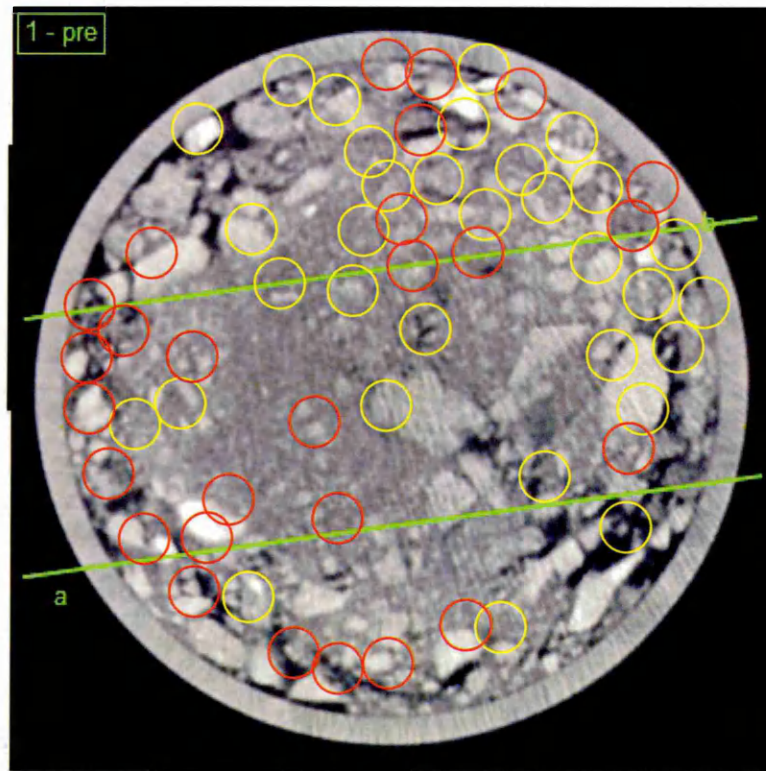
CT Scans of
Test 10



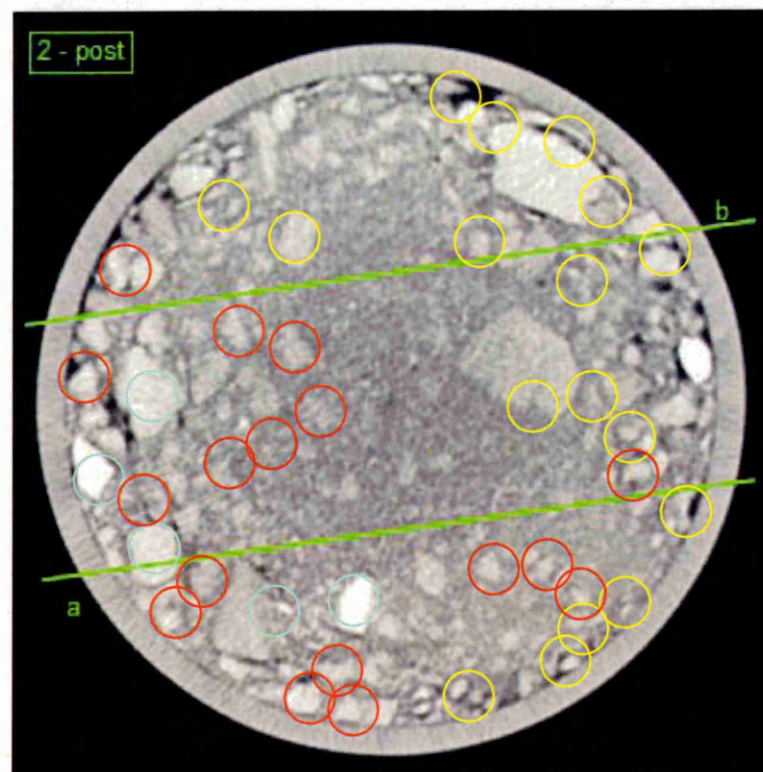
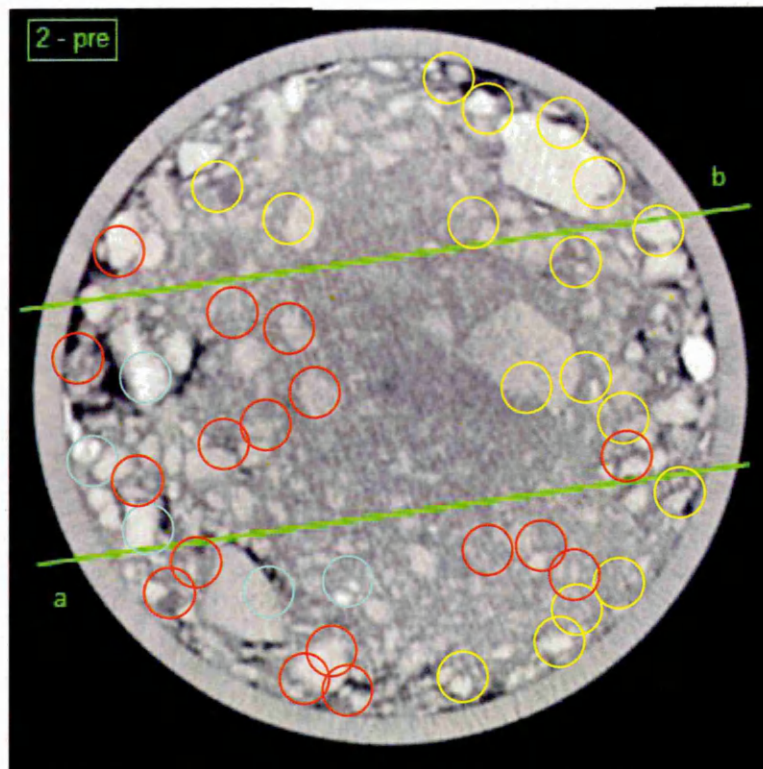
CT Scans of
Test 10



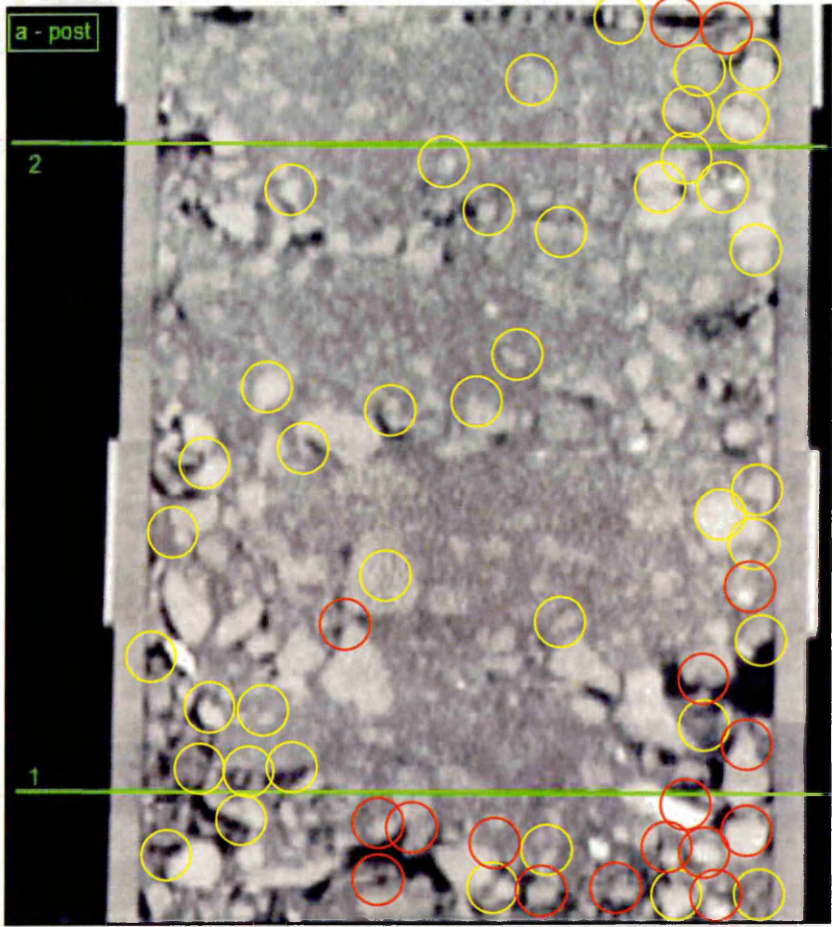
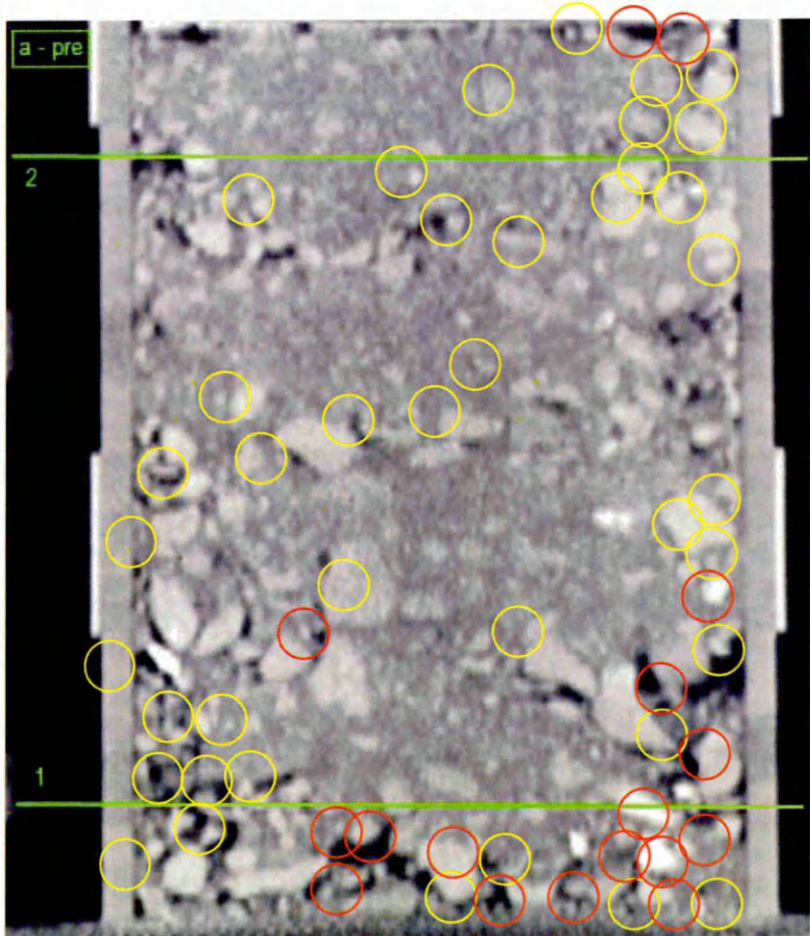
of Test 5



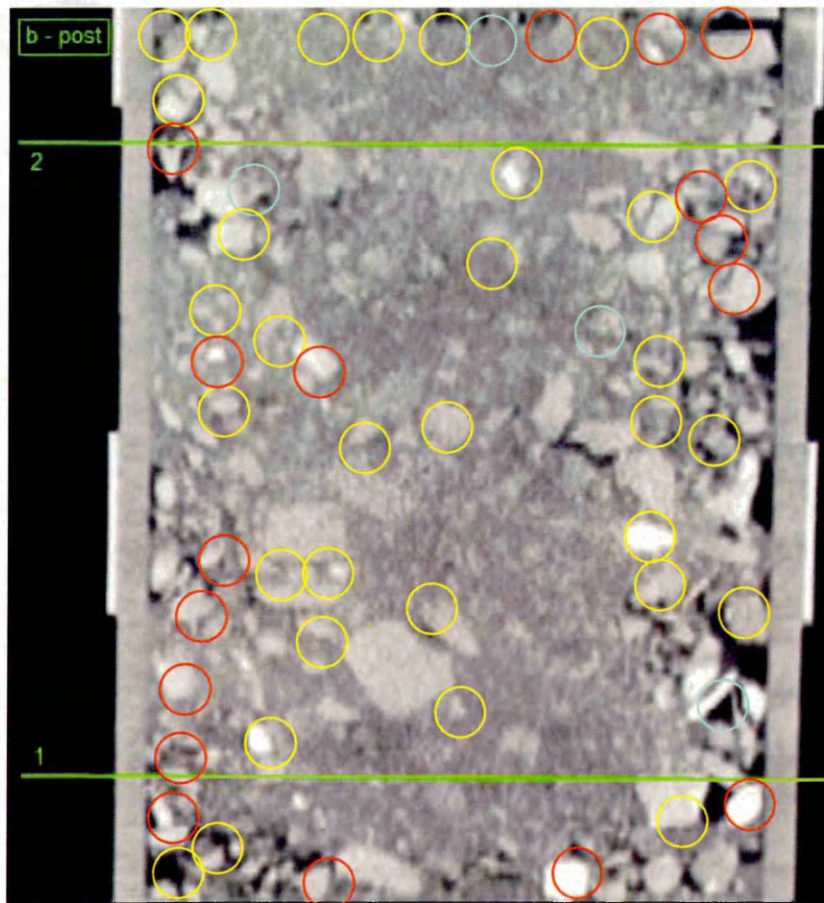
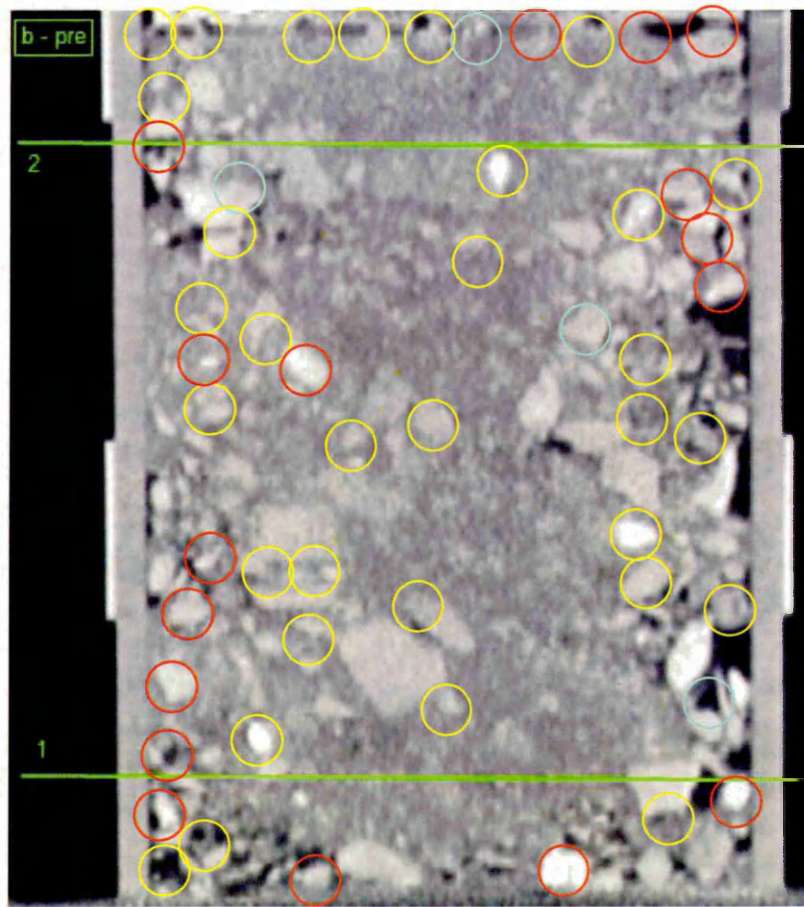
CT Scans of
Test 11



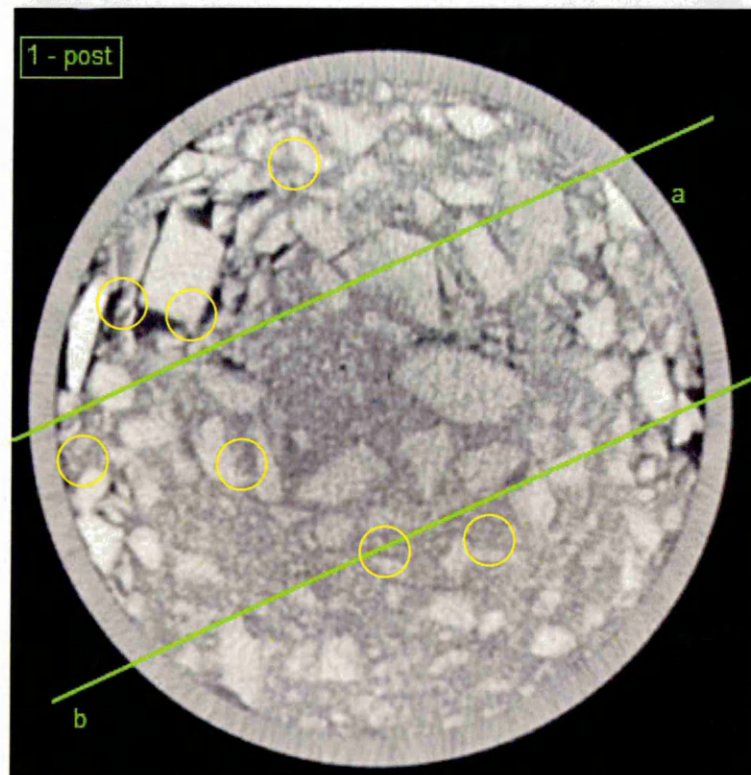
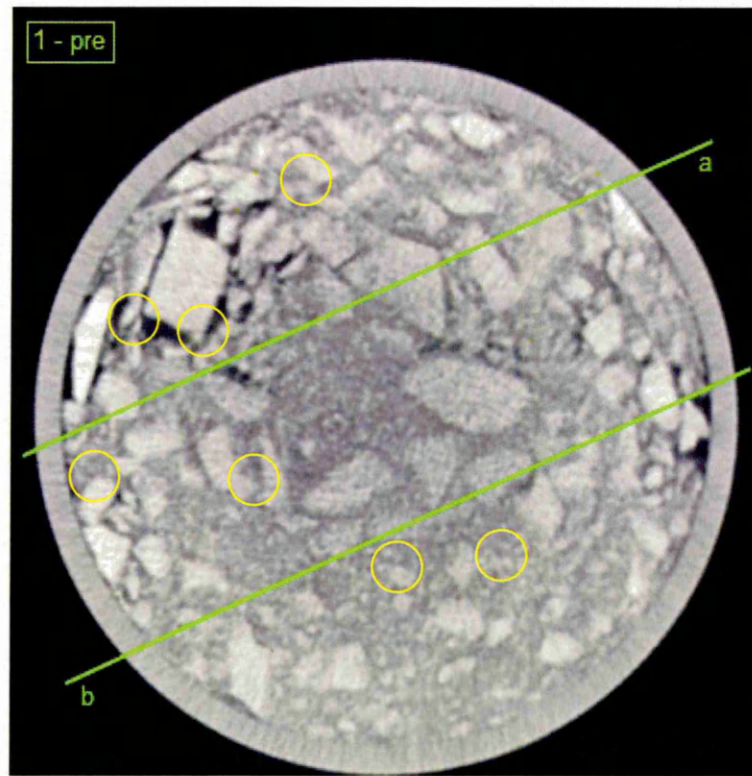
CT Scans of
Test 11



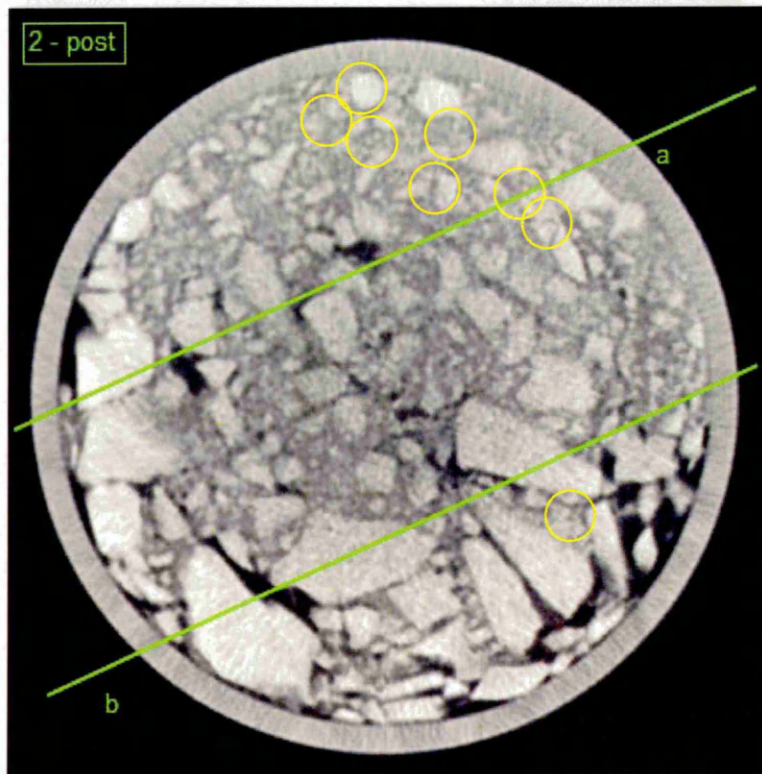
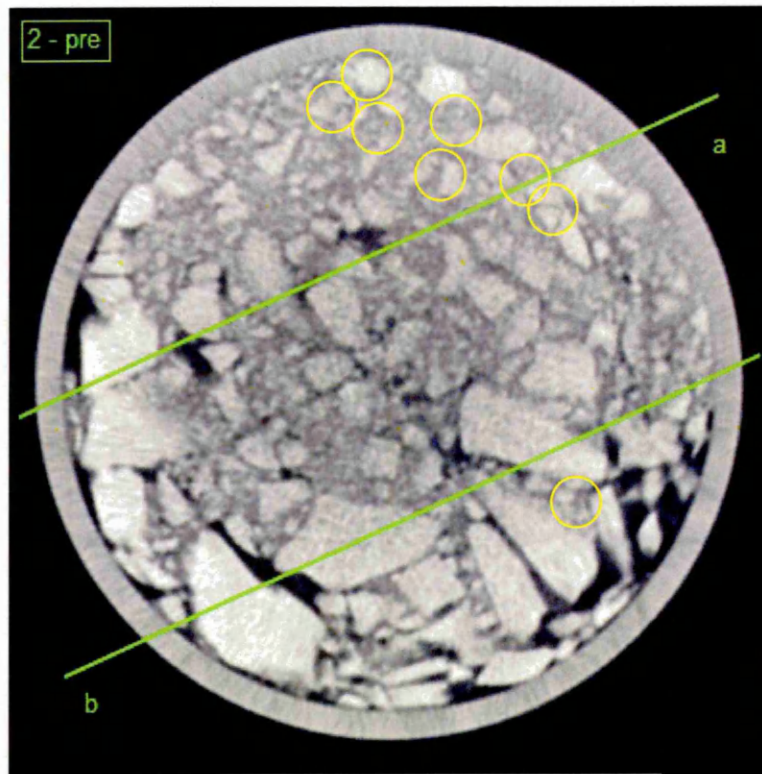
CT Scans of
Test 11



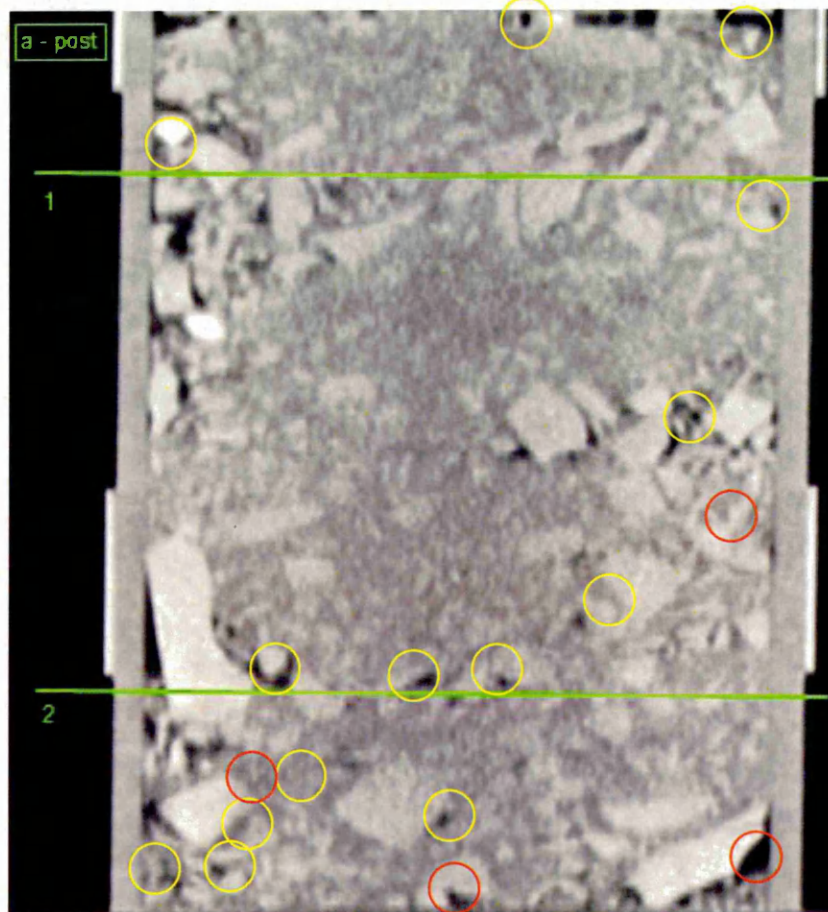
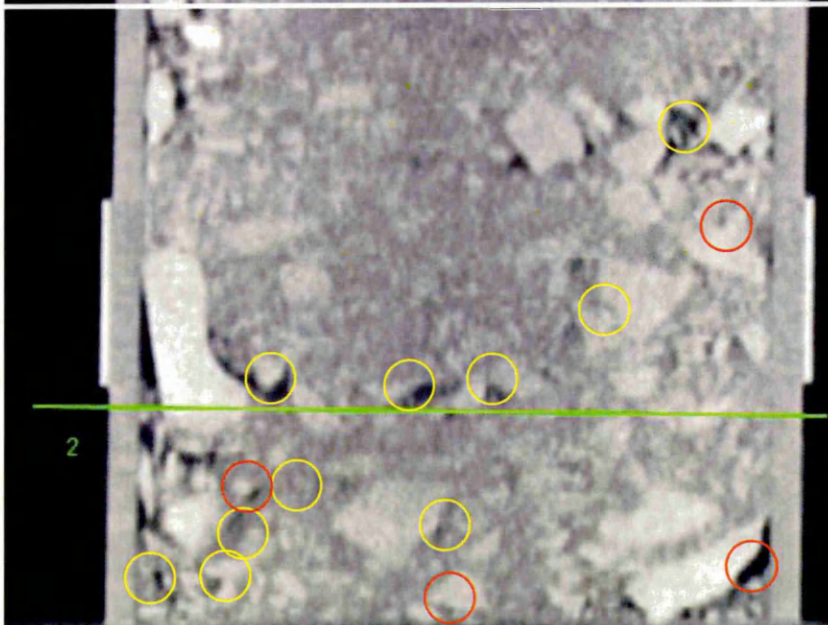
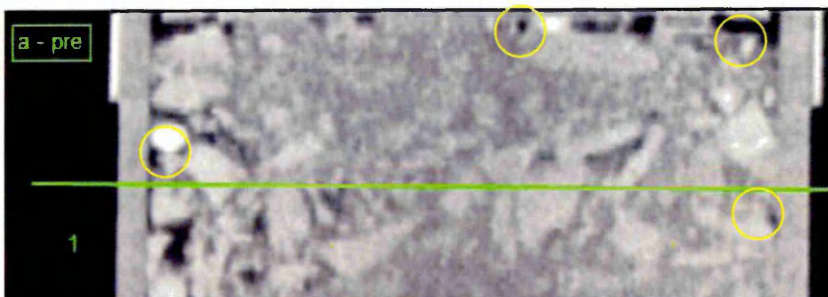
6.4.2.7 CT Scans of Test 12



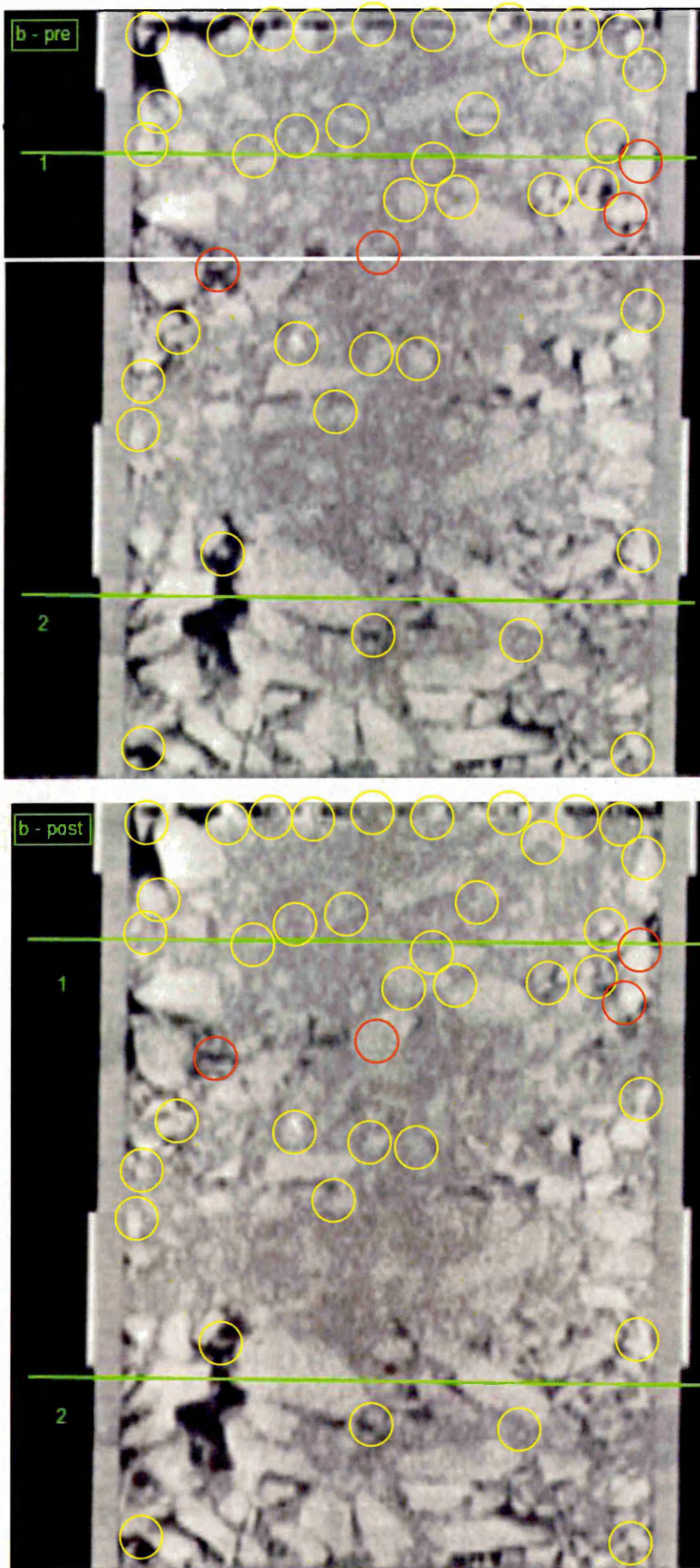
CT Scans of
Test 12

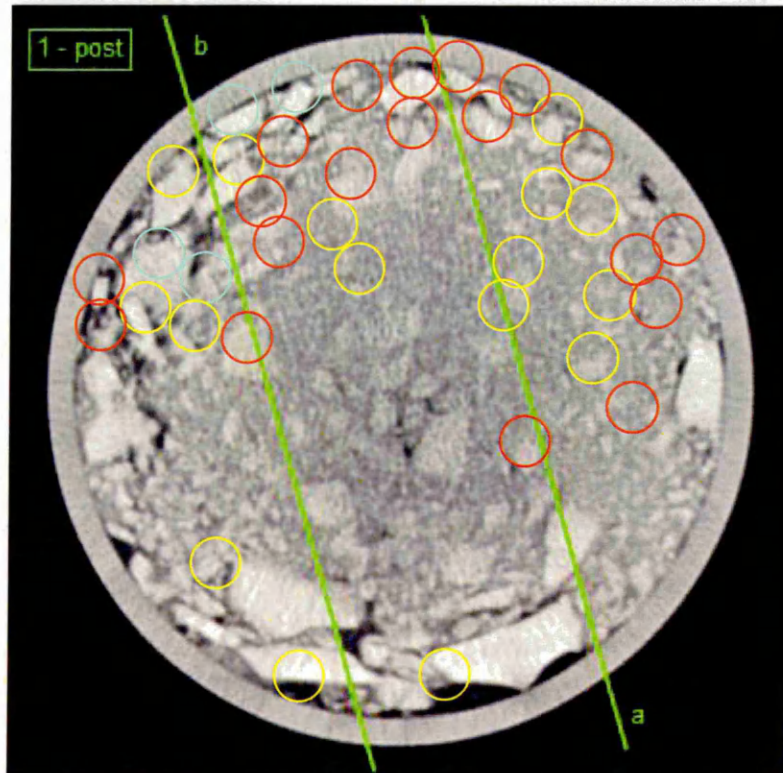
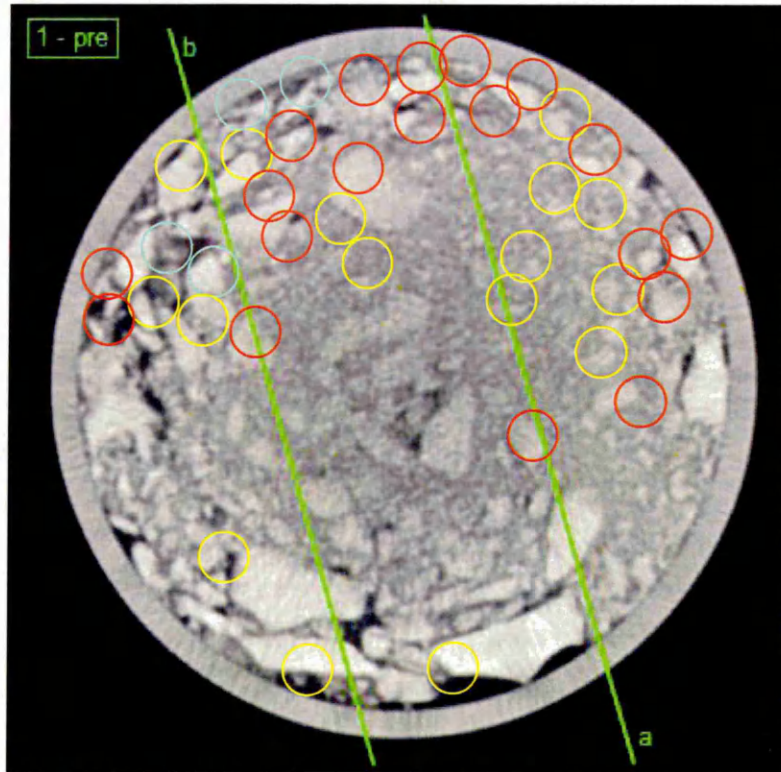


CT Scans
of Test 12

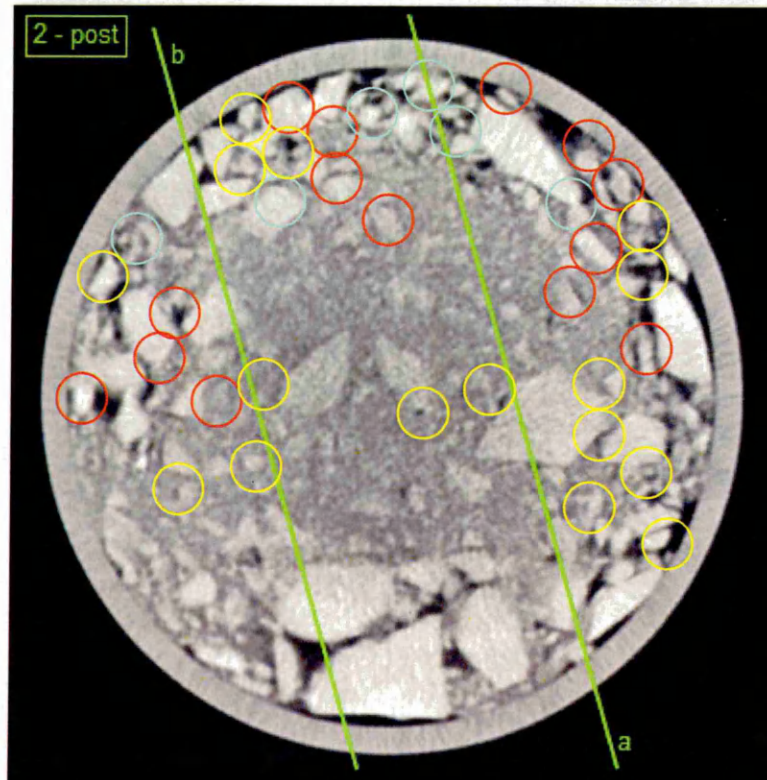
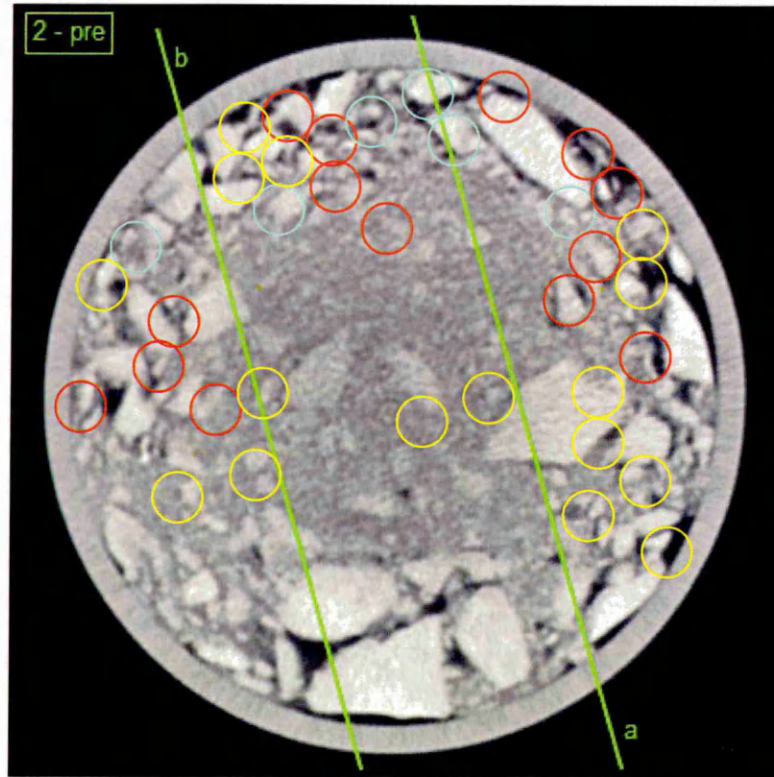


CT Scans
Test 12

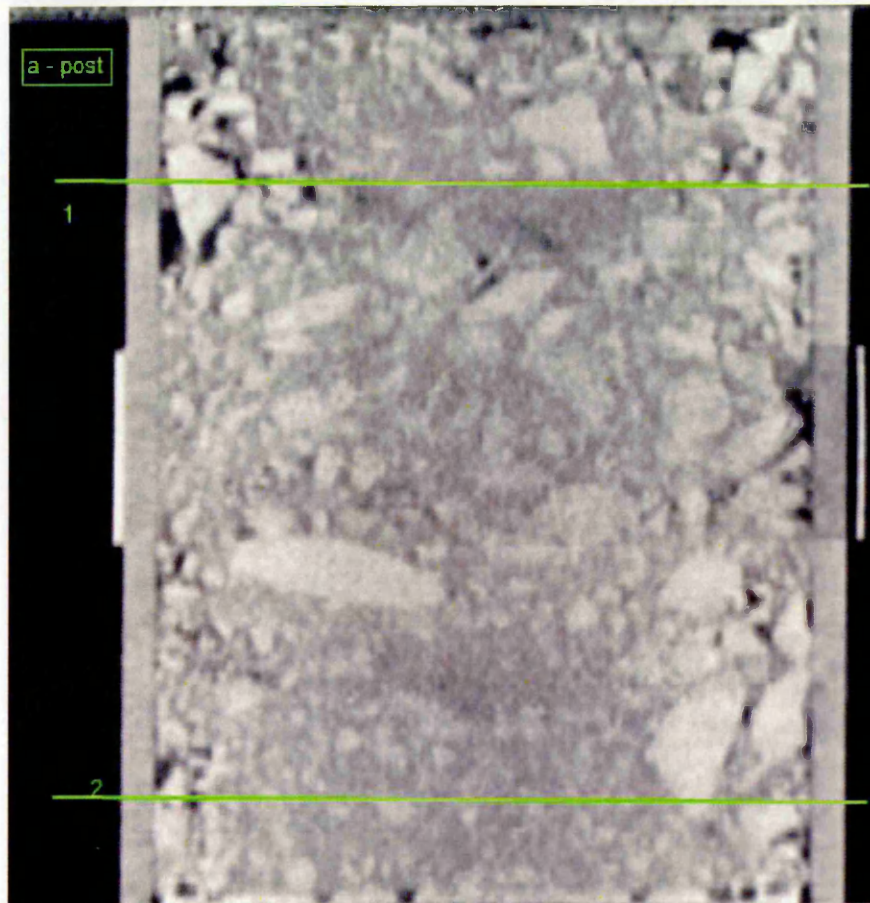
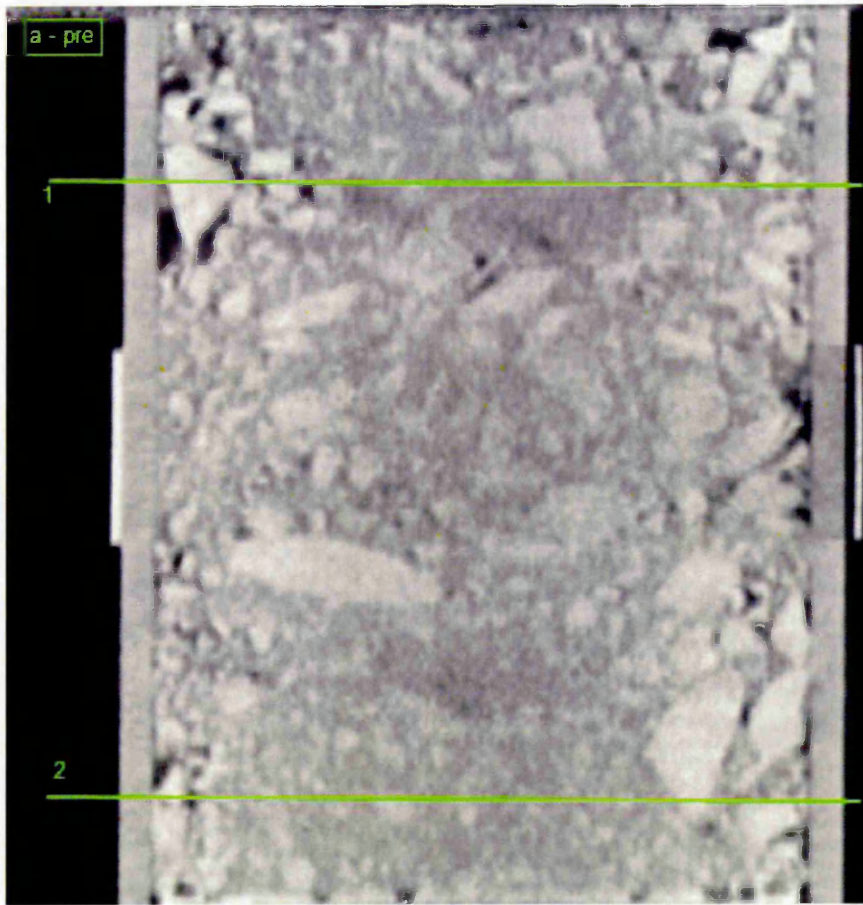




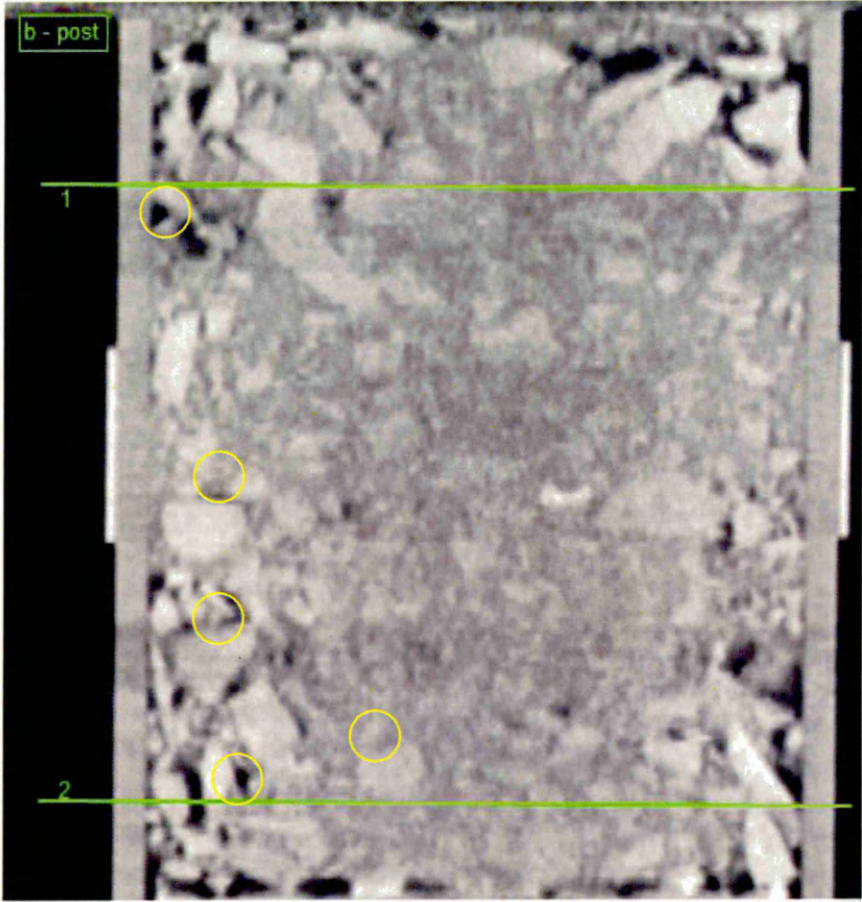
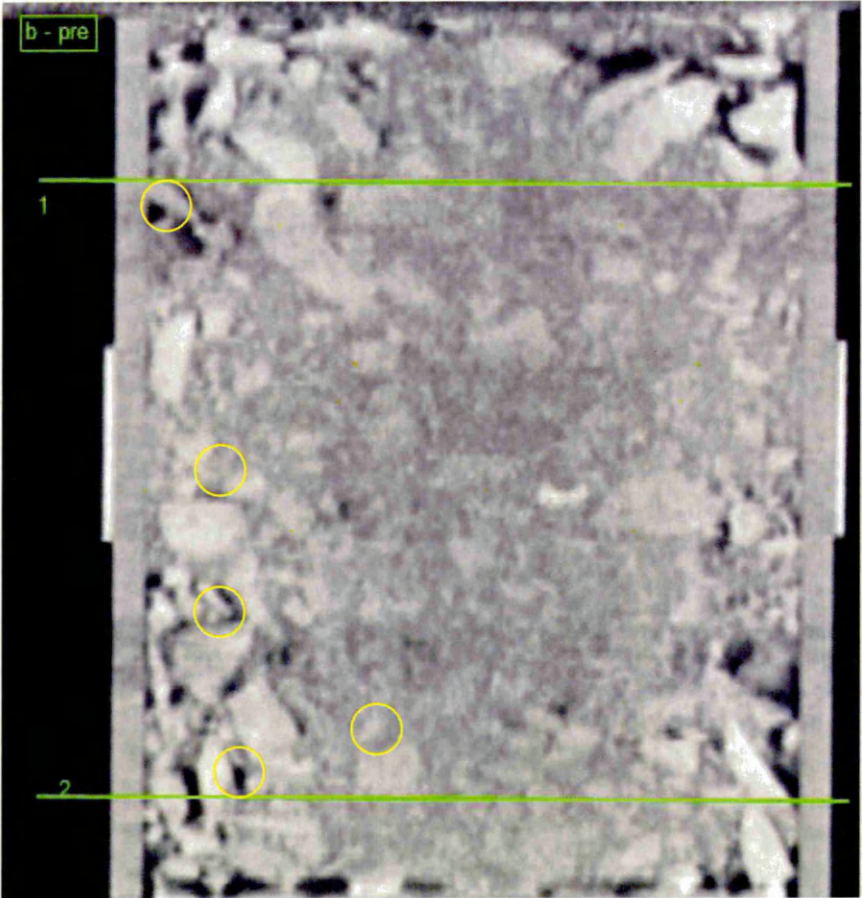
CT Scans of
Test 13

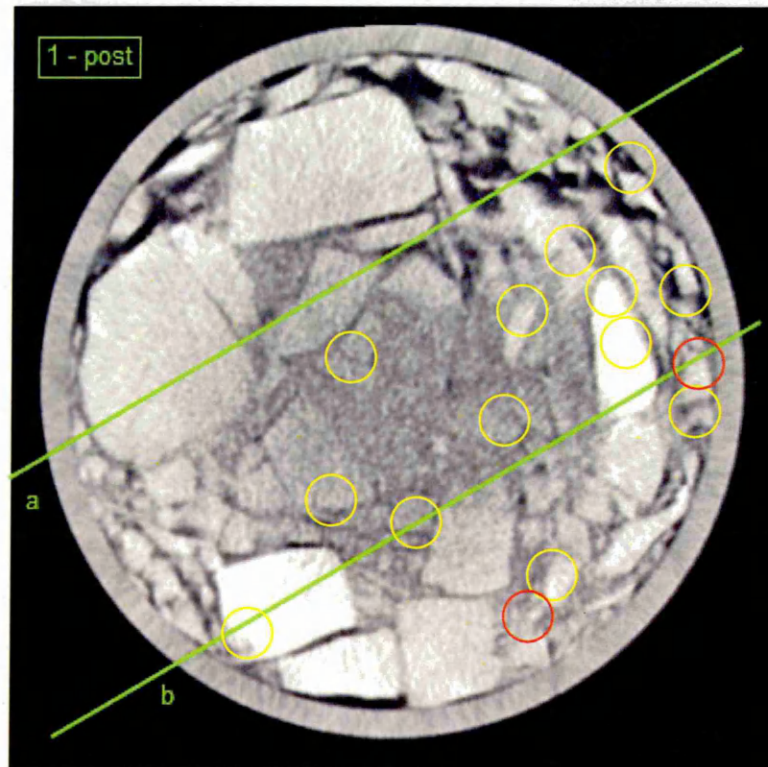
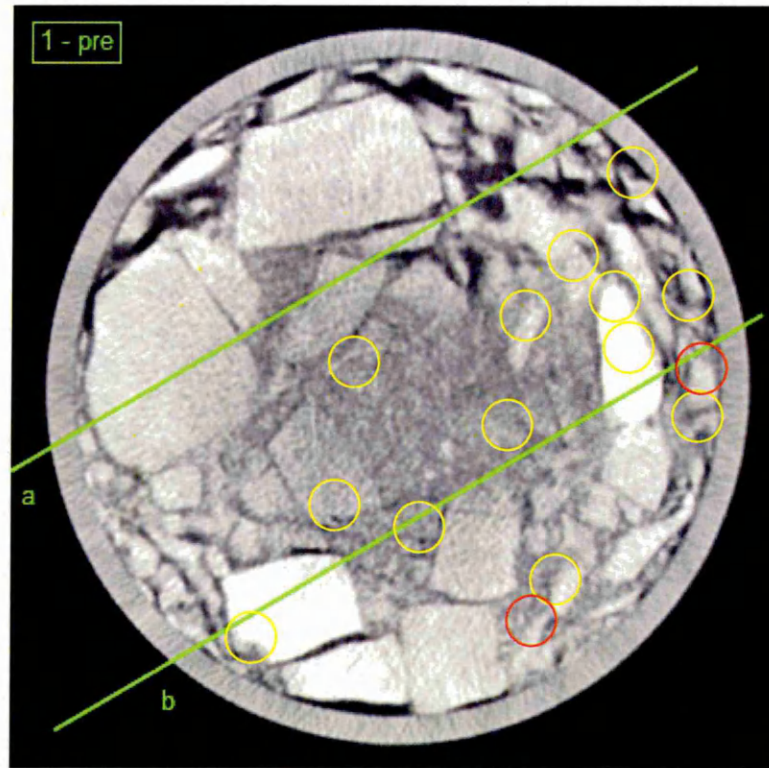


CT Scans of
Test 13

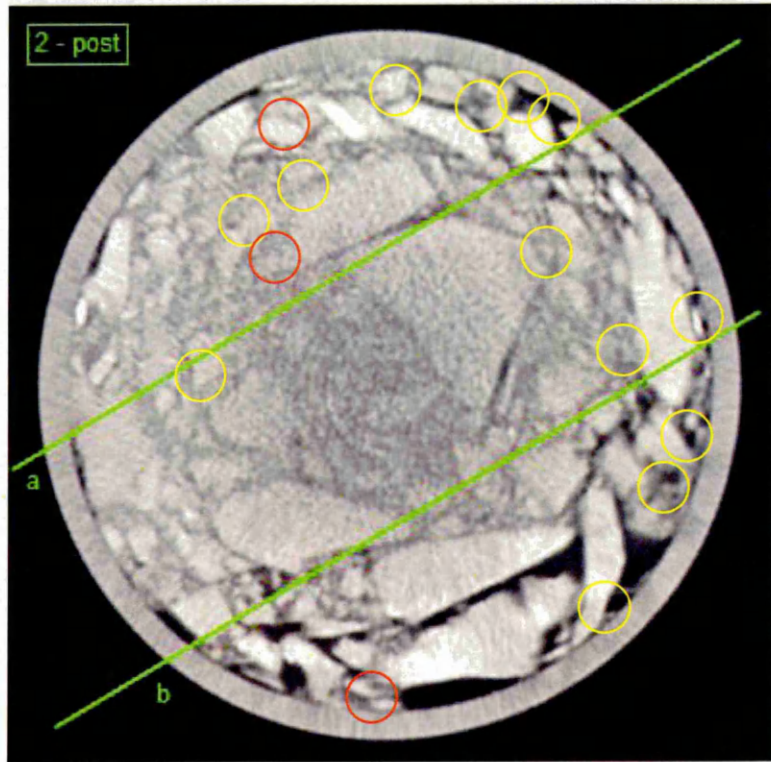
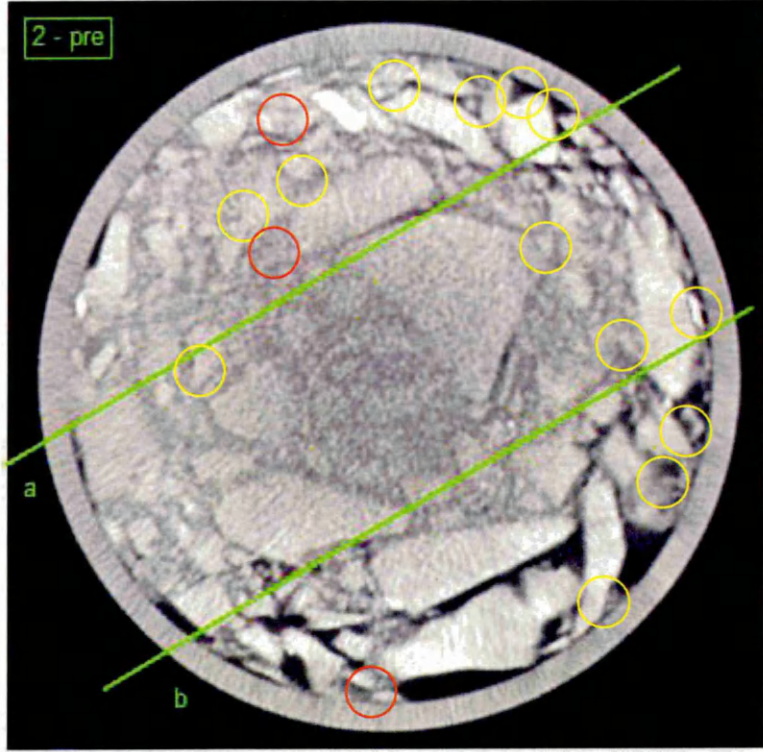


CT Scans of
Test 13

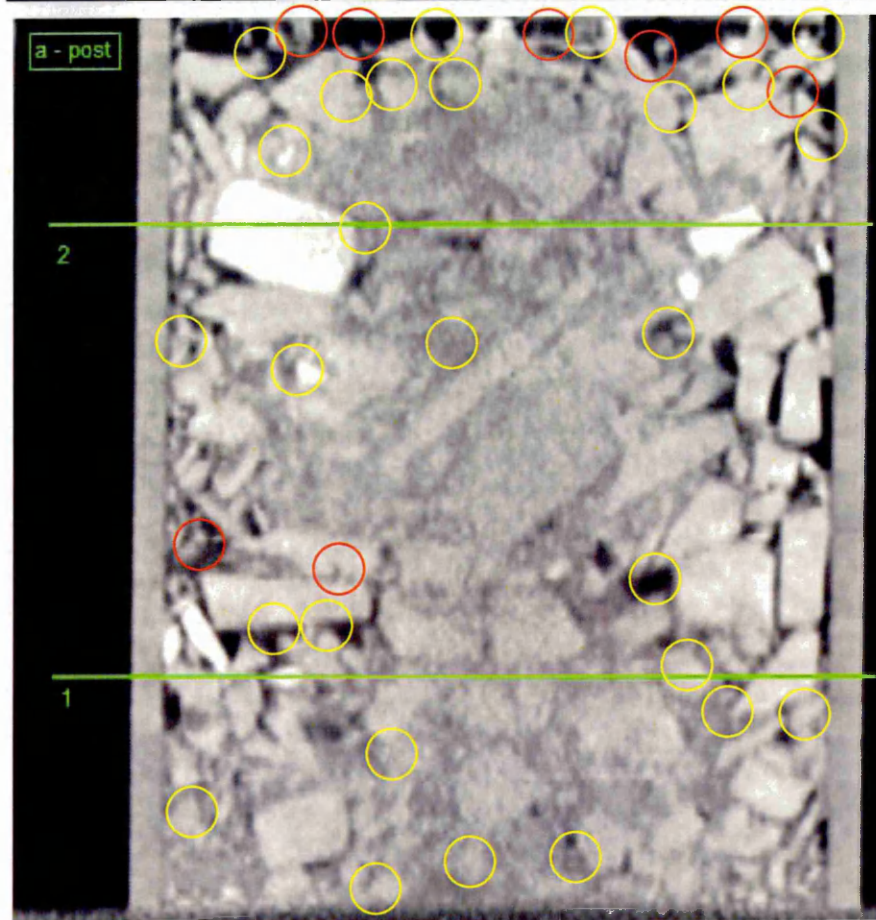
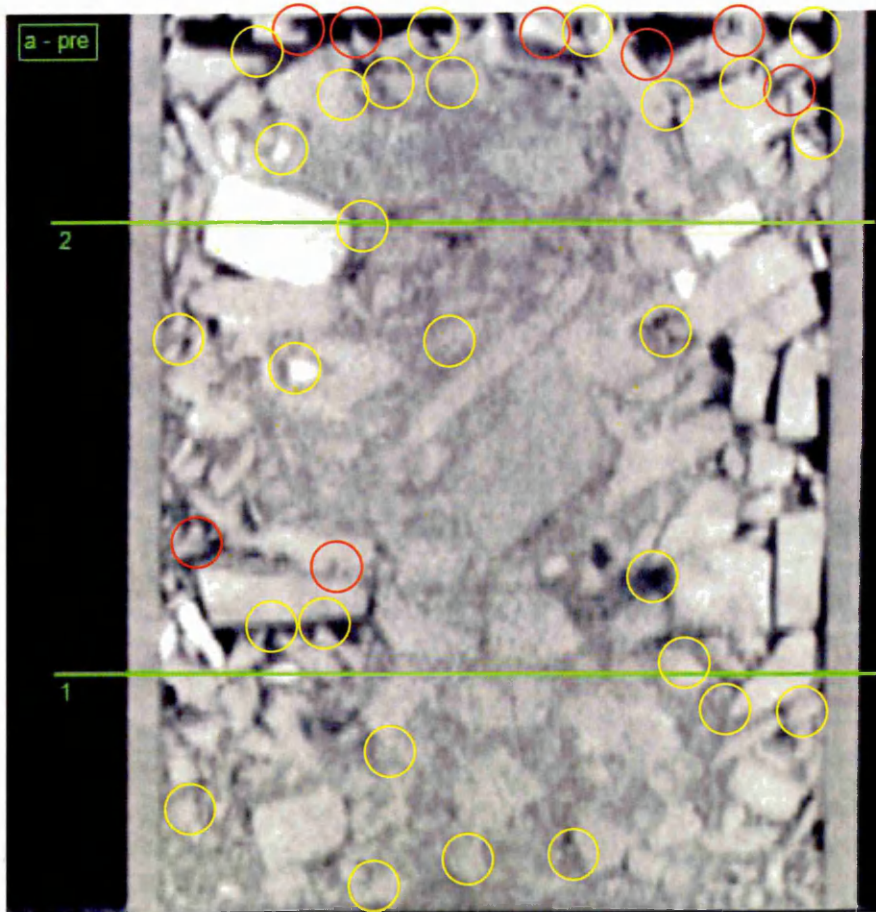




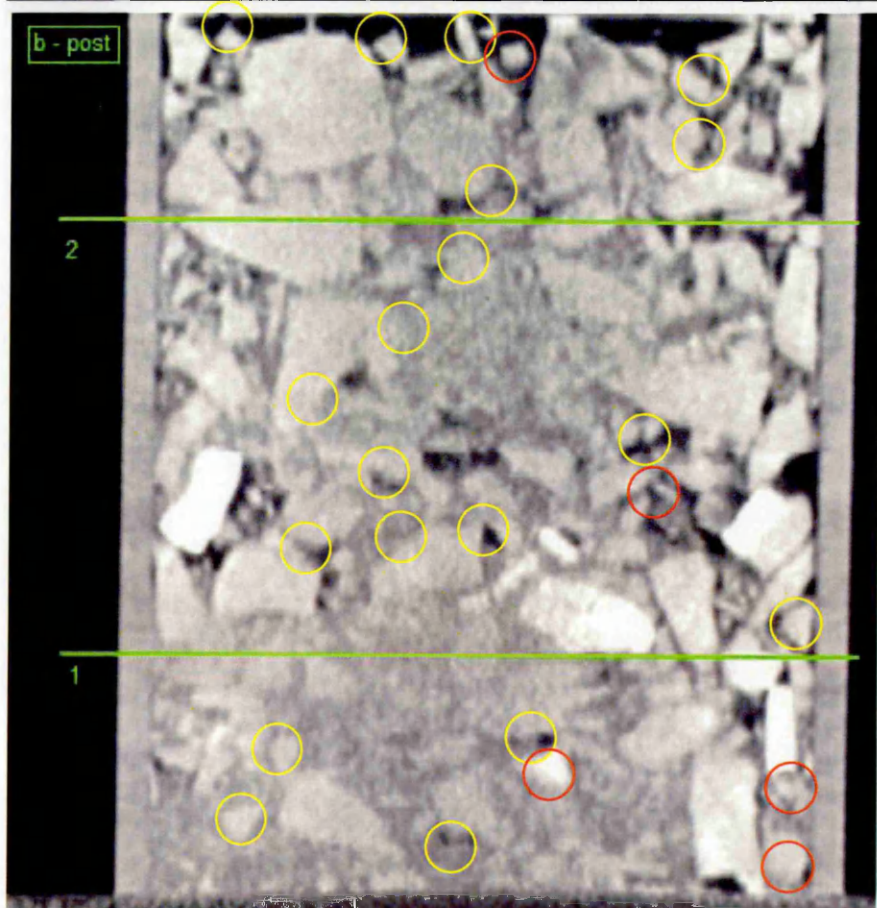
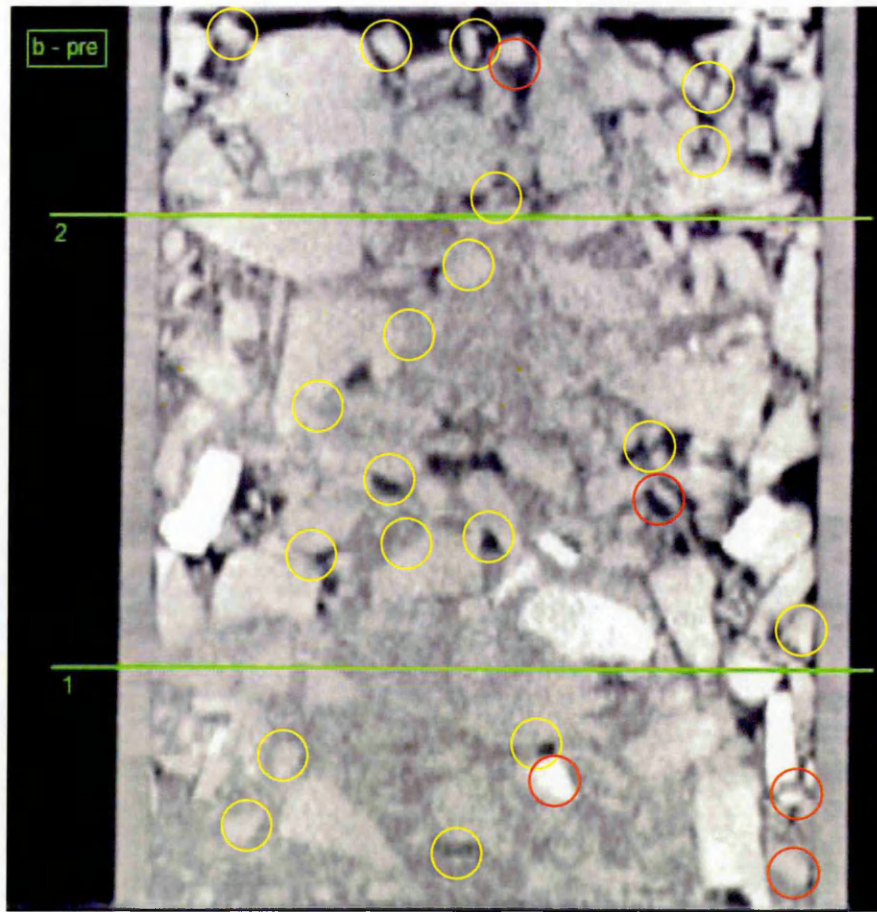
CT Scans
of Test 14

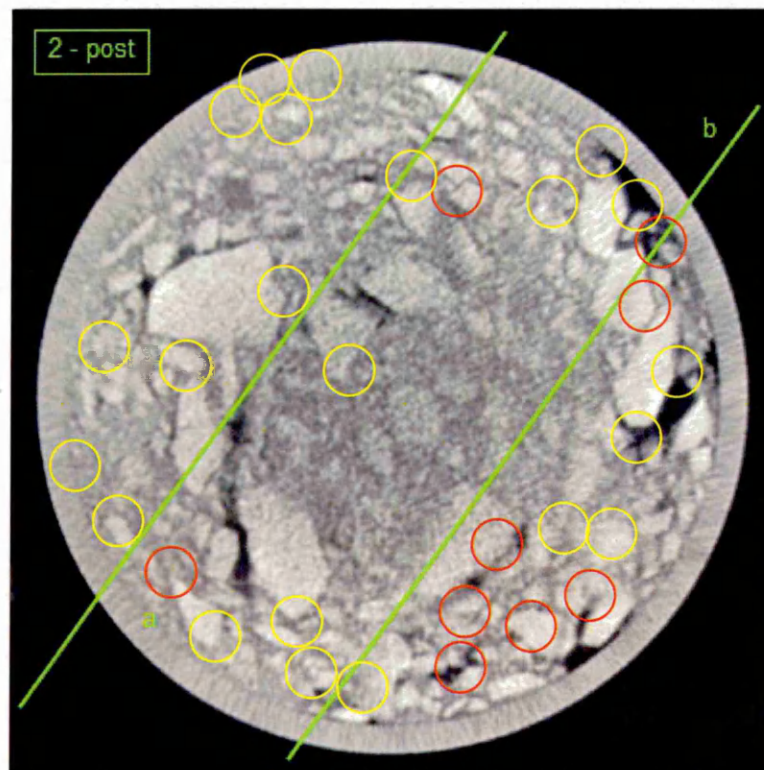
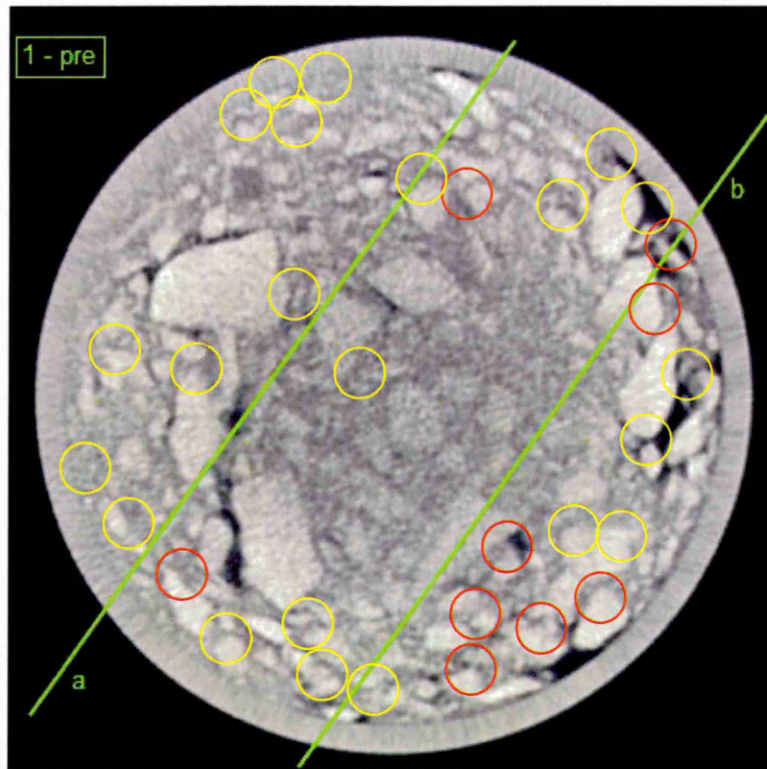


CT Scans
of Test 14

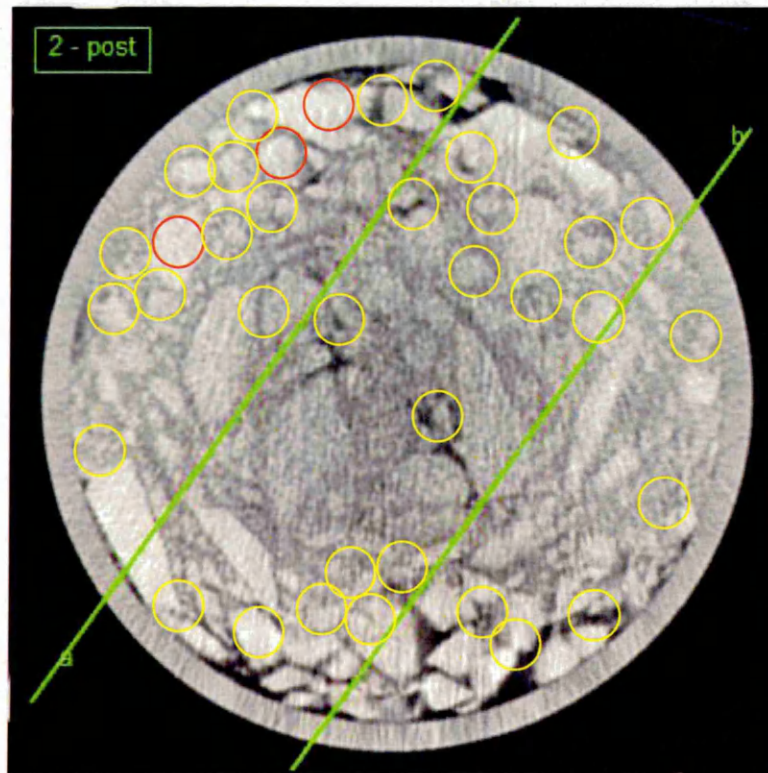
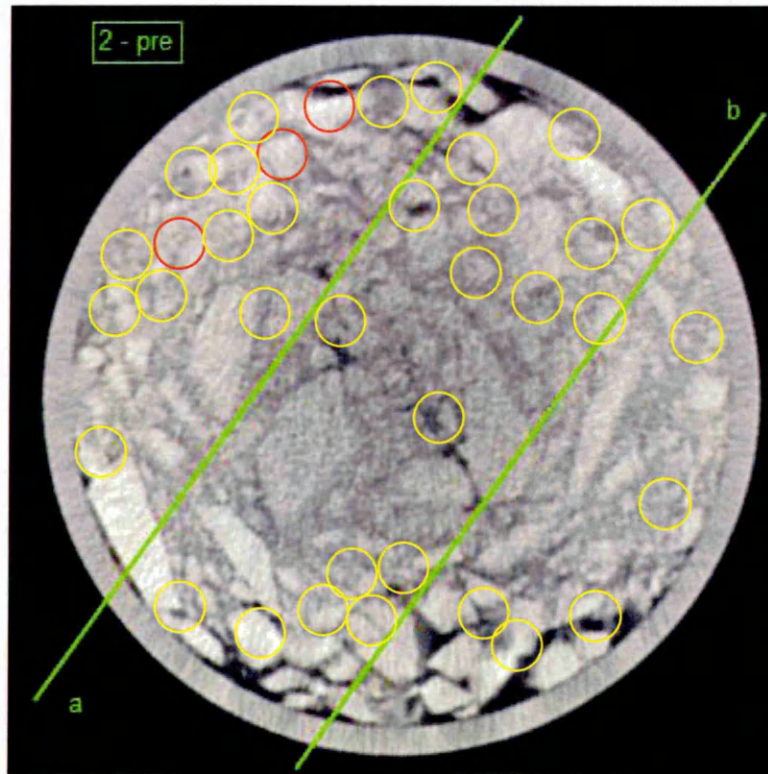


CT Scans
of Test 14

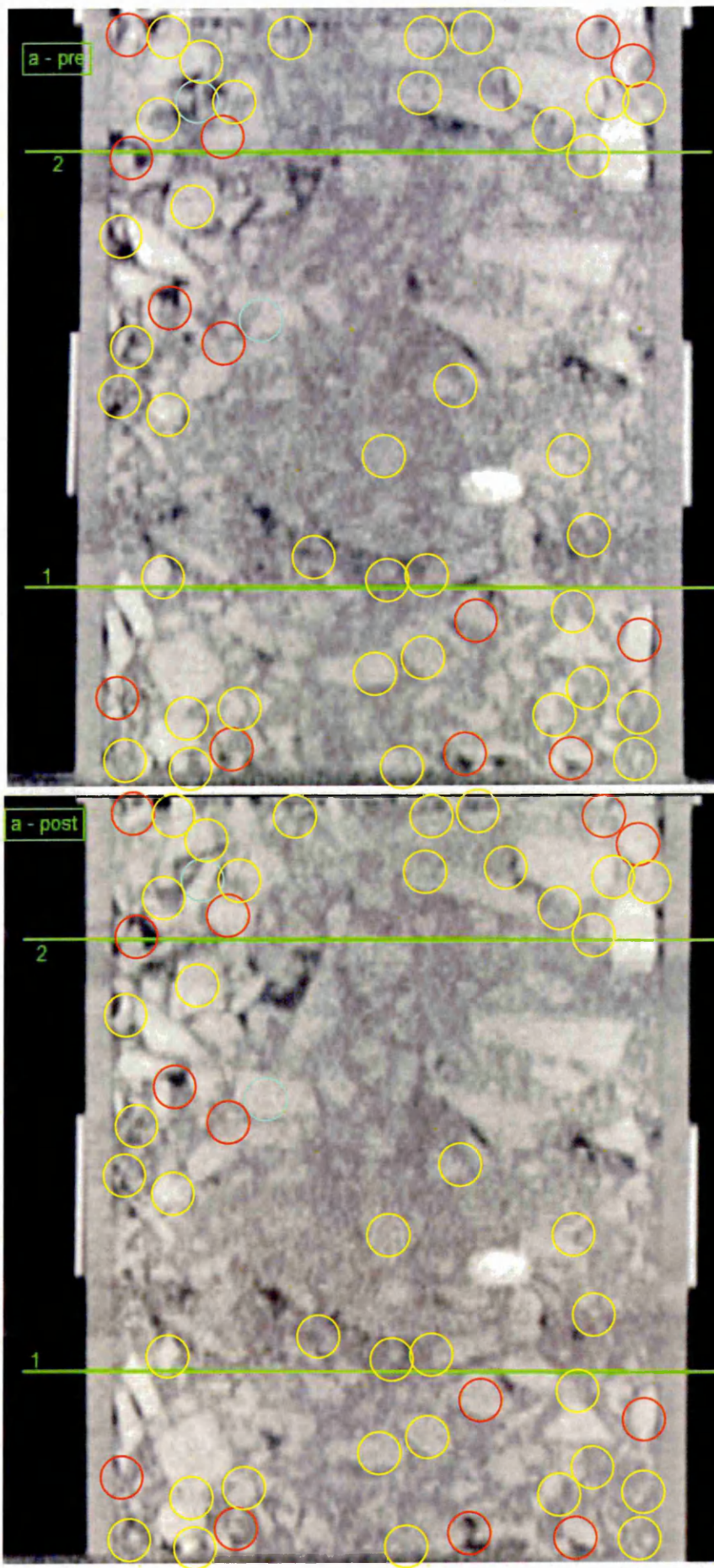




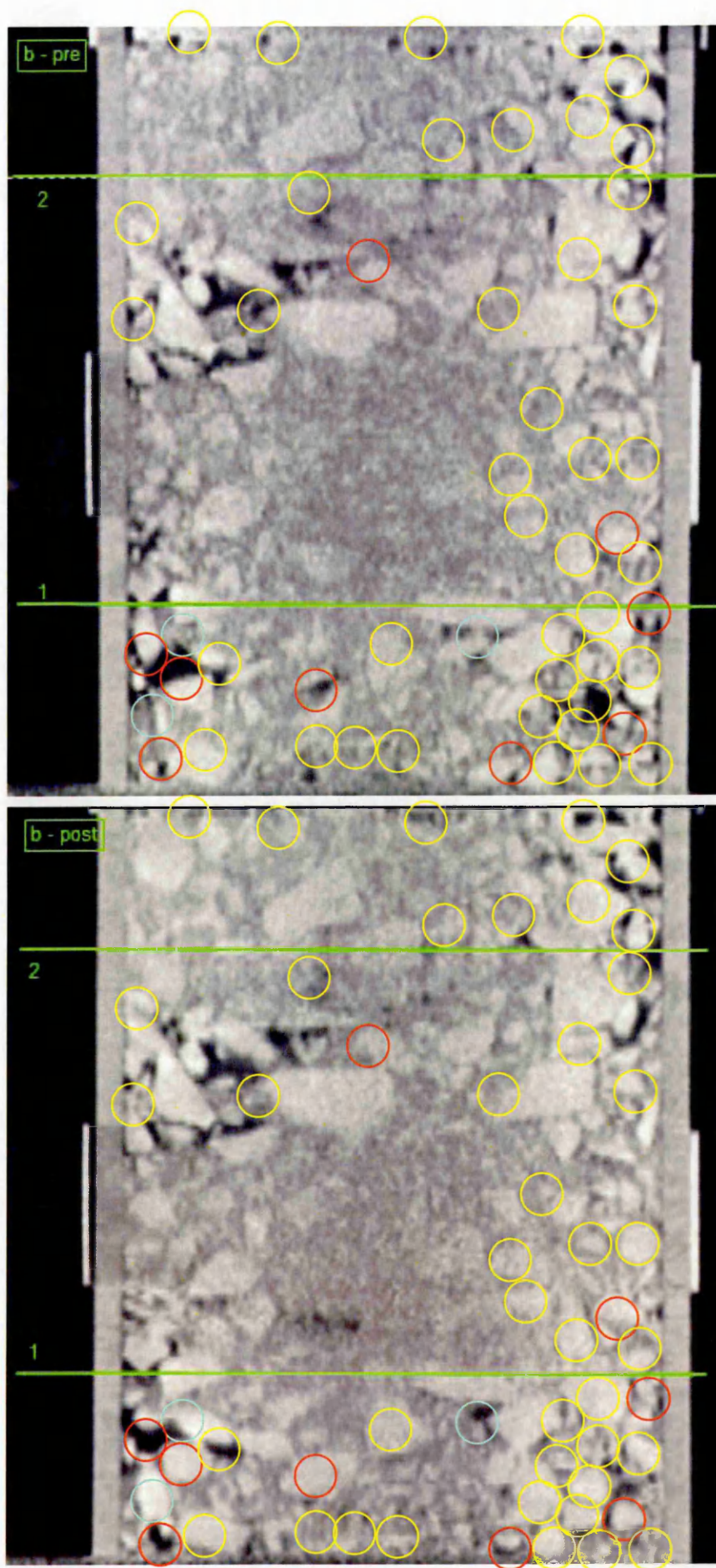
CT Scans
of Test 15



CT Scans
of Test 15



CT Scans
of Test 15



| Test number | Section | Differences (by scale) | | | Differences score | |
|-------------|-----------|------------------------|-----------------|-----------|-------------------|------|
| | | Minor (1) | Significant (3) | Major (5) | Image | Test |
| 5 | cross - 1 | 9 | 13 | 0 | 48 | 194 |
| | cross - 2 | 16 | 11 | 2 | 59 | |
| | long - a | 14 | 5 | 0 | 29 | |
| | long - b | 12 | 12 | 2 | 58 | |
| 6 | cross - 1 | 16 | 3 | 0 | 25 | 170 |
| | cross - 2 | 21 | 6 | 0 | 39 | |
| | long - a | 20 | 6 | 0 | 38 | |
| | long - b | 35 | 11 | 0 | 68 | |
| 8 | cross - 1 | 19 | 12 | 2 | 65 | 233 |
| | cross - 2 | 14 | 8 | 5 | 63 | |
| | long - a | 19 | 11 | 3 | 67 | |
| | long - b | 29 | 3 | 0 | 38 | |
| 9 | cross - 1 | 15 | 19 | 3 | 87 | 241 |
| | cross - 2 | 10 | 2 | 0 | 16 | |
| | long - a | 14 | 12 | 5 | 75 | |
| | long - b | 15 | 16 | 0 | 63 | |
| 10 | cross - 1 | 9 | 1 | 1 | 17 | 78 |
| | cross - 2 | 19 | 0 | 0 | 19 | |
| | long - a | 20 | 3 | 0 | 29 | |
| | long - b | 13 | 0 | 0 | 13 | |
| 11 | cross - 1 | 33 | 27 | 0 | 114 | 399 |
| | cross - 2 | 17 | 17 | 5 | 93 | |
| | long - a | 38 | 17 | 0 | 89 | |
| | long - b | 32 | 17 | 4 | 103 | |
| 12 | cross - 1 | 7 | 0 | 0 | 7 | 89 |
| | cross - 2 | 8 | 0 | 0 | 8 | |
| | long - a | 14 | 4 | 0 | 26 | |
| | long - b | 36 | 4 | 0 | 48 | |
| 13 | cross - 1 | 16 | 19 | 4 | 93 | 186 |
| | cross - 2 | 16 | 14 | 6 | 88 | |
| | long - a | 0 | 0 | 0 | 0 | |
| | long - b | 5 | 0 | 0 | 5 | |
| 14 | cross - 1 | 13 | 2 | 0 | 19 | 126 |
| | cross - 2 | 13 | 3 | 0 | 22 | |
| | long - a | 27 | 8 | 0 | 51 | |
| | long - b | 19 | 5 | 0 | 34 | |
| 15 | cross - 1 | 21 | 9 | 0 | 48 | 251 |
| | cross - 2 | 34 | 3 | 0 | 43 | |
| | long - a | 37 | 13 | 2 | 86 | |
| | long - b | 35 | 8 | 3 | 74 | |

6.5 Other Observations

In addition to the data gathered and presented in detail above and summarised in Table 6-4, Section 6.4.3 and Table 6-4, other observations were made during the undertaking of the testing.

Sowers et al. (1965) reported hearing popping sounds during the loading of samples of rockfill in confined compression tests. These sounds were also reported to have been heard following sudden changes in the water load on dams (Sowers et al, 1965). During the testing for this research, similar noises (that could be described as popping) were also heard. The noises were, possibly, of a lower pitch than a “pop” and were often preceded by a short period of creaking culminating in a snapping noise.

These noises were relatively frequent during the loading stage of the testing and were often, but not always, accompanied by a marked compression of the specimen. The occurrence of these noises was most frequent on the application of load and then quickly decreased. No change in the frequency of the occurrence of the noises was noted on the application of the different load increments, *i.e.* the frequency was noted to be the similar at the application of 50 to 100 kPa stress increment as the 200 to 400 kPa increment. It was in the loading stage of the testing that vibrations associated with noises could be felt in the cells’ structure and walls.

During the inundation stage of testing the occurrence of these noises were very infrequent or went unnoticed; despite large specimen compressions being measured.

In the longer periods of testing that consisted of the application of constant stress conditions on the specimens only very occasional noises were noted. Again these were often accompanied by significant specimen compressions.

Following the completion of a test the insides of the cells were inspected. The cell walls were found to be in a generally good condition following the testing

with only minor surface scratching being in evidence. No noticeable dimples or indentations were observed.

| Test number | Test information | | | | Testing results | | |
|-------------|------------------|-----------------|-------------------------|--|-----------------|-------------------|-------------------|
| | Cell type | Specimen source | Inundation condition | Compaction / Dry density ρ_d (Mg/m ³) | Strain (%) | Creep rate (%) | Differences score |
| 1 | large | Houghton | not inundated | heavy | 2.04 | 0.50 | - |
| 2 | large | Orgreave | inundated* ¹ | heavy | 5.88 | n/a* ² | - |
| 3 | large | Orgreave | inundated* ¹ | light | 2.40 | 0.12 | - |
| 4 | large | Houghton | inundated | light | 2.10 | 0.20 / 0.27 | - |
| 5 | small | Houghton | not inundated | light | - | 0.48 | 194 |
| 6 | small | Orgreave | not inundated | light | >0.54 | 0.19 | 170 |
| 7 | small | Houghton | not inundated | light | - | 0.25 | - |
| 8 | small | Orgreave | not inundated | light | 0.81 | 0.15 | 233 |
| 9 | small | Houghton | not inundated | light | - | 0.21 | 241 |
| 10 | small | Orgreave | not inundated | heavy | - | 0.08 | 78 |
| 11 | small | Orgreave | not inundated | heavy | 0.84 | 0.07 | 399 |
| 12 | small | Houghton | not inundated | heavy | 1.99 | 0.12 | 89 |
| 13 | small | Orgreave | not inundated | light | 1.00 | 0.10 | 186 |
| 14 | small | Houghton | not inundated | heavy | >1.00 | 0.13 | 126 |
| 15 | small | Orgreave | not inundated | light | 1.34 | 0.10 | 251 |

Notes:

1. Due to a diaphragm failure the specimen was inundated during initial loading, after the diaphragm was replaced the specimen was loading in it wet state.
2. A constant creep rate was not measured; the specimen demonstrated a linear deformation with time at a rate of approximately 0.2%.

Table 6-4: Summary of Laboratory and CT Data.

7 Interpretation and Discussion

The interpretation and discussion of the work undertaken is approached under four headings. Firstly the methodology employed in the research is discussed. Then the equipment used in the research and the test materials are discussed, followed by the results. The detailed results are presented in the preceding chapter and discussion is made in two sub-sections: the first discuss the data from the laboratory programme and the second discuss the computered tomography (CT) data and compares and contrasts it with the laboratory data.

7.1 Methodology

In order to achieve the aims and objectives of the research the methodology outlined in Chapter 3 was derived. This methodology required that large scale testing be carried out in cells of two sizes for periods between 3 months and more than 2 years. Further, that this testing be supplement by non-destructive testing; this used CT and was undertaken in a location remote from the main laboratory. This long term testing required that bespoke test cells be designed and manufactured and that new CT protocols to be developed. These achievements, the limitations and their implications are discussed in subsequent sections.

7.2 Equipment

7.2.1 Laboratory Based

Relevant information about the equipment used in this study is presented in detail in Chapter 4.

7.2.1.1 Laboratory environment

Details of the laboratory environment are given in Section 4.1.1. Guidance on the appropriate range in which temperature of a soils' testing environment should be maintained is given in BS1377:1990. Specifically,

BS1377:1990:Part 5 advocates that the temperature in the area in which one-dimensional consolidation testing is carried out, be maintained to within $\pm 4^\circ$. As shown by the data presented in Section 4.1.1 this requirement was met.

7.2.1.2 Compression cells

The main pieces of equipment used were the compression cells. They also presented some of the greatest obstacles to the research.

A major aim of the design of the cells was to identify and source materials from which they could be constructed and were suitable for use in conjunction with computed tomography and possibly other non-destructive techniques. The resulting cell design was to utilise plastic cell walls, the other structural elements being manufactured from aluminium.

The use of a plastic as the cell side walls presented particular concerns about long-term deformations similar to the ones under investigation. In order to understand the full implications of this potential problem information on the behaviour of these material's was sought. Figure 4-4 and Figure 4-5 present the behaviour of this material and indicate that the materials behaviour could be controlled by pre-stressing them. Further pre-stressing the cell wall to a greater level than was to be used in the testing programme would further reduce the likelihood of this behaviour impacting on the investigation.

With these precautions in place dimensional checks were carried out on the cell walls such that if the cell walls were exhibiting behaviour other than that predicted it would be identified. As stated in Section 4.1.2.1 no such behaviour was measured.

The potential for movements in the other structural elements of the cells (*i.e.* the aluminium and steel components) was accounted for in their design. Details of these design considerations and how they were accounted for is included in Appendix A.

In order to mitigate the influence of large temperature changes on the cells, the testing was generally carried out in a controlled laboratory environment. The details of the environmental monitoring of the laboratory can be found in Section 4.1.1.

7.2.1.3 Compression cells' commissioning

Section 4.1.3 describes the commissioning of the cells. The commissioning included an investigation into the likelihood of the occurrence of the side wall friction and the magnitude of the side wall friction was quantified. Table 4-1 presents the findings of this investigation.

It was found that the side wall friction varied considerably dependent on the size of the cell. In the main, it was found that the load lost to friction in the small cells was relatively minor, whilst in the large cells it accounted for a 5% loss in load. An account of this is made, explicitly, in Chapter 6 and Table 6-1.

Whilst this study of the effect of side wall friction is not considered exhaustive, it is seen as offering strong indications in respect to what degree equipment induced friction reduces the effective stress on the specimen.

7.2.1.4 Loading arrangements

The stress on the specimens was transferred through a plate and diaphragm arrangement within the cells, details of this arrangement can be found in Sections 4.1.2.4 and 4.1.2.5. This arrangement was based on a similar proven arrangement in use at the University of Sheffield (Blanchfield, 1998).

In this particular case this arrangement was found to be problematical, with the diaphragm being prone to rupture. A number of measures were implemented to prevent this rupturing occurring and these are detailed in Sections 4.1.2.4 and 4.1.2.5.

The implications of these ruptures significantly impacted on the proposed programme of testing. However, despite these failures the aims of the research

were fulfilled. Sufficient testing was undertaken examining a number of variables pertinent to the phenomenon of creep settlement; more detailed discussion is given in Section 7.4.2.1. In addition, a number of repeatability tests were undertaken, the results of which are discussed in Section 7.4.2.9.

During the Christmas break 2000 the university suffered a power failure. This caused the testing underway to be unloaded, with no means of monitoring the consequence in terms of specimen volume change. In order to assess the impact of this unloading and reloading an investigation was undertaken, whereby – under controlled – conditions the specimens were once again unloaded and reloaded. The details of this are shown in the results for Test 1, Test 5 and Test 7.

As can be seen from the graphs for these tests (see Figure 6-2, Figure 6-9, Figure 6-10, Figure 6-14 and Figure 6-13) the specimen undergoes some slight heave before, on the reapplication of load, undergoing a short period of non-linear (with the decadic logarithm of time) settlement. It then returns to the settlement rate (linear with the decadic logarithm of time) it was previously exhibiting to prior to the unloading.

This behaviour could be expected based on observations by Sowers *et al.* (1965) who identified that creep settlement rates were constant both before and subsequent to an inundation event. That is in an inundation event the soil structure is partially unloaded, due to the buoyancy effect. Section 7.4 contains further discussion with regards the behaviour of the specimens under stress.

7.2.1.5 Data Acquisition

The displacement and pressure transducers used in the laboratory testing were double calibrated; the results of the calibration undertaken on receipt of the transducers from the manufacturer agree with the manufacture's calibration which was supplied as a certificate with the transducers.

The computed tomography (CT) equipment and protocols used in this study are described in Section 4.2.

The scanner used in this study was located in a busy modern hospital and was employed as the diagnostic tool it was designed to be. As such, certain limitations were imposed on its use in this study; these are outlined in Section 4.2. The implications of these were mitigated as far as possible by the adoption of an optimised scanning protocol, which is described in Section 3.2.2. These limitations have meant that the CT images reproduced in Section 6.4 are a compromise between the aspirations of the study and the capabilities of the scanner. However, as shown by O'Neill et al. (2003) and Anderson *et al.* (2003) the technique offers some large and tangible benefits to the visualisation of particulate behaviour within a soil mass.

It is apparent from the review made in Section 4.2.3 that applications of CT in the Geosciences are relatively few. What applications have been reported are often borne of the needs and aspirations within the oil and gas industry. The capital cost of a typical modern medical CT scanner is in the region of £790k plus a further £50k to £100k for installation (LGI, 2007). Add to these costs the expense of running and maintaining the scanner and it is not difficult to appreciate that the cost of technique could be prohibitive. This may be the reason why many previous applications of this technique have been limited to the relatively rich oil and gas industry. Further, it is likely with the wider acceptance and use of CT in the medical world the effects of a mass market have reduced the costs from those quoted above.

A further reason for limited applications in the past could also be the image resolution that can be typically be achieved with a medical scanner. A resolution of 1 mm by 1mm by 1 mm is perfectly acceptable for use in medical diagnostics. When in order to achieve higher resolutions would mean exposing patients to higher doses of radiation, it is easy to understand why such scanners have not, until recently, been developed to produce higher resolutions. That has meant that for investigations requiring examination of particles smaller

than a gravel, the technique is only useful for making general measurements, e.g. the work reported by Braz *et al.* (2000) looking at the measurement of porosity and density of compacted soils. However, as shown by O'Neill *et al.* (2003), investigations on soils containing larger particles than gravel utilising CT can produce useful insights into the mechanics of soil behaviour. Further discussion is given in Section 7.4.3.

The resolutions of modern medical scanners have been increased in recent years due to the development of more advanced detector arrays and increasingly sophisticated reconstruction algorithms. For example the Philips Medical Systems' scanner the Brilliance CT – 64-channel is capable of reconstructing images to an isotropic resolution of 0.34 mm.

The limited use of industrial CT scanners is likely to be similarly due to cost. It is probably that as there is only a limited market for such scanners the capital and running cost are likely to be much more than those for a medical scanner.

It is evident that micro-focus CT has been found to be useful by researchers such as Van Geet *et al.* (2001) and Oda *et al.* (2004). This is possibly due to the fact that, relatively speaking, high isotropic resolution (10 μ m) images can be obtained at relatively little expense. Micro-focus CT scanners are commercially available at a capital cost of approximately £160k (Skyscan). However, the largest specimen size that can be accommodated by these scanners is approximately 75mm in size.

7.3 Materials

7.3.1 Material sources

Details about the locations from which the samples were taken are given in Section 5.1. The samples were taken from two, then, operational opencast coal mines, Houghton Main and Orgreave, from similar stratigraphic levels within the Middle Coal Measures. Both materials are typical of the strata encountered as overburden in coal extraction and, therefore, as fill in the restoration of opencast mines. The main difference affecting the testing material is in its

excavation method. The sample from Houghton Main was excavated from an undisturbed stratum of massive mudrock, whereas, the sample from Orgreave was excavated from a stratum that had recently been blasted.

The results of this difference were anticipated to be visible in the engineering properties, the determinations of which are outlined in Chapter 5 and discussed below.

7.3.2 Engineering Properties

The determinations of the engineering properties reported in Chapter 5 when compared with the values reported by Rainbow (1987) summarised in Table 2-7 (Section 2.1.5) are discussed below and, in summary, show that:

- The natural moisture contents of the materials used in this research were at the very bottom or slightly below the range encountered by Rainbow (1987).
- Particle Density (or Specific Gravity) of the materials were slightly higher, on average, than the range given by Rainbow (1987).
- Atterberg limits were within the ranges given; further the values were close to the mean average values given by Rainbow (1987).
- Compactive behaviour (optimum moisture content, w_{opt} , and maximum dry density, ρ_d) of the test materials was found to be slightly outside the ranges reported by Rainbow (1987), with w_{opt} being dry of the range given and ρ_d being slightly more dense than the range given.

A similar situation, with regards to the relative values of natural moisture content values was encountered by Blanchfield (1998) when the materials used in that study were compared with those in reported by Rainbow (1987). Blanchfield concluded that this difference was due to the timeliness of the moisture content determination relative to the materials excavation. That is, in its undisturbed state the mudrock will have a very low voids ratio and, thus, a relatively low moisture content when fully saturated. For the material used in the Blanchfield (1998) study a void ratio of 0.08 was determined and a

corresponding fully saturated moisture content of 3.2% for the undisturbed rock was calculated. The materials for which Rainbow (1987) determined moisture contents had all been stockpiled for sometime. As such these materials will have undergone some additional weathering and would have had access to moisture that the stockpiled material could have taken up.

Blanchfield cited O'Hara (1988) in support of this explanation. O'Hara measured the moisture content of various materials from the South Yorkshire coalfield and found that freshly excavated material typically had a moisture content of 5.0% to 9.0%. The values determined for the materials within this study are, in the most part, within this range. Only two moisture content determinations were found to be very slightly below this range. These undertaken on material taken from the Houghton Main site and were 4.7% and 4.8%, *i.e.* below the quoted range by 0.3% and 0.2% respectively.

In themselves the slightly higher particle densities determined for the materials used within this study than those reported by Rainbow (1987) are of little concern. Values at the upper end of, and slightly above, the range given by Rainbow (1987) are common. For example, Thompson *et al.* (1990) reported particle densities of 2.75Mg/m^3 for materials encountered on the Lounge Opencast Coal Mine Site and the Flagstaff site.

Compaction behaviour of the test materials used in this study was determined using the 4.5kg rammer method outlined in BS1377:1990:Part 4 as modified by the NCB Technical Memorandum (1971). As such the values determined in this study should not be directly compared with either those in Table 2-7 (after Rainbow, 1987) or those reported by Thompson *et al.* (1990), because both of these sources use different test methods to those employed here and to each other.

The values reported by Thompson *et al.* (1990) were determined using the 2.5kg rammer method (or Proctor method) whereas the values summarised in Rainbow (1987) were determined using a vibrating hammer method. The Thompson *et al.* (1990) values are comfortably within the ranges (for w_{opt} and ρ_d) given by Rainbow (1987); this suggests that the two methods, 2.5kg

rammer and vibrating hammer methods used, impart a comparable level of compactive effort on to the samples.

A higher energy would be imparted by the 4.5kg rammer method over the 2.5kg method and, as suggested, the vibrating hammer method. As can be seen from Figure 2-7, with an increase in the application of a higher compactive effort comes a higher achieved compacted density and corresponding lower optimum moisture content.

It is also noted that the standard compaction tests, mentioned above, are all undertaken on modified samples. To render the testing manageable the tests are either carried out in either a CBR mould, in the case of the vibrating hammer and heavy rammer methods, or a Proctor mould in the case of the 2.5kg rammer. In order for these moulds to be used and the test to be repeatable the samples used have a scalped grading. That is the particles not passing a certain sieve size (37.5mm aperture sieve, in the case of a CBR mould) are discarded. A similar approach is used in generating the specimens placed in the compressions cells; this is discussed in more detail in Section 7.4.1.

7.3.3 Houghton Main – Orgreave Sample Differences

Given the differences in excavation treatment between the material from each of the two sites, some differences in material properties were anticipated. Further, it was expected that the greatest difference would be seen between the particle size distributions for the fill materials.

The blasted material from the Orgreave site was expected to contain much more fine material, by proportion, whilst the material from the Houghton Main site would contain relatively little fine material. This was based on the perception that the amount of disturbance caused by the excavator digging the material from the Houghton Main site would be less than that caused by first blasting the material then excavating it.

The particle size distributions shown on Figure 5-4 do not confirm this expectation. There is little difference between the curve for the material from Orgreave and that from Houghton Main. What differences there are show the opposite from what was expected, *i.e.* the material from Houghton Main contains more fine particles by proportion than the material from Orgreave.

A simple explanation for this would be that the materials from the Houghton Main site were weaker than those from the Orgreave site, such that, even when exposed to greater disturbance forces, the Orgreave material did not fragment as much as the Houghton Main material. No direct evidence for this explanation is apparent however. Whilst no direct rock compressive strength testing was undertaken on either of the two samples the materials' strength was assessed in the field and recorded in accordance with BS5930:1999. The use of blasting at Orgreave was common practice at the site and was used to speed excavation rates rather than render rock suitable for excavation.

There is a slight difference in moisture content values for the two materials. The material from Houghton Main generally has a lower moisture content value than the Orgreave sample. Material with a higher moisture content would typically contain more fine particles and thus have a greater surface area and more particle contact points where moisture could be retained. However, this is not the case as can be seen from Figure 5-4. It is therefore speculated that the materials' diagenesis, particularly the resultant mineralogy, is the controlling factor for moisture content.

Slight differences in typical particle shape are also noted. From Section 5.4.1 it can be seen that the Houghton Main sample contains particles that are typically equi-dimensional in shape, whilst relatively few particles are rod or blade shaped. The Orgreave material also contains a preponderance of equi-dimensional particles but also contains a significant number of blade and rod shaped particles. It is probable that this is predominantly a result of the production methods used on the two sites (blasted before being dug at Orgreave and simply excavated at Houghton), though some other factors would have an influence, such as mineralogy of the parent materials.

Whilst the materials are of a similar stratigraphic level, they do not represent the same stratum nor are they from the same geographical location. With this in mind, it is likely that the differences between the materials are a function of their geological history and mineralogy.

The Atterberg limit determinations carried out for the two materials are reported in Section 5.6. They indicate some difference in mineralogy between the materials. The plastic limit for the Houghton Main Sample is significantly lower than that for the Orgreave sample. Similarly significant differences are apparent in the liquid limits for the materials and these carry through to the plastic and liquidity indexes. The generally accepted explanation for the differences in soil plasticity is difference in its mineralogy.

These factors are discussed further with respect to their influence on the behaviour of the materials under compaction in Section 7.4.1.2 and under stress in Section 7.4.

7.4 Results

7.4.1 Specimen Preparation

The specimens used within this work were derived from material taken from the Houghton Main and the Orgreave opencast coal mine sites. The details of the materials are given in Chapter 5 and interpretation and discussion is given in Section 7.3. The specimens were prepared as outlined in Section 3.1.2.

7.4.1.1 Maximum particle size

In order to render the laboratory testing as representative as possibly of conditions typically found in opencast coal mines it was necessary to maximise the size of the particle within the specimens as well as the specimens themselves. The specimens' particle size distributions are shown on Figure 5-4. As can be seen the specimens used in the small compression cells did not contain particles greater in size than 37.5 mm in nominal diameter. Similarly the specimens used in the large cells did not contain particles greater in size

that 120 mm in nominal diameter. This was done so that the effects of side wall friction on the behaviour of the stressed specimen could be minimised.

These maximum sizes were arrived at following the guidance contained in BS1377:1990:Part 5; which recommends that a ratio of greater than 5 to 1 (cell diameter to maximum nominal particle diameter) is used. The ratios used in this testing were 5 to 1 in the large cells and 6 to 1 in the small cells. Similar guidance can be found in BS1377:1990:Part 4 with respect to particle sizes used in standard compaction testing. The guidance for compaction testing also extends to the proportions of a soil of a particular nominal diameter. With some interpretation this guidance can be applied to the ratios used within this study.

A ratio of ~3 to 1 is required for a soil containing up to 5% of its particles exceeding 37.5 mm nominal diameter for a test in a CBR mould. In this case the material and cell combinations are:

- 5% of the particles used in the large compression cells exceed 110 mm nominal diameter, giving a ratio, similar to that in BS1377:1990:Part 4, of ~5.5 to 1.
- 5% of the particles used in the small compression cells exceed 34 mm nominal diameter, giving a ratio of ~6.5 to 1.

The use of different maximum particle sizes in the different cell sizes provided an opportunity to investigate its affect on creep rate, this is discussed in Section 7.4.2.6.

7.4.1.2 Specimen compaction

The specimens were compacted in the cells using the equipment described in Section 4.1.6. The densities achieved are presented through out Section 6.2 alongside other relevant information.

Comparison of compaction effectiveness is commonly measured against standard tests, such testing was carried out as part of this study and the details

and results are reported in Section 5.7. In the field, during the restoration of an opencast mine, the requirements of a compaction regime are specified. Such specification, such as that contained in SARCOB (1993) or Trenter and Charles (1996), often require that the compacted material meet an end-product requirement. Most frequently the end-product criterion is in relation to the achieved end-product density measured against that achieved with a standard test. For example, the end-product requirement might be, put simply, that the dry density of the soil compacted by the compaction regime be at least 90% of the maximum dry density achieved in the lab with a standard test. With this in mind the resulting specimen density achieved in the laboratory are presented in Table 7-1 and Figure 7-1 against the results from the standard testing carried for the same material.

| Test number | Material source | Specimen density (Mg/m ³) | | Moisture content (%) | Air voids ¹ (%) | %age maximum dry density ² |
|-------------|-----------------|---------------------------------------|------|----------------------|----------------------------|---------------------------------------|
| | | Bulk | Dry | | | |
| 1 | Houghton | 1.84 | 1.74 | 5.5 | 22.2 | 86 |
| 2 | Orgreave | 1.97 | 1.83 | 7.1 | 20.0 | 84 |
| 3 | Orgreave | 1.76 | 1.65 | 6.7 | 28.5 | 75 |
| 4 | Houghton | 1.74 | 1.66 | 5 | 31.5 | 76 |
| 5 | Houghton | 1.76 | 1.68 | 4.7 | 31.0 | 77 |
| 6 | Orgreave | 1.84 | 1.67 | 6.9 | 25.1 | 76 |
| 7 | Houghton | 1.75 | 1.67 | 4.7 | 31.4 | 77 |
| 8 | Orgreave | 1.75 | 1.65 | 6.2 | 29.4 | 75 |
| 9 | Houghton | 1.74 | 1.66 | 5.1 | 31.4 | 76 |
| 10 | Orgreave | 1.84 | 1.72 | 7.1 | 24.9 | 79 |
| 11 | Orgreave | 1.85 | 1.73 | 7.1 | 24.5 | 79 |
| 12 | Houghton | 1.85 | 1.77 | 4.8 | 27.3 | 82 |
| 13 | Orgreave | 1.68 | 1.57 | 7.1 | 31.4 | 72 |
| 14 | Houghton | 1.84 | 1.76 | 4.7 | 27.8 | 81 |
| 15 | Orgreave | 1.74 | 1.62 | 7.1 | 29.0 | 74 |

Notes:

1. Particle density testing results for the samples are included in Section 5.2.
2. Standard compaction testing results for the samples are included in Section 4.1.6.

Table 7-1: Comparison of the compaction achieved in specimen preparation with standard compaction.

As can be seen from Table 7-1 and Figure 7-1 the bulk densities achieved in the compression cells vary from 1.68 Mg/m³ to 1.97 Mg/m³, the dry densities of the specimens vary from 1.57 Mg/m³ to 1.83 Mg/m³. When compared to the maximum dry density (MDD) determined for each material presented in Section 5.7 the results show that between 74% and 86% of the maximum dry density was achieved.

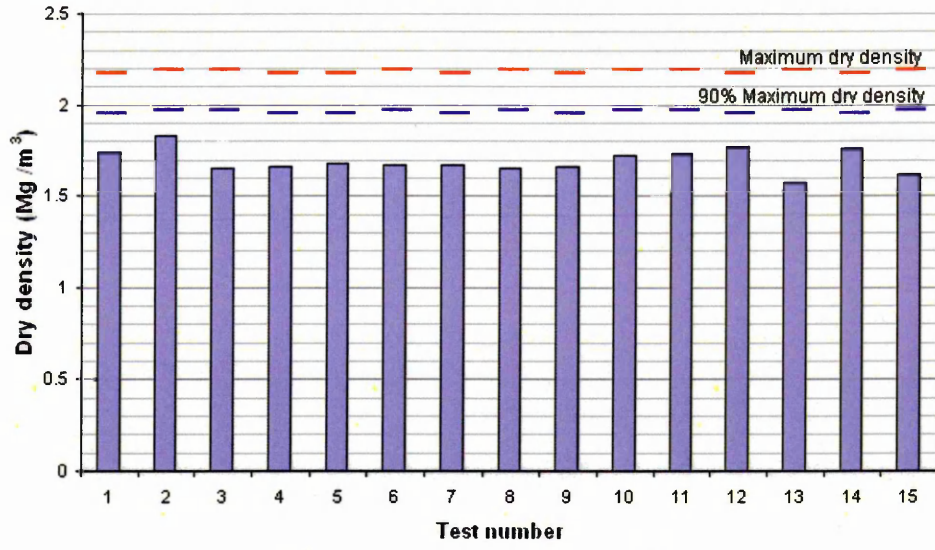


Figure 7-1: Graph showing compaction achieved for each test specimen compared to MDD and 90% of MDD.

A comparison can be made between the densities achieved during cell preparation when using the light compaction method against those achieved using the heavy method (see Table 6-1 and Figure 7-1) in similar sized cells. This comparison is summarised in Figure 7-3. As can be seen the heavy compaction method consistently produced higher density specimens.

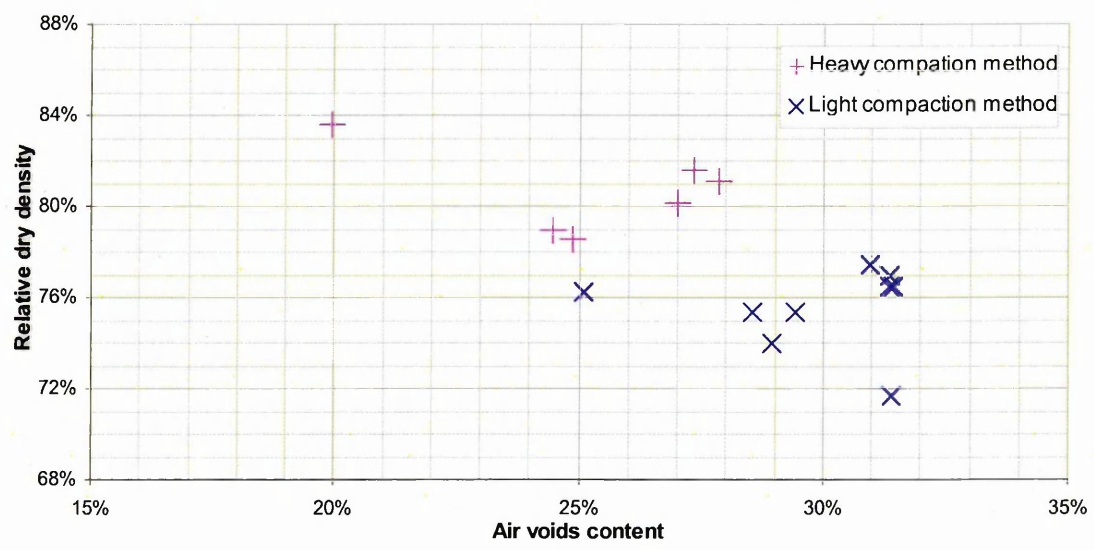


Figure 7-2: Graph showing relative effectiveness of compaction energies used in specimen preparation for creep testing.

Under different compaction the materials used were also found to behave differently. Figure 7-3 shows that the material sourced from the Houghton Main site had consistently higher air voids for similar relative compaction than the material sourced from the Orgreave site. Had the particle size distribution for the Houghton Main and Orgreave fill samples (Figure 5-4) been as anticipated, see Section 7.3.3, it would be possible to explain this behaviour by referring to the relative fractions of fine to coarse particles. That is, the larger volume of finer particles in one material resulting in a more efficient packing state than in the other material thus resulting in lower air voids in the compacted specimen. As is apparent from the grading curves shown in Figure 5-4, which do not evidence a significant difference between to two materials, this explanation is unlikely.

The next logical explanation is that some change from the starting particle size distribution occurred during the compaction process; such that the resulting air void contents of the compacted specimens were reduced following breakdown of some of the material particles. It may be that the Orgreave sample, which has fewer air voids, was predisposed to such breakage under compaction due to its excavation method. This predisposition could be caused by the blasting of the material whilst it was insitu. This would have caused increased micro fracturing in the material, weakening it so that it broke down more readily than the other material when compacted.

The layers of the specimens used in the large cells were typically 130 mm when compacted using the heavy method and 215 mm when using the light. Similarly, in the small cells the layer thicknesses were typically 75 mm when using the heavy method and 150 mm when using the light method. It is normal practise to limit the ratio of particle maximum size to layer thickness to less than 2 to 3 (SARCOB, 1993), i.e. for a layer of 300 mm the maximum particle size would be 200 mm.

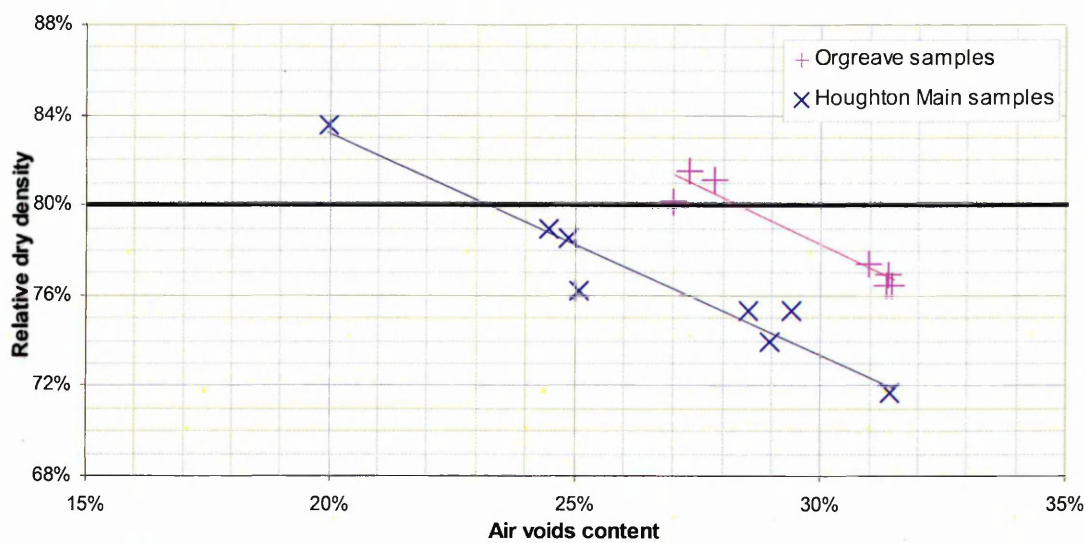


Figure 7-3: Graph showing relative effects of compaction energies on each material type.

In order to achieve densities close to those found in opencast coal mine restorations it was necessary to exceed the ratio of layer thickness to particle maximum size in all of the compaction regimes employed in this study with the exception of the light compaction method when applied to the specimens in the small cells. However, the methods of compaction used in the restoration of mines are likely to be much more abrasive to particles than the methods used in this study.

7.4.2 Laboratory Results

7.4.2.1 Test variables

The following variables, potentially affecting the creep behaviour of the specimens, were examined in the testing reported here:

- Degree of Compaction.
- Inundation state.
- Material properties through use of two different but typical materials. These properties and characteristics include:
 - Particle size distribution (inc. maximum particle size)
 - Mineralogy
 - Petrology

- Physical weathering (through excavation)
- Plasticity

Both the materials and the degree of compaction have been discussed in the preceding section of this chapter from the aspect of specimen preparation and material. They are further discussed in subsequent sections from the perspective of the specimens' exhibited behaviour.

The inclusion of specimen inundation as a test variable was considered important because of the apparent contradictory states found within the literature. It was generally acknowledged by Sowers *et al.* (1965) that the rate of creep strain continued unchanged following an inundation event. However, the effect of wetting materials, particularly soft rock materials, is shown to increase or further weather the material (e.g. Bally, 1988). The effect of inundation on exhibited behaviour is discussed in subsequent sections.

7.4.2.2 Exhibited behaviour – creep rate

The settlement behaviour exhibited by the stressed specimens is shown the various plots in Chapter 6. Generally, the settlement plots (presented in terms of strain) show typical creep behaviour. That is, under conditions of constant stress a linear relationship of strain with decadic logarithm of time is apparent.

The one test that did not clearly display this behaviour was test 2, see Figure 6-3. The strain rate measured from this test was approximately linear with time. The reason for this is not obvious though the most likely possibility is an equipment failure. It is considered that the behaviour exhibited could be the result of a leak in the diaphragm arrangement causing a gradual inundation of the specimen and with it the gradual plastic deformation measured.

7.4.2.3 Exhibited behaviour – creep rate establishment

The establishment of the generally constant creep rate can be seen to take some time after a constant stress has been achieved. This can be seen at intermediate stages of loading and / or on the completion of loading on Figure 6-2 for Test 1,

Figure 6-8 for Test 4, Figure 6-10 for Test 5, Figure 6-14 for Test 7, Figure 6-16 for Test 8, Figure 6-22 for Test 11, Figure 6-26 for Test 13, Figure 6-28 for Test 14, and Figure 6-30 for Test 15.

This behaviour is also noticeable on those tests for which an unload / reload cycle was carried out, *i.e.* Test 1 (Figure 6-2), Test 5 (Figure 6-10), and Test 7 (Figure 6-14).

Also, following the inundation events undertaken as part of this research a similar non-linearity of the strain rate with decadic logarithm of time is noted. See Figure 6-8 for Test 4.

This similarity is marked and it is logical to conclude that this similar behaviour following the establishment, or re-establishment, of a constant stress is due to similar mechanisms.

7.4.2.4 Exhibited behaviour – sudden strains

A number of the figures (Figure 6-2, Figure 6-12, Figure 6-16, Figure 6-22, Figure 6-24, and Figure 6-30 for Tests 1, 6, 8, 11, 12, and 15, respectively) show similar non-linearity occurring with no corresponding stress change. These sudden strains may also be due to the same types of mechanisms as those responsible for the non-linearity identified in Section 2.3.

It may be that these mechanisms represent the large scale movements of particles, such as those identified as major differences identified in Section 6.4.2 and discussed late in Section 7.4.3. Attributing such movements to large scale movements suggests that the constant creep rate typical of the linear relationship is due to smaller scale movements. Again, these small scale movements may be identified as the minor differences identified in Section 6.4.2 and discussed late in Section 7.4.3.

Further discussion of this is also made in Section 7.4.2.10 with regards to snapping noises heard whilst the testing was underway.

7.4.2.5 Exhibited behaviour – creep rate comparison

The creep rates measured within the compression cells are presented in Figure 7-4 along side the typical rates of creep for compacted opencast coal mine backfills, identified from the literature in Section 2.4.4. As can be seen in Figure 7-4, the majority of the creep rates from the testing are within typical limits observed in the field.

Two notable exceptions are Tests 1 and 5, the creep rates for these two tests are significantly above those observed in the field. It may be that this is a function of the compaction state achieved in the specimen preparation. It is noted in Section 7.4.1.2 that the compaction achieved in the laboratory is below that typical of a controlled fill.

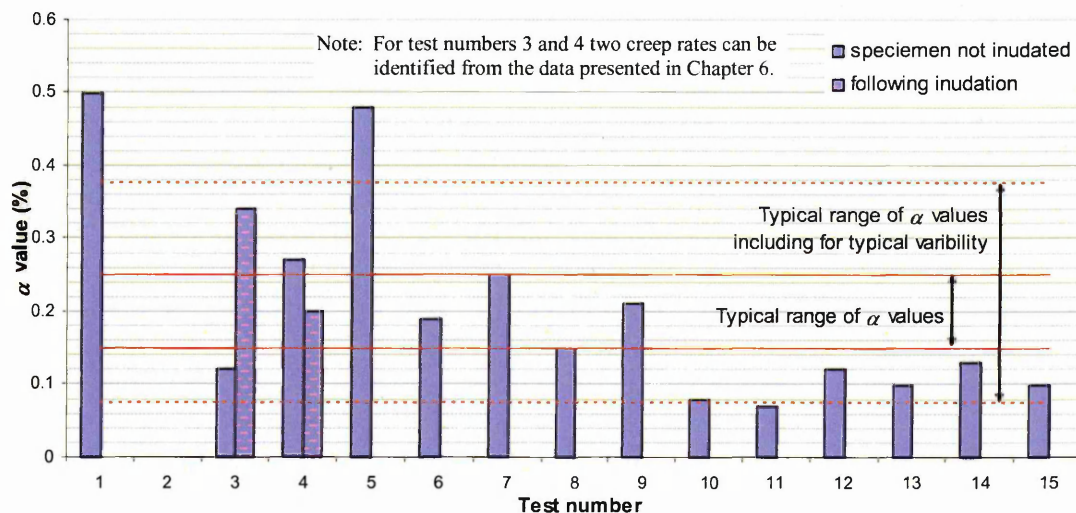


Figure 7-4: Comparison of test α values with typical values observed in the field.

7.4.2.6 Exhibited behaviour – creep rate with cell size and maximum particle size

The information shown in Figure 7-5 indicates that the creep rate observed in the large cells (containing a larger maximum particle size) was greater than in the small cells. However, the available data set for the large cells is relatively small and has a large variability. With this in mind, it is possible to say that there is some indication that maximum particle size affects creep rate and creep rate variability.

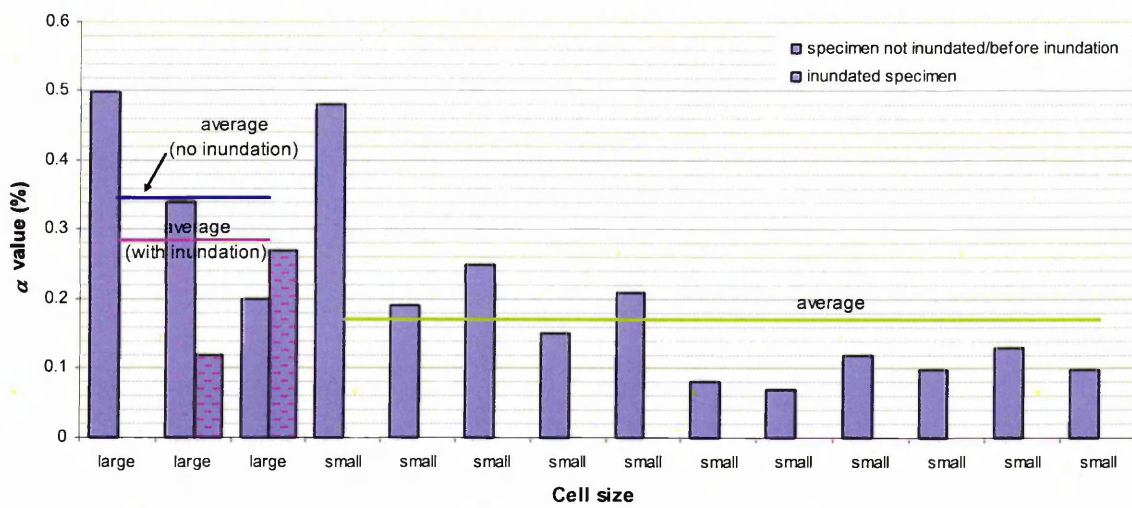


Figure 7-5: Graph of α values against cell size.

It is postulated, e.g. Kettle (1990), that with an increase in particle size comes an increased potential for particle breakage. This is attributed to the greater probability of a larger particle containing more and more significant irregularities from which particle breakage could propagate. This is somewhat supported by the results of this study.

7.4.2.7 Exhibited behaviour – creep rate with density

Figure 7-6 compares the α values obtained from the laboratory testing against density of the specimen. Based on this figure there appears to be no obvious correlation between the creep rate parameter, α , and specimen density, although, there is some tendency for those samples with a higher density to exhibit a lower creep rate parameter. The outlying data points (approximately on the 0.5% α line of the graph) however, mask this.

Two groups of data points illustrate this and these groups are highlighted on the graph and labelled (a) and (b). Group (a) has an average dry density of $\sim 1.745 \text{ Mg/m}^3$ and a corresponding α value of 0.1%. Whereas, group (b) has an average density of $\sim 1.655 \text{ Mg/m}^3$ and a corresponding α value of 0.2%.

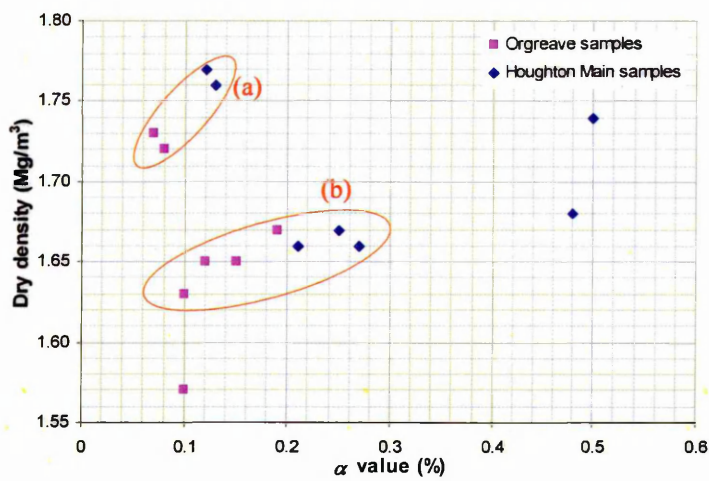


Figure 7-6: Comparison of test α value with sample dry density.

This is further supported by Figure 7-7, which shows that samples which received a greater degree of compaction generally exhibited lower rates of creep compression.

Two noteworthy anomalies are apparent in Figure 7-7. One of the heavily compacted samples is shown to have undergone creep at a rate of 0.5% (per \log_{10} cycle). This rate is five times that of the average of other samples that were compacted using the heavy sample compaction method. This value, inevitably, increases the average creep rate for the samples compacted using this method.

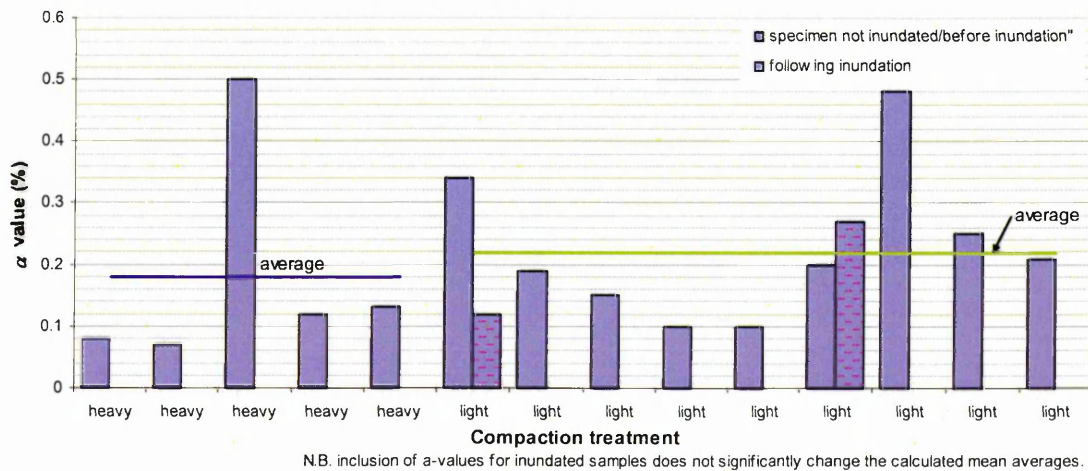


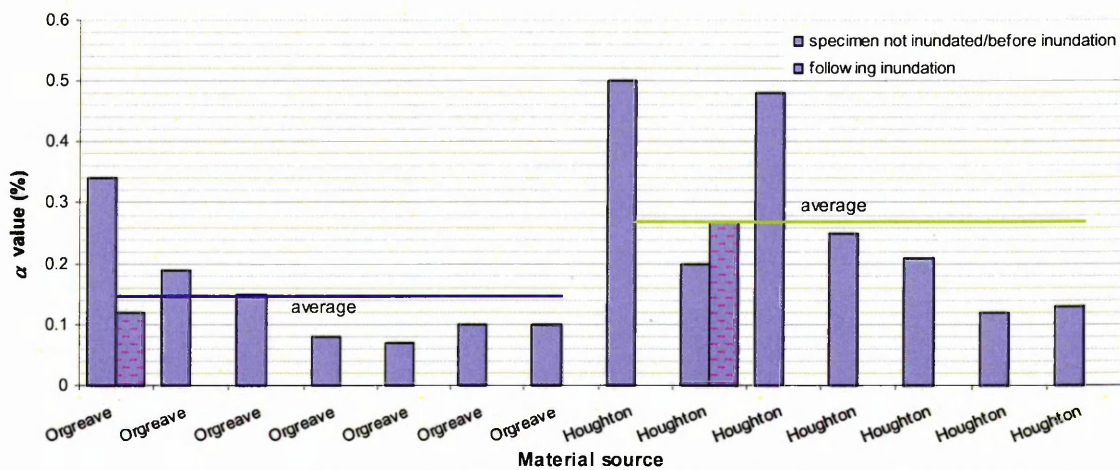
Figure 7-7: Graph of α values against compaction treatment.

The second anomalous value is not as significant. For the samples compacted using the light method one exhibited a creep rate of 0.48%. This elevated rate is more than double the average rate exhibited by the other lightly compacted samples.

7.4.2.8 Exhibited behaviour – creep rate with material

A difference in creep rate behaviour can be seen between the two material sources used and this is shown clearly in Figure 7-8. With the Houghton Main material exhibiting greater rates of creep than the material taken from the Orgreave site.

The results described as anomalous in the preceding section were both from samples of the material taken from the Houghton Main site. This may indicate that the results were in fact not anomalous but were still representative of the Houghton Main material. If this is the case then it suggests that material properties are more significant than compacted density.



N.B. inclusion of α -values for inundated samples does not significantly change the calculated mean averages.

Figure 7-8: Graph of α values against material source.

7.4.2.9 Repeatability

Four pairs of similar tests were carried out as part of the testing for this study. These repeatability pairs are listed in Table 7-2.

| Repeatability | Test numbers that |
|---------------|-------------------|
|---------------|-------------------|

| pair number | make the pair | |
|-------------|---------------|----|
| 1 | 5 | 7 |
| 2 | 10 | 11 |
| 3 | 12 | 14 |
| 4 | 13 | 15 |

Table 7-2: Repeatability pairs.

Comparisons of the dry densities, total strains and creep rates are shown in Figure 7-9, Figure 7-10, and Figure 7-11, respectively.

As can be seen from Figure 7-9 the compaction regime used has produced samples of similar densities.

As can be seen from Figure 7-10 the total strain experienced by each of the repeatability pairs, numbers 1, 2 and 4 are similar. Pair 3 shows that one of the tests has undergone greater strain than other. However, consulting Table 6-1 and Figure 6-28 it is apparent that not all of the strain experienced by the sample in Test 14 was necessarily recorded. Pair 3 should, therefore, be ignored for this comparison.

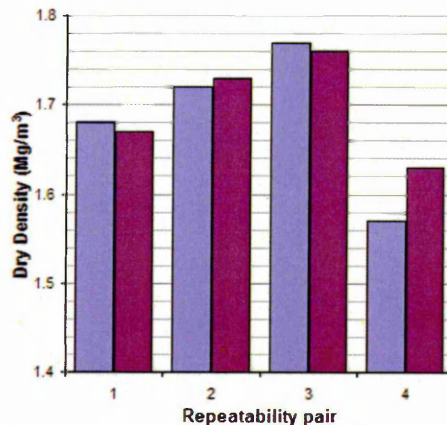


Figure 7-9: Comparison of sample dry density of Repeatability Pairs.

The comparison of the creep rate (α value) for the repeatability Pairs 2, 3 and 5, shown on Figure 7-11, is good. However, the comparison of Pair 1 shows that for these similar tests (Test 5 and 7) the creep rates were significantly different. However, the comparisons for this repeatability pair shown in Figure 7-9 and

Figure 7-10 are good. Further, the creep rates for either Test 5 or 7 are not considered anomalous.

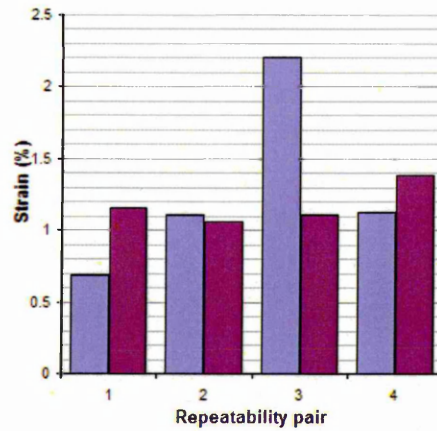


Figure 7-10: Comparison of sample strain of Repeatability Pairs.

On the basis of the comparisons and discussion above the repeatability of the testing method is considered to be satisfactory.

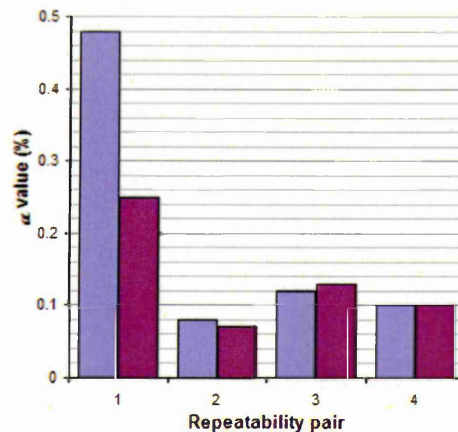


Figure 7-11: Comparison of sample α values of Repeatability Pairs.

7.4.2.10 Popping noises

As noted in Section 6.5 cracking noises were occasionally heard emanating from the samples. These noises were most frequent during the loading phase of the testing with the occurrence of a snapping sound usually accompanied by a large deformation of the sample.

These sounds may be indicative of the large scale changes first discussed in 7.4.2.4. The occurrence of such a large scale change could conceivably produce such a noise. For example the breakage of a particle by delaminating along a bedding plane, dislocation along incipient discontinuities or the rotation of a particle ploughing against an adjacent particle would be accompanied by significant amounts of kinetic energy.

It was noted that the cracking noises were shortly preceded by creaking sounds. It is speculated that this creaking was the relatively small movements along structural plane that ultimately built up, transferring enough energy, to a larger movement. The release of this energy, in the larger movement, is thought to be the cause of the snapping sound.

Such noises are typically encountered in soil and rock testing. When testing rock samples in a triaxial cell such noises accompany fragmentation and spalling of the sample (M Czerewko, *pers. comm*). Thus it is reasonable to speculate that similar spalling or fragmentation also occurs with the samples used in this study. This is further supported by observations made of mudrock exposures. Following a period of rain when the mudrock surface is drying the surface weathers. This weathering comprises of desiccation producing spalling of fragments of mudrock from the exposure and similar 'popping' sounds have been noted (M Czerewko, *pers. comm*).

Similar noises are noted to accompany crack propagation in brittle materials, including rock (Cox and Meredith, 1993) and Shearer (1999) reports on work on other materials.

These popping noises may also be akin to those observed in active slope failures where it has been shown that movement within the soil mass during failure emits acoustic vibrations, Dixon *et al.* (2003).

Following testing, the insides of the cells were inspected for damage and little was observed. It is probable that the plastic of the cell walls was sufficiently robust to resist the majority of any damage that could be caused by the mudrocks used within this study. The rocks are relatively soft and the pipe

material's typical use is in underground applications, where it will have to resist similar and more extreme damage.

7.4.3 Computed Tomography Results

7.4.3.1 Individual images

An inspection of the individual images shows various features resulting from the compression of the sample under the applied stress. Similar features have been noted in the publications O'Neill *et al.* (2003) and Anderson *et al.* (2003). The visualisation of behaviour through these features is quantified by the differences scoring scale and analysis described in Section 6.4.2. The interpretation and discussion of this analysis is contained in 7.4.3.2.

These features include:

- i. Movements of individual particles and the corresponding changes in the size and shape of surrounding voids.
- ii. Particle breakage.
- iii. Changes in localised conglomerations of fine particles.
- iv. Breakage of particle asperities.

Other features apparent on the long-sectional images that were not included in either O'Neill *et al.* (2003) or Anderson *et al.* (2003) are listed below.

- v. Localised movements of either individual particles or conglomerations of fine particles located at the interfaces of the cells' bottom plate or loading plate.
- vi. Some images show a concentration of differences close to the cell walls.
- vii. The concentration of differences in one area of a sample, whilst in the remainder of that sample (at the plane of the image) no differences are apparent.

The grouping of differences identified in some of the images and noted in point 'vi' (above) implies that, in some cases, the compression of the samples is due to movement of relatively few particles.

It is also clear from the relative frequency of ‘small’ compared to ‘large’ that it is the ‘small differences’ that are most responsible for the creep compressions observed. This extends to the relative infrequency of ‘significant differences’ compared to ‘small differences’ and infrequency of ‘major differences’ compared to ‘significant differences’.

This approach could be automated and refined using an image analysis software package; such an approach has recently been used successfully by White *et al.* 2003.

7.4.3.2 Differences score

As described in Section 6.4.2 the images taken from the computed tomography (CT) scans has been analysed using a scale of differences. Three degrees of difference have been used: minor, significant and major.

As might be expected the frequency of these differences decreases with severity, *i.e.* there are fewer large (major) differences than small (minor) ones. This is shown in Table 7-3, which shows that there was more than sixteen times the number of minor difference as major ones.

| Scale of differences | Scale value | | |
|-----------------------------------|-------------|-------------|-------|
| | 1 | 3 | 5 |
| | minor | significant | major |
| Number of difference noted | 760 | 324 | 47 |

Table 7-3: Summary of totals of differences scores.

By multiplying the scale value by the number of differences identified at that scale a weighted total was arrived at. Thus the total difference score is indicative of the internal structural changes that have occurred during the testing. This is described in more detail in Section 6.4.2.

This total (total difference score) is plotted against dry density for each sample in Figure 7-12. This figure shows that there is a discernable relationship between dry density and the number of differences noted.

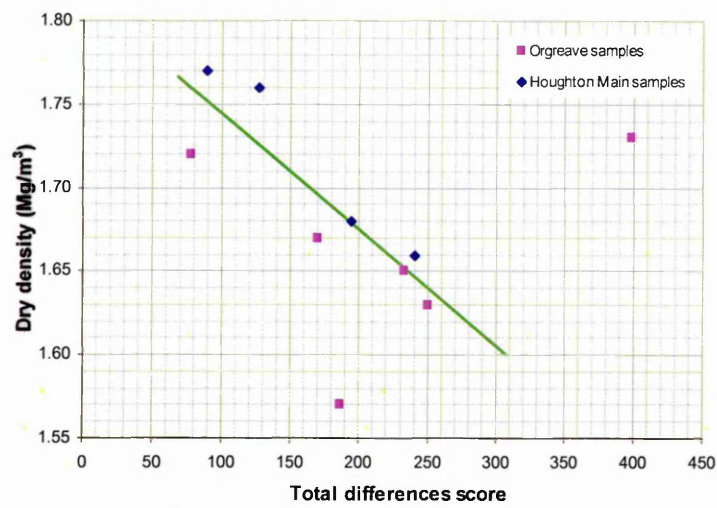


Figure 7-12: Comparison of test difference score with sample dry density.

The right most data point does not follow this relationship. One likely reason for this is that the sectional images selected and analysed for this sample are coincident with volumes within the sample that have undergone the most movement.

As with the α values in Sections 7.4.2.7 and 7.4.2.8, the total differences scores can be compared with the sample materials' source and compactive treatment. This comparison is shown graphically in Figure 7-13 and Figure 7-14, respectively.

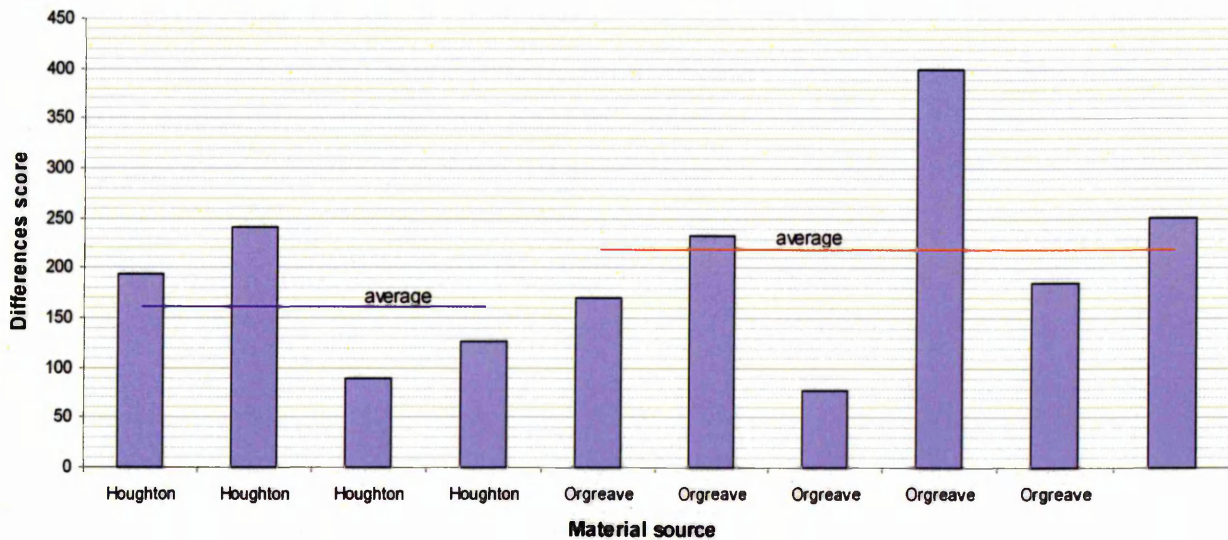


Figure 7-13: Graph of difference score against material source.

Comparison of the differences score with material source, shown in Figure 7-13, does not show a marked difference as the comparison of material source with α value did (Figure 7-8).

The comparison of differences score with compaction treatment (Figure 7-14) shows a similar relationship to that observed in the comparison of compaction treatment with α value in Figure 7-7. The larger differences score of ~400 for one of the heavily compacted samples is an exception, with the remainder of the heavily compacted samples having lower scores than any of the lightly compacted samples.

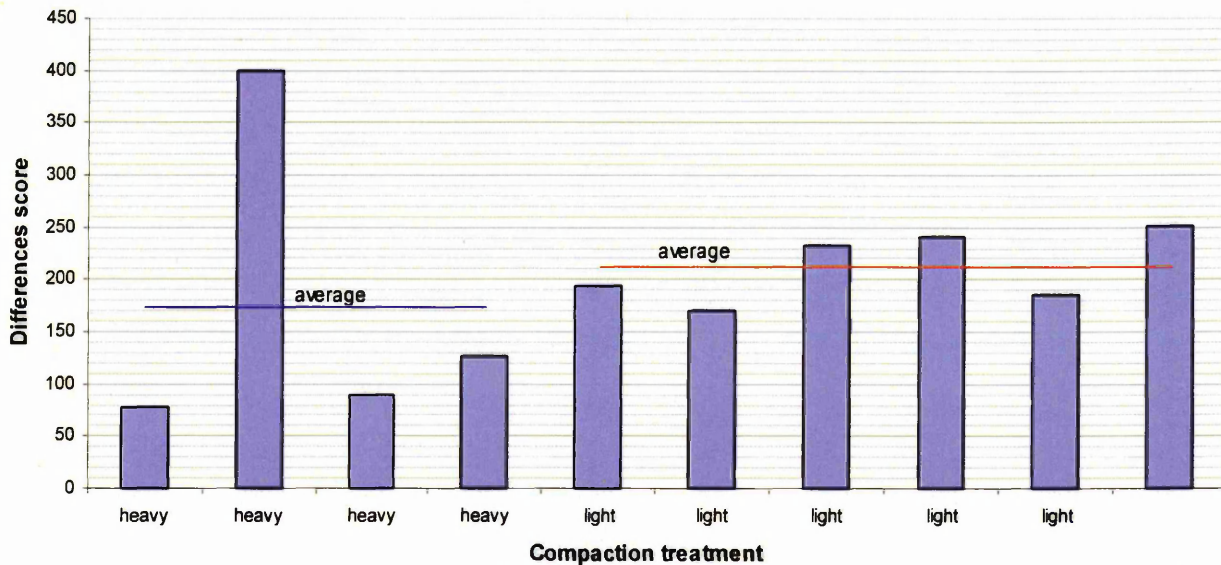


Figure 7-14: Graph of difference score against compaction treatment.

7.4.4 Laboratory and Computed Tomography Results Comparison

Figure 7-15 and Figure 7-16 compare the differences scores for each test against the α values.

Figure 7-15 shows a correlation of increasing total differences score with increasing creep rate (α value). This correlation remains true if the data point to the right of the main grouping of data points is ignored, as unrepresentative.

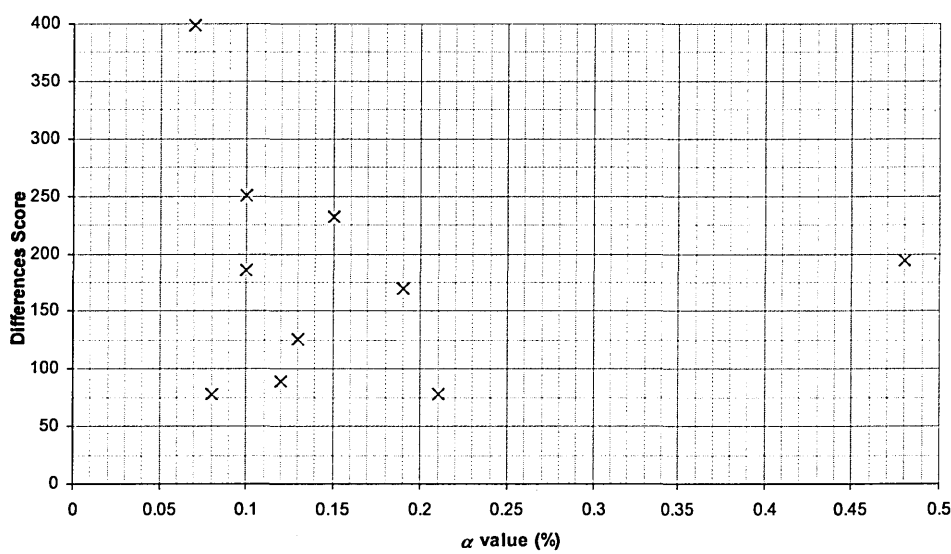


Figure 7-15: Comparison of total differences scores against α values for each test.

Figure 7-16 shows that the occurrence of major differences is independent of the creep rate. A similar correlation as that for total differences is apparent for the significant differences. This correlation remains true if the data point to the right of the main grouping of data points is ignored, as unrepresentative.

If the data point shown to the right of the main grouping of data points for the minor differences is excluded from the assessment then a similar correlation can be observed.

The outlying data point could be attributed to the selection of the sectional images analysed. It is possible that the images used in the analysis passed through areas of the sample which have undergone the greatest compression and account for the majority of the creep measured. Further, that other areas of the sample have not undergone similar compression and had the images been taken through these areas the difference score for the sample would reflect this.

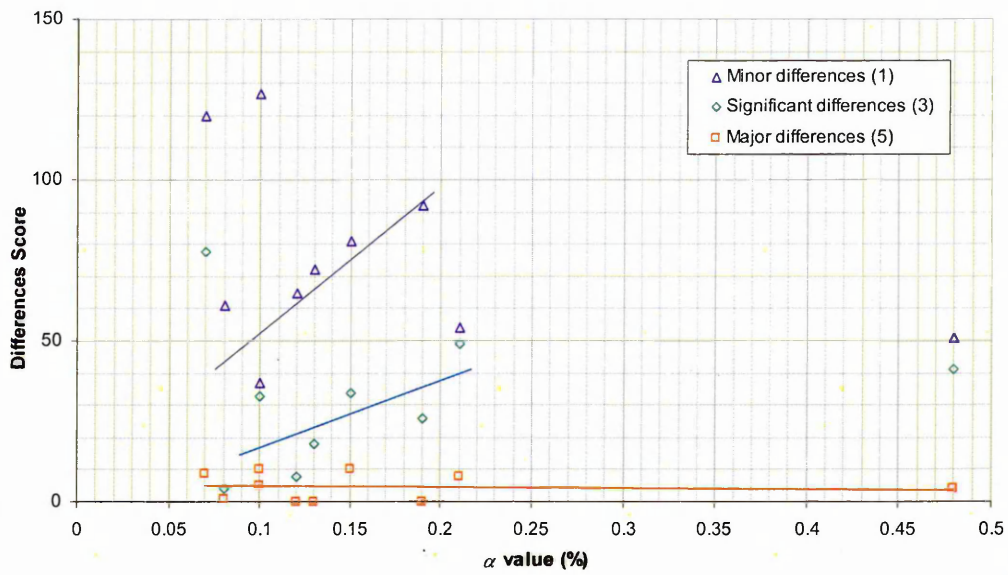


Figure 7-16: Comparison of differences scores against α values for each test.

Based on the discussion above and the comparisons of differences scores for each test with the corresponding α value it is reasonable to speculate that the differences noted in the images of the CT scans are the cause of the creep compression recorded in the main testing.

8 Conclusions & Recommendations

A programme of laboratory based testing, supplemented and integrated with a programme of non-destructive testing using a x-ray computed tomography technique has been completed. The information obtained through this testing is useful in testing the hypothesis presented in Section 1.4, i.e. that creep settlement is due to redistribution of forces within a soil through particle breakage and/or rotation. That is, the aims and objectives of this research, also listed in Section 1.4, have generally been achieved.

Following a brief summary of the work undertaken, the conclusions drawn from the work are presented and, subsequently, recommendations for future work are given.

8.1 *Summary of work*

Bespoke test cells that could be used in the research's testing programme were designed and commissioned. The use of a diaphragm and piston arrangement, like that detailed in Section 4.1.2.5, proved problematic in use. Despite this, long-term testing into the creep behaviour of opencast mine backfill was been successfully undertaken.

As the test programme required that the cells and the specimens contain within be scanned in a medical computed tomography (CT) scanner the materials from which they were manufactured was a major consideration. The use of very dense materials would have increased the likelihood of artefacts compromising the results from the CT scanner.

As anticipated the use of a medical x-ray CT scanner has yielded good quality results. It was found that by developing an appropriate and optimised scanning protocol the technique could be successfully used for research in the field of soil mechanics. The relatively low isotropic resolution of the images produced has meant that a simplified approach to the CT image's interpretation has been adopted. Only larger particles within the soil can be clearly identified. Along

with limited access, the high capital and running cost of equipment, this explains lack of widespread use of CT in soil mechanics.

The use of the non-standard soil mechanics technique, i.e. CT, in this research has aided the understanding of the phenomena of creep settlement investigated.

8.2 Conclusions

8.2.1 General Creep Settlement Behaviour

The programme of testing has produced high quality data evidencing the occurrence of creep settlement within the specimens being tested. This test data reveals compression of the sample under conditions of constant stress and moisture content.

The cross-sectional images taken through the specimens soon after the application of load and again prior to its removal show a greater number of “major differences” in those specimens exhibiting larger creep rates (see Figure 7-16). This correlation extends through to the “significant changes” but to a lesser degree. No such correlation is apparent between “minor differences” and the creep rate. This adds weight to the assertion that creep settlements are attributable to rotations and breakage of particles which are most frequently highlighted as “major differences”.

8.2.2 Field Creep Values

As can be seen from the results the laboratory based testing has yielded creep rates comparable with those observed in the field (see Figure 7-4 and Section 2.4.4). It is reasonable to conclude from this that the objective of investigating creep behaviour whilst simulating field conditions has been achieved. Further, the additional control of variables and increase in monitoring possible in the laboratory has allowed the effects of the variables: “compaction regime” and “soil composition” to be investigated.

8.2.3 Repeatability

The experimental regime included sufficient testing to allow repeatability testing to be carried out. The discussion on this aspect of the regime is made in Section 7.4.2.9. This section also presents the interpretation of the results with their repeatability in mind. Whilst a relatively few tests have been carried out a good level of repeatability is shown to have been achieved. In addition to that provided by the good practice and quality testing employed within the research, the repeatability achieved adds further confidence to the conclusions drawn from the results and their interpretation.

8.2.4 Source Materials

The effects of material composition on creep behaviour were investigated by this research. The composition of the test material was varied by using material taken from two sources. The sources of the materials used in this study were active mine sites, Houghton Main and Orgreave opencast coal mine sites. These sites were located in coal bearing Carboniferous geologies; at each site different but typical methods of overburden removal were employed. With this in mind it can be said that the materials used are typical of materials encountered as overburden to coals that exist at a shallow enough depth such that they can be won by opencast mining methods.

Further, it can be said that these materials are representative of the materials used in the restoration of opencast coal mines in the United Kingdom and this is illustrated by the comparisons with data published from other sources, see Section 7.3.2. Based on the classification testing undertaken and reported herein, the materials used within the research were reasonably consistent through out the period beginning with their excavation and collection to their final use in the test programme.

However, the material sourced from the Houghton Main site appears to be significantly different to that sourced from the Orgreave site. It is evident from the classification testing presented that these differences are not fully explained by standard engineering testing. It is likely that these differences are due to the

excavation method and mineralogy of the parent material. It is reasoned that the excavation method is the most significant single cause, see Section 7.3.3.

The composition and diagenetic history of a material is believed to have a significant effect on the creep behaviour of the samples. This is clear from the creep rates recorded for the two materials tested. Figure 7-8 shows the tests carried out on the material sourced from the Houghton Main site to exhibit higher creep rates than that sourced from the Orgreave site. However, the data from the analysis of the CT scans (see Figure 7-13) does not show any notable difference.

8.2.5 Compaction Regime

Two compaction regimes (light and heavy) were employed to produce specimens for testing. The compaction regimes have been shown to have produced consistently compacted samples, as illustrated throughout Section 6.2 where details of the test specimen's preparation are presented.

It was expected that with an increase in compactive effort that the creep rate would be reduced. The testing reveals that this expectation is accurate; with the data indicating that with an increase in density (i.e. high compactive effort) comes a reduction in creep rate. Figure 7-3 clearly shows this. Similarly, the analysis of the computed tomography data indicated that samples subjected to a greater degree of compaction underwent fewer internal structural changes.

8.2.6 Test Scale

Two cell sizes were employed during the investigation, the larger cells contained specimens with a maximum particle size of 75mm nominal diameter. The specimens contained in these cells exhibited greater creep rates than those in the smaller cells, containing specimens with a maximum particle size of 37.5mm nominal diameter. Whilst the data set available for the large cells is both small and variable the results do indicate that with a larger particle size comes an increase in creep rate, see Figure 7-5.

From the variability in creep rates exhibited in the specimens contained in the large cells it could be inferred that an increase in variability may also be expected with an increase in particle size.

8.2.7 Non-linear and Inundation Behaviour

Non-linear behaviour (that is strain not directly proportional to the decadic logarithm of time) was noted to occur:

- during the loading phases of the testing,
- on the inundation of specimens, and
- immediately prior to the onset of the linear behaviour typically associated with creep settlement.

This non-linearity also was noted in isolated and spontaneous events when a typical linear creep rate relationship had been established. It is speculated that these sudden movements may be due to large scale particle rearrangements or breakages, thus implying that the linear creep relationship is attributable to smaller scale mechanisms. This speculative view is somewhat supported by the occurrence of major soil structure differences and some of the significant differences identified in the computed tomography images. Further, these sudden movements are likely to be associated with the snapping or popping noises heard emanating from within the tests.

Only a small number of the tests were inundated, however these tests reveal data (see creep rates for tests numbers 3 and 4 in Figure 7-4) that confutes the generally accepted view that the creep rate prevalent before an inundation event is re-established once inundation is complete.

8.3 Recommendations

- The classification of soils used in similar projects to the one reported here should be extended to include the geological classification and variability of the source materials. This is true, even when the materials are of a similar nature.

- A further study of creep behaviour that investigates the influence of stress on creep rate would further the understanding of the mechanisms and nature of creep.
- The benefits of computed tomography in the investigation of soil behaviour are clear. This technique should be exploited further, possibly using a scanner which can resolve to a higher resolution and, therefore, track individual particles.
- Where possible the computed tomography scanner employed in future studies should be designed for the purpose. This would allow the imaging to be reconstructed at of a much higher quality and resolution.
- The use of computed tomography requires the processing of large amounts of data this could be automated using the type of software already available and developed by White *et al.* 2003.
- The use of such software alongside a computed tomography scanner, with a higher specification, would allow the tracking of individual particles.

References

- Anderson, W. F. and Cripps, J. C. (1990) The effects of acid leaching on the shear strength of namurian shale. *Proceedings of the 26th Regional Conference of the Engineering Group of the Geological Society*. Leeds, 181-192.
- Anderson, W.F., O'Neill, M.A. and Goodwin, A.K. (2003) Creep settlement of opencast coal mine restorations. *Proceedings of the 13th European Conference on Soil Mechanics and Geotechnical Engineering*, Prague, 1, 533-538.
- ASTM D2922-05 (1991). Standard Test Methods for Density of Soil and Soil-Aggregate in Place by Nuclear Methods (Shallow Depth).
- ASTM D3017-05 (1993). Standard Test Method for Water Content of Soil and Rock in Place by Nuclear Methods (Shallow Depth).
- Bally, R. J. (1988) Some specific problems of wetted loessial solid in civil engineering. *Engineering Geology* 25, 303-324.
- Barden, L., McGown, A. and Collins, K. (1973) Evaluation and control of collapsible soils. *Journal of Geotechnical Engineering*, ASCE 118(10), 1491-1504.
- Barnes, G.E. (2000) *Soil mechanics: principles and practice*, 2nd Edition, Palgrave.
- Barnes, G.E. & Staples, J.G. (1988) The acceptability of clay fill as affected by stone content. *Ground Engineering*, 21(1), 22-30.
- Bates R.L. and Jackson J.A.J. (1980) *Glossary of geology*, 2nd edition. American Geological Institute.
- Behringer, R.P., Howell, D., Kondic, L., Tennakoon, S. and Veje, C. (1998) Gravity and Granular Materials. *Proceedings of the Fourth Microgravity, Fluid Physics and Transport Conference*. Cleveland, OH.
- Bell, F.G., Entwisle, D.C. and Culshaw, M.G. (1997) A geotechnical survey of some British Coal Measures mudstones, with particularly emphasis on durability, *Engineering Geology* 46, 115-129.
- Bishop, A.W. (1959) The principle of effective stress. *Tecknisk Ukeblad*, 106(39): 859-863.
- Blanchfield, R. (1998) Volume Change Characteristics of Opencast Coal Mine Backfill, PhD Thesis, University of Sheffield.
- Blanchfield, R. & Anderson, W.F. (2001). Settlement of opencast coal mine backfill in large scale laboratory tests. *Proceedings Of The 3rd International Symposium On Geotechnics Related to the European Environment, GREEN3*, Berlin, 447-456.

- Blight, G.E. (1965) Effective stress evaluation for unsaturated soils. *Journal of Soil Mechanics and Foundation Design*, ACSE, **93(SM2)**, 125-148.
- Boespflug, X., Long, B.F.N. and Occhietti, S. (1995) CAT-scan in marine stratigraphy: a quantitative approach. *Marine Geology* **122**, 281-301.
- Bolt, G. H. (1956) Physico-chemical analysis of the compressibility of pure clays: *Geotechnique* **6**, 86-93.
- Bowman, E.T., Soga, K. and Drummond, T.W. (2000) Particle Shape Characterisation using Fourier Analysis. Technical Report, Department Of Engineering, University of Cambridge.
- Brady, K. C. and Kirk, G. (1990) The compressibility of Crushed Limestone Backfill, Research Report 251. Transport and Road Research Laboratory, Department of transport.
- Braz, D. Lopes, R.T. and Motta, L.M.G. (2000) Dual-energy computerized tomography in compacted soil. *Geotechnical and Geological Engineering* **18**, 221-238.
- British Coal Opencast (1993) Facts and figures. Information Bulletin, Mansfield, Nottinghamshire.
- British Geological Survey (2006) Mineral Planning Factsheet Coal and Coalbed methane.
- British Standard (BS) 1377:parts 1 to 9 (1990) Soils for civil engineering purposes. British Standards Institution, London.
- British Standard (BS) 5930 (1999) Site investigation methods. British Standards Institution, London.
- British Standard (BS) 812 (1989) Testing Aggregates. British Standards Institution, London.
- Burgers, J. M., and Scott Blair, G. W. (1948) Report on the principles of rheological nomenclature (Joint Committee on Rheology of the International Council of Scientific Unions): *Proceedings of the International Rheologie Congress*, Amsterdam.
- Burland, J.B. (1965) The yielding and dilation of clay (correspondence). *Geotechnique* **15**, 211-214.
- Casagrande, A. (1932), The structure of clay and importance in foundation engineering. *Journal of the Boston Society of Civil Engineers* **19**, 4, 168-209.
- Challinor, J. (1967) *A Dictionary of Geology*, Cardiff, University of Wales Press.
- Charles, J.A., Watts, K.S. (2001) *Building on fill: geotechnical aspects*. 2nd Edition, BRE Report 424.

- Charles, J.A., Skinner, H.D., Watts, K.S. (1998) The specification of fills to support buildings on shallow foundations: the "95% fixation". *Ground Engineering*, January, 29-33.
- Clements, R. (1984) Post-Construction deformation of rockfill dams, *Journal of the Geotechnical Engineering Division*, ASCE, July, 821-840.
- Coop, M. (1997) Personal Parameters - A report on the BGS meeting selection of parameters for geotechnical design. *Ground Engineering* 11, 32-37.
- Cox, S. J. D., and Meredith, P. G. 1993. "Microcrack formation and material softening in rock measured by monitoring acoustic emission." *International Journal of Rock Mechanics, Mining Science and Geomechanics Abstracts*, 30, 11-21.
- Cripps, J. C. and Taylor, R. K. (1981) The engineering properties of mudrocks. *Quarterly Journal of Engineering Geology*, 14, 325-346.
- Croney, D, Coleman, J.D. and Black, W.P.M. (1958) Movement and distribution of water in soil in relation to highway design and performance. From Highway Research Board Special Report 40: Water and its conduction in soils.
- Curtis C.D. (1976) 'Unmixed' Ca²⁺/Mg²⁺ saponite at Calton Hill. *Clay Miner.* 11, 85-89. Derbyshire.
- Czerewko, M. (1997) Diagenesis of mudrocks, illite crystallinity and the effects on engineering properties, PhD Thesis, University of Sheffield.
- Day, R. W. (1989) Relative compaction of fill having oversized particles. *Journal of Geotechnical Engineering*, ASCE 115(10), 1487-1491.
- Department of Transport. Specification for Highway Works (1986).
- Department of Transport. Specification for Road and Bridge Works (1969).
- Department of Transport. Specification for Road and Bridge Works (1976).
- Dixon N., Hill R., and Kavanagh J. (2003) Acoustic emission monitoring of slope instability: development of an active waveguide system. *Geotechnical Engineering* 156(2), 83 – 95
- Fair, P. I. (2003) Geotechnical behaviour of ballast materials for railway track maintenance. PhD Thesis, University of Sheffield.
- Feda, J. (1982) *Mechanics of Particulate Materials – The Principle*. Elsevier, Amsterdam.
- Feda, J. (1989) Interpretation of creep of soils by rate process theory. *Geotechnique* 39(4), 667-677.

- Fredlund, D. G. (1995), "The Scope of Unsaturated Soils Problems", *Proceedings of the First International Conference on Unsaturated Soils*, Paris, September 6 - 8, Vol. 3.
- Fredlund, D.G., and Rahardjo, H. (1993) *Soil mechanics for unsaturated soils*. John Wiley & Sons, New York.
- Gillott, J.E. (1968) *Clay Engineering in Geology*. Elsevier, Amsterdam.
- Goodwin, A. K. (1991) One Dimensional Compression Behaviour of Unsaturated Granular Soils at Low Stress Levels, PhD Thesis, University of Sheffield
- Goodwin, A K, O'Neill, M A & Anderson W F. (2001) 'Investigation of the Fundamental Mechanisms Affecting Creep Settlement of Restored Opencast Coal Mine Sites', Proc. 3rd British Geotechnical Association Geoenvironmental Engineering Conf., Edinburgh, September 2001
- Grimshaw, P. N. (1992) *Sunshine Miners. Opencast Coalmining in Britain*, British Coal Opencast, Mansfield, Nottinghamshire. 1942–1992.
- Hardin, B. O. (1985) Crushing of Soil Particles. *Journal of Geotechnical Engineering*, ASCE 111(10), 1177-1192.
- Hassani, F. P., Whittaker, B. N., and Scoble, M. J. (1979) Strength characteristics of rocks associated with opencast coal mining in the UK. *U.S. Symposium on Rock Mechanics*. Texas. 347-356.
- Hawkins, A. B. and Pinches, G. M. (1987) Sulphate analysis on black mudstones. *Geotechnique* 37(2), 191-196.
- Highways Agency (1998), *Manual of Contract Documents for Highways Work*, Volume 1 - Specification for Highway Works, Series 600 Earthworks.
- Hills, C.W.W. (1994) *The Examination & Prediction of Opencast Backfill Settlement*. PhD Thesis, University of Nottingham.
- Hills C. W. W. & Denby D. (1996) 'The prediction of opencast backfill settlement', *Proceedings of the Institution of Civil Engineers, Geotechnical Engineering*, 119, 167-176.
- Howell, D. (2000) *Stress Distributions and Fluctuations in Static and Quasi-static granular assemblies*, PhD Thesis, Duke University.
- HP Vee, *Visual Engineering Environment*– a visual programming language supplied by Hewlett Packard (2000).
- Hughes, D.B. and Clarke, B.G (2003) Surface Coal Mining and the reclamation of tips, landfills and quarries – some geotechnical cases studies from Northern England. *International Journal of Surfacing Mining, Reclamation and Environment* 17, No. 2, 67-97.

- Human, C. (1992) Time dependent property changes of freshly deposited or densified sands, PhD Thesis, University of California, Berkley.
- Jennings, J.B. and Burland, J.B. (1962) Limitations to the use of effective stresses in partially saturated soils. *Geotechnique* 12. 125-144.
- Kalender, W. (2000). *Computed Tomography: Fundamentals, System Technology, Image Quality, Applications*. MCD, Verlag, Erlangen & Munich.
- Kestenbaum, D. (1995) Sand castles and cocktail nuts - Innocent-looking piles of seeds, sand or powder are liable to drive grown men and women to tears - or even to the extreme edges of theoretical physics. *New Scientist* 154(2083), 25-28. ipc magazines.
- Kettle, R. J. (1990) The Influence of Particle Size on the Performance of Cement Bonded Minestone. *Reclamation, Treatment and Utilization of Coal Mining Wastes*. 33-40. Rotterdam, Balkema.
- Kilkenny, W.M. (1968) A study of the settlement of restored opencast sites and their suitability for building development. Bulletin No 38 Department of Civil Engineering, University of Newcastle-Upon-Tyne.
- Kjaernsli, B. and Sande, A. (1963) Compressibility of some coarse grained materials. *Proceedings of Wiesbaden European Conference on Soil Mechanics and Foundation Engineering*.
- Knipe, C. (1979) Comparison of settlement rates on backfilled opencast mine sites. *Conference on Urban and Industrial Fills*. Birmingham. E81-E98.
- Kolbuszewski, J., and Frederick, M.R. (1963). "The significance of particle shape and size on the mechanical behaviour of granular materials" *European Conference on Soil Mechanics and Foundation Engineering* 1
- Kolbuszewski, J. & Alyanak, I. (1964) Effects of vibrations on the shear strength and porosity of sands. *The Surveyor and Municipal Engineer*, 123, 3756: 23-27 and 3757: 31-34.
- Krumbein, W.C. (1941) Measuring of Geological significance of shape and roundness of sedimentary particles. *Journal of Sedimentary Petrology* 11, 64 -72.
- Lambe, T.W., and Whitman, R.V. (1969). *Soil Mechanics*. John Wiley & Sons, New York.
- Lawton, E.C., Fragaszy, R.J. and Hetherington, M.D. (1992) Review of wetting induced collapse in compacted soil. *Journal of Geotechnical Engineering* 118, September 1376-1394.
- Lees, G. (1963) The Measurement of Particle Shape and its Influence in Engineering Materials. *Journal of the British Granite and Whinstone Federation*. 4(2).

- Léés, G. (1964) A New Method for Determining the Angularity of Particles. *Sedimentology* 3, 2-21.
- Leonards, G.A. and P. Girault (1961) "A study of the One-Dimensional Consolidation Test," *Proceedings 5th International Conference on Soil Mechanics and Foundation Engineering*, Paris, 1. 213-218.
- Leung, C.F., Lee, F.H. and Yet, N.S. (1996) The role of particle breakage in pile creep in sand. *Canadian Geotechnical Journal* 33, 888-898.
- Lu, M. and McDowell, G. (2007) The importance of modelling ballast particle shape in the discrete element method. *Granular Matter* 9, 1-2, January, pp. 69-80.
- Marsal, R.J. (1963) Contact Forces in Soils and Rockfill Materials. *Proceedings of the Panamerican Conference in Soil Mechanics and Foundation Engineering*. 2, 67-98.
- Marsal, R.J. (1965). Soil properties-shear strength and consolidation, *Proceedings of the 6th International Conference Soil Mechanics and Foundation Engineering*, 3, 310-316.
- Marsal, R.J. (1973) *Mechanical properties of rockfill*. Embankment dam engineering, Casagrande volume John Wiley and Sons, New York
- McDowell, G. R. & Bolton, M. D. (1998). On the micromechanics of crushable aggregates. *Geotechnique*, XLVIII, 5, 667-679.
- McDowell, G.R. and Khan, J.J. (2003) Creep of granular materials. *Granular Materials*. 5(3). 115-120.
- Mees, F., Swennen, R., Van Geet, M. & Jacobs, P. (eds) 2003. Applications of X-ray Computed Tomography in the Geosciences. Geological Society, London, Special Publications, 215, 1-6.
- Mesri, G. (1973) Coefficient of Secondary Compression. *Journal of Soil Mechanics and Foundations Division*, ASCE, Vol.99, No.SM1, 123-137.
- Minerals Planning Guidance 3: Coal mining and colliery spoil disposal (MPG3). Office of the Deputy Prime Minister, 1999.
- Mitchell, J. K. (1960) Fundamental Aspects of Thixotropy in Soils. *Journal of Soil Mechanics and Foundations Division*. SM 3. 19-52.
- Mitchell, J. K. (1993) *Fundamentals of Soil Behaviour* 3rd Edition, Wiley, New York.
- Monroe, J. S. and Wicander, R. (1992) *Physical Geology: Exploring the Earth*, West Group.
- Morgenstern, N. R. and Eigenbrod, K. D. (1974) Classification of Argillaceous Soils and Rocks. *Journal of the Geotechnical Division*, ASCE 100(GT10), 1137-1156.

- Naderian, A.R. and Williams, D.J. (1996) Simulation of groundwater rise and its effects on settlements of open-cut coal mine back-fills. *International Journal of Surface Mining, Reclamation, and Environment*, 10, 83-89.
- Nakashima, Y. Hirai, H. Koishikawa, A. Ohtani, T. (1997) Three-dimensional imaging of arrays of fluid inclusions in fluorite by high-resolution X-ray CT. *N. Jb. Miner. Mh.* 559-568.
- National Coal Board (1971) Application of British Standard 1377 : 1967 to the Testing of Colliery Spoil, Technical Memorandum, joint Working Party on Soil Mechanics Testing, NCB, London.
- Newland, P.L., and B.H. Allely (1957) Volume changes in drained triaxial tests on granular materials, *Geotechnique*. 7, 1734.
- Oda, M., Takemura, T. and Takahashi, M. (2004) Microstructure in shear band observed by microfocus X-ray computed tomography. *Geotechnique* 54, 539-542.
- O'Neill M., Goodwin A.K. & Anderson W.F. (2001) The Use of Computerised Tomography (CT) in the Investigation of the Settlement Behaviour of Mudrock. *Applications of X-ray Computed Tomography in the Geosciences*. Geological Society, London, Special Publications 2003 volume 215: 199-204.
- Otani, J., Mukunoki, T. and Obara, Y. (2000) Application of X-ray CT method for characterization of failure in soils. Japanese Geotechnical Society *Soil and Foundations*, 40, 111-118.
- Parkin, A. K. (1971) Application of rate analysis to settlement problems involving creep. *Proceedings 1st Australian - New Zealand Conference in Geomechanics*. 138-143.
- Parkin, A. K. (1977) The Compression of Rockfill. *Australian Geomechanics Journal*, 33-39.
- Penman, ADM, (1953). Shear characteristics of a saturated silt, measured in triaxial compression. *Geotechnique*, 1.3(8). 312-329.
- Penmen, A.D.M (1971) Rockfill British Research Establishment CP15/71
- Peterfi, T. (1927). Die abhebung der Befruchtungsmembran bei Seeigeleiern. *Archiv für Entwicklungsmechanik der Organismen* 112, 660-695.
- Pigeon Y. (1969) 'The compressibility of rockfill', PhD thesis, Imperial College, London.
- Rainbow, A. K. M. (1987) Minestone Fill in Reinforced Earth Abutments. *The Journal of the Institution of Highways and Transportation*. 25-31.

- Ramsbottom, W. H. C., Sabine, P. A., Dangerfield, J., and Sabine, P. W. (1981) Mudrocks in the Carboniferous of Britain, *Quarterly Journal of Engineering Geology* 14, 257-262.
- Rowe, P.W. and Barden, L. (1966) A new consolidation cell. *Geotechnique*, 16 (2), 162—170.
- SARCOB (1993) State of the art review of the compaction of opencast backfill, Scott Wilson Kirkpatrick & Co. Ltd. for British Coal Opencast, Mansfield, Nottinghamshire.
- Schoeck, G. (1961) Thermodynamic principles in high-temperature materials. *Mechanical behaviour of materials at elevated temperatures*. 57-78, New York, McGraw-Hill.
- Scholz, C. H. and Engelder, J. T. (1976a) The Role of Asperity Indentation and Ploughing in Rock Friction - 1, Asperity Creep and Stick-slip. *International Journal of Rock Mechanics and Mining Sciences* 13, 149-154.
- Scholz, C. H. and Engelder, J. T. (1976b) The Role of Asperity Indentation and Ploughing in Rock Friction - 2, Influence of Relative Hardness and Normal Load. *International Journal of Rock Mechanics and Mining Sciences* 13, 155-163.
- Shearer, P. M. 1999. *Introduction to seismology*, Cambridge University Press, Cambridge, England.
- Shi, B., Murakami, Y., Wu, Z., Chen, J. and Inyang, H. (1999) Monitoring of internal failure evolution in soils using computerization X-ray tomography. *Engineering Geology*. 54, 321-328.
- Skyscan Microtomography Equipment (2007, 29 May – last updated). Available: www.skyscan.be [30 May 2007]
- Slobod, R.L. and Claudle, B.H. (1952) X-Ray shadow studies of aerial sweep out efficiencies. *Transactions of the American Institute of Mining, Metallurgical, and Petroleum Engineers* 195, 265–270.
- Sowers, G. F., Williams, R. C., and Wallace, T. S. (1965) Compressibility of Broken Rock and the Settlement of Rock fills. *Montreal. Proceedings of the 6th International Conference of Soil Mechanics and Foundation Engineering* 2, 561-565.
- Soydemir, C. and Kjaernsli, B. (1979) Deformation of membrane-faced rockfill dams, *7th International Conference on Soil Mechanics and Foundation Engineering*, Brighton, UK, 3, 281-284
- Spears, D. A. (1969) A laminated shale of Carboniferous age from Yorkshire, England, *Journal of Sedimentary Petroleum* 39, 106-112.

- Spears, D. A., Taylor, R. K., and Till, R. (1971) A mineralogical investigation of a spoil heap at Yorkshire Main Colliery. *Quarterly Journal of Engineering Geology* 3, 239-252.
- Sridharan, A. and Rao, A. S. (1982) Mechanisms Controlling the Secondary Compression of Clays. *Geotechnique* 32(3), 249-260.
- Steudi, J.S., Hopkins, F. and Ander, J.E. (1994) Industrial X-rays computed tomography applied to soil research. *Proceedings of the Symposium Soil Science Society of America*, Minneapolis, Minnesota, American Society of Agronomy, Madson, WI, 29-41.
- Stow, D.A.V. (1981) Fine-grained sediments: Terminology. *Quarterly Journal of Engineering Geology* 3, 239-252.
- Swennen, R. Poot, B Marchal, G. (1990) Computerized tomography as a tool in reservoir characterization. *Zbl. Geol. Paläont. Teil I*, 1105-1124.
- Taylor, D.W. (1948). *Fundamentals of Soil Mechanics*. John Wiley, New York.
- Taylor, R. K. and Spears, D. A. (1970) The breakdown of British Coal Measures rocks. *International Journal of Rock Mechanics and Mining Sciences* 7, 481-501.
- Taylor, R. K. and Spears, D. A. (1981) Laboratory investigation of mudrocks. *Quarterly Journal of Engineering Geology* 14, 291-309.
- Taylor, R. K. (1988) Coal Measures mudrocks: composition, classification and weathering processes. *Quarterly Journal of Engineering Geology* 21, 85-99.
- Terzaghi, K. (1943) *Theoretical Soil Mechanics*. John Wiley, New York.
- Terzaghi, K. and Peck, R.B. (1948). *Soil Mechanics in Engineering Practice*. John Wiley, New York.
- Thompson, J., Holden, J.M.W., Yilmaz, M. (1990) Compaction of opencast backfill beneath highways and associated developments. *Reclamation, Treatment and Utilization of Coal Mining Wastes*. Edited by Rainbow, Balkema, Rotterdam. 293-312.
- Timoshenko, S. (1955) *Strength of Materials, Part 1: Elementary theory and problems*. 3rd Edition, Van Nostrand Reinhold Company.
- Trenter, N. A. (2001) *Earthworks: A Guide*, Thomas Telford, London.
- Trenter, N. A. and Charles, J. A. (1996) A model specification for engineered fills for building purposes. *Proceedings of the Institution of Civil Engineers Geotechnical Engineering* 119, 219-230.

- Van Geet, M., Swennen, R. and David, P. (2001) Quantitative coal characterisation by means of microfocus X-ray computer tomography, colour image analysis and back-scattered scanning electron microscopy, *International Journal of Coal Geology* 46, 11-25.
- Vinegar, H.J. (1986) X-Ray CT and NMR imaging of rocks. *Journal of Petroleum Technology*, March, 257-258.
- Wahl, A.M. and Lobo, G. (1930) Stresses and deflections in flat circular plates with central holes, *Transactions of American society of Mechanical Engineers*, 52, APM-53-30, 29-43.
- Wahls, E. H. (1962) Analysis of Primary and Secondary Consolidation. *Journal of Soil Mechanics and Foundations Division*, ASCE, 88(SM6), 207-231.
- White, D.J., Take, W.A. and Bolton, M.D. (2003) Soil deformation measurement using particle image velocimetry (PIV) and photogrammetry. *Geotechnique* 53, 619-631.

List of Personal Communications

- Czerewko, M. Principal Engineering Geologist, Scott Wilson Ltd. Chesterfield. In discussion, March 2007.
- D'Souza, J. Materials Engineer, Hepworth Plumbing, Pollard Moor, Padiham, Burnley, Lancashire, England. By letter and email, 27 January 2000.
- Stevens, T. Principal Engineer, Uponor Ltd., Heighton Lane, Newton Aycliffe, Co. Durham, England. By facsimile communication, 05 January 2000..

Appendix A Metal Cell Component Design Calculations

A.1 Introduction

This appendix is intended to present the design calculations and concepts for the design of the structural elements of the creep cells as discussed in Chapter 3 of this thesis. The structural elements are the top and bottom plates of the cells and the tie bars between them, these three elements clamp the plastic pipe that forms the cell walls. These elements can be seen, for design purpose, as to two plates on with a central hole large enough to reduce the plate's structural integrity and a series of bars subjected to a tensile force. The plates will be subjected to a uniformly distributed load whilst being supported at the edges.

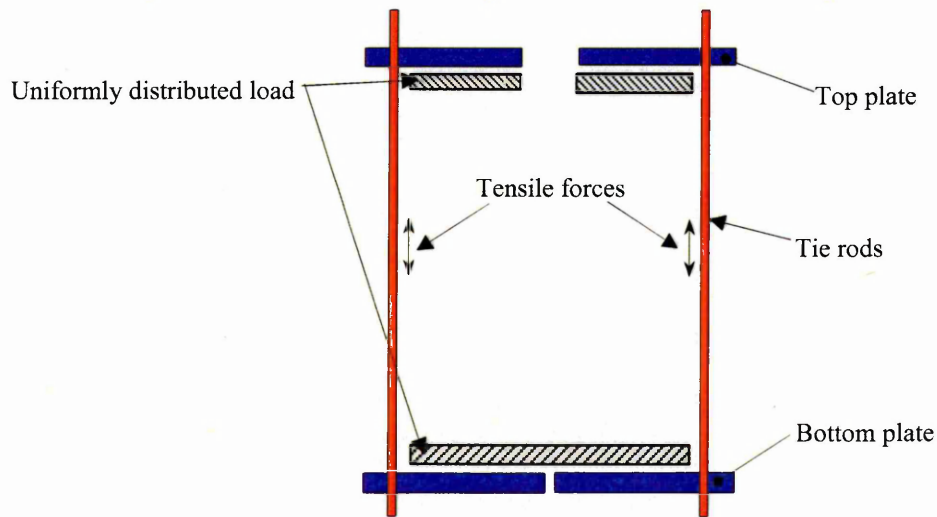


Figure C-1 Cell components and forces acting upon them.

A.2 Tie Rod Design

Looking at the design of the tie rods of the cells first; the design problem is straight forward with the bars subjected to a tensile load equal to the working pressure of the cell divided by the number of bars. The only complication to the design arises from the requirement imposed by the use of the radiological techniques. In order to get the most information from the radiological techniques employed the cells must have the maximum number of "lines of sight" possible through the sample and unencumbered by a dense material, such as that used to form the structural elements of the cells. In order to accomplish this, a spreadsheet was set up in which the number of bars required for a certain bar diameter is calculated or the bar diameter for a certain number

of bars is calculated. This enabled the speedy comparison of different bar configurations.

Finally, an allowance for the thread depth had to be made, effectively reducing the bar diameter, and a factor of safety for the design had to be applied; these are given more consideration in the design in Section A.6.

A.3 Bottom Plate Design

The detailed design calculations for the small and large cell bottom plates are shown in Section A.6, the design equations have been taken from Timoshenko (1955). The small hole required to accommodate the cell plumbing has been ignored due to its negligible effect on the design.

A.4 Top Plate Design

The top plate design is based on the design equations proposed by Wahl and Lobo (1936), which provides the means for the calculation of the thickness and deflection of a plate with a central hole subjected to a uniformly distributed load. Two situations for the plate are considered the first with the inner edges restrained against rotation the second where the inner edges are unrestrained. The most conservative of these situations will be used to identify the required plate thickness.

A.5 Design Summary

| | Small Cell | Large Cell |
|------------------------|------------|------------|
| Top plate thickness | 33mm | 67mm |
| Bottom Plate Thickness | 25mm | 52mm |
| Number of bars | 12 | 14 |
| Bar diameter | 15mm | 19mm |

A.6 Design Calculations

Small cell - tie bar design

Tensile strength of plate material - aluminium, $\sigma = 150 \text{ N/mm}^2$

Load, $q = 0.8 \text{ N/mm}^2$ cell diameter = 360 mm

loaded diameter = cell diameter = greatest distance between any two tie bars

Loaded area = 101787.6 mm^2 Total load = 81 kN

Factor of safety

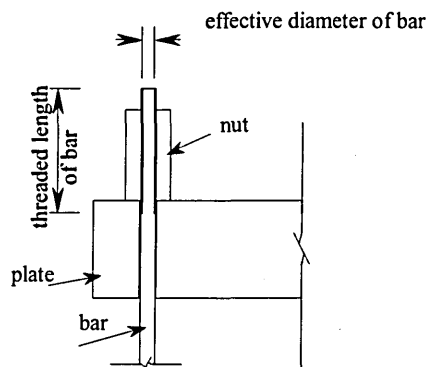
A factor of safety is applied to the strength of the material, i.e. σ , giving $\sigma_a = \frac{\sigma}{f}$

$f = \text{factor of safety} = 1.75$ $\sigma_a = 85.714286 \text{ N/mm}^2$

Total cross sectional area of tie bars required, $A_{\text{tot}} = 950.0 \text{ mm}^2$

Effective diameter

By threading the ends of the bars the effective diameter is reduced by twice the depth of the thread



assuming bar thread, $f = 1.5 \text{ mm}$

Required bar diameter when specifying numbers of bars

Specified number of tie bars, $N_{\text{spec}} = 12$

$$\text{Required diameter, } d_{\text{req}} = 2f + \sqrt{\frac{4A_{\text{tot}}}{\pi N_{\text{spec}}}} = 14 \text{ mm}$$

OR

Required number of bars for specified diameter

Specified diameter of tie bars, $d_{\text{spec}} = 12$

$$\text{Required numbers of bars, } N_{\text{req}} = \frac{4A_{\text{tot}}}{\pi(d_{\text{spec}} - 2f)^2} = 15 \text{ bars}$$

Tensile strength of plate material - steel, $\sigma = 260 \text{ N/mm}^2$

Load, $q = 1 \text{ N/mm}^2$ cell diameter = 720 mm

loaded diameter = cell diameter = greatest distance between any two tie bars

Loaded area = 407150 mm^2 Total load = 407 kN

Factor of safety

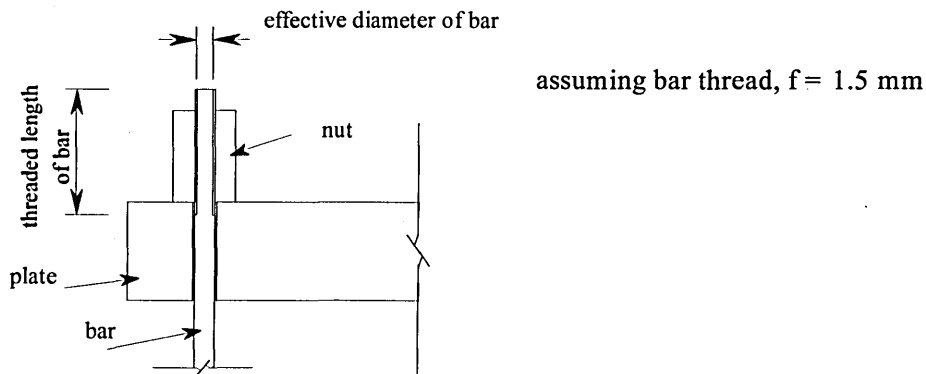
A factor of safety is applied to the strength of the material, i.e. σ , giving $\sigma_a = \frac{\sigma}{f}$

$f =$ factor of safety = 1.75 $\sigma_a = 148.57143 \text{ N/mm}^2$

Total cross sectional area of tie bars required, $A_{tot} = 2740.4 \text{ mm}^2$

Effective diameter

By threading the ends of the bars the effective diameter is reduced by twice the depth of the thread



Required bar diameter when specifying numbers of bars

Specified number of tie bars, $N_{spec} = 14$

$$\text{Required diameter, } d_{req} = 2f + \sqrt{\frac{4A_{tot}}{\pi N_{spec}}} = 19 \text{ mm}$$

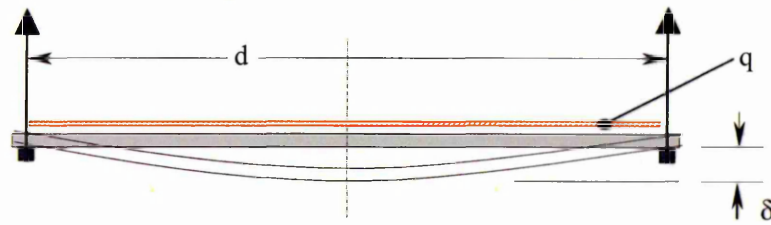
OR

Required number of bars for specified diameter

Specified diameter of tie bars, $d_{spec} = 19$

$$\text{Required numbers of bars, } N_{req} = \frac{4A_{tot}}{\pi(d_{spec} - 2f)^2} = 14 \text{ bars}$$

Small Cell - Bottom plate design



| | | | | | |
|------------------------------|-----|----|------------------------|-------|--------------------|
| loaded diameter, $d =$ | 360 | mm | Load, $q =$ | 0.8 | N/mm ² |
| radius of loaded area, $a =$ | 180 | mm | Elastic Modulus, $E =$ | 70 | kN/mm ² |
| | | | | 70000 | N/mm ² |

Tensile strength of plate material, $\sigma = 110$ N/mm² Poissons ratio, $\mu = 0.3$

Minimum required thickness, t_{min}

$$t_{min} = \sqrt{\frac{6(3 + \mu)qa^2}{\sigma_a}} = 24.1 \text{ mm}$$

where: σ_a is the allowable tensile strength of plate material and is $\frac{\sigma}{f}$, $f =$ factor of safety = 2

$$\sigma_a = 55 \text{ N/mm}^2$$

Deflection for plate of minimum thickness, δ

$$\delta = \frac{12(1 - \mu^2)(5 + \mu)qa^4}{64(1 + \mu)Et_{min}^3} = 0.6 \text{ mm}$$

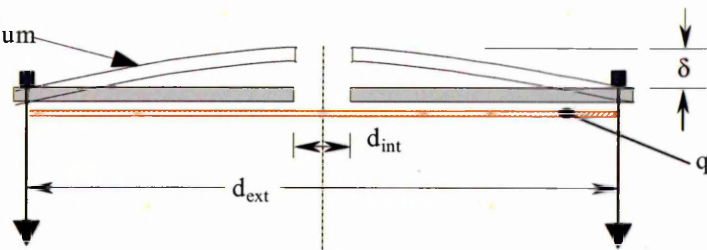
Required thickness for a specified deflection, t_{def}

specified deflection, $\delta_{spec} = 1.0$ mm

$$t_{def} = \sqrt{\frac{12(5 + \mu)(1 - \mu^2)qa^4}{64(1 + \mu)E\delta_{spec}}} = 20.3 \text{ mm}$$

Required thickness, $t_{req} = 24.1$ mm Determined by the stress criteria

Plate material - Aluminium



| | |
|---|--|
| external diameter, $d_{ext} = 720$ mm | Load, $q = 0.8$ N/mm ² |
| internal diameter, $d_{int} = 80$ mm | Elastic Modulus, $E = 70000$ N/mm ² |
| external radius, $0.5d_{ext} = 360$ mm | Tensile strength of material, $\sigma = 110$ N/mm ² |
| internal radius, $b = 0.5d_{int} = 40$ mm | |
| $\alpha = a/b = 9$ | |

NOTE: Poissons ratio, $\mu = 0.3$

Constants

$$k = \frac{-3.9 \log \alpha + 2.475 \alpha^2 - 3 + 0.525 / \alpha^2}{\alpha^2 - 1} = 2.361$$

$$M = \frac{-2.425 \alpha^2 + 2.768 - 1.037 / \alpha^2 + 0.694 \alpha^4 + 3.22 \alpha^2 \log_e \alpha - 3.22 \log_e \alpha - 5.07 (\log_e \alpha)^2}{\alpha^2 (\alpha^2 - 1)} = 0.7564$$

Minimum required thickness, t_{min}

$$t_{min} = \sqrt{k \frac{q a^2}{\sigma_a}} = 66.7 \text{ mm}$$

where: σ_a is the allowable tensile strength of plate material and is $\frac{\sigma}{f}$, f = factor of safety = 2

$$\sigma_a = 55 \text{ N/mm}^2$$

Deflection at minimum required thickness, δ

$$\delta = M \frac{q a^4}{E t_{min}^3} = 0.5 \text{ mm}$$

Required thickness for a maximum deflection, t_{def}

required maximum deflection, $d_{req} = 1.0$ mm

$$t_{def} = \sqrt[3]{\frac{M q a^4}{E \delta_{req}}} = 52.6 \text{ mm}$$

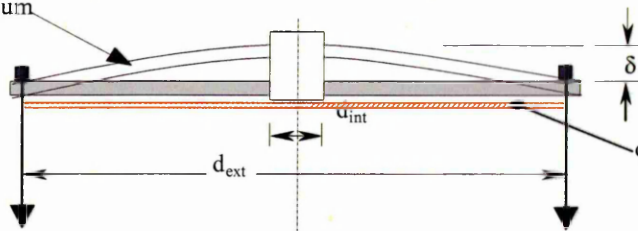
Checks to confirm use of theory

$$t \leq \frac{2}{3}(a - b) \text{ TRUE}$$

$$\delta \leq \frac{t}{2} \text{ TRUE}$$

Required thickness, $t_{req} = 66.7$ mm Determined by the stress criteria

Plate material - Aluminium



| | |
|---|--|
| external diameter, $d_{ext} = 360$ mm | Load, $q = 0.8$ N/mm ² |
| internal diameter, $d_{int} = 50$ mm | Elastic Modulus, $E = 70$ kN/mm ² |
| external radius, $0.5d_{ext} = 180$ mm | Modulus, $E = 70000$ N/mm ² |
| internal radius, $b = 0.5d_{int} = 25$ mm | Tensile strength of material, $\sigma = 110$ N/mm ² |
| $\alpha = a/b = 7.2$ | |

NOTE: Poissons ratio, $\mu = 0.3$

Constants

$$k = \frac{0.525}{\alpha^2} - 3.9 \log_e \alpha - 3 + 2.475 \alpha^2 = 1.755$$

$$M = \frac{0.905\alpha^2 - 3.498 + 2.235/\alpha^2 + 0.358/\alpha^4 + 6.350 \log_e \alpha / \alpha^2 - 2.25 \log_e \alpha + 6.350(\log_e \alpha)^2 / \alpha^2}{1.3\alpha^2 + 0.7} = 0.5836$$

Minimum required thickness, t_{min}

$$t_{min} = \sqrt{k \frac{qa^2}{\sigma_a}} = 28.8 \text{ mm}$$

where: σ_a is the allowable tensile strength of plate material and is $= \frac{\sigma}{f}$, f = factor of safety = 2

$$\sigma_a = 55 \text{ N/mm}^2$$

Deflection at minimum required thickness, δ

$$\delta = M \frac{qa^4}{Et_{min}^3} = 0.3 \text{ mm}$$

Required thickness for a maximum deflection, t_{def}

required maximum deflection, $d_{req} = 1.0$ mm

$$t_{def} = \sqrt[3]{\frac{Mqa^4}{E\delta_{req}}} = 19.1 \text{ mm}$$

Checks to confirm use of theory

$$t \leq \frac{2}{3}(a-b) \text{ TRUE}$$

$$\delta \leq t/2 \text{ TRUE}$$

Required thickness, $t_{req} = 28.8$ mm Determined by the stress criteria